THE EFFECT OF REVERSE OSMOSIS MEMBRANE MICROSCOPIC STRUCTURE ON ITS PERFORMANCE AND REVERSE OSMOSIS PERFORMANCE IN OILY WATER

Subhi Al-Jeshi

Thesis submitted for the degree of Doctor of Philosophy

To Heriot-Watt University, Edinburgh, UK

on completion of research in the

School of Engineering and Physical Sciences

June 2004

DECLARATION

This is to declare that the thesis is an account of the author's work carried out at Heriot-Watt University, Edinburgh, except where acknowledgement is made, and has been submitted for any other degrees.

Sobhi Al-Jeshi (candidate)

Professor Anne Neville (Supervisor)

TABLE OF CONTENTS

LIST OF FIGURES

LIST OF TABLES

ACKNOWLEDGEMENETS

I would like to thank my supervisor Professor Anne Neville for her outstanding support, understanding and continuous encouragement during this research. I would also like to thank my parents, especially my mum. Special thanks for the emotional support from my very special sisters and brothers. I am deeply indebted to my brother Mohammed who positioned himself into my deep heart by his exceptional support. Very special thanks to my wife who has supported me during my study and has been very patient and understanding. My thanks also to my friends in Saudi.

I would like to thank also Saudi Aramco who provided my scholarship. I would like to thank all the Mechanical and Chemical Engineering Department staff for their assistance specially, Marian Millar, Ian Galloway, Aftab Aziz, Craig Bell, Ann Blyth and John Pritchard. I would like to thank finally all my friends in the department who made my stay enjoyable and full of laughs with special thanks to Myrna Rayes.

NOMENCLATURE

C_{A1}	Dissolved solids concentrations in feedwater
C_{A3}	Dissolved solids concentrations in reject water
R_{avg}	Average plan surface roughness
Ra	Average plan surface roughness
R_{rms}	Square mean plan roughness
P-V	Maximum difference between peak and valley
a b	Length of two sides of the area
S	A specified area
f(x,y)	Height in the specified area
AFM	Atomic Force Microscopy
SEM	Scanning Electron Microscopy
NMR	Nuclear Magnetic Resonance
MF	Microfiltration
UF	Ultrafiltration
NF	Nanofiltration
RO	Reverse Osmosis
COD	Chemical Oxygen Demand
v	Velocity
σ	Taft number

ABSTRACT

The objective of this thesis is to provide a comprehensive discussion of RO membrane microscopic structure by using atomic force microscopy (AFM), light microscopy and scanning electronic microscopy (SEM). The effect of RO membrane surface roughness and cross-section thickness on flux has been assessed. Additionally, the effect of AFM operation mode on membrane surfaces was studied. The performance of two commercial polyamide RO membranes was studied in clean water and in the treatment of up to 50% oil contamination.

It was found that surface properties of RO membranes can vary significantly from one location to another and for this reason characterization using microscopy must be conducted in a comprehensive manner, taking into account the spatial variation. From this research a methodology for the proper assessment of membrane surface characteristics was established. It was also found that a universal relationship between membrane surface roughness and flux does not exist and that membrane thickness affects flux rate. It was found that the thicker the membrane the lower the permeation rate. In contact mode operation excellent quality AFM images were obtained for membranes imaged in air. However, the AFM tip was found to cause damage to the membranes imaged in water under some circumstances.

The two tested membranes showed excellent performance in not only tolerating high oil contamination (no fouling) but also in producing high quality product water. More than 99.9% oil rejection was achieved. Drinking water quality (less than 5 ppm TOC) was achieved by optimizing operating parameters. It was found that feedwater pH and pressure have a significant effect on membrane oil rejection properties.

CHAPTER 1- INTRODUCTION

1.1 Introduction

This research is designed to provide a comprehensive discussion of RO membrane microscopic structure, properties and performance in pure water and oily water and to link the membrane structure properties to performance. It will be divided into three broad categories. The first deals with RO membrane cross-section and surface morphology properties characterized by Atomic Force Microscope (AFM), light microscope and Scanning Electronic Microscope (SEM). The second deals with RO membrane performance under various operating conditions in pure water. The third deals with RO membrane performance in the treatment of oil-contaminated water.

Four RO membranes are examined in this research. Each RO membrane surface morphology and cross-section structure is characterized. Then an investigation is conducted to determine the effect of membrane surface roughness and cross-section thickness on membrane performance. The results from pure water tests are used as baseline performance data for the last part of the research, which is to examine RO membrane performance in oil-contaminated water at various operating conditions.

1.2 The effect of membrane microscopic structure on its performance

Reverse osmosis technology is a desalination process used mainly to produce drinking water from seawater and brackish water. Since the early days, the main emphasis of reverse osmosis (RO) membrane development has been directed in the improvement of RO performance: namely high salt rejection and permeate flux. There are two types of RO membranes: 1) thin film composite, which have a thin salt rejecting layer (0.25-0.5 microns) separately deposited or formed on the surface of a non-salt-rejecting porous membrane substrate, and 2) asymmetric membranes that have one layer formed in one operation where the surface facing the feed stream has very small pores or no porosity to a depth of about 0.1 micron. The porosity then increases through the thickness of the membrane [1].

Over the last two decades, reverse osmosis (RO) thin-film-composite (TFC) membranes have found a variety of applications such as in the production of ultra pure water, and in wastewater treatment. Recently, it has become important to control the membrane performance and specialize it for the intended application to meet the tight environmental regulations in terms of wastewater toxic contaminant limits. Various methods have been followed, and they generally fall into two categories. The first is to synthesize and develop new thin-film polymeric materials. The second involves two routes which are surface modification by post-treatment with various chemicals and some modification of the polymer chains and hence control of the surface morphology by using additives during formation of the thin films.

The improved properties of the resulting composite membranes that have been achieved are either by enhancing water flux accompanied with a loss of salt rejection, or vice versa. Lately, a number of studies have been performed where an increase in water flux without any loss in salt rejection has been reported.

An understanding of the relationship between membrane surface properties and separation characteristics is very important in the development of membrane technology. Such understanding can determine the choice of membrane for particular separation and can also lead to development of better membranes. Atomic Force Microscopy (AFM) offers a valuable means of imaging membrane surfaces and characterizing topography at different length scales. AFM can be used to image membrane surfaces in air or in liquid without any special surface preparation, which offers benefits over SEM, which requires a conductive coating to be applied. In this work a full analysis of the membrane surfaces using principally AFM, and supported by SEM and light microscope, is presented.

To date several studies of the effect of RO membrane surface roughness on membrane performance have been presented in the literature and the results and conclusions are not yet clear. Contradictory findings are reported; higher RO membrane surface roughness can mean higher flux, lower flux or have no effect on flux. There are issues in the selection of surface roughness data using AFM related to the nature of the tip-surface interaction. These issues are addressed in this thesis for the range of membranes included in the study.

1.2.1 Objective of the study

The objective of this study is to understand the role of membrane surface morphology on its performance. AFM is applied to characterize four RO membrane active surface layers and SEM and light microscopy are applied to characterize the membranes cross-section thickness. The flux of the four tested membranes is assessed and then the relationship between membrane surface roughness, cross-section thickness with membrane flux is investigated. In addition, the effect of scanning RO membrane surfaces with the AFM tip in contact mode is investigated.

1.3 RO membrane technology performance in pure water and oil contaminated water

Global water shortage is an issue that is inflating in magnitude, severity and urgency. The global search for alternative water sources began some decades ago and has found two promising technologies: seawater desalination and wastewater reclamation. Seawater desalination has been considered to provide additional water. However, although there has been rapid development in desalination, its operation is still costly because of high-energy consumption. Parallel efforts have also been directed at exploring the option of wastewater reclamation. One of the solutions is to reuse water by reclaiming wastewater and boost the water supply with such recycled water. Therefore research in recent years has been focused to finding more efficient and cost effective technologies. Membrane processes have been shown to offer promise in the treatment of wastewater.

Membrane processes are filtration processes and are normally divided into four types based on membrane pore size: microfiltration, ultrafiltration, nanofiltration and reverse osmosis. Reverse osmosis (RO) is the finest filtration process. It uses a semi-permeable membrane to separate an extremely high percentage of particles from water. RO has the ability to remove ions from solution [2].

In recent decades, membrane filtration has become a novel technology in wastewater reclamation. It has been applied in the purification of wastewater from the metal-finishing industry (usually contaminated with heavy metals), pulp and paper industry (mainly to recycle and reduce water wastage), textile and petroleum industries, many of which are contaminated with oil and grease [3]. Rapid advances in membrane technology

have resulted in improvement in membrane performances and increased tolerance to contaminants. However, controlling membrane fouling continues to be a major challenge in wastewater reclamation. In highly oil-contaminated waters, microfiltration and ultrafiltration membranes processes are employed and they undergo severe fouling problems, which leads to high operational costs. Many new techniques were discovered such as back flushing to minimize fouling and extending the operational cycle between chemical cleaning.

RO membranes are used primarily for the treatment of low oil contaminated water (mostly in ppm ranges) to produce high quality water. RO has not been employed in the treatment of above 10% oil water contamination because it was believed that RO is a much more delicate process than other filtration processes due to a very tight structure. Fouling is therefore expected and other filtration processes having much higher flux rates are preferred. Smaller plant is needed in this case for handling high feedwater flow because they generally have much larger pore sizes. Another possible reason is that RO membrane is a young technology and recently many new developments were achieved in producing new membranes, which have not been tested in various treatment conditions. Currently, to produce high quality water from highly oil contaminated water two steps are usually required: 1) a microfiltration or ultrafiltration step to remove the majority of oil and 2) a RO membrane process to remove traces of oil left behind to achieve the desired product water quality.

1.3.1 Objective of study

The ultimate objective of this part of the research is to examine RO membrane technology in the purification of up to 50% oil contaminated water to assess the feasibility of avoiding the ultrafiltration or microfiltration step. In addition to that, the limiting factors and the optimum operating conditions at which highest water quality is achieved with minimum fouling and highest production rate are assessed. Prior to studying oil contaminated water, an extensive study in "clean" water was conducted with the objective of producing reliable baseline data and to comprehensively assess the parameter relationships in the RO process.

1.4 Outline of the thesis

The layout of the thesis is as follows: Chapter 2 presents mainly the historical background of RO technology, principles of RO technology, RO membrane physical and chemical structure, RO design configuration and pretreatment system design. This chapter gives the reader a full understanding of the RO process. Chapter 3 is designed to provide a comprehensive discussion of RO membrane technology performance in various environments and operating conditions reviewed from the current existing literature. There is a special emphasis on membrane surface morphology and its relation to flux and salt rejection. Chapter 4 covers the application of membrane technology in purifying industrial wastewater contaminated mainly with oil, lubricants, and heavy crude oil. It deals with the application of the following membrane technologies: Microfiltration (MF) membranes, Ultrafiltration (UF) membranes, Nanofiltration (NF) membranes, and Reverse Osmosis (RO) membranes. Because this research deals with the performance of RO membranes in oily wastewater, a thorough literature review will be covered in this part. Chapter 5 presents the experimental procedures and gives description of the analysis techniques used in this research. Chapter 6 covers membrane surface and cross-section property characterization and the role of membrane structure properties in membrane permeation rate. In addition, the effect of operating AFM in contact mode with different tip force settings on RO membranes surfaces will be assessed.

Chapter 7 presents results from experiments to assess membrane performance in pure water and the effect of operating parameters on the membrane permeation rate and salt rejection are evaluated. In Chapter 8, RO membrane fouling tendency in the treatment of oily water is assessed. Then results from tests to assess membrane oil rejection properties at various operating conditions are presented. Chapter 9 discusses in depth the experimental results in relation to the literature and details the main contributions made in this thesis. In Chapter 10, conclusions from the work are summarized and further work is suggested. Finally, the appendix is given in chapter 11.

CHAPTER 2

THEORETICAL REVIEW OF RO MEMBRANE TECHNOLOGY

2.1 Introduction

The objective of this chapter is to describe reverse osmosis (RO) membrane processes. The chapter will cover the following headings:

1) The historical background of RO technology,
2) Industrial membrane processes,
3) Principles of RO technology,
4) RO membrane physical and chemical structure,
5) RO process performance parameters,
6) RO design configuration, and
7) Pretreatment system design.

2.2 Historical background of reverse osmosis

For many years it was thought that no filter could retain salt while passing water because a salt solution represents a single phase. But experiments in the late 1920s and early 1930s demonstrated small filtration effects in very dilute solutions with membranes [4]. Reid in 1953 at the University of Florida appears to be the first person who recognized that salt filtration by membranes might be useful in desalination. Many membrane materials were investigated at that time. The one showing most promise was cellulose acetate, which rejected 98% or more of the salt from salt solutions of seawater concentration. Permeation rates, however, were small and therefore posed a large constraint on the practical use of this finding.

Loeb and Sourirajan [5-9] at the University of California worked along similar lines and developed a cellulose acetate membrane, which could handle a greatly enhanced flow by casting them from solutions containing perchlorate salts. The fluxes (flow per membrane surface area) were high enough to arouse an interest in practical applications, and this has

been growing ever since. Many variations have been made on this membrane material since then [10]. A range of membranes with different salt rejection and water flux properties were made [6].

Nowadays many new types of membranes are available, leading to an increase in various applications. Improvements have been made in membrane materials making them more pH, temperature and chlorine resistant [11-17]. The industrial development of noncellulosic, thin–film composite (TFC) membranes has provided better flux performance by surface modifications [1,18].

Reverse Osmosis membranes are currently used in the treatment of water and hazardous wastes, separation processes in the food, beverage, and pulp and paper industries, and recovery of organic and inorganic materials from chemical processes [1,19-22].

2.3 Industrial membranes processes

Membranes for industrial separation processes can be divided into the following categories; reverse osmosis, nano-filtration, ultra-filtration, micro-filtration, and filtration [2,23]. Table 2.1 shows typical production rates expected from each filtration process, which could vary significantly upon changing operating conditions. Figure 2.1 is a self-explanatory diagram. It compares these membranes in terms of pore diameter and the types of particles and contaminants that can be filtered.

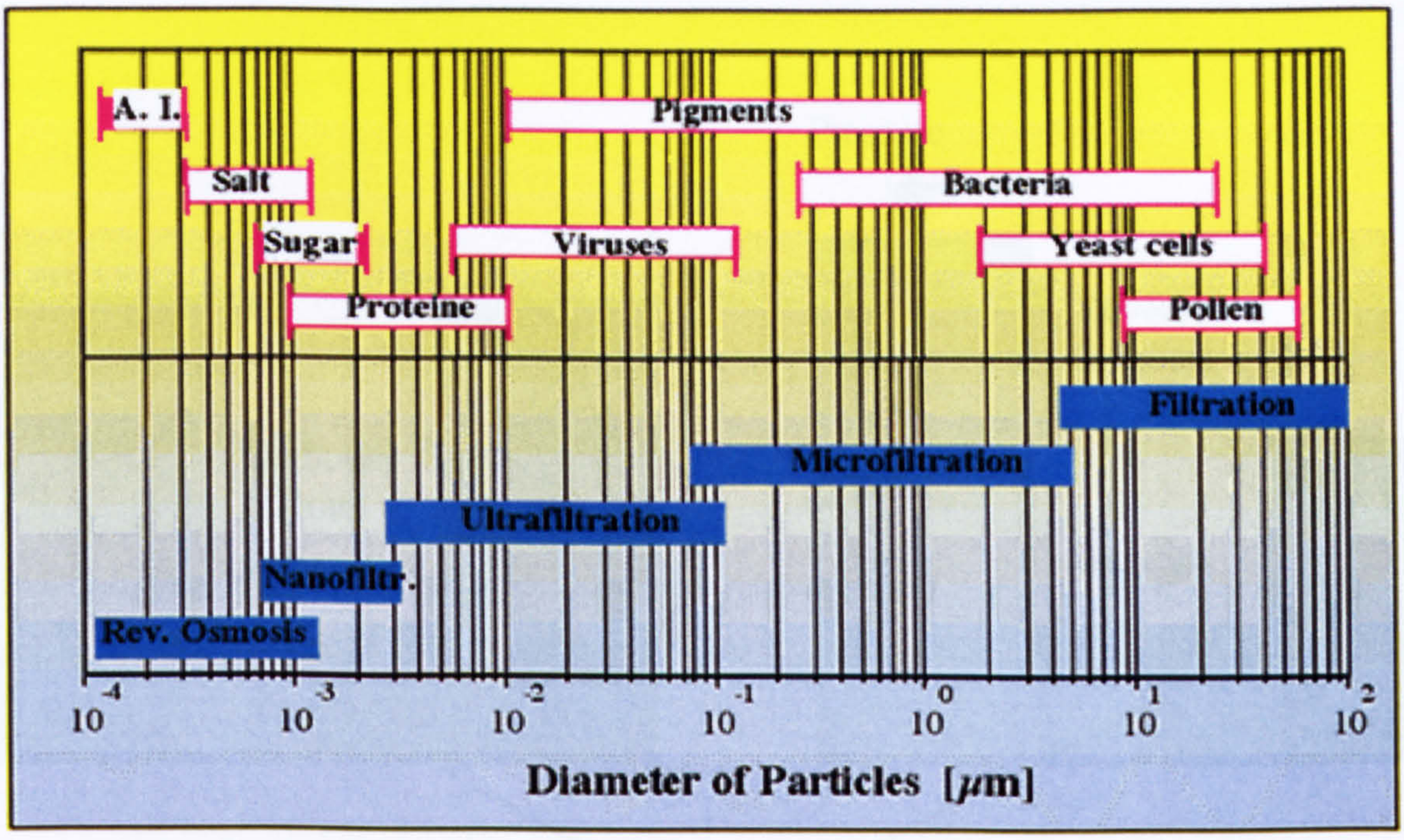

Figure 2.1. Membrane average pore diameters [2,24]

2.4 RO process principles

Reverse osmosis membranes are permeable to water but not to salt (see Figure 2.2). They are called semi-permeable membranes. When a semi-permeable membrane is placed between seawater and pure water, which are both at the same pressure, diffusion of fresh water into seawater will occur because of the natural tendency to equalize concentrations. This process, called osmosis is exactly the opposite of the desired action, namely, the transfer of water from salt solution into the fresh water. To make the process occur in the desired direction, pressure must be exerted on the salt water. The applied pressure must be higher than the osmotic pressure, which increases with salt concentration [2,3,5,6,23].

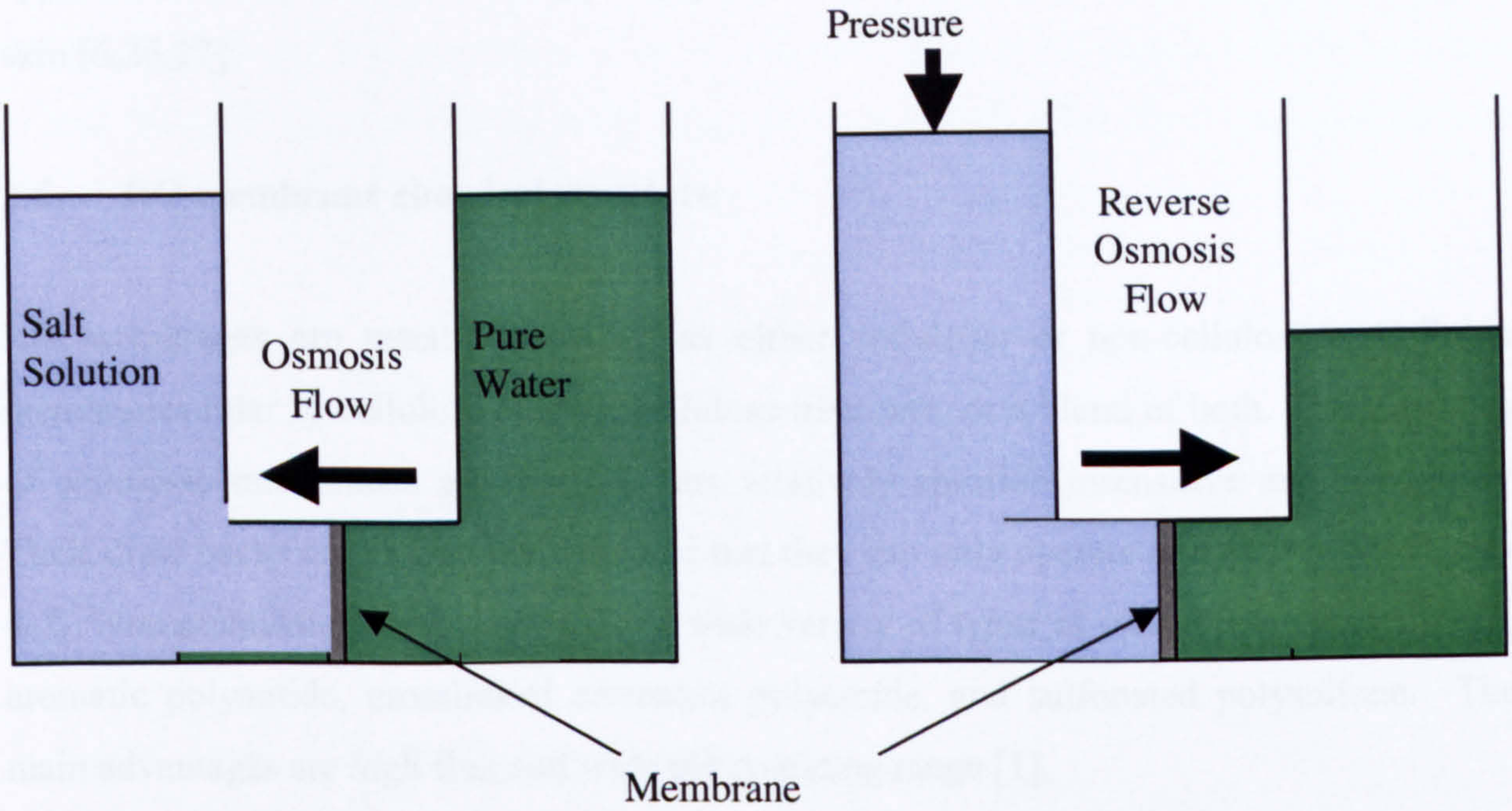

Figure 2.2. Principle of RO process [25]

2.5 RO membrane physical structure

RO membranes have a dense skin layer (active layer) on the top side of the membrane that is supported by a relatively thick porous sub-layer [3]. The surface of the membrane facing the feed stream has very small pores or no porosity (see Figure 2.3).

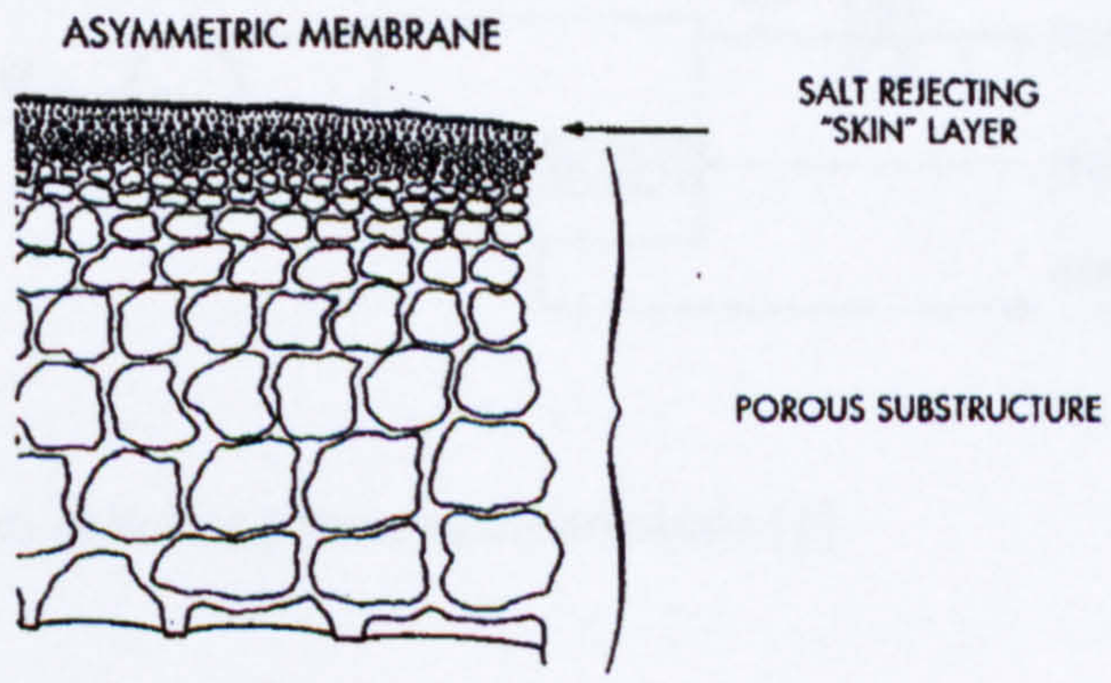

Figure 2.3. Membrane physical structure [1]

The porosity then increases through the thickness of the membrane. Salt rejection is a surface phenomenon; it is independent of membrane thickness. Membrane flux, however, is

inversely related to the thickness of the solute rejecting skin layer [1]. The skin depth is approximately 1 μm whilst the support layer can be up to 100 times as thick as the rejection skin [6,26,27].

2.6 RO membrane chemical structure

RO membranes are usually classified as either cellulosic or non-cellulosic. Cellulosic membranes refer to cellulose acetate, cellulose triacetate, or a blend of both. The advantages of cellulosic membranes are that they are relatively chlorine insensitive and inexpensive. Their draw backs are mainly low flux and that they can only operate in a narrow pH range of 4-7. Non-cellulosic membranes cover a wide variety of types of synthetic polymers such as aromatic polyamide, crosslinked aromatics polyamide, and sulfonated polysulfone. Their main advantages are high flux and wide pH operating range [1].

2.7 RO process performance parameters

Before discussing the RO process it is important to define some of the terms used to describe membrane performance. Typically membrane performance is characterized in terms of flux and separation as illustrated in Figure 2.4.

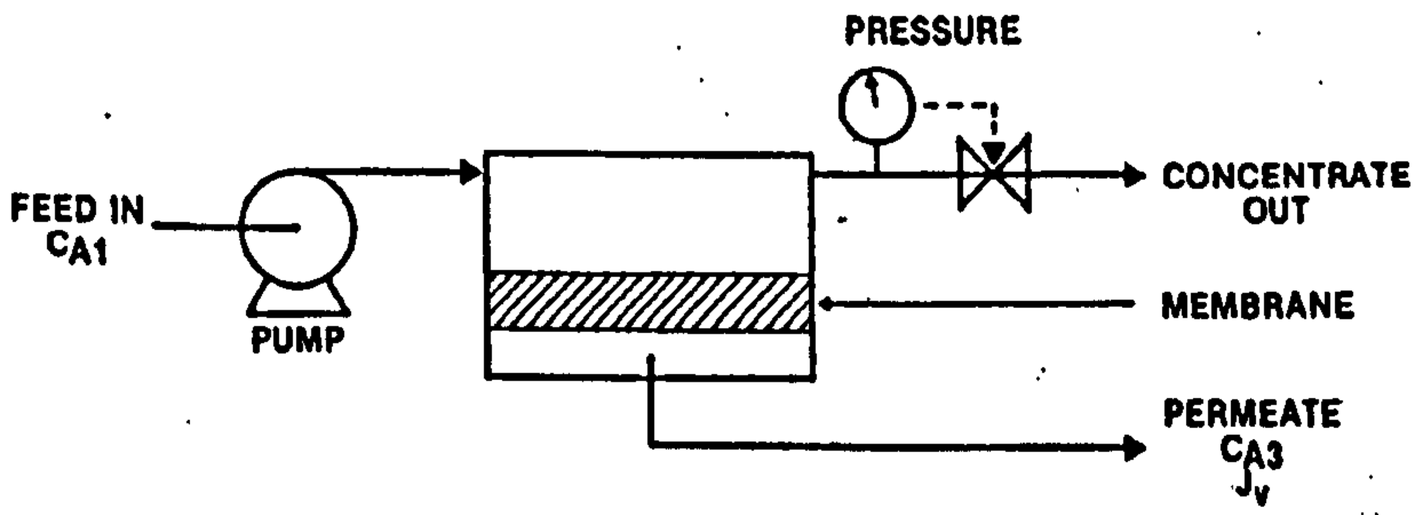

Figure 2.4. Reveres osmosis process performance [1]

Flux = Volumetric flow passing through membrane /membrane area/time ($m^3/m^2/s$)

Separation % = rejection % = $\{(C_{A1}-C_{A3})/ C_{A1}\}$ x 100

Where C_{A1} is the dissolved solids concentrations in feedwater and C_{A3} is dissolved solids concentrations in reject water.

In operation, RO membranes are arranged so that a high pressure feed stream contacts the salt rejection face of the membrane. The feed stream continuously passes over the membrane so that the fluid velocity sweeps away much of the retained solute from upstream face (see Figure 2.5)

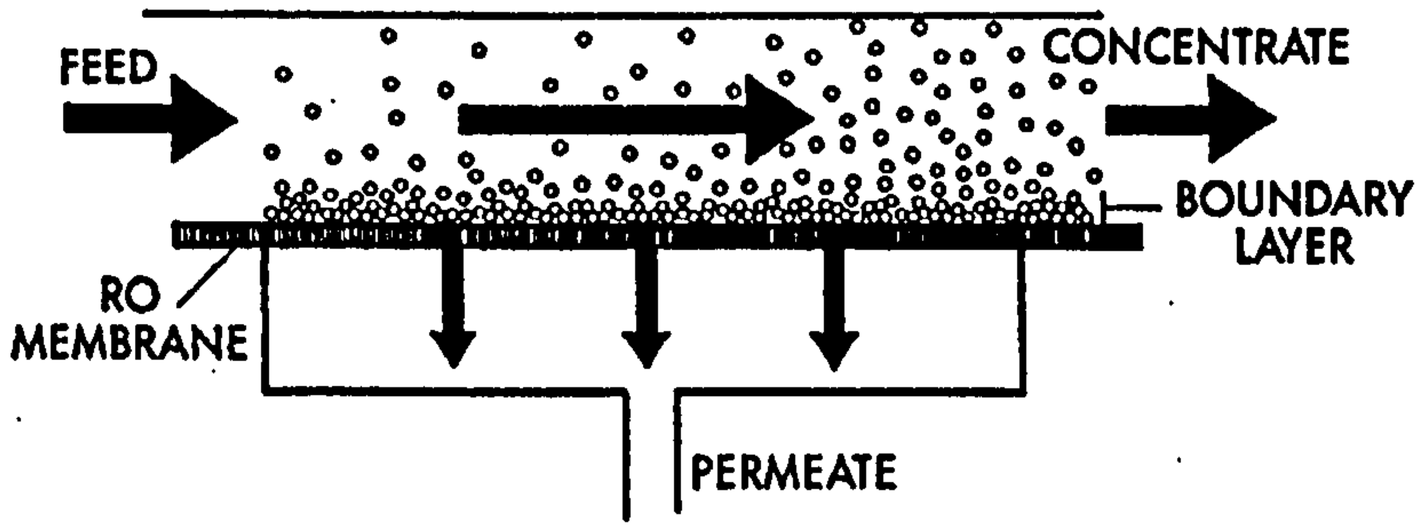

Figure 2.5. Fluid stream in RO operation [1]

The feed flow generally sweeps away all except a boundary layer thickness of this concentrated feed. The phenomenon causing the resultant layer is termed concentration polarization. The possible negative effects of concentration polarization include a decrease in water flux, increase in solute flux, precipitation of solute on the membrane surface, and fouling [1,3].

2.8 RO design configurations

In designing RO processes, the manufacturers' main interests are: a) to provide mechanical support for the membrane, which must operate at high pressure, b) to maximize the efficiency with which flow energy is used to control concentration polarization, and c) to provide an adequate exit path for the permeate [2]. Four design configurations for the membrane have became popular: 1) hollow-fibre, 2) spiral-wound, 3) tubular, and 4) plate and frame. The hollow-fibre and spiral wound configurations have received the most attention due to their efficiency [10]. Both tubular and plate and frame RO units have been developed for food applications where sanitary design is paramount, but would not be

considered as efficient designs where costs must be contained as in seawater desalination [2,6]. An explanation of each design system is given in the following sections.

2.8.1 Spiral-wound system

General Atomic Co., San Diego, California, developed the concept of a spiral-wound system as early as 1968 [2,5]. In construction of spiral-wound systems, pairs of membranes are separated by a tricot nylon spacer (typical thickness 0.2-0.4 mm) and are glued on three sides. The fourth, open side, is attached to the central permeate collection tube. A plastic net then separates the membrane pairs from each other which functions to distribute feed flow and assist feed side mass transfer. The sets of membranes plus spacers are scrolled to give a spiral wound configuration as shown in Figure 2.6.

During operation, pressurized feed water passes through the membrane into the nylon spacer, which contains flow channels allowing the water to proceed to the perforated central tube where it is collected and removed from the system. This design has high packing density, low manufacturing cost, and can be cleaned chemically and hydraulically with relative ease. The primary disadvantage is that it cannot be used on highly turbid feed water due to the high packing that leads to small spaces for water to travel through. These spaces are easily clogged with impurities [6,28].

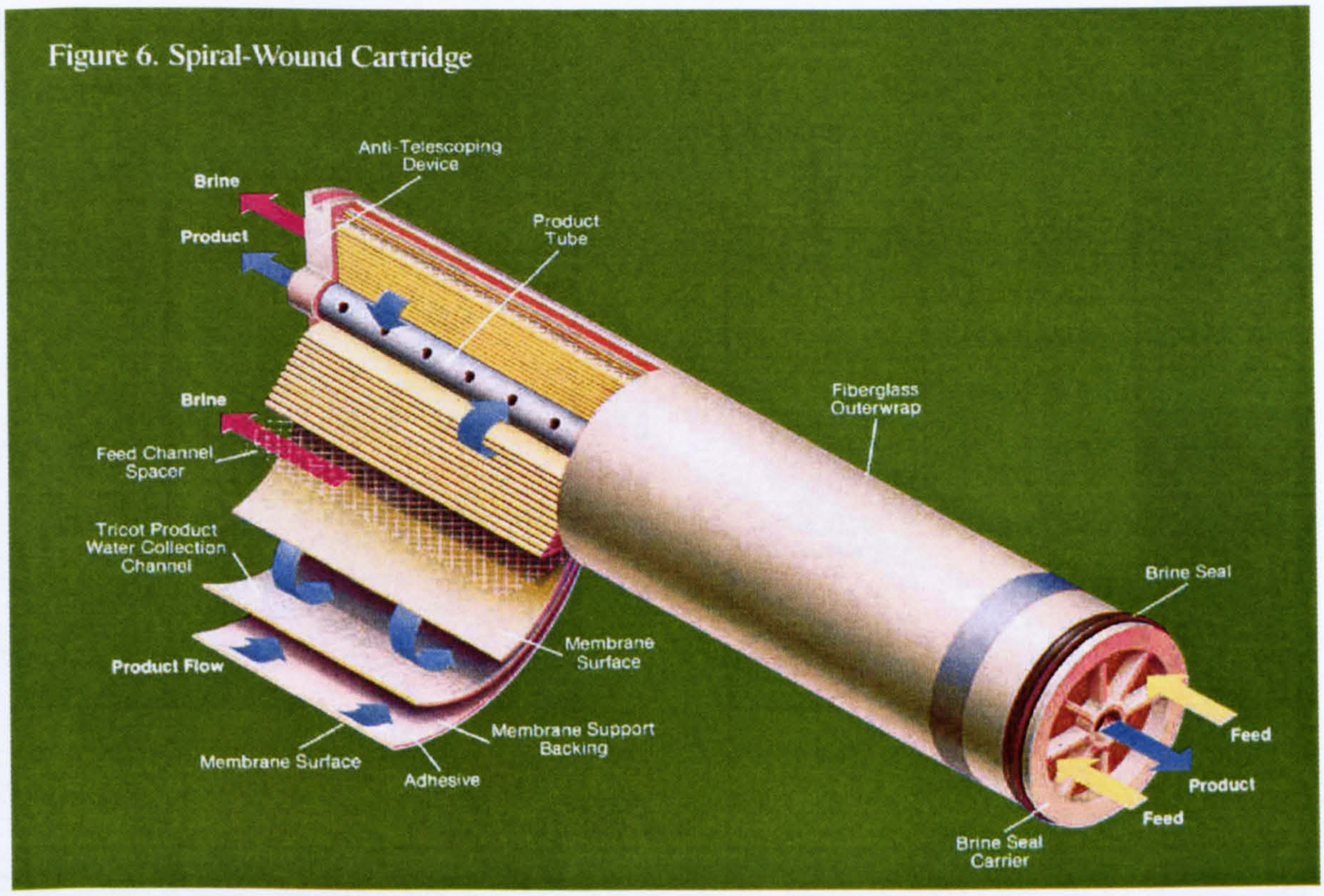

Figure 2.6. Spiral wound cartridge, [24]

2.8.2 Hollow-fibre system

The hollow-fibre membranes used in this configuration are inherently less water permeable than the flat sheet thin film composite membranes used in the spiral-wound configuration (see Figure 2.7). However, hollow-fibre membranes have higher salt rejection, can be operated often at higher pressure, thus making higher packing densities possible. As a result, the cost per unit of water produced are comparable to those of spiral-wound modules. In the hollow-fibre configuration, the fibres are pressurized from the outside, and the product water passes into the interior of the fibres. The product water flows down the fibre through a tube sheet and into a product water header. Because the fibres are pressurized from the outside, fibres with less mechanical strength can be used than if fibres were pressurized from the inside. Furthermore, the pressure drop down the fibres is reduced because the permeate stream has a lower flow rate than the feed stream [3,6,24].

Figure 5. Hollow-Fiber Permeator

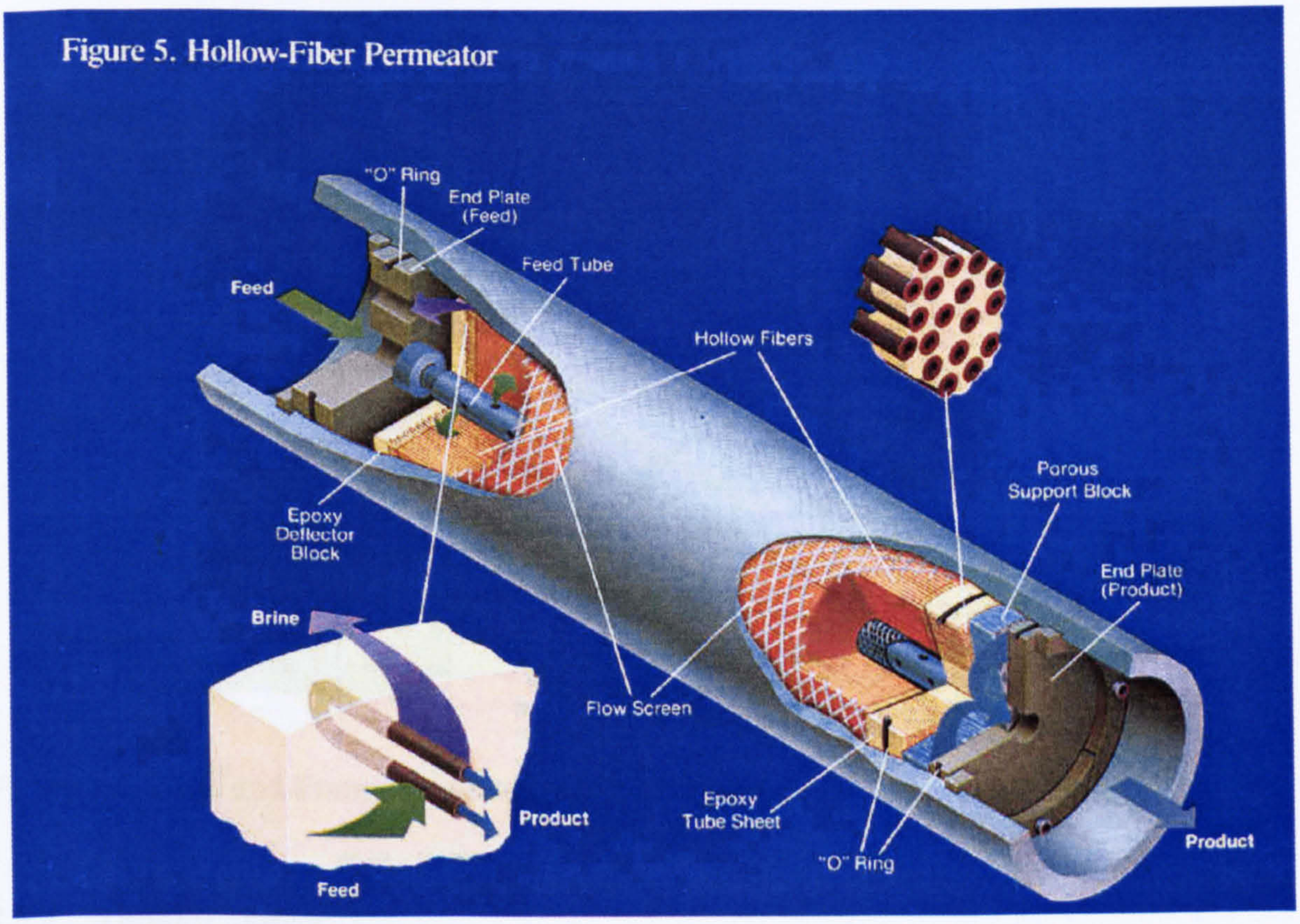

Figure 2.7. Hollow-Fine Fibre Permeate [9]

2.8.3 Plate and frame system

This design has been constructed by the University of California at Los Angeles and by Aerojet General Corp. Membranes in flat sheets are laid on each side of porous plates, and the plates are stacked in a filter-press arrangement, inside a pressure vessel (see Figure 2.8). Brine flows between the membranes, and product through the porous materials. Product conduits may be porous metals or plastic, or metal sheets overlaid with a porous cloth. Connections of successive channels between membranes are necessary, and rather complex seals are required. Since a uniform flow pattern is difficult to attain, concentration polarization and fouling difficulties are anticipated. The concept appears to have lost favour in recent years as it was concluded from an economic analysis that large plate and frame plants would not be competitive with other arrangements [2,6].

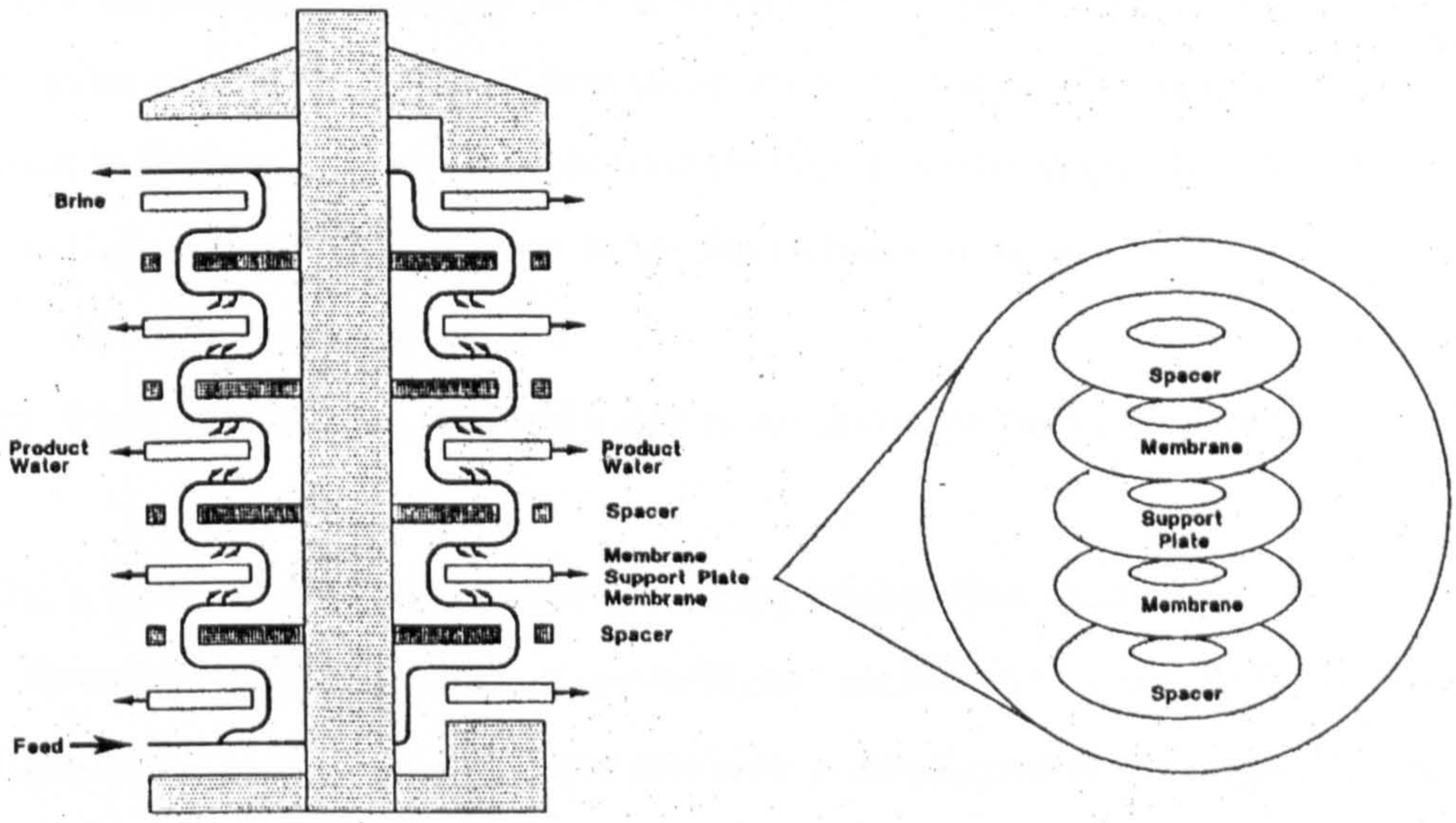

Figure 2.8. Plate and Frame System [2,6]

2.8.4 Tubular system

Havens Industries, San Diego, California first marketed fibreglass tubes, lined on the inside with cellulose acetate membranes [5]. Tubular modules can contain up to 30 tubes and can be up to 20 ft in length (see Figure 2.9). The membranes are normally supported within stainless steel tubes. The tubes are connected in series in most designs. With this design, the feed channels and most importantly, the permeate channels can be easily cleaned, making the modules appropriate for food and dairy applications in which frequent cleaning is necessary.

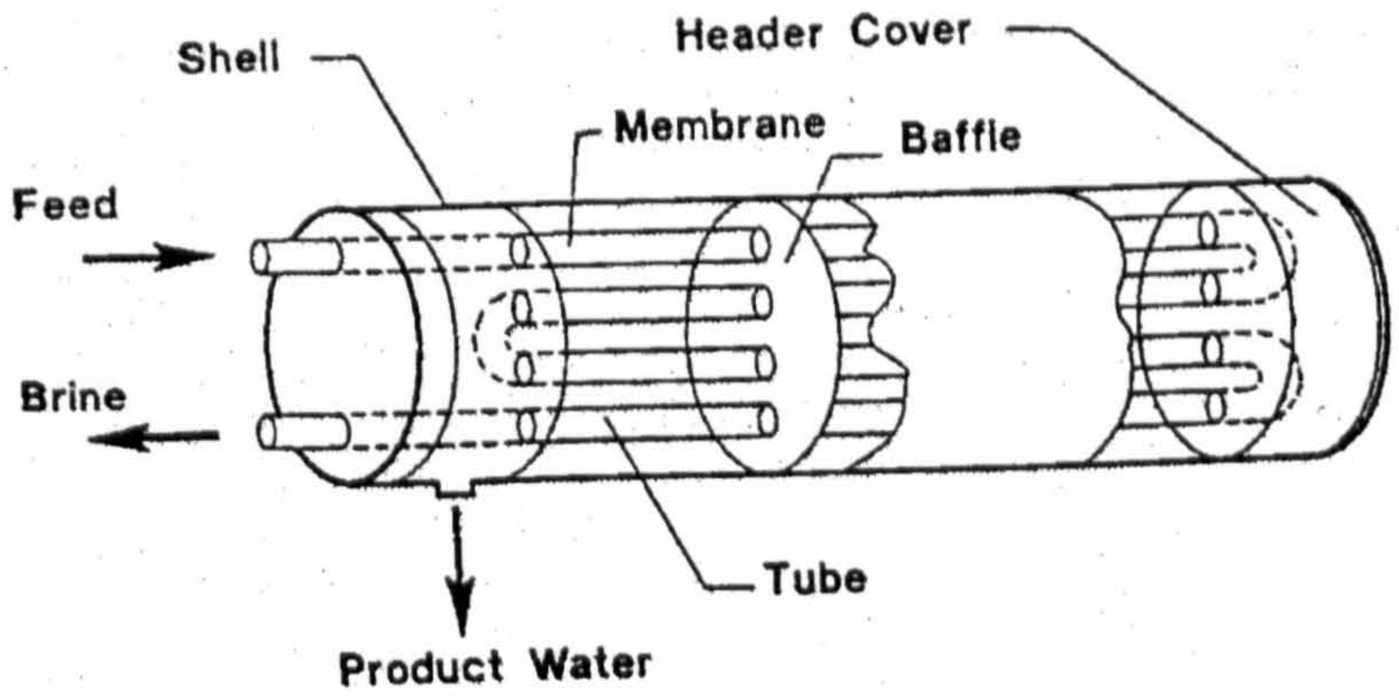

Figure 2.9. Tubular System configuration

Besides ease of cleaning, a major advantage of the tubular configuration is that the tube diameter (typically 0.5 in. for RO applications) is large enough to promote turbulent flow under most conditions without excessive pressure drop. This feature makes the module very resistant to fouling. However, this module type has two major disadvantages:

1) High energy cost due to large feed channels (need to pump large volume of water through the modules) and
2) High capital cost, primarily due to module low packing density [3,6].

Lately, a new design configuration showing higher flux than the conventional design system was developed [29]. It is a centrifugal membrane separation system (CMS) design configuration. In CMS the process pressure is developed at the edge of a centrifuge rotor and the fluid cross-flow direction across the membrane surface is fixed with respect to the rotational direction. The CMS was compared with conventional (non-rotating) pressure-driven RO separations of NaCl and $MgSO_4$ solutions. At low salt concentrations the CMS system is equivalent to the conventional system, but shows progressive flux enhancement over conventional RO as the salt concentration of the feed-stream is increased. The enhancement is related to a reduction in concentration polarization due to rotation-induced instabilities, which diminish the boundary layer thickness at the membrane interface.

2.9 Desalination by RO process

The available RO membranes (see Figure 2.10) are generally not robust enough to operate directly on typical feed water streams. Feed waters usually contain components that can adversely affect the performance and lifetime of an RO membrane system. Therefore, the performance of a RO system will only be as good as the system used to pre-treat the water before it enters the system [30]. Virtually every RO system includes some level of feed pretreatment designed to; a) extend the lifetime of the membranes, b) prevent fouling of the membranes, and c) maintain the performance (i.e., rejection and recovery) of the system [3]. Figure 2.10 shows schematic diagram of the Jeddah RO desalination plant, Saudi Arabia.

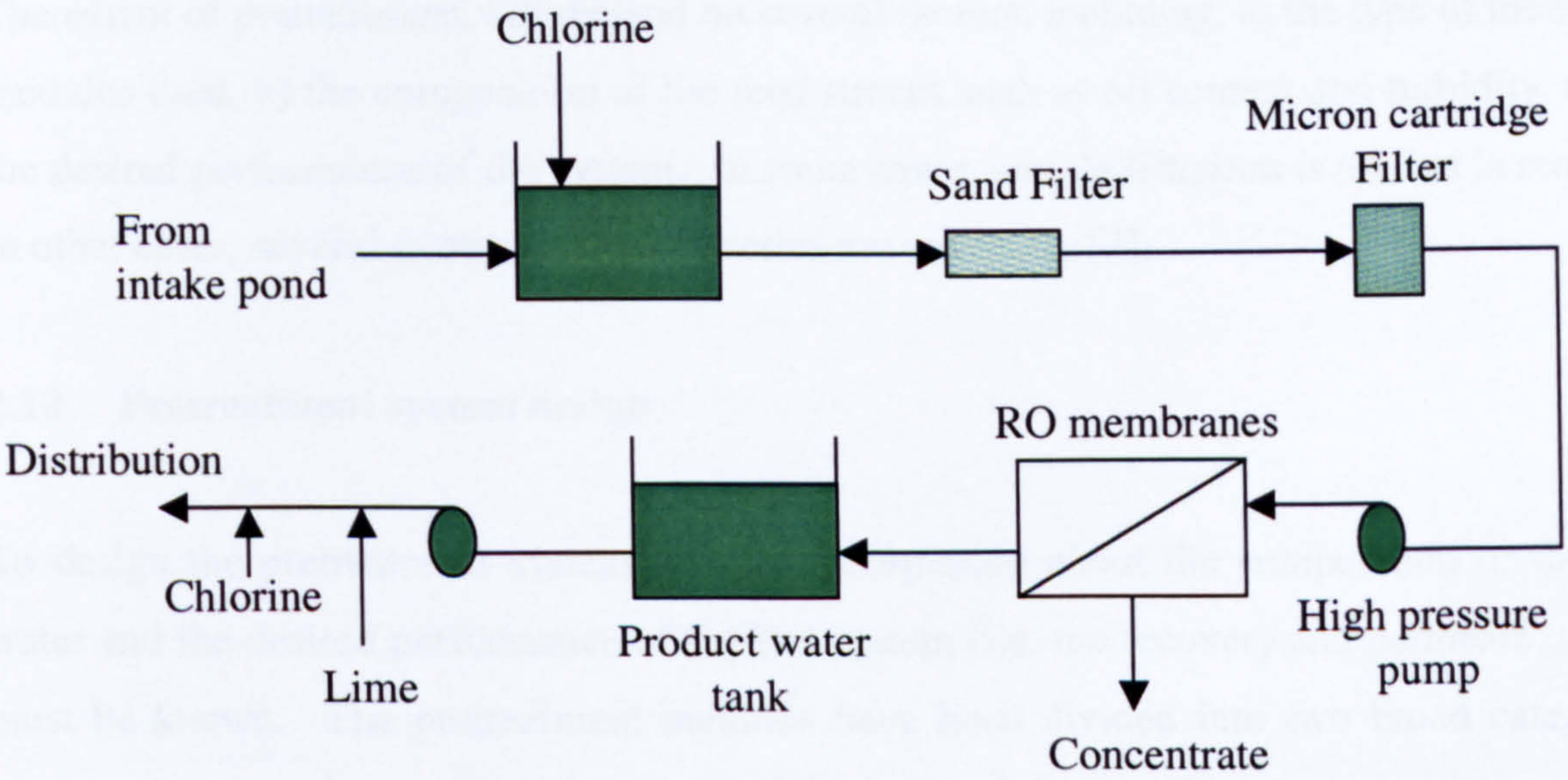

Figure 2.10. Schematic of Jeddah RO desalination plant, Saudi Arabia [3]

Figure 2.11 shows an actual RO desalination plant for a 5 million gallons per day production located in California, USA. In the picture, hundreds of RO membrane cartridges are stacked on top of each other, which are considered the heart of the plant. The pretreatment system is not shown.

ESPA installation, 5 MGD, in Carson, California

Figure 2.11. 5-MGD RO desalination plant located in California, USA

The extent of pretreatment will depend on several factors, including; a) the type of membrane modules used, b) the composition of the feed stream such as oil content and turbidity, and c) the desired performance of the system. In some cases, simple filtration is all that is required. In other cases, several treatment steps in series are necessary [3].

2.10 Pretreatment system design

To design the pretreatment system detailed information about the composition of the feed water and the desired performance of the RO system (i.e. the recovery and permeate quality) must be known. The pretreatment methods have been divided into two broad categories: pretreatment to prevent membrane chemical damage and fouling [3].

2.10.1 Prevention of membrane chemical damage

The concentration of chlorine and the pH of the feed water are the most common factors that can result in chemical damage of the RO membranes. Chlorine is added to feed waters to control microbial growth. Many RO membranes are damaged by even 0.1 ppm concentration of chlorine. Chlorine causes chain deformation and depolymerization of the polymer leading to breakage of the thin film layer allowing salt to pass [10]. Therefore, the feed water must be dechlorinated before it enters the membrane system. There are several methods used to dechlorinate. The most popular ones are; a) treatment with sodium bisulfate, b) carbon filtration, and c) treatment with gaseous sulfur dioxide [3,6].

While dechlorination is vital for most polyamide membranes, control of pH is particularly important for membranes based on cellulose acetate. These membranes undergo rapid hydrolysis (fast breakage of the thin film layer) below pH 4 and above pH 7. Therefore, tight control of pH is essential. In most applications, the pH of the feed must be lowered by adding hydrochloric acid or sulfuric acid. In some situations, where the pH must be increased, NaOH is usually used [3,6].

2.10.2 Prevention of membrane fouling

Most feed waters contain contaminants that reduce membrane productivity (flux) over time. The extent to which a membrane fouls will depend on the module configuration and the types of contaminants and their concentrations in the feed water. For example, spiral-wound and hollow-fibre modules foul readily and therefore require an extensive pretreatment system. On the other hand, tubular modules are more resistant to fouling due to the hydrodynamics within them. Therefore, minimal pretreatment is required. The types of contaminants that foul RO membranes can be divided into the following categories: (i) suspended solids, (ii) colloids, (iii) scale forming salts, (iv) metal oxides, (v) biological foulants, and (vi) organic foulants. The pretreatment must be designed specifically for specific applications [3].

CHAPTER 3

LITERATURE REVIEW OF THE RO MEMBRANE PERFORMANACE

3.1. Introduction

This chapter is designed to provide a comprehensive discussion of RO membrane technology performance expectations in various environments and operating conditions. There will be a special emphasis on membrane surface morphology and its relation to flux and salt rejection. The chapter will be divided into two main sections, namely:

1) The effect of operating parameters and system design on RO membrane performance, and
2) The effect of membrane physical properties on RO membrane performance.

3.2. The effects of operating parameters on RO membrane performance

Based on publications from manufacturers [31], it might be perceived that each membrane has a characteristic performance (that is, flux and separation) for each solute independent of operating conditions. However, the actual performance of the membrane can be strongly dependent on the operating conditions. In this section all the relevant literature relating to the effect of feed water 1) pressure, 2) temperature 3) pH, 4) flow, and 5) conductivity on RO membrane performance will be discussed.

3.2.1 Effect of feedwater pressure

Generally, increasing feedwater pressure increases water flux [1,3,32-35]. In terms of salt rejection, all publications have reported that increasing pressure will result in higher permeate quality. In the literature there are two possible causes for higher permeate quality: 1) Porteous *et al* [6] and Sablani *et al* [33] reported that salt rejection across a membrane is not affected by pressure; increased water flow with pressure dilutes the salt passing through the membrane, which results in lower permeate salt concentration and 2) Parekh [1] reported

that based on calculated salt rejection performance by Kimura-sourirjan analysis for several cellulose acetate membranes it was found that salt rejection increases rapidly with operating pressure and then levels off to a constant value. Unfortunately, Parekh did not report what determines the plateau values. The primary effect of increasing feed water pressure is to increase the driving force for the solvent (water). Mattheus *et al* [32], showed that the permeate flux increases linearly with increasing pressure and at higher temperature the flux is more sensitive to pressure due to the reduced viscosity (Figure 3.1). The experiments were conducted in a pilot scale UF/RO unit (Model 25M 100AL, Hydranautics Inc., USA) containing spiral wound membrane. Feed pressure was varied from 10.9 to 55 bar (1090 to 5500 KPa) and feed flows were 9 and 18 l/min. The experiments were conducted with a NaCl-water solution of 0, 1, 2, 3, 4, and 5% w/v. The membrane material was not given in the paper.

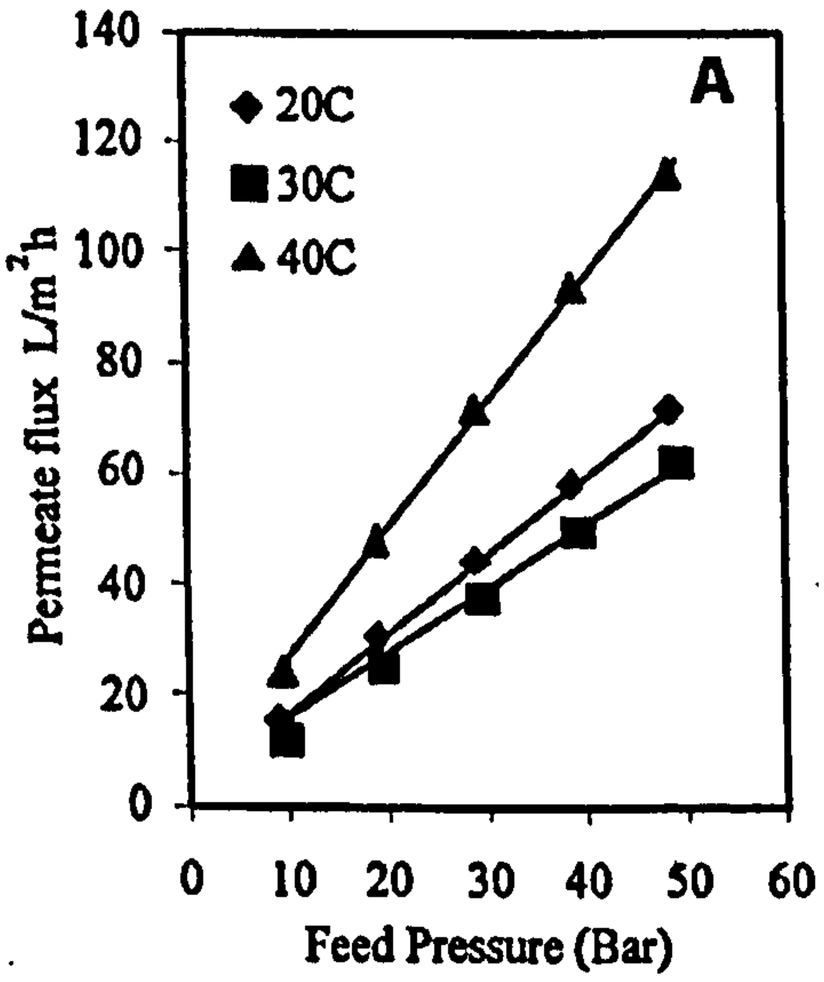

Figure 3.1. Effect of temperature and pressure on permeate flux [32]

As can be seen from Figure 3.1, increasing the pressure has a great effect on membrane productivity. Although increasing pressure leads to higher permeate production, optimization of feedwater pressure is required [36,37] because an increase in pressure results in an increase in membrane fouling as a result of cake compression in systems containing scaling ions such as calcium and magnesium [36]. Mohammadi *et al* [36] studied the influence of pressure on fouling and permeate flux using a FilmTech polyamide FT30 RO membrane flat sheet in an experimental cell. Experiments were carried out within a range of

8–17 bar pressure with river water (pH 6.5, Na^+ = 354, Ca^{2+} = 139, Cl^- = 538, and SO_4^{2-} = 489 ppm) used as the feed to the experimental cell. It was found that the optimum pressure is 13 bar at which the best production with low fouling rate is achieved. This conclusion is valid for FT30 RO membranes but cannot be generalized for other membranes, which have different water permeability and design pressure. However, the concept of balancing pressure and fouling is likely to be a generalized finding.

In some situations RO membranes can be operated in a fluctuating pressure regime. An interesting study was done by Al-Bastaki *et al* [38]. He operated RO spiral wound membranes in a cyclic mode to reduce the effect of concentration polarization. He operated the unit by fluctuating the operating pressure between 15 and 25 bar once every 5 minutes and managed to achieve a 6.5% increase in the permeate flow rate over that obtained from steady-state operation of 25 bar. The main cause for that improvement was reported as a reduction of the effect of concentration polarization.

3.2.2 Effect of feedwater pH

The feedwater pH has an effect on RO membrane performance [1,36,39,40,41]. However, the effect of pH can be ignored in some cases because manufacturers limit the operating pH. However, if the pH is too high or low then the solute can be ionized. One example of this is the case of phenol solute with cellulose acetate membranes. At lower pH (up to pH 8) the phenol is completely undissociated and separation is about zero. However, as pH increases phenol dissociates and separation increases until at pH 12 the phenol is totally dissociated and the separation reaches about 100% [1]. The pH also plays a very important role in the process of removing toxic compounds from water [41,42]. In treating water contaminated with arsenic, elevating feedwater pH is one of the approaches for greater removal [42] because it tends to be ionized in water at neutral pH (7-8) that makes separation low. Studies on the effect of pH on flux are not commonly found in the literature. Mohammadi *et al* [36] studied the influence of pH on permeate flux using FilmTech polyamide FT30 RO membrane flat sheet in an experimental cell. Experiments were carried out within a range of pH 3-9.6 (refer to section 3.1.1 for experiment conditions). It was found that the minimum flux was achieved at pH 6 because at that pH the electrostatic forces between solute and between

solute and membrane surface are attractive. The permeate flux was between 22, at pH 6 and 27 l/m^2.h, at pH 9.5 (see Figure 3.2).

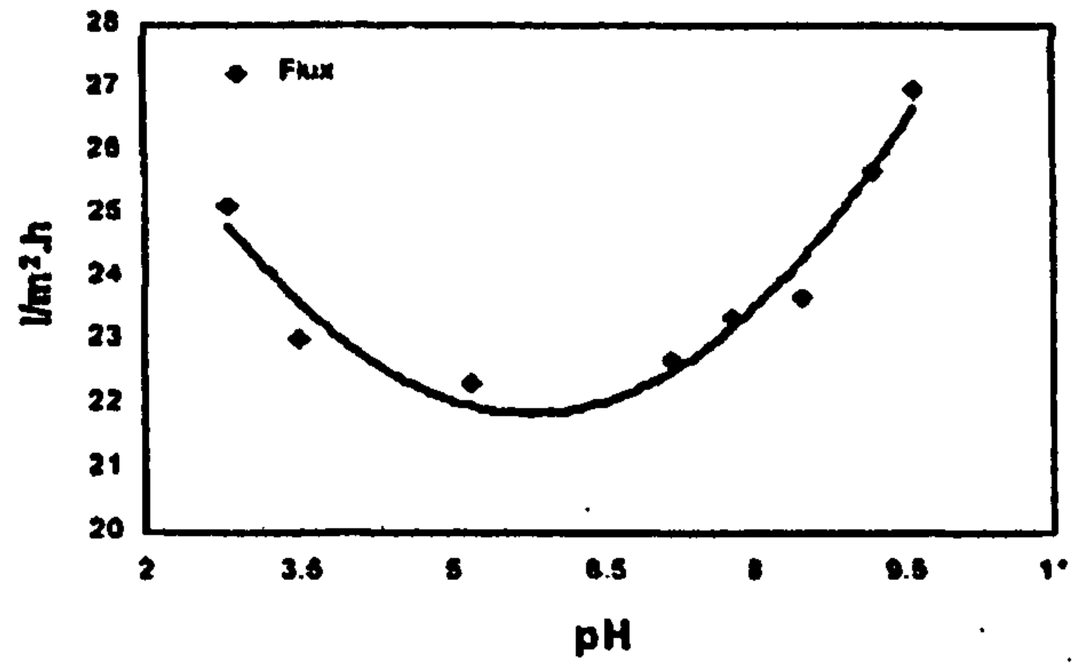

Figure 3.2. Effect of pH on Permeate flux [36]

The pH becomes an important factor in controlling fouling in feedwater contaminated with silica [43-46]. Silica is commonly present in seawater and brackish water. Silica fouling is a serious problem because it is a very hard and tenacious scale once it is formed. At pH 8 the silica solubility is 120-150 ppm at 25 °C and increasing pH to 11 increases silica solubility to 1500 ppm. For best silica separation the operating pH range should be below 6.5, which precludes silica polymerization as well as precipitation of silicates.

3.2.3 Effect of feedwater temperature

Temperature changes can affect both flux and salt rejection [6,7,32,36]. Temperature affects water viscosity and a rule of thumb is that membrane capacity increases about 3 percent per degree Celsius increase in water temperature [7]. Mattheus [44] found that polymeric membranes are very sensitive to feedwater temperature. There was up to 60% increase in permeate flux when the feedwater temperature was increased from 20 to 40 °C. The relationship between viscosity and membrane flux was not reported. Experiments details are given in section 3.1.1. It was noticed that the permeate flux goes through a minimum at an intermediate temperature. Explanation for the cause of this phenomenon was not reported. There was up to a 100% difference in the permeate flux between feed temperatures of 30 and 40°C. At 30 °C, the permeate was 12.4 l/m^{2}h and at 40 °C it was 24.1 l/m^{2}h at 9.5 bar pressure and 0% NaCl (feed flow was not mentioned). At 20 °C, the permeate was 15.4

l/m^{2}h at the same operating conditions. The flux change could possibly be due to changes in the physical properties of the polymeric membrane such as pore size.

Temperature optimization is required in some situations to control fouling [47]. In the event of having high silica in feedwater an increase in temperature leads to silica polymerization and the temperature must be lowered to 25 °C to control formation of hard scale, although some researchers found that silica polymerization processes at the membrane surface are kinetically controlled [47].

3.2.4 Effect of feedwater salinity

Feed water salinity has a large effect on membrane performance, and the primary reason for this is the increase in osmotic pressure with increasing concentration polarization [1,32,48,49]. In experiments conducted by Mattheus [32] it was found that at 40 bar (4000 kPa) feedwater pressure, an increase of feedwater salinity from zero to 3% NaCl dropped permeate flux from 55 to 22 l/m^{2}h. Khan and Hamad [50] evaluated the performance of aromatic polyamide hollow fibre membranes at various dissolved solids feedwaters ranging from 20,000-53,000 ppm. The experiments were carried out using a membrane module system 9/200, designed by Horizon Reverse Osmosis Desalinators. The feedwater pressure and flow were maintained at 800 psig (5515 kPa) and 14 l/min respectively in all experiments. The tests were carried out at low (17-19 °C), room (24-26 °C), and high temperatures (33-35 °C). A heating coil and the addition of ice to the feedwater tank was used to control the temperature. It was found that increasing feedwater conductivity from 20,000-50,000 ppm has almost no effect on salt rejection (above 99% in all tests) but membrane percent recovery {(feed flow-product flow)/feed flow} drops with increasing feedwater dissolved solids. It was 53% at 20,000 ppm and 30% at 50,000 ppm for the same operating parameters.

3.2.5 Effect of feedwater flow

When feed rate is decreased the permeate flux decreases [1,32]. At a salt concentration of 2% w/v and 50 bar feedwater pressure, decreasing feed flow from 18 to 9 l/min at constant temperature resulted in a decreasing permeate flow from 18 to 16 l/m^{2}h [32]. Parekh [42]

showed that as feed flow increases the permeation rate increases and that is due to the increased mixing in the test system. In the experiments conducted by Mohammadi *et al* [36], it was found that as feedwater velocity increases permeate flux increases. However, they reported a limiting 0.7 m/s velocity is reached where the flux does not increase further, where the reason(s) for that was not reported. Experiments were carried out within a range of 0.1–0.97 m/s. Moreover, the permeate flux increase is minor. It was 25 $l/m^2.h$ (at 0.1 m/s) and 28 (at 0.7 m/s).

3.2.6 Summary

In summary, all operating parameters have an effect on the membrane performance but the degree can vary substantially from one parameter to another. It was found that pressure and temperature variation has a great effect on the membrane production rate. Feedwater flow and pH cause very minor effects on permeation rate. The feedwater pH influences the membrane ability in rejecting some species whereas feedwater conductivity does not. Increasing feedwater conductivity reduces permeation rate. Ho [3] summarizes the effect of each parameter in Figure 3.3. The pH effect on the membrane performance was not given. So it can be said from literature review that the effect of each operating parameters is generally as given by Ho in Figure 3.3 and the slope is likely to change for each type of membrane.

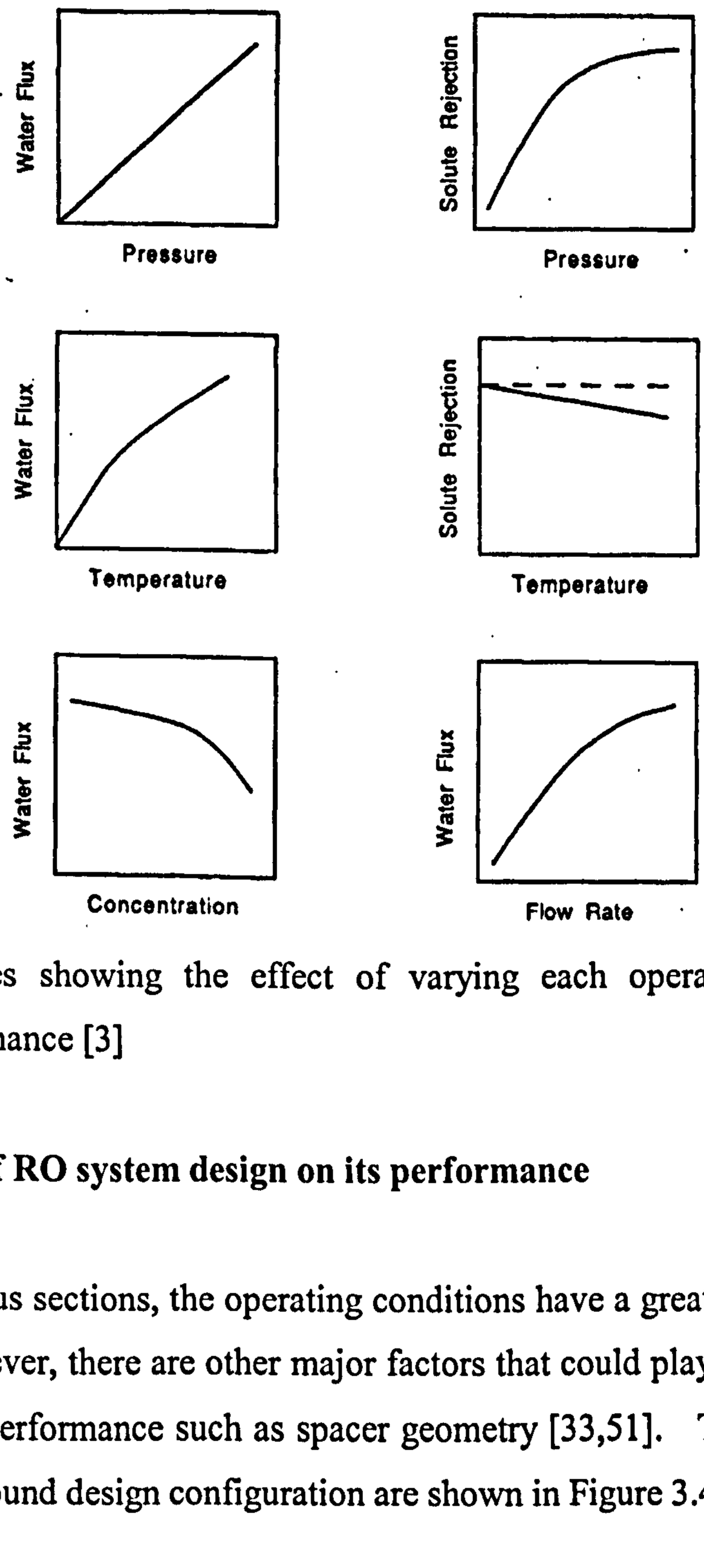

Figure 3.3. Curves showing the effect of varying each operating parameter on RO performance [3]

3.3 The effect of RO system design on its performance

As shown in previous sections, the operating conditions have a great influence on membrane performance. However, there are other major factors that could play an important role in the overall membrane performance such as spacer geometry [33,51]. The spacer geometry and location in spiral wound design configuration are shown in Figure 3.4.

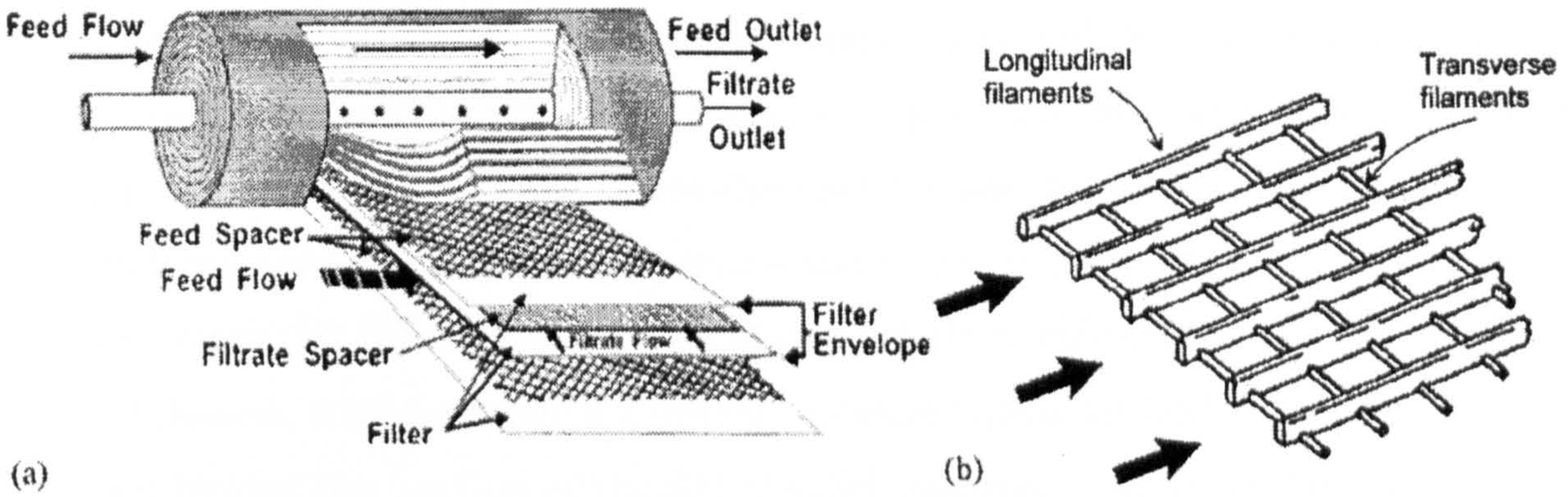

Figure 3.4. Schematic of a) spiral wound module and b) ladder-type spacer [51].

Sablani [33] observed that reducing the spacer thickness, in the spiral wound model design, from 0.1168 to 0.0508 cm decreases flux by up to 50%. The different geometry/configuration of the spacer influences turbulence at the membrane surface which, in turn, affects concentration polarization. In spiral wound types several flat membranes are sandwiched between plastic screen supports (known as spacers) and then rolled into a "swiss roll" around a central tube. The spacers come in different thicknesses and geometries. Sablani [33] tested three different spacer thicknesses: 0.0508, 0.0711, and 0.1168 cm. A pilot-scale UF/RO unit model 25M 100AL from Hydranautics Inc., USA was used in the study. The membrane material was not mentioned. Experiments were carried out at several feed pressures (between 9.5 and 52.5 bar). The temperature of the feed was maintained at 30 °C, feed flow was 9.0 l/min, and sodium chloride solutions were prepared at concentrations ranging from 0 to 5% w/v. The solution pH was not given in the paper. At maximum feed pressure (52.5 bar), for feed concentration of 0% NaCl, the fluxes were 63, 58, 29 l/m^{2}h for spacer thicknesses of 0.1168, 0.0711, and 0.0508 cm respectively. So, reducing the spacer thickness from 0.1168 to 0.0508 cm dropped permeation rate by 50% where it was expected that reducing spacer thickness increases turbulence and reduces concentration polarization. This indicates that spacer design geometry is important.

Over the last two decades, RO membrane permeability improved significantly as a result of developing enhanced membrane materials and surface modifications. However, the outcome was quite disappointing, the average permeate flux per long vessel was virtually unchanged

based on Liafa reaserch [52]. That is because the RO membrane cartridge is not designed to handle this increase in pure water production. Lianfa examined the mechanisms controlling the performance of a full-scale reverse osmosis (RO) process under various operating conditions. She demonstrated that thermodynamic equilibrium imposes a strong restriction on the performance of a full-scale RO process under certain circumstances. Thermodynamic restrictions mean that the osmotic pressure of concentrate significantly increases downstream in the RO channel, such that when the osmotic pressure equals the feed water pressure, water production beyond that portion of the RO channel vanishes. Lianfa did not carry out any laboratory experiments but her findings are based on theoretical calculations using mass transfer and thermodynamic analysis. Wilf [53] also reported that the low pressure and high rejection membranes at operating conditions of high temperature, high feed water salinity or high permeate recovery rate, conditions could create excessive permeate flux rate from the lead elements and negligible NDP (net driving pressure) at the end of the system. This is also based on mathematical calculations and no experiments were conducted. So based on the above it can be seen that flux enhancement is not a straight forward issue and many parameters should be considered. In the following section further discussion on membrane surface properties will be carried out to give the reader better understanding for RO membrane technology science.

3.4 The effect of RO membrane structure on its performance

The Atomic Force Microscope (AFM) and Scanning Electronic Microscope (SEM) provide excellent means to investigate and analyze the morphological structure of RO membranes. The structures of RO membranes require microscopic techniques to the level of micron and sub-micron resolution to enable the features to be resolved. In the literature there are several studies utilizing AFM [54-64] and or SEM [65-71] to characterize membrane structure. The application of AFM in characterizing RO membrane surface roughness is relatively new. Most papers have been published since 1995 although ultrafiltration and microfiltration membranes have been studied using AFM since 1992. In early research, AFM images were visually analyzed [72]. Today software is incorporated into AFM instruments to give more quantitative details of the membrane surface, such as its roughness, its peak and trough

distribution and other statistical analysis of the surface. AFM is found to be a useful tool for characterization of the membrane surface due to the ability of analyzing dry or wet samples without any pretreatment.

AFM can be operated on three modes: contact, non-contact, and tapping mode. Because membrane surfaces can be sensitive and can potentially be damaged by AFM tips many researchers have operated AFM in tapping mode [58,61,73-75] or non-contact mode [72,76,77,78]. However others have used contact mode operation and produced images without any damage to the membrane surface [18,54].

AFM has the advantages over SEM that the resolution is higher, and more importantly sample preparation is minimal and no electron beam damage can occur [58]. The use of SEM to characterize RO membranes has been found in the literature since 1976 [26]. Very good images have been produced for RO membranes during that time (see Figure 3.5)

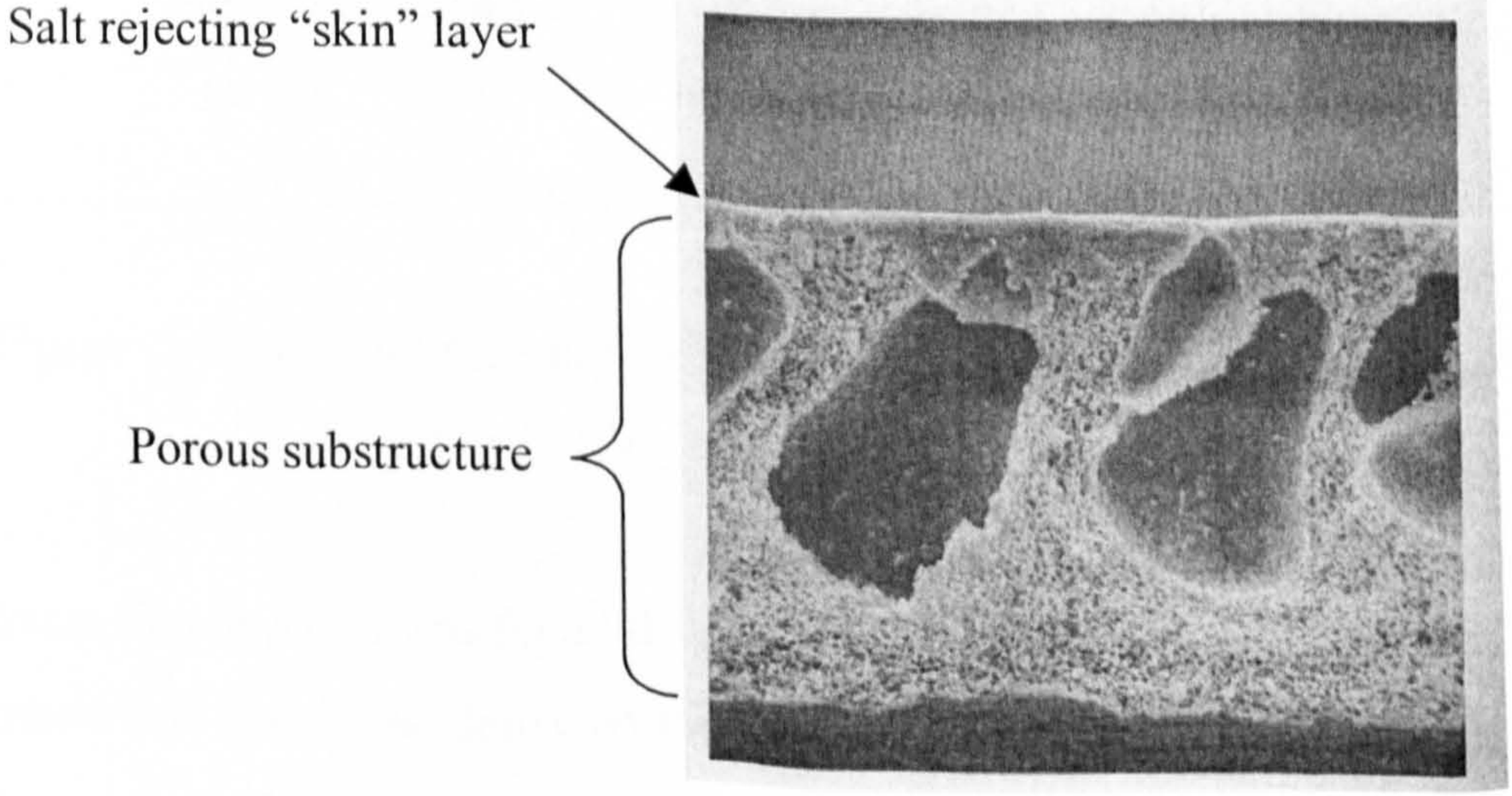

Figure 3.5. SEM image for cross-section of asymmetric cellulose acetate membrane containing microbubble irregularties [26]

AFM has been used in a number of studies to correlate membrane surface roughness with flux. In 1996, Hirose *et al* [54] suggested an approximately linear relationship between membrane surface roughness and flux for cross-linked aromatic polyamide RO membranes,

where permeability increased with increasing surface roughness (see Figure 3.6). Six membranes were tested in Hirose's investigation. All tests were conducted at 150 MN/m^2 (15 bar) using 1500 ppm NaCl solution (pH 6.5) at 25 degrees Celsius (°C) in a cross-flow cell.

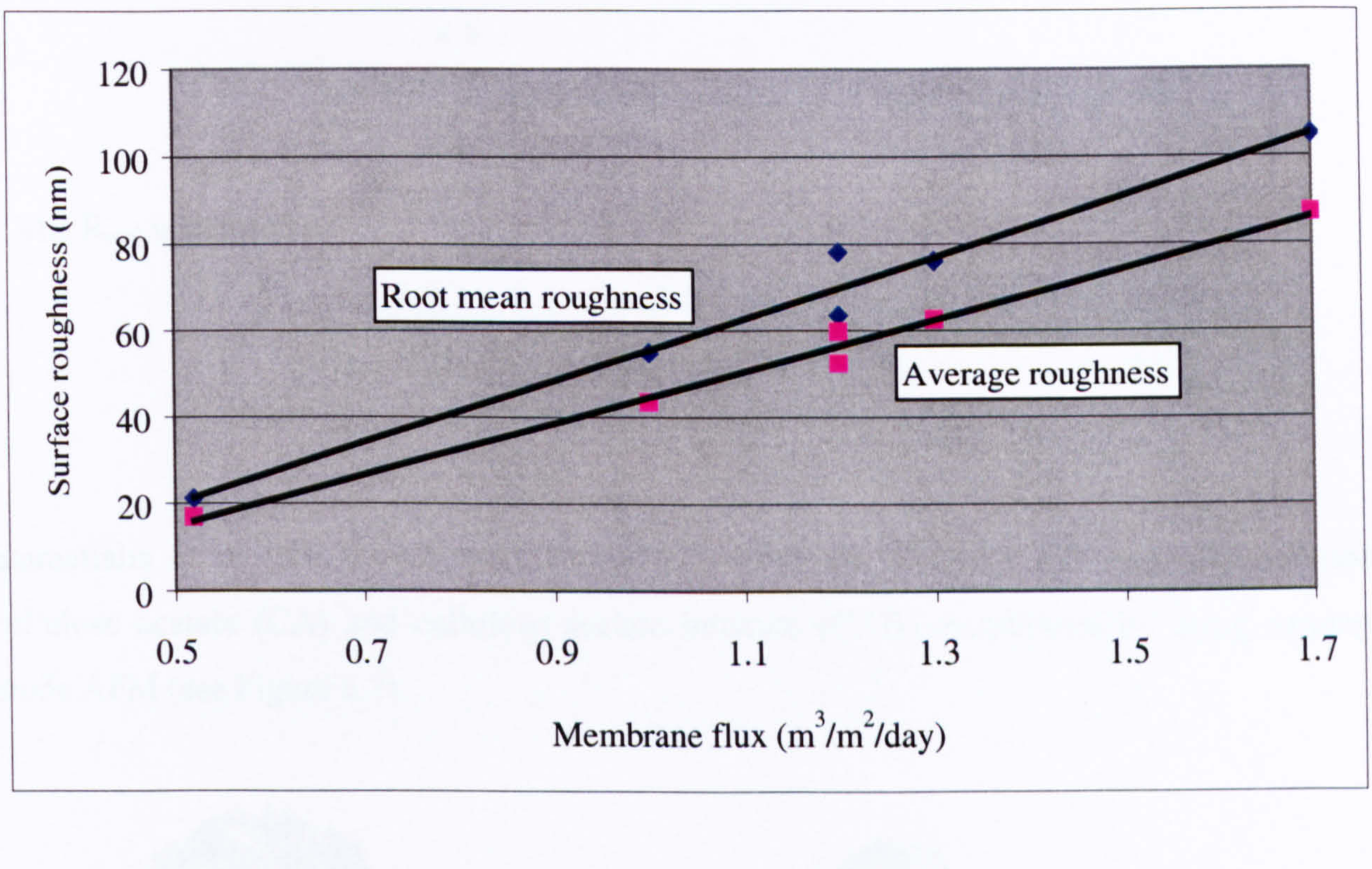

Figure 3.6. The relationship between surface roughness and flux for six membranes evaluated by in Hirose *et al* [54]

From Figure 3.6, it was found that the roughest membrane delivered the highest flux and the smoothest membrane delivered the lowest flux and a linear relationship was established. It was reported that the rougher the membrane surface the higher the flux because the unevenness (roughness) resulted in enlargement of the effective surface area.

The R_a is the average plane roughness, R_{rms} is square mean plane roughness and they are calculated by a computer software incorporated in the AFM. The mathematical equation used to calculate each are presented in the following page.

$$R_{avg} = 1/S \int_0^a \int_0^b |f(x,y) - z_0| \, dxdy \quad \text{.....(1)}$$

Where S is the specified area, $f(x,y)$ is the height in the specified area, a and b are the length of two sides of the area, and z_0 is the mean height. z_0 is given by the following:

$$z_0 = 1/S \int_0^a \int_0^b f(x,y) \, dxdy \quad \text{.....(2)}$$

The R_{rms} is defined as

$$R_{rms} = [1/S \int_0^a \int_0^b \{f(x,y) - z_0\}^2 \, dxdy]^{1/2} \quad \text{.....(3)}$$

Stamatialis *et al* [58] investigated the surface structure of dense and integrally skinned cellulose acetate (CA) and cellulose acetate butyrate (CAB) membranes by using tapping mode AFM (see Figure 3.7).

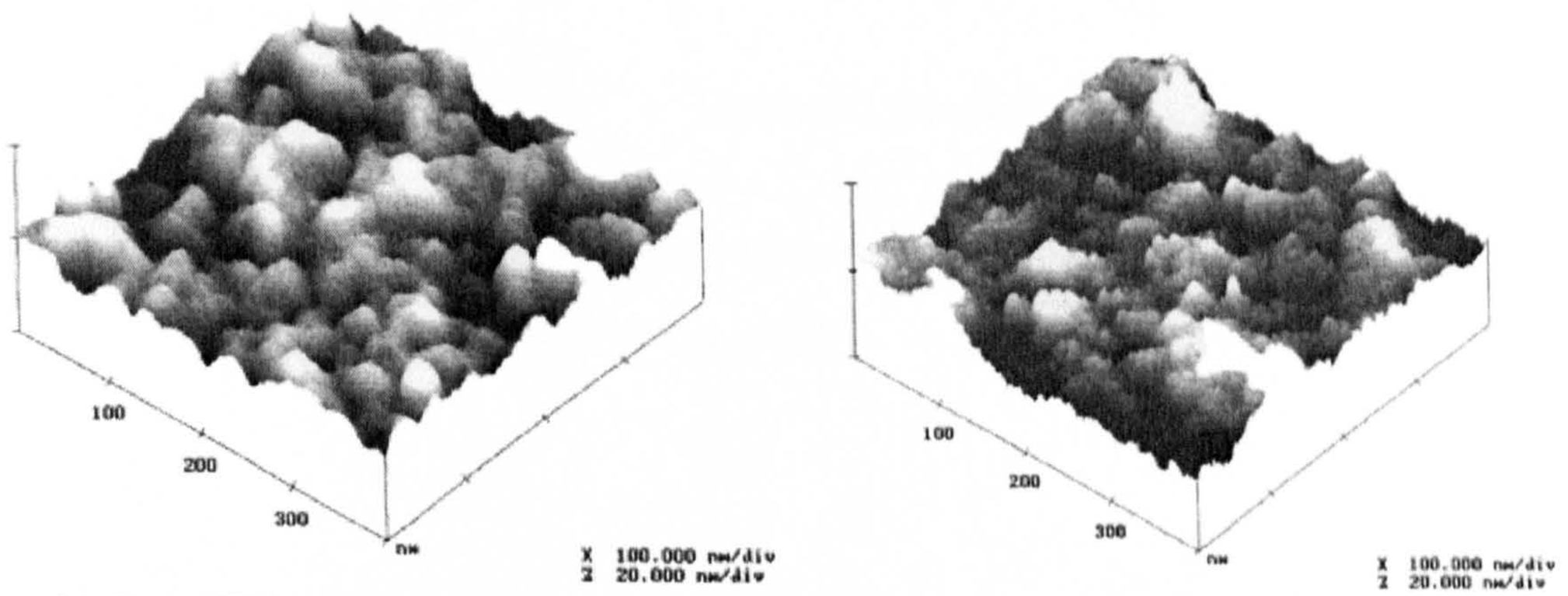

Figure 3.7. AFM images for CA (to left) and CAB active layer (to right) [58]

The membrane performance tests were carried out at 40 bar, 25 °C, and using 3500 ppm NaCl solution. Small pieces were cut from each membrane, glued onto metal disks and then scanned by AFM at 25 °C. All the membranes were fitted the same way before imaging. The tested membranes were asymmetric membranes prepared under different casting

conditions and showed a wide range of Nanofiltration/Reverse Osmosis permeation characteristics (NaCl rejection varied between 30 to 98.2%). It was observed that the surface morphology is associated with permeation properties; the lower values of roughness the lower the flux and the higher the rejection. However, the relationship was not linear. Figure 3.8/9 illustrate the relationship. Figure 3.8 shows the relationship between membrane surface roughness and flux and Figure 3.9 shows the relationship between membrane salt rejection and flux for 4 membranes.

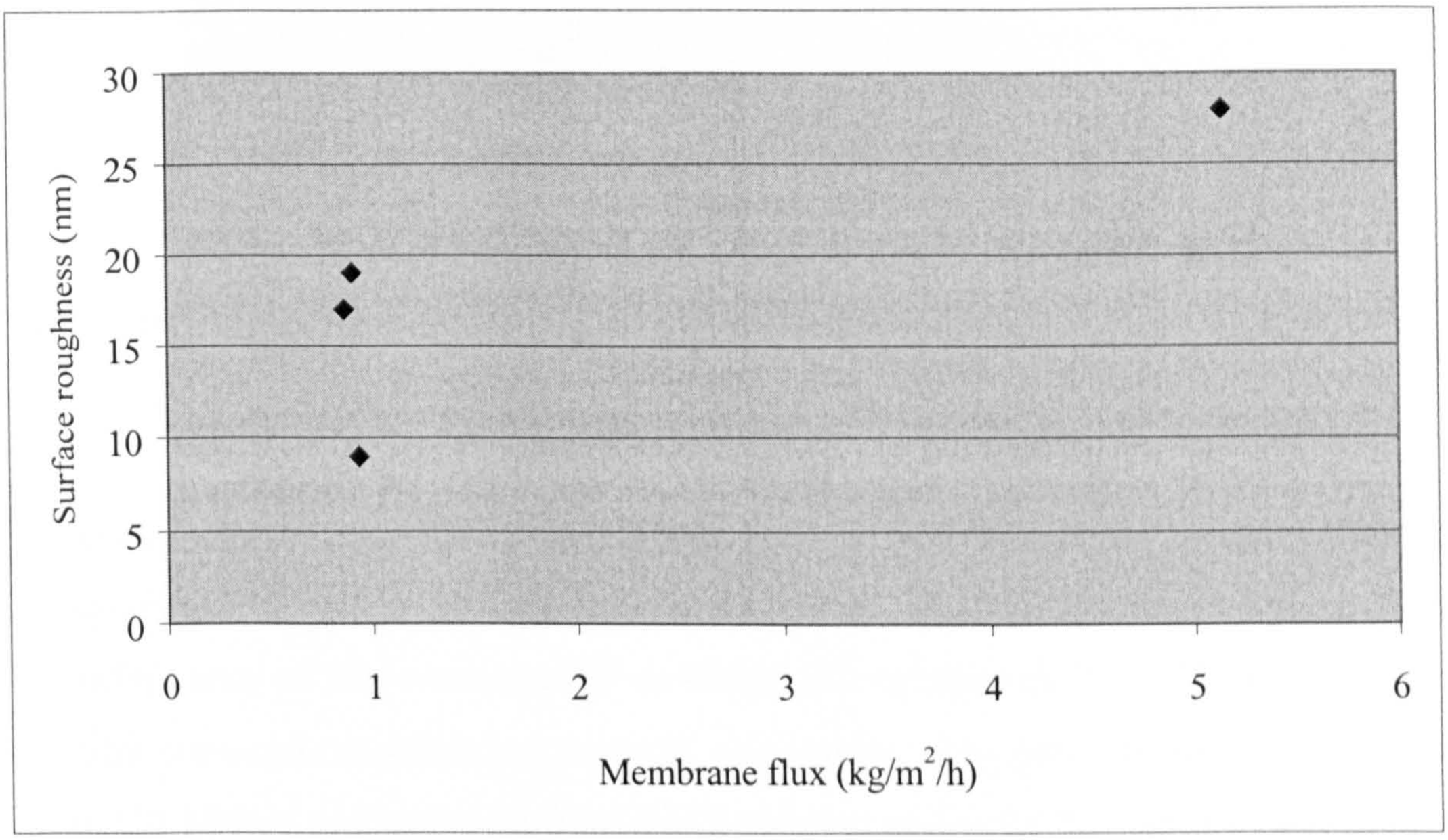

Figure 3.8. The relationship between membrane surface roughness and flux for 4 membranes evaluated by Stamatialis *et al* [58]

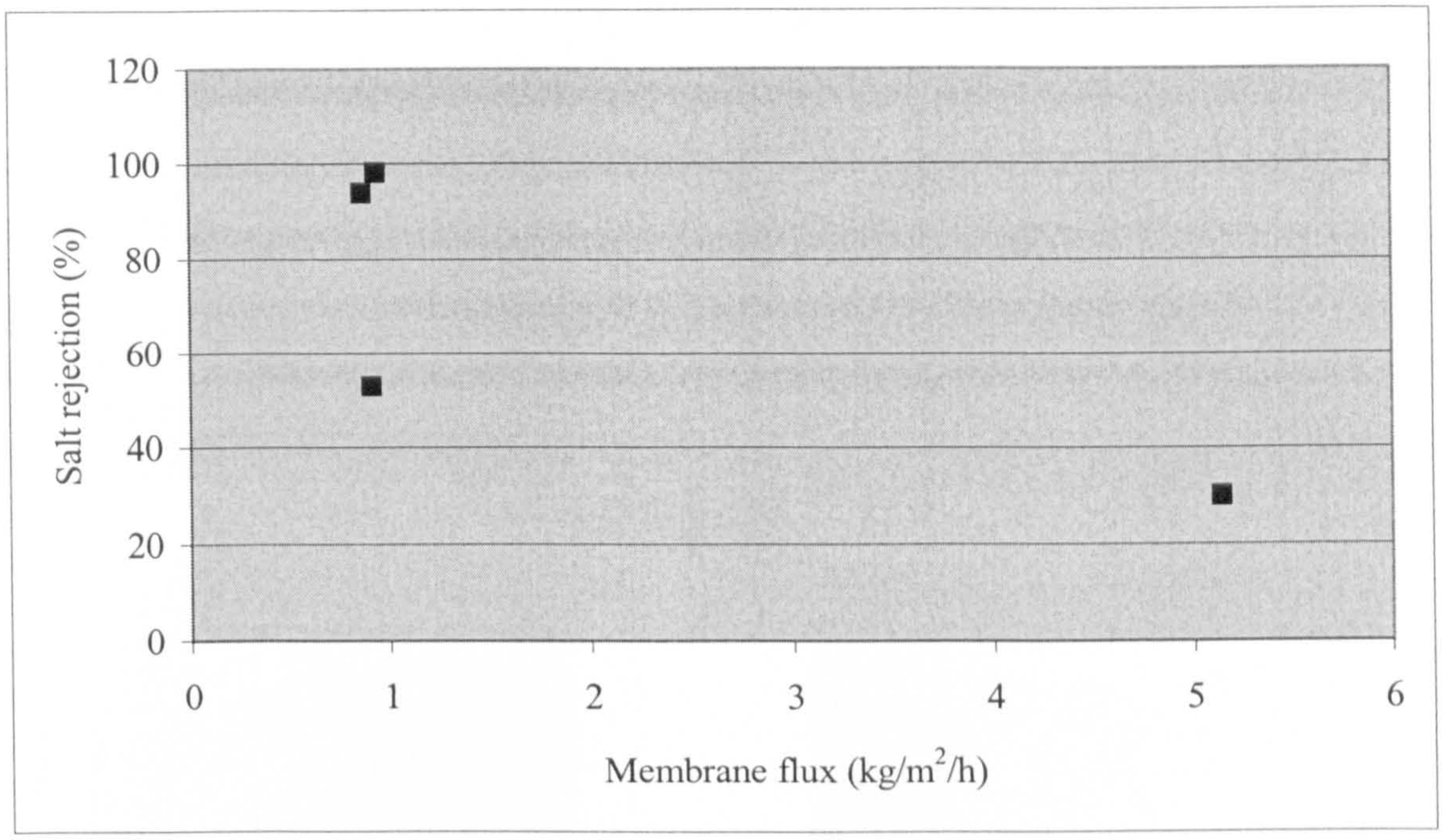

Figure 3.9. The relationship between membrane flux and salt rejection for 4 membranes evaluated by Stamatialis *et al* [58]

In one experiment, the AFM, the FE-SEM (Field Emission-Scanning Electron Microscope) and solid state H nuclear magnetic resonance (NMR) spectroscopy were employed to study the performance of four commercially available RO membranes [55]. The membranes were thin film composite membranes (aromatic polyamide). The performance tests were carried out at 150 MN/m^2 (15 bar) with 0.2% NaCl solution and at 25 °C. AFM imaging was done with the membranes dry in non-contact mode (see Figure 3.7).

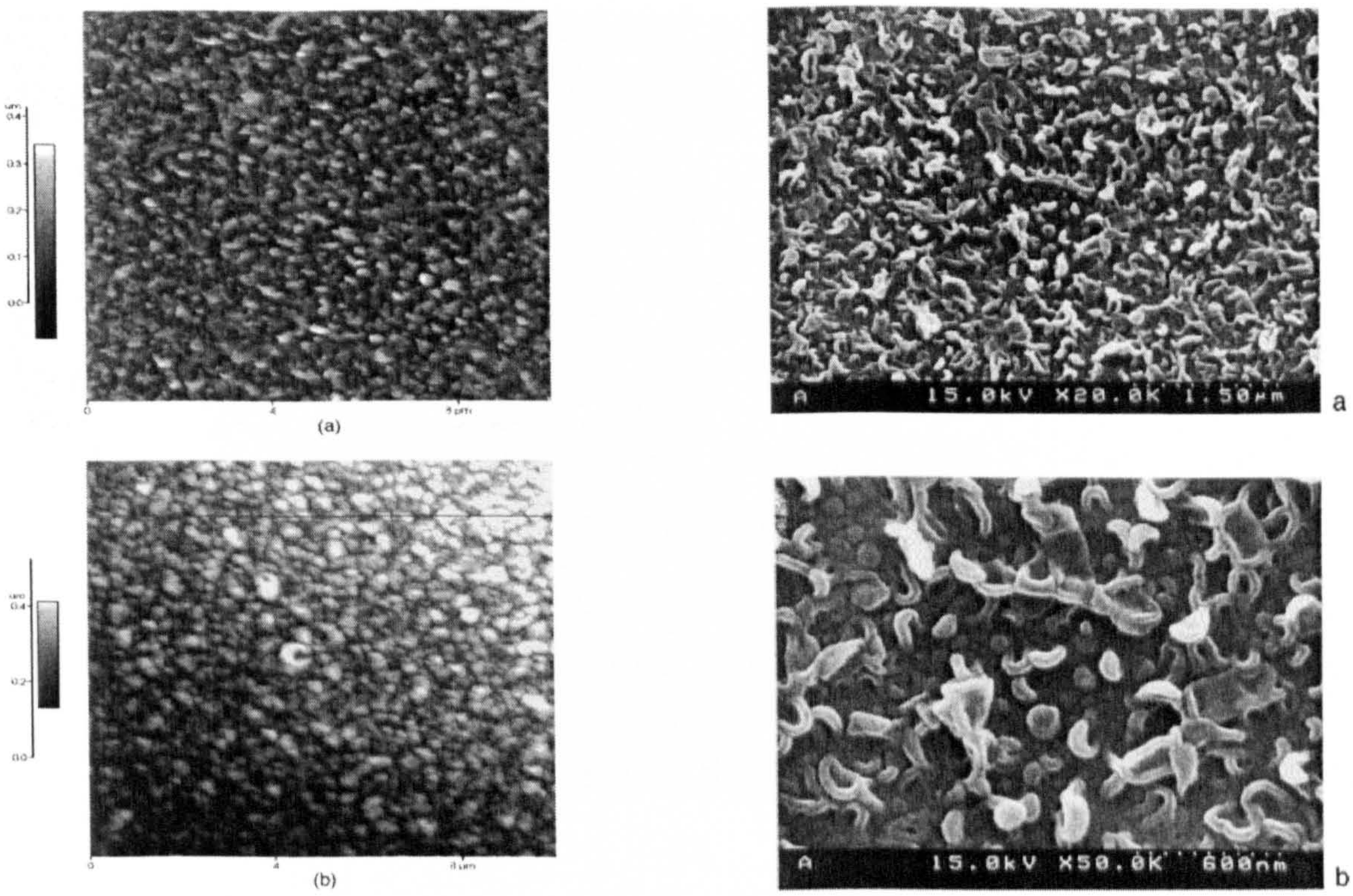

Figure 3.10. a) AFM surface images of two membranes and b) SEM images [55]

The membrane preparation procedure for AFM testing was not disclosed. It would appear that imaging (in contact mode) was done in dry conditions. It was reported that the membrane performance depends primarily on the nature of the thin film layer. The improvement in performance was correlated with the change in the inherent material property of the active layer, particularly in the wet state. The relaxation behavour and molecular motion of the wet thin film polymers were characterized by NMR and it was found that the local polyamide chain motion plays a crucial role in RO permeability. A linear relationship between membrane surface roughness and flux was not found. However, the roughest membrane did have the highest flux. Figure 3.11 illustrates the relationship.

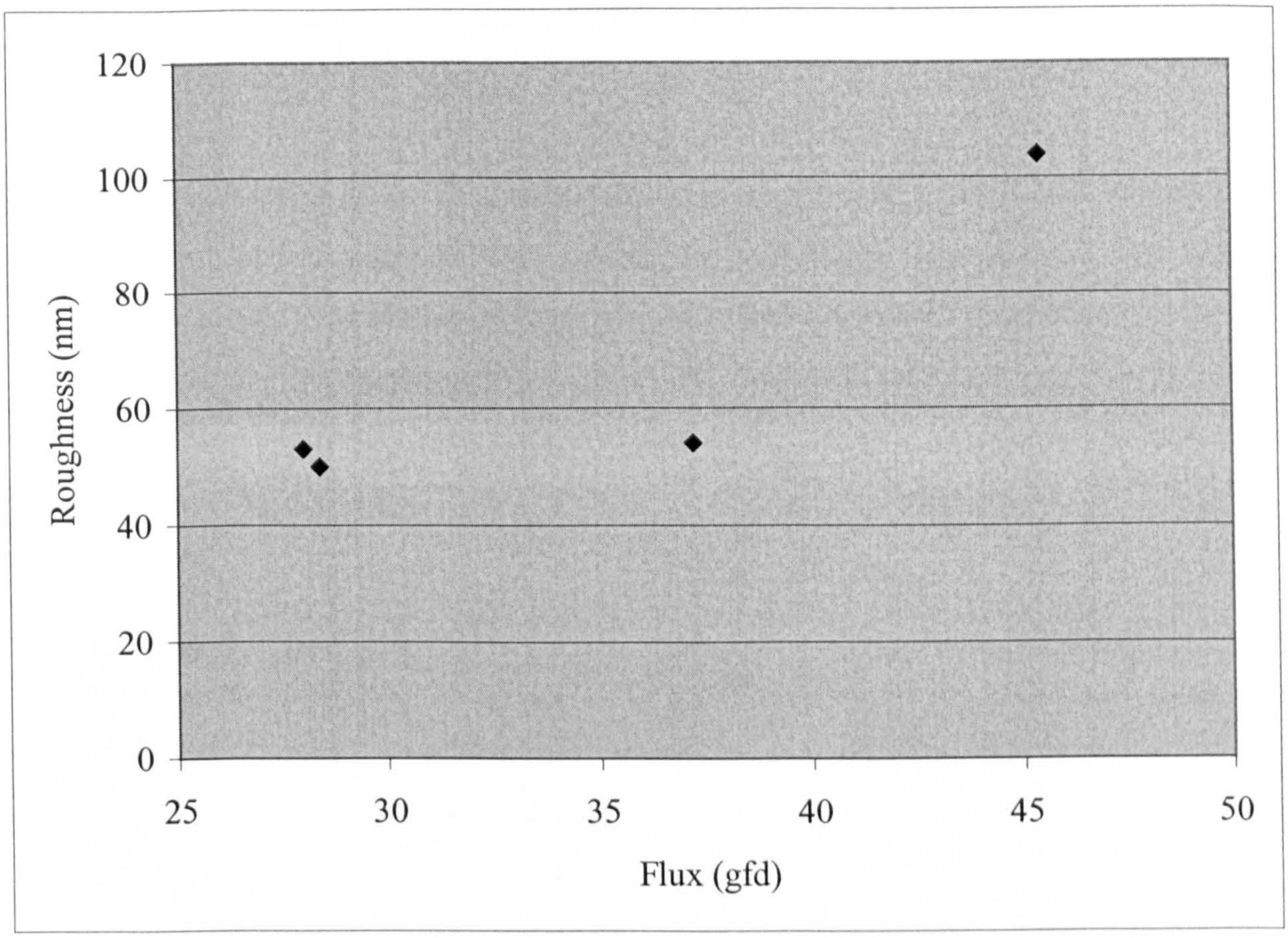

Figure 3.11. The relationship between membrane surface roughness and flux for 4 membranes evaluated by Kwak and Ihm [55]

In 2001, Madaeni [59] showed that the rougher the membrane the lower the permeation rate due to the adsorption and trapping of the ions on the rough surface membrane. His finding was based on evaluating two commercial RO membranes performance in tap water (exact details of the experiments were not available in the paper). However, above finding is based on only evaluating two membranes, which is believed to be difficult to prove.

The AFM has also been used to study membrane fouling. It was found that the increase in membrane surface roughness causes an increase in particle attachment. The colloid fouling of RO membranes is nearly perfectly correlated with membrane surface roughness. AFM images show that more particles are deposited on rough membranes than on smooth membranes. Particles preferentially accumulate in the "valleys" of rough membranes,

resulting in "valley clogging" which causes more severe flux decline than in smooth membranes [63,55,79,80,81].

SEM was used to examine the cross-sectional morphology of RO membranes by Ferjani *et al* [82]. Three series of membranes were studied: (a) membranes manufactured from Cellulose Acetate (CA) solutions as reference materials, (b) membranes cast from a blend of CA with 2 wt.% polymethylhydrosiloxane (PMHS) as bulk modified materials, (c) CA membranes coated by a thin PMHS film as surface modified materials. All membrane thicknesses were 90-110 μm (see Figure 3.12).

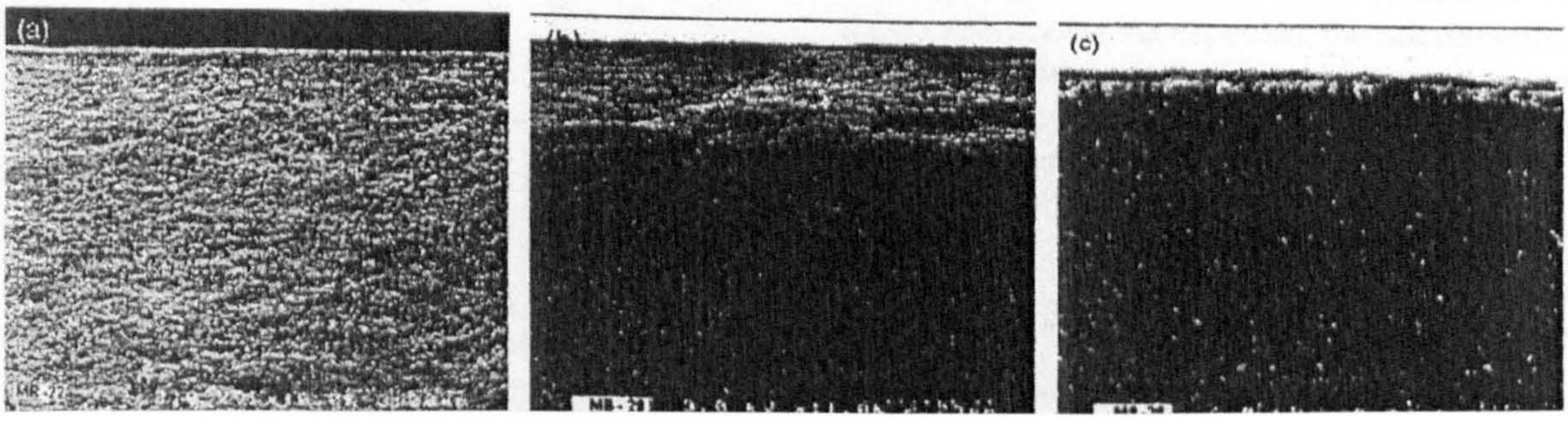

Figure 3.12. Cross-sectional view for tested membranes, a) CA membrane, b) CA-PMHS blend, and c) CA membrane coated with a thin film of PMHS [82]

The membranes were characterized in terms of permeation rate and solute separation using NaCl solution (2000 ppm). Experiments were carried out using a conventional frontal cell with an effective membrane area of 38.5 cm^2 at an operating pressure of 15 bar and at room temperature. The feed flow and pH were not given in the paper. Modification by PMHS both in bulk and onto the surface enhanced the salt rejection and reduced the transmembrane flux compared to the corresponding reference membrane. It is believed that the more dense top layer is responsible of higher salt rejection and lower permeation rate. It is generally assumed by many researchers that the porous support layer affords a negligible resistance to transmembrane flux. However, Ferani *et al* [82] found that more open substructure (based on visual evaluation) leads to easier penetration of water through it thus resulting in higher flux.

3.4.1 Summary

Based on the review of the literature a universal relationship between surface roughness and RO membrane flux is not presented in work carried out to date. More work in this area needs to be done to understand the relationship between surface roughness and membrane performance. Contradictory findings are reported; higher RO membrane surface roughness can mean higher flux, lower flux or have no effect on flux. Moreover, the application of SEM in the area of understanding the main parameters that control membrane flux is very limited. From surveying the literature relating to AFM imaging of polymeric membranes no conclusive findings to confirm the best AFM operation mode for scanning membranes surfaces are approved.

CHAPTER 4

LITERATURE REVIEW FOR THE APPLICATION OF MEMBRANE TECHNOLOGY IN THE TREATMENT OF OILY WATER

4.1 Introduction:

Membrane processes have received considerable attention for the separation of toxic material from wastewater mainly to protect the environment and human health. Most industrial plants use oil in their processes, which eventually ends up in wastewater steams. Membrane technology has been used over recent years and has proved its ability in purifying wastewater steams. In some circumstances the product water from membrane processes is recycled as a process water to reduce water consumption especially in arid areas. In this chapter, the application of membrane technology in the treatment of industrial wastewater contaminated mainly with oil, lubricants, and heavy crude oil to recycle or meet environmental regulations before discharge to sewer will be presented. It will deal with the applications of the following membrane technologies:

1. Microfiltration (MF) membranes,
2. Ultrafiltration (UF) membranes,
3. Nanofiltration (NF) membranes, and
4. Reverse Osmosis (RO) membrane.

Because the research presented in this thesis is based in evaluating the performance of RO membranes in oily wastewater, a thorough literature review will be carry out for RO membrane technology. A very brief overview will be given for the performance of MF, UF, and NF membranes in oily wastewater treatment to give the reader an overall picture of this area of research.

4.2 Microfiltration membranes in oil/waste water treatment

MF membrane technology is a process used to separate micron-sized particles (0.02 – 10 μm) from fluids and uses relatively low pressure to drive fluid through the filter. There are principally two types of MF membrane materials: polymeric and ceramic membranes [3]. Several studies have been conducted to investigate the performance of polymeric membranes [83-85,86], ceramic membranes [87,88, 89] and to compare the performance of both materials [90, 91] in various environments. The effects of crossflow velocity, feed pressure, and membrane pore size, or membrane surface properties on MF membranes performance are the main issues in this area of research [83,90].

Cross flow velocity plays an important role in microfiltration process. As cross flow velocity increases membrane permeation rate increases and also organic rejection increases [83,88]. However, that cannot be generalized in some circumstance the cross flow velocity could have no effect on the membrane performance characteristics. This depends on the type of treated wastewater. Microfiltration tends to be relatively insensible to cross flow velocity in the treatment of contaminated water with heavy crude oil [91].

Microfiltration membrane pore size plays an important role in oil rejection; the smaller the pore size the higher the rejection [92]. It is found that membranes with larger pores are more permeable but that leads to more deposition on the surface of the rejected oil. Moreover, any increase in feedwater pressure leads to an increase in flux but microfiltration process was found to suffer from fouling in the treatment of oily contaminated water. In most circumstances they undergo significant fouling which could be internal or external fouling [88,89,91]. The internal fouling is irreversible fouling in which foulants are trapped within the membrane structure and cannot be removed by chemical cleaning. External fouling is reversible fouling and foulants can be removed by basic chemical cleaning. The addition of suspended solids increases usually membrane flux because suspended solids adsorb oil.

Upon comparing the behavior of the polymeric membranes with ceramic membranes, it is found that polymer membranes are sensitive to both polar and chlorinated solvents, which

limits their application. The ceramic membranes have higher thermal and chemical stability, pressure resistance, and hence tend to have long life times [88,89]. In summary, MF membranes offer effective processes for oil separation from water but they are prone to internal and external fouling in some conditions.

4.3 Ultrafiltration membranes in oil/waste water treatment

Ultrafiltration membranes typically have pore sizes in the range from 1-100 nm and are capable of retaining species in the molecular weight range of 300-500,000 [15]. Interestingly some researchers have referred to 0.5 μm pore size membranes as an ultrafiltration [93] and others considered 0.1 μm pore size membranes as MF membranes [90]. There is therefore overlap between the MF and UF membrane classification in pore size but typically below 0.08 μm pore size is regarded to be ultrafiltration [2,24].

Ultrafiltration is used in treating effluent from the metal working industries [94, 95, 96], water contaminated with heavy oil [97], refinery and petrochemical effluents [98-104] and emulsified oil-water streams [105-108]. Most investigations have been carried out to study flux decline [98,101,105], and the optimum operating conditions [93]. The application of ceramic membranes is not limited to MF membranes but also a number of studies have evaluated the performance of ceramic UF membranes [93,97,109,110], and some have compared ceramic membranes with polymeric membranes in treating oily water [111]. Ceramic ultrafilters have been developed in industry for 20 years and widely used in oily wastewater treatment because they offer chemical, thermal, and pressure resistance to a wide variety of feed conditions [93,112].

Srijaroonrat *et al* [93] studied ceramic membranes for the treatment of oily wastewater. The tested membranes are asymmetric ceramic made of zirconium and capable of withstanding the full pH range 0-14, temperatures from 0-1000 °C and pressure of at least 100 bar. They investigated the optimum operating conditions (forward and reverse backflushing time, pressure, velocity and feed concentration) to obtain the best permeate flux. Backflushing is a method for improving the performance in crossflow ultrafiltration by reducing the

concentration polarization and fouling effect on the membrane surface. Backflushing can be attempted with air, water or permeate. In the backflushing cycle, the permeate flow is applied through the membrane in the reverse direction to the filtration for a few seconds once in every several minutes or longer, and leads to the removal of the deposited gel layer. Moreover, the compaction of the gel layer under high pressure, which causes membrane fouling, is also prevented. The backflushing process for crossflow filtration is shown in Figure 4.1.

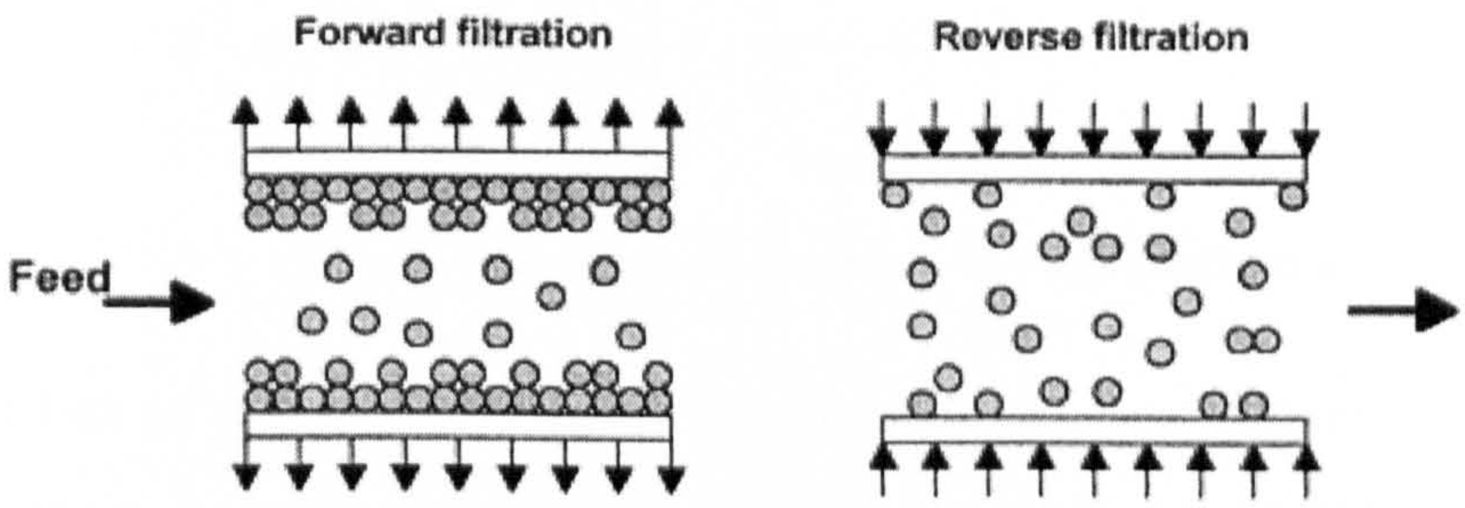

Figure 4.1. Schematic representation of backflushing technique [93]

The influent feed emulsion of kerosene in water was applied at a concentration of 1000 mg/l. The average diameter of emulsion droplets was 11 μm. The optimum forward filtration and reverse filtration time were found to be 60 s and 0.7 s. Applied pressure, crossflow velocity and feed concentration also have an important influence on the flux. The higher the crossflow velocity the higher the flux but transpressure behaves differently. Experiments were performed at pressures of 1, 2, 3 and 4 bar. The effect of operating pressure on permeate flux is shown in Figure 4.2.

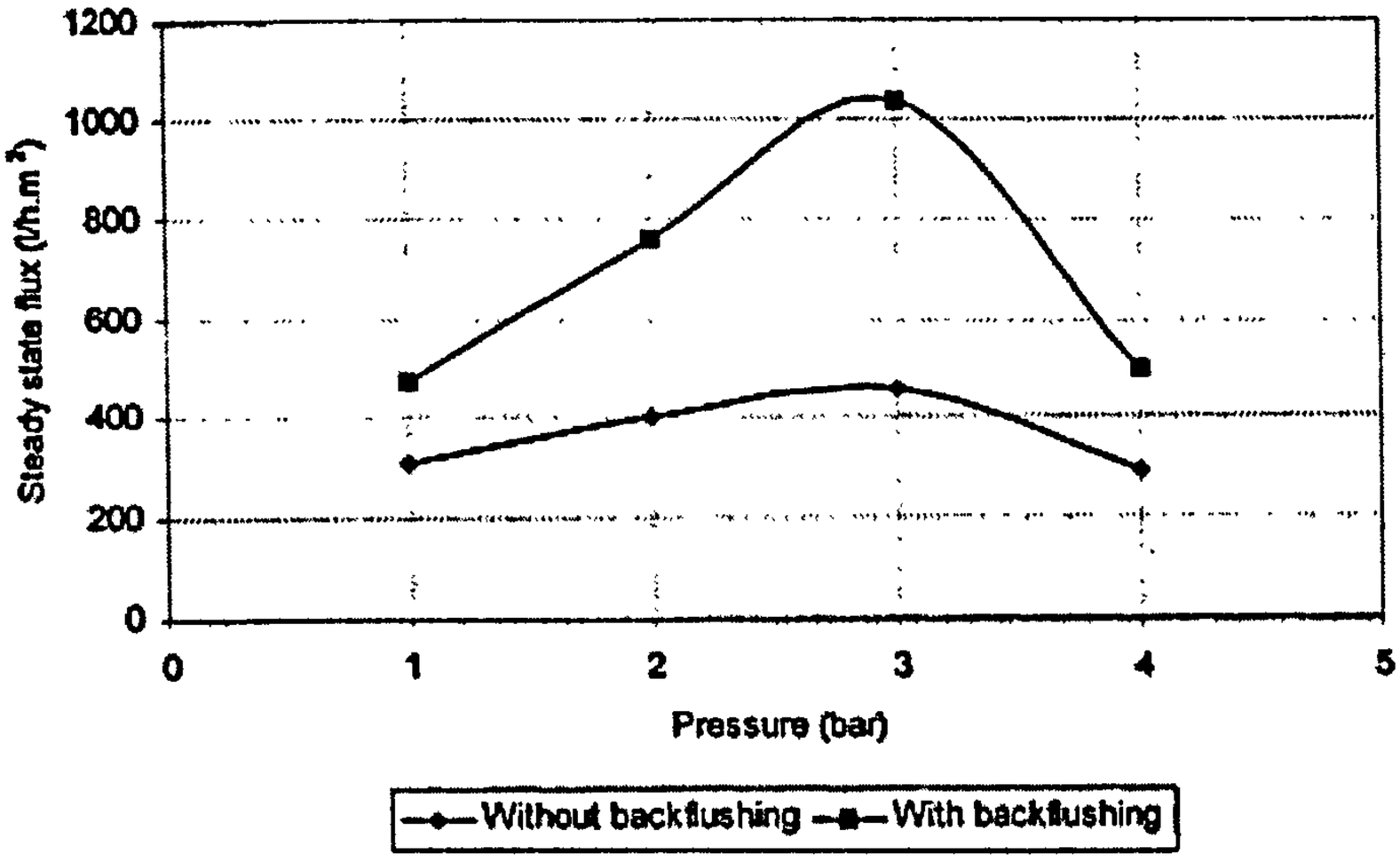

Figure 4.2. Effect of pressure on flux in the absence and presence of backflushing, crossflow velocity v=0.94 m/s and emulsion concentration =1 g/l [93]

It was observed that there was no oil phase contamination of the permeate and the concentration of hydrocarbon was found to be negligible at all operating pressures.

It was also found that flux increases with pressure up to the threshold region at 3 bar. Above 3 bar, the flux was found to decrease. Also with backflushing, the flux is much higher. At higher driving pressure, oil can easily pass and deposit in the membrane pores thus decreasing membrane pore sizes and increasing membrane fouling For the effect of feedwater oil contamination, it is found that the higher the influent concentration, the greater the flux reduction because it leads to a higher oil–gel layer build-up on the membrane surface as filtration proceeds. Actually many researchers have observed severe fouling in ultrafiltration membranes in oily water treatment [80,87,88,91] but the fouling can be controlled by good backflushing or injection of a coagulant agent in feed water [81-84,89].

In some experiments, the performance of ceramic tubular membranes and polysulphone hollow fibre membranes in treating crude soybean oil were compared. The influence of temperature and transmembrane pressure on the crude soybean oil permeate flux were evaluated. Temperature and pressure values are 50, 60 and 70°C, 3.0, 4.5 and 6.0 bar, for the

ceramic membrane and 50, 60 and 70°C, 0.7 and 1.4 bar, for the polysulphone membrane It was found that the flux was lower for the ceramic membrane than polysulphone membrane Permeate flux in the ceramic membrane increased with pressure but was not effected by temperature change. However, the polysulphone membrane flux increased with temperature and pressure. The ceramic membrane rejection for soaps is 97% (36 ppm in permeate) whereas polysulphone membrane rejection is 85% (269 ppm in permeate). It is understood that ceramic membrane filters are not sensitive to temperature which explains their stable performance over a wide range of temperatures but unfortunately the author did not report the reason for the superiority of ceramic filter on polysulphone in rejecting oil. The only information reported is that polysulphone membrane pore size is 100 KDalton (Dalton refers to molecular weight) and the ceramic membrane is 0.01 μm. Unfortunately, it was not possible to compare both membranes in terms of porosity because the author identified polysulphone membrane by its ability to reject molecules with molecular weight of above 100,000 whereas ceramic filter pore size was given. Moreover, reporting that the ceramic filter permeate is lower than polysulphone is questionable since the experiments were conducted at different pressures [111].

Polyetherimide (PEI) was used as the membrane material and polybenzimidazole (PBI) and poly ethylene glycol (PEG 600) as the additives, to investigate the asymmetric hollow fibre membranes prepared from wet-spun 25 wt% solids of 20:5:75 (wt ratio) PEI/PEG 600/DMAc and 19:1:5:75 PEI/PBI/PEG 600/DMAc solutions for oil-surfactant-water separation. DMAc is *N,N*-dimethyl-acetamide. It was found that for oil-surfactant-water emulsion systems (1600 ppm surfactant of sodium dodecylbenzenesulfonate and 2500 ppm oil of n-decane), the rejection rates for surfactant, total organic carbon and oil were 51.4-79.1%, 83.1-92.7% and more than 99%, respectively [113]. It was found that PEG existed in hollow fibre membranes and increased the hydrophilicity of membranes and that is the reason for high performance and that was found by other researchers [96, 93] too. With hydrophobic membranes, flux was found to be lower than with hydrophilic membranes, indicating that oil is easily wetted on the hydrophobic membrane surface and induced more fouling of the membrane. Hydrophilic membranes are more fouling resistant [102,114,115].

In summary, ultrafiltration is an effective process for treating oily water when using backflushing techniques or the addition of coagulants agents in the feedwater to control fouling and enhance performance. Without these, severe and rapid fouling is usually observed.

4.4 Nanofiltration membranes in oil/waste water treatment

Nanofiltration (NF) membrane technology is considered as a new process. Nanofiltration membranes are called low desalinating RO membranes and possess intermediate properties between ultrafiltration and RO membranes [116,117]. The pore sizes are usually between 0.8 and 2 nm [2,24]. From the literature review, it appears that NF is not applied widely in the treatment of oily water. A number of researchers have reported that NF is severely fouled in the treatment of oily water [117–122]. However, Afonso *et al* [121] used a ceramic membrane in his experiments and reported that although the membrane undergoes severe fouling, it can be effectively cleaned through a basic acid wash cycle. Also Meier *et al* [119] showed that fouling can be controlled by non-chemical flushing procedure consisting of a combination of feed cross flow, air flushing and permeate back flushing.

The use of nanofiltration membranes for separating organic solvents (such as ethanol from hexane) is found in several studies [117,120, 123, 124]. White [124] has used NF polyamide membranes to separate six solutes dissolved in toluene. The six compounds range in molecular weight (MW) from 142 to 311 Da, contain branched and unbranched compounds, and have varying degrees of aromaticity. Results for permeation tests are shown in Table 4.1.

ID	Name	Feed (wt.%)	Permeate (wt.%)	Rejection (%)
Solvent	Toluene	88.05	95.51	
C10	*n*-Decane	1.99	1.12	44
C11	1-Methyl-naphthalene	2.02	2.00	1
C16	Hexadecane	2.02	0.43	79
C19	Pristane	1.92	0.10	95
C17	1-Phenyl-undecane	1.99	0.68	66
C22	Docosane	1.98	0.16	92

Table 4.1. Test conditions were temperature at 50 °C, pressure at 41.4 bar, and flux = 35.58 $l/m^2/h$

The membrane performance in concentrated toluene is good and White expects practical applications of NF membranes to large-scale refining and chemical separations to be demonstrated in the near future.

In summary, research in evaluating the performance of NF membranes in oily wastewater is very limited, presently because it is a new technology.

4.5 RO technology in oil separation industry

The application of RO technology in wastewater treatment has been reported since the 1970's [125,126,127]. Considerable attention was given to RO technology after the introduction of ultra low-pressure reverse osmosis (ULPRO) membranes in 1995 [3, 128]. That is because ULPRO offers high fluxes and solute separations and can operate over a wide range of temperatures and pH values. These membranes are comparable to conventional composite membranes in terms of salt rejection whilst requiring only 7 bar net driving pressure instead of 28 bar for older ones [10] because they have thinner ultra thin film layers in which pressure drop across them is much lower than conventional membranes. The RO membranes have been applied in removing oil pollutants [59,60], organics compounds [129], humic substances [131-133], vegetable oil [134], and pesticides [135] from water to recycle or meet environmental regulations before discharge to sewer. RO membranes also were used successfully in organic environments such as separation of linear hydrocarbons and carboxylic acids from ethanol and hexane solutions [136]. Many studies showed that RO technology is an effective technology to remove organic compounds from water but the key factors that directly affect the rejection of organics are not yet clear [129].

From a thorough literature review it is apparent that most studies are either studying the effect of operating conditions (pressure, pH, organic concentrations, organic molecular weight, etc) [137] or the effect of membrane properties (surface charge, pore size distribution, wettability etc) on RO membrane performance in treating oil-contaminated water. Therefore the role of: 1) organic molecular weight, 2) pressure and feedwater organic

concentrations and 3) membrane properties on the performance of RO membranes will be discussed in detail. Afterwards the application of RO membrane technology in wastewater recycling will be discussed.

4.5.1 The role of organic molecular weight

A commercial ULPRO membrane (ES20) manufactured by the Nitto Denko Company was used by Ozaki and Li to study the rejection of 19 low molecular weight organic compounds using laboratory scale experiments [129]. The tested membrane was aromatic polyamide with an active layer consisting of charged chemical groups (carboxyl groups and amine groups). The surface charge was analyzed quantitatively by measurement of the surface zeta potential using Laser-Doppler electrophoresis equipment. The membrane is negatively charged at pH above 5 as a result of the dissociation of the carboxyl group present in the skin layer. It is positively charged at low pH due to dissociation of the amine group in the skin layer. During the experiments the feedwater temperature, pressure, sodium chloride concentration, and flow were maintained at 25±2°C, 3 kg/cm^2, 500 mg/l, and 1.20 l/min respectively. The concentrations of each organic compound in the feedwater were not mentioned in this study. The rejection of the organic compounds was measured at different pH values of 3, 5, 7, and 9. It was found that the higher the molecular weight or the larger the molecular width, the higher the rejection. However, that is not always true for all organic compounds. For example, the molecular weight of the undissociated organic compounds with a benzene ring, and the molecular width of the undissociated organic compounds with a long chain, do not follow the general argument. It was found that the rejection of some organic compounds is almost constant in the pH range of 3–9 but for acetic acid and urea, which have the same molecular weight of 60, the rejection values are quite different (see Figure 4.3).

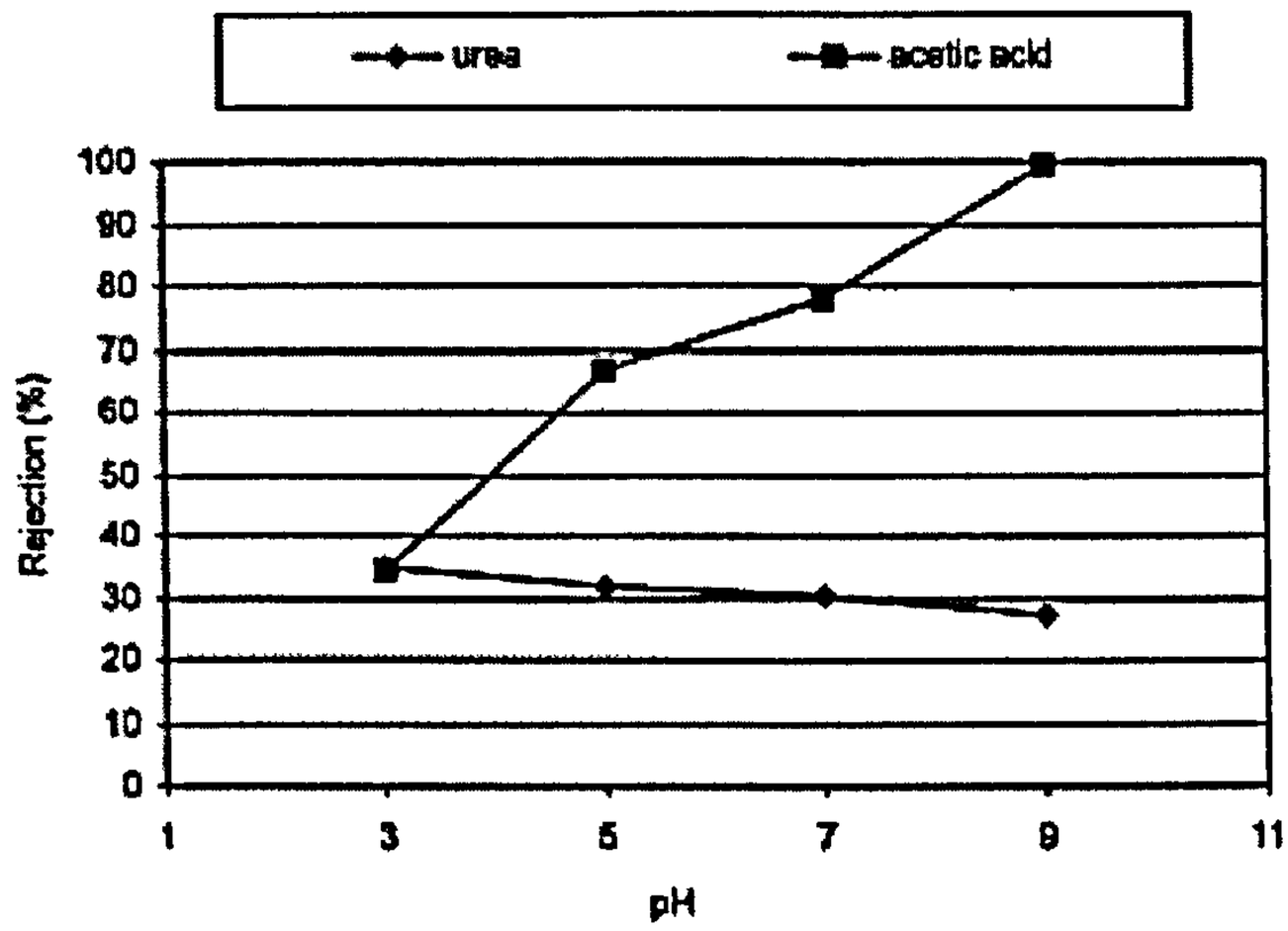

Figure 4.3. The effect of pH on rejection of urea and acetic acid [129]

When the pH is changed from 3 to 9, the rejection of acetic acid increased from 34.3 to 99.7%. The possible explanation is that the carboxyl group in membrane has anion characteristics under alkaline condition and the dissociation of acetic acid occurred with an increase in pH. This might cause an electrostatic repulsion between membrane and acetic acid.

The separation properties of crosslinked polyacrylic acid (PAA) composite membrane for aqueous solutions of organics, such as alcohols, amines, aldehydes, acids, ketones, and esters was evaluated. All tests were conducted at 5.0 MPa, 30°C and a feed flow rate of 800 ml/min. All membranes were tested with a single-solute solution. The concentration of organic solute in the feed solution was 1000±50 ppm. Each test solution was circulated over the membrane surface under test conditions for at least 3 h prior to collecting the permeate samples. It was found that the solute rejections increase with the increase of the molecular weights of alcohols, amines and aldehydes. The main factor is the increase of hydrophobicity of organics with the increase of molecular weights, which causes the decrease of distribution and permeability in the membrane, and therefore the increase in separation [138].

In one experiment, it was found that there is no correlation between the organic pollutant separation and the molecular weight, and it was reported that the RO membrane cannot be

thought of as a simple sieving process. FT30 membranes (thin film composite membrane type) manufactured by the FilmTec Corporation of Dow Chemical Company were used to study the separation of seven organic chemicals present in low concentration in wastewater (less than 100 ppm). The membranes were tested in a simple laboratory RO apparatus. The feedwater temperature, pressure, pH, sodium chloride concentration and flow were 25 °C, 17 and 34 bar, 6.8-7.0, 3500 ppm, and 350 ml/min respectively. Kunst calculated the pore size distribution of the membrane. The detail of the method was not given. The pore size distribution for FT30 was between 5.5 and 6.5 Å. It was found that the interaction between solute molecules, solvent and membrane material is an important parameter affecting membrane separation characteristic. A linear relationship (see Figure 4.4) was found between the separation data of the organic pollutants and their Taft number (a measure of the polar character of solute molecules) [139]. Taft numbers data are available in the literature.

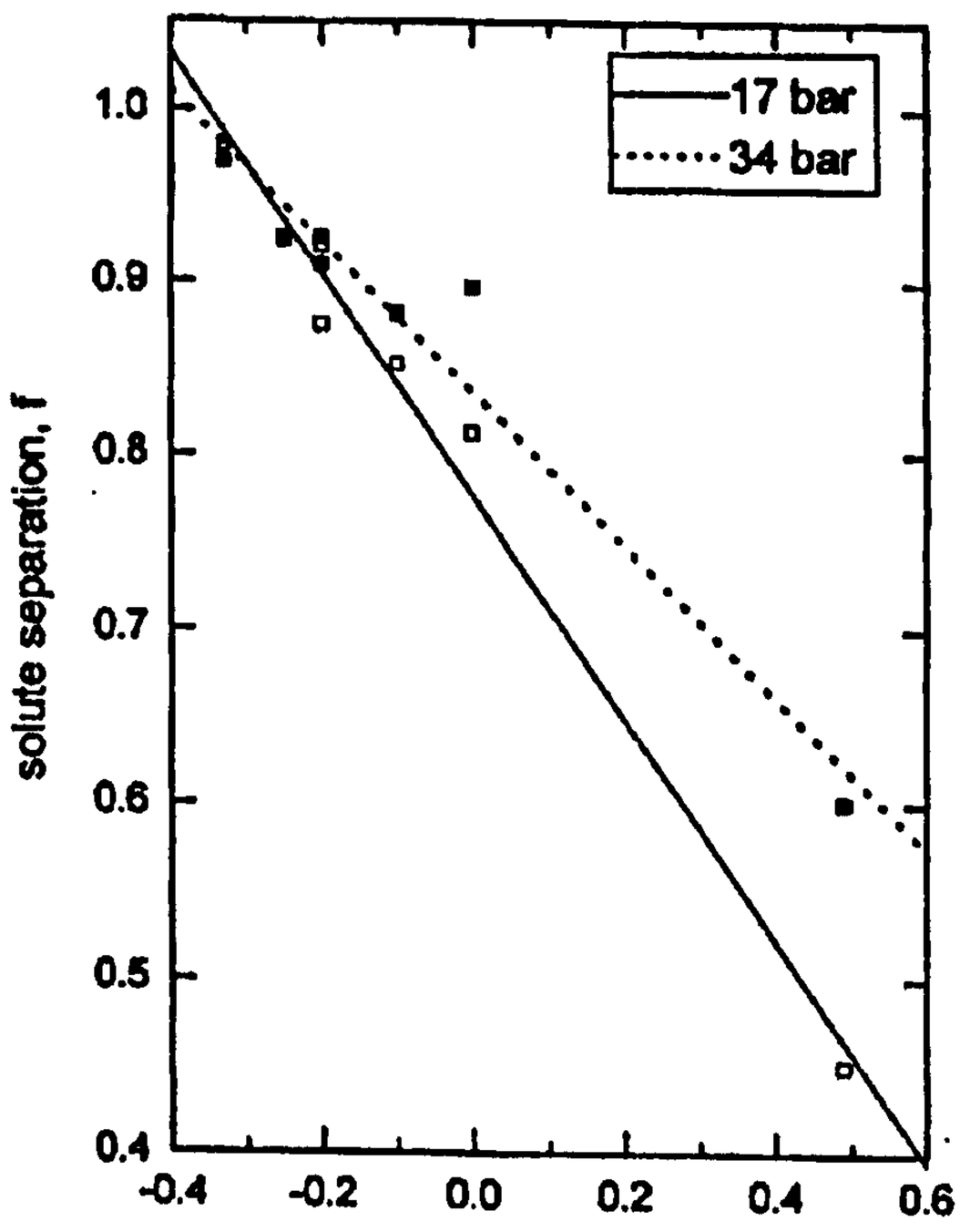

Figure 4.4: Relationship between the average separation data and the examined organic pollutants and their Taft numbers (σ) [139].

The experiments were carried out at feedwater pressure of 17 and 34 bar. However, the conclusion is based on very limited number of organic molecules and from the graph it appears that more data is required to confirm this finding by selecting organics with wide range of Taft numbers.

Some commercial reverse osmosis (RO) and nanofiltration (NF) membranes were studied in the removal of organic pollutants of petrochemical and agrochemical origin from water. The rejection of organics was shown to depend on both the membrane properties like pore size, membrane material, membrane charge and solute characteristics such as molecule size, charge and polarity [140]. The pore size distribution (PSD) of UF/MF membranes usually can be measured directly by SEM, AFM, or bubble pressure/solvent permeability but that can't be applied for RO membranes. Therefore an indirect determination method based on selective solute permeation and using the surface force-pore flow model of material transport through the membrane is used [141]. The detail of this procedure will not be reported since the interest in his study is membrane performance in rejecting organics. The tested RO membranes were HR95PP (HR) from Dow Danmark, TFC-8821(ULP) from Fluid Sys Corporation, and CPA2 from Hydranautics. The nano-fitration membrane is TS80 from TriSep Corporation. Calculated pore size is given in Figure 4.7.

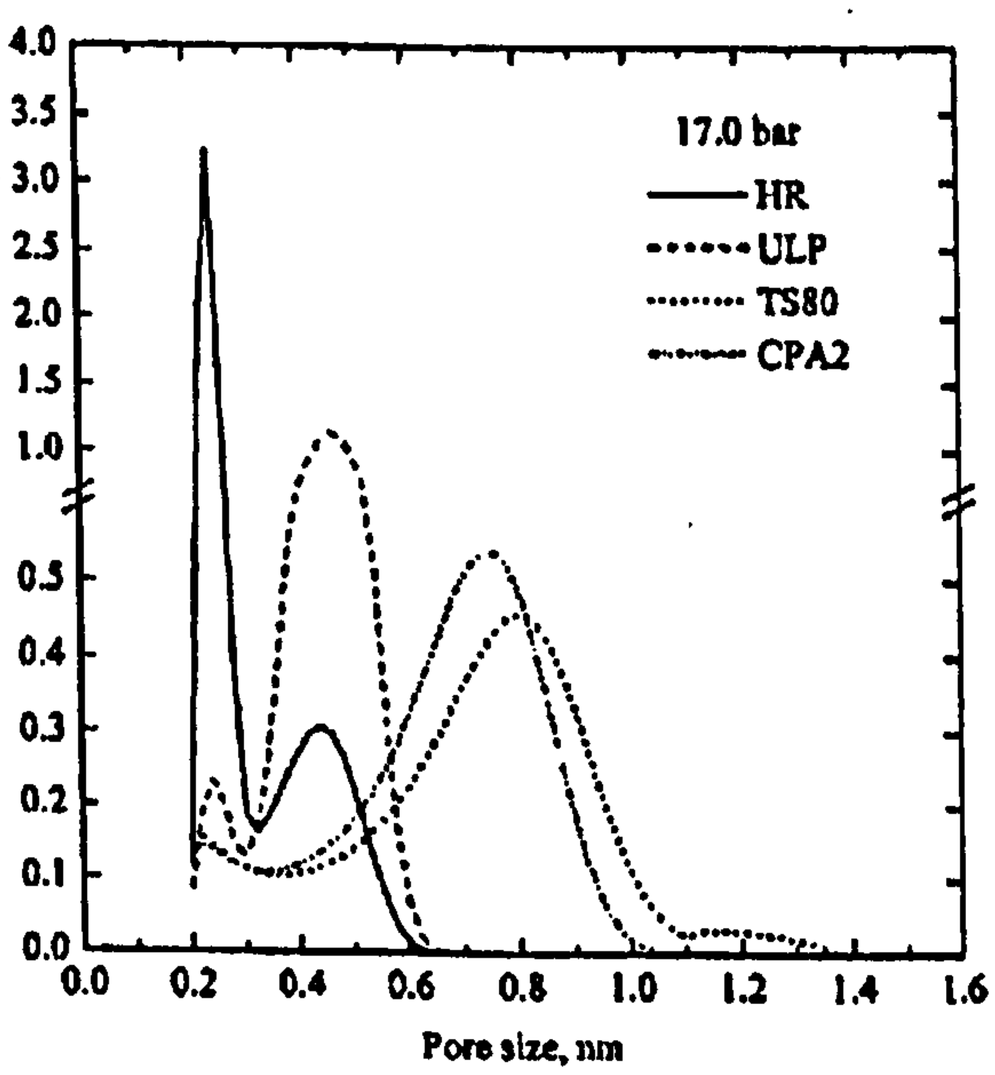

Figure 4.5. Pore size distribution for the tested membranes [140]

From Figure 4.7 it appears that for HR and ULP RO membranes the active layer surface has small pores and for the NF TS80 has large pores. The experiments were carried out in a laboratory apparatus. The feedwater temperature, pressure, and solution concentration of sodium chloride and calcium chloride were at room temperature, 17 bar, and 300 ppm respectively. The rejections of the tested petrochemical organics are given in Table 4.2.

	R, formaldehyde (methanediol)	*R*, 1,2-ethanediol	*R*, 2-butanone	*R*, ethyl acetate
HR	0.274	0.569	0.542	0.657
ULP	0.308	0.623	0.607	0.751
CPA2	0.186	0.501	0.776	0.553
TS80	0.164	0.364	0.651	0.455
Molecular mass	48.03[a]	62.07	72.11	88.11

Table 4.2. Petrochemical chemical rejection ratio [140]

From Table 4.2 it can be seen that in general increasing molecular weight increases rejection but that is not true for all membranes and also membranes with smaller pore size has higher rejection for organics than larger pore size membrane and again that is not true in every situation. So based on that the molecular weight and the pore size do play an important role but there are other factors that influence organic rejection such as molecule charge and membrane material properties.

4.5.2 The role of pressure and feedwater organic concentrations

The operating pressure and feedwater organics concentrations have an effect on the performance of RO membranes. Lin and Lan [142] employed ultrafiltration (UF) and reverse osmosis (RO) to reduce the COD (chemical oxygen demand), Cu^{2+} concentration, suspended solids (SS) and to improve the turbidity and conductivity of waste drawing oil. The COD is used to determine the organic matter concentrations. A semi-batch UF/RO experimental apparatus was used which consists of a prefilter and UF and RO cells. The RO membranes were spiral-wound polyamide membrane. The feedwater was supplied by a copper cable and wire manufacturer in northern of Taiwan. The RO feed water COD concentration, pH, conductivity were 4,347 ppm and 7.92, 1800 μmho/cm respectively. The overall COD

removal is between 98 and 99%. It was found that the COD concentration was lowered from 97 mg/l to 46 mg/l after increasing the pressure from 0.24 MPa to 0.8 MPa (Figure 4.6).

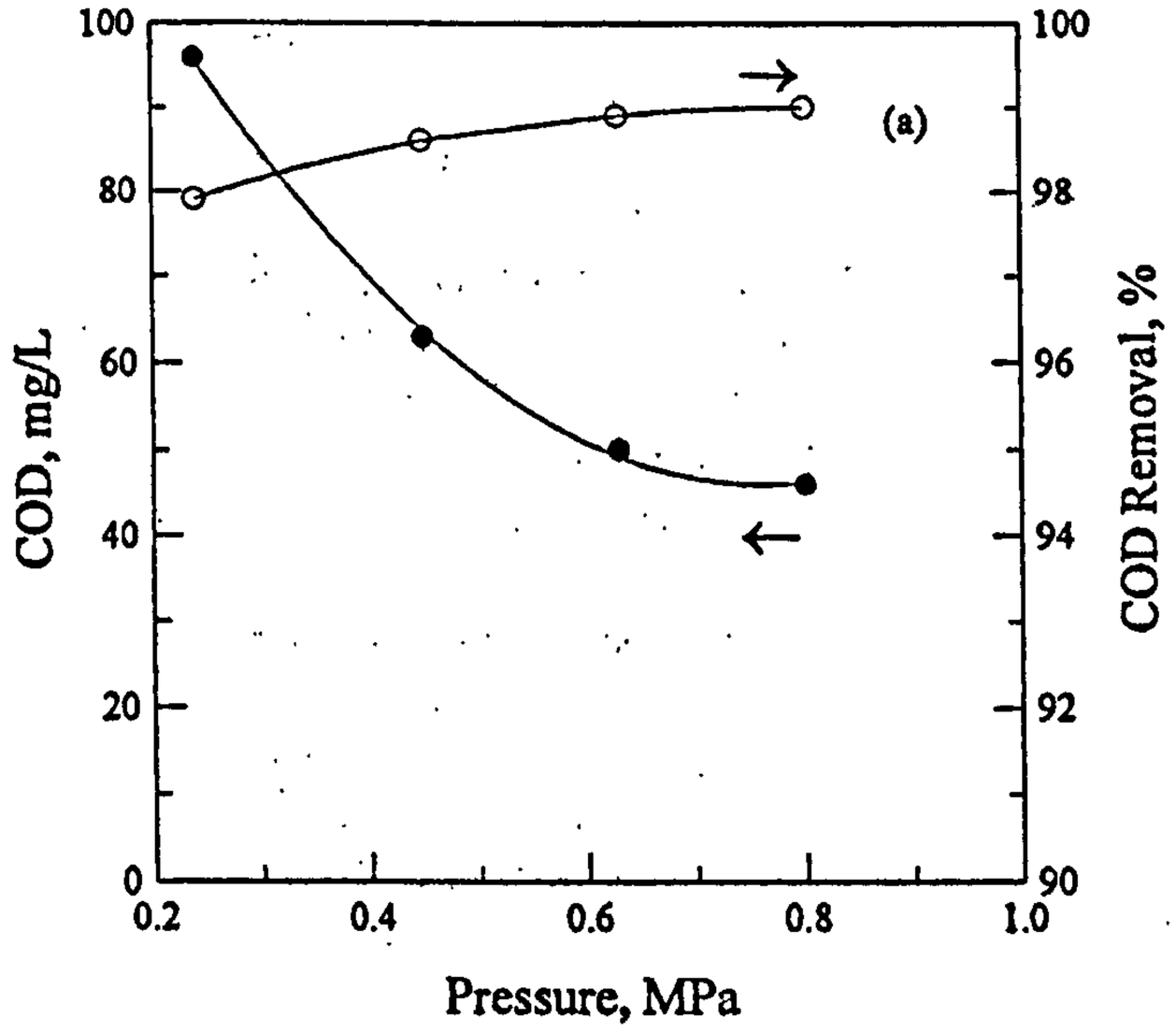

Figure 4.6. RO feedwater pressure versus permeate COD level and percent removal [142]

The reason(s) for higher rejection at higher pressure was not mentioned but is most probably that pressure leads to higher water permeation, which dilutes the organic content.

Sridhar *et al* [134] used a pilot-scale RO unit to study the treatment of wastewater from a vegetable oil industry. The effect of varying feed pressure (0–69 bar) and feed TDS concentration (0.54–5.2% w/v) on separation performance of the thin film composite (TFC) polyamide RO membrane was investigated. At feed pressure of 55.2 bar, high rejection of TDS (99.4%) and COD (98.2%) along with complete rejection of color was achieved with a reasonably high flux of 52.5 l/(m^2 h). The flux and percent rejection of pollutants improved with increasing transmembrane pressure at constant feed concentration (see Figure 4.7).

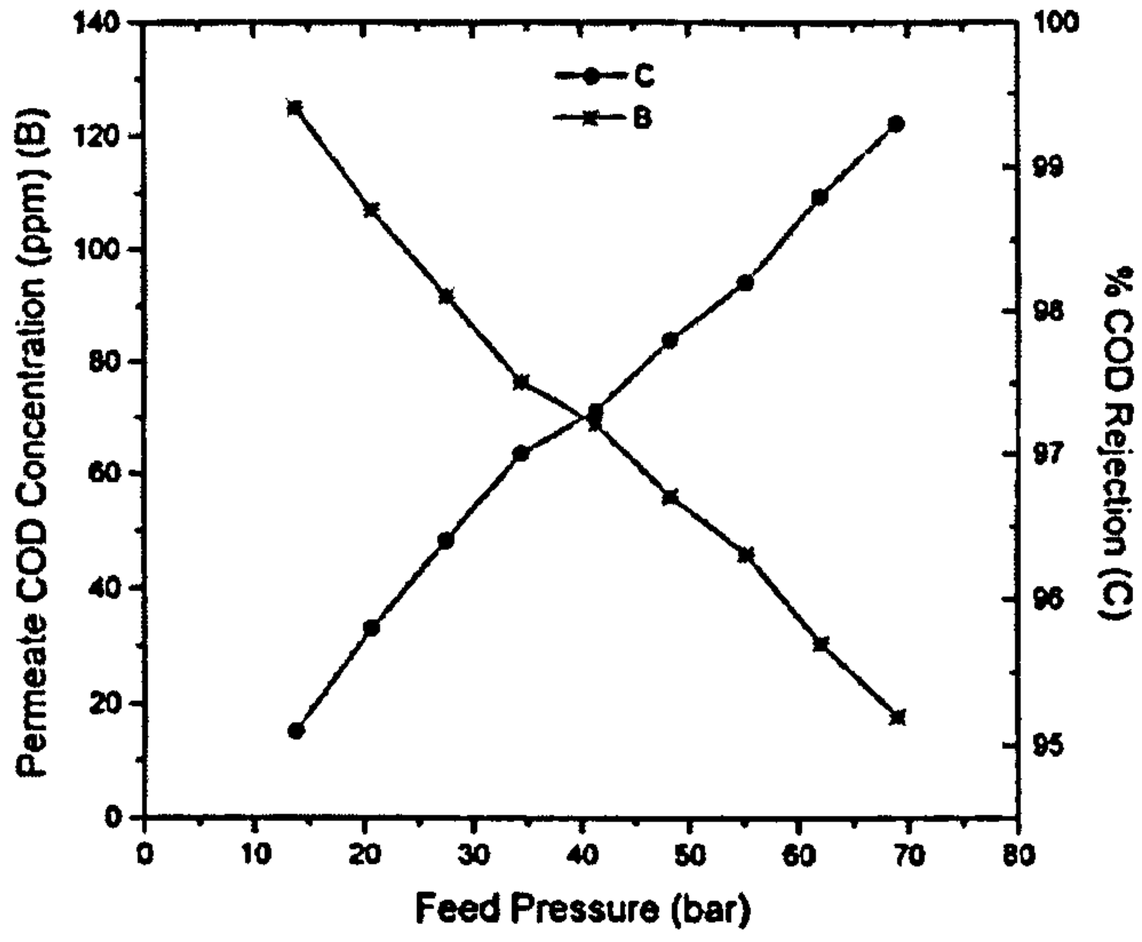

Figure 4.7. Variation of permeate COD with feed pressure (feed concentration:2,550 ppm COD, 10,411 TDS)

It is found that as feedwater COD concentration increases COD rejection decreases (see Figure 4.8). Also increasing feedwater TDS concentration from 0.54 to 5.22% (w/v) lowered the flux from 60 to 7 l/(m^2 h) while the rejection decreased from 99.5 to 96.2% for TDS and from 98.6 to 92.3% for COD. The decreasing flux and rejection is due to rising concentration polarization of solute, which increases the osmotic pressure at the membrane surface and causes a loss in effective transmembrane pressure.

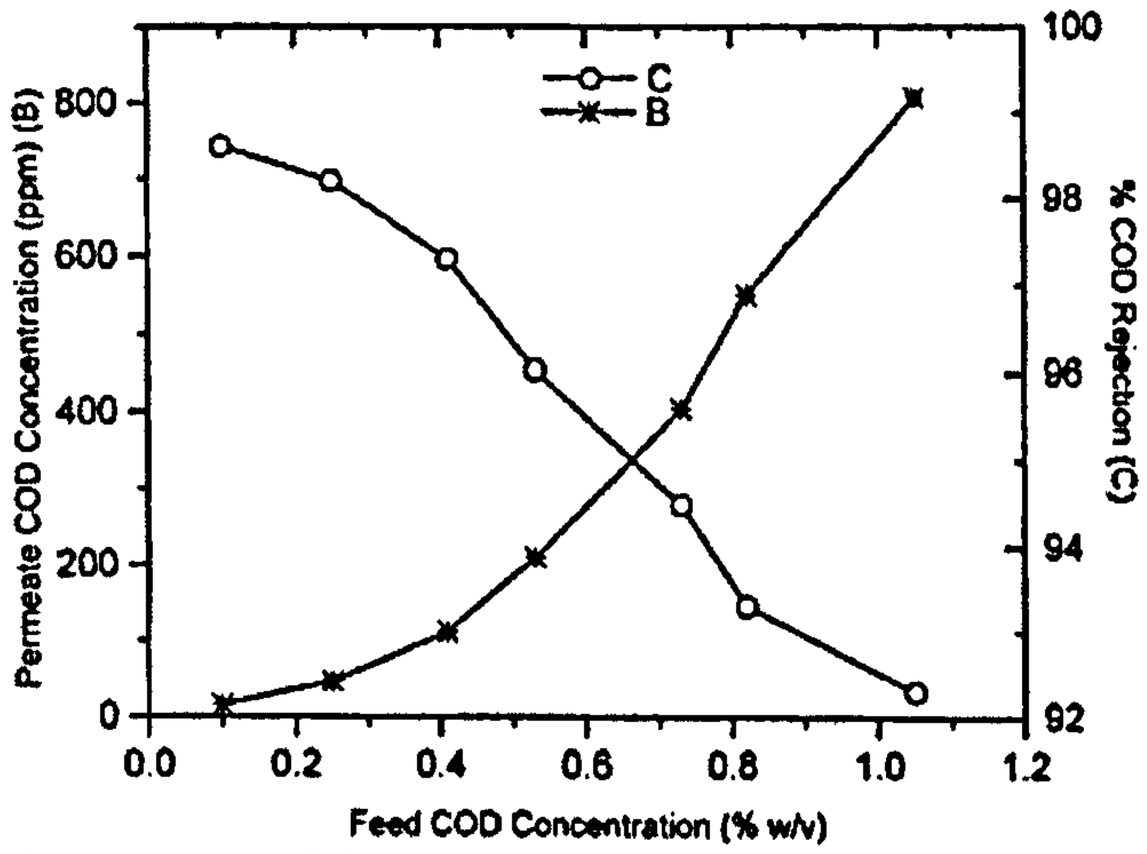

Figure 4.8. Variation of permeate COD content with feed concentration (feed concentration: 55.2 bar, temperature 28 °C). [134].

4.5.3 The application of RO membranes in recycling wastewater

RO membranes were applied successfully in purifying contaminated water with lubricant and degreasing agent. That was based on an experiment conducted by using a new, high-temperature-resistant, thin-film RO polyamide membrane from Osmonics-Desal in a heat-exchanger manufacture plant (Alfa Laval in Sweden) to study the influence of a lubricant and an alkaline degreasing agent on the membrane performance. The aim was to investigate the possibility of treating the contaminated water and then recycling the permeate. The feedwater pressure, temperature, and flow velocity across the membrane were 4.0 MPa, 65 °C, and 7.5 m/s respectively. The feedwater degreaser and lubricant were 0.3 and 0.5 wt%. The plant was run for almost 500 hours without cleaning. The COD rejection was 97% (corresponding to 250 ppm in permeate). Based on these results it was concluded that recycling permeate was possible even though 250 ppm is considered in other papers as a high COD concentration [108].

Gerard *et al* [128] tested the performance of two new RO membranes and compared them with conventional commercially available composite membranes. Over a three year test period, the new membranes showed high flux, maintained good salt and organic rejection due to improvement in active layer surface. The improvement includes increasing membrane surface hydrophilicity and reducing surface charge. Membrane surface charge is believed to play an important role in the fouling mechanism because it can determine the nature of potential absorption site for foulants. The surface charge of the new membranes was analyzed quantitatively by measurement of the surface zeta potential (see Figure 4.9).

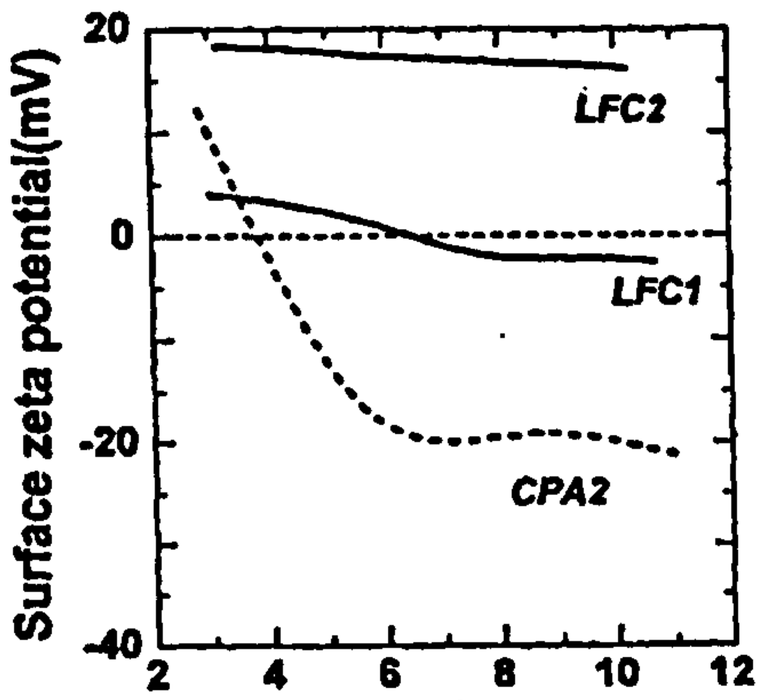

Figure 4.9. Surface zeta potential for the membranes [128]

The effect of neutral surface charge for LFC1 (low fouling membrane) is that when the performance of LFC1 was tested in a municipal effluent system in Japan, 87% rejection of TOC was achieved. The system was operated at feed flow rate, pressure, and system recovery of 20 $l/m^2.h$, 10 bar and 50% respectively. The feedwater characteristics were not mention. It is believed that the neutral surface charge has reduced the organic adsorption and that lead to stable operation for LFC1 for about 150 hour (see Figure 4.10).

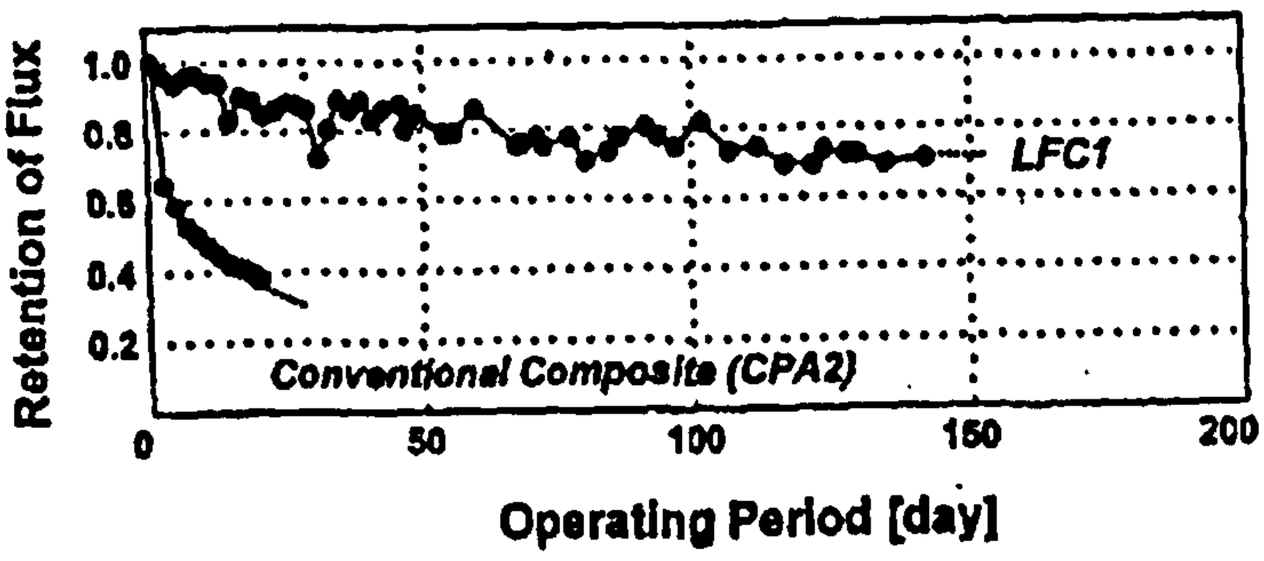

Figure 4.10. Performance of LFC1 and CPA2 in municipal effluent system in Japan [128]

Although many researchers showed that RO membranes is an effective technology to remove organics from water [35,143,144,145,146], Hodgkiess *et al* [147] found that polyamide RO membrane is severely damaged once exposed or soaked into hydrocarbons. In his experiments polyamide seawater RO membranes and brackish water RO membranes were tested after exposure to crude oil, crude oil/water mixtures, diesel and diesel/water mixtures, hexane and hexane/water mixtures. A serious degradation of desalination performance was

observed for these membrane causing extremely severe reductions of RO membrane performance.

In summary, RO membrane technology is an effective process to separate organics from water. Most of the research is focused toward determining. the governing factors that influence organics separation such as molecular weight and membrane properties in addition to operating parameters. It was observed that RO technology is mostly used to separate small fraction (in ppm ranges) of organics from water, in some studies it was applied to treat up to 0.5% wt% whereas microfiltration processes are employed to treat up to 30% oil contamination. In this work RO membrane will be applied to purify up to 50% oil contamination.

CHAPTER 5

EXPERIMENTAL PROCEDURES AND ANALYSIS TECHNIQUES

5.1 Introduction

To evaluate RO membrane performance in various operating conditions and environments, an extensive experimentation and detailed membrane analysis using advanced surface analysis apparatus was necessary. A series of tests were carried out for four RO membranes in an experimental test rig designed and built specifically for this study. The rig facilitated study of the membrane performance in pure water and in oil-contaminated water. The membranes were examined at various feedwater pressures, temperatures, pH values, conductivity values and with different levels of oil-contamination. In this chapter the experimental test rig design, configuration and operating conditions to evaluate membranes performance in oil contaminated water and in pure water will be presented. Membrane manufacturer operating parameters limits will be specified. Also a brief description for the analytical techniques used to characterize the membranes will be presented. The analytical techniques are Atomic Force Microscopy (AFM), Environmental Scanning Electronic Microscopy (ESEM), Light Microscope (LM) and ATR-FTIR spectroscopy.

5.2 Membranes studied

Four membranes were studied: Osmonics SG, Osmonics AD, Osmonics AG and TriSep X20. TriSep X20 membrane was received from Tri-Sep Corporation, USA and Osmonics SG/AD/AG were received from Osmonics Inc., France. TriSep X20 membrane was received rolled in a flat sheet (1x5 m^2) and Osmonics Inc. membranes were received in flat sheets (30x30 cm^2). The membrane properties, as specified by the manufacturer, are given in Table 1. The TriSep X20 membrane thin film layer is aromatic polyamide-urea and the support layer is polysulfone. Osmonics Inc. membranes materials of construction were not provided.

Membrane	Maximum Pressure	Maximum Temperature	pH range	% Salt rejection (NaCl)
TriSep X20	410 MN/m^2	45 °C	4 - 11	99-99.5%
Osmonics AD	540 MN/m^2	50 °C	4 - 11	99.5%
Osmonics SG	150 MN/m^2	50 °C	1 - 11	99.5%
Osmonics AG	400 MN/m^2	50 °C	4 - 11	99.5%

Table 5.1. Manufacturer specified operating parameters

The membranes were cut into 10x19 cm^2 areas to fit into the experimental test cell compartment after wetting by distilled water.

5.3 Experimental test rig design configuration

Part of this research involved a complete system design of the RO membrane test rig followed by fabrication of the rig. Initially, the operating ranges were specified and based on that the rig was built. The operating rages are as follows:

Pressure: 10-250 MN/m^2

Temperature: 20-50 °C

Feedwater conductivity: 0-30,000 μS/cm

Feedwater pH: 1-12

Feedwater flow: 0-1.9 x 10^{-4} m^3/s

The central part of the rig is the RO membrane cell, which was from OSMONICS Inc. It simulates an actual operating RO plant and it is easy to fit and remove the tested membrane sheets. The major components of the experimental rig are shown in Figure 5.1. The rig, as built, is shown in Figure 5.2. The system consists of a feed tank, 5-micron cartridge filter, high-pressure pump, SEPA CF membrane test cell from OSMONICS, and a flow meter. The specification of each component is given in Appendix A. One of the major properties that was considered in the design of the rig is to sustain high pressure, up to at least 250 MN/m^2, to enable testing the membranes under high pressure conditions. The system was fabricated

as shown in Figure 5.2. Because membrane cell installation is a very important part of the study, a detail procedure supported by figures is given in Appendix B.

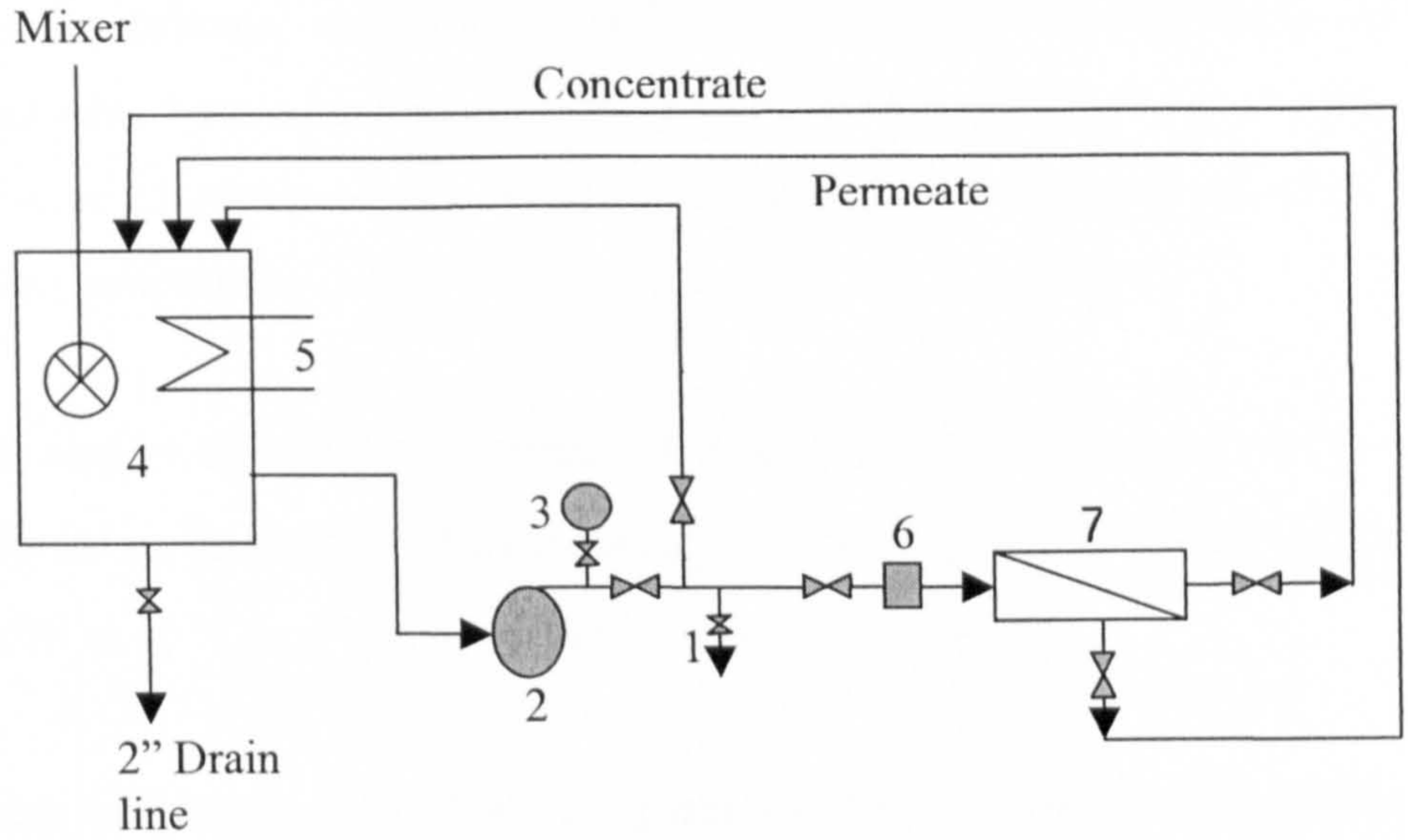

1. Sample Point 2. Pump 3. Pressure Gauge 4. Tank
5. Heating coil 6. Flow meter 7. Membrane cell

Figure 5.1. Schematic diagram of the test rig design

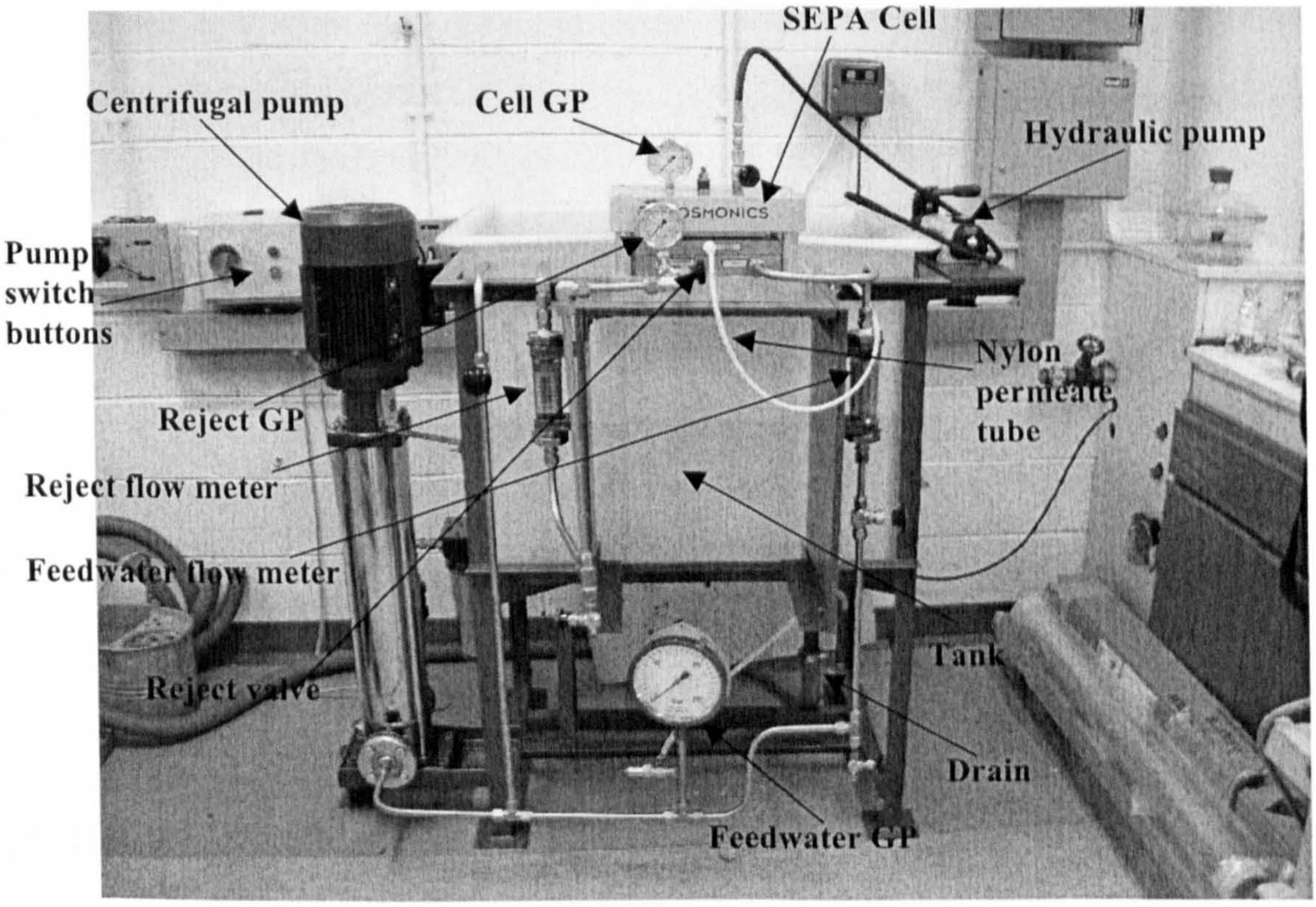

Figure 5.2. The experimental rig as built

The SEPA CF membrane cell is a lab scale cross-flow membrane filtration unit that can be used for membrane evaluation. RO, nanofiltration, ultrafiltration and microfiltration membrane can be used in the cell. Based on the Osmonics Inc., the SEPA CF simulates the performance of commercially available spiral-wound membrane elements with easy to use flat sheet membranes.

The oil used in this study is purchased from ESSO Petroleum Company Limited, UK and was referred as Priol 352. The oil density is 0.86 g/ml at 15 °C, boiling at 316 °C, viscosity 67 mm2/S at 40 °C and it is not volatile. It is safe to handle.

Shimadzu analyzer (model: TOC-500) was used to analyze Total Organic Carbon (TOC) in feedwater and permeate.

5.5. SEPA CF start-up

Once the cell is installed the rig is ready to work. The following is a list of procedures for the operation of the system.

1. Fill out the tank with distilled water. Make sure that the system piping and pump casein is fully occupied with water to avoid pump cavitations.
2. Turn on the feed flow pump. Check for any leaks in the piping and the cell holder.
3. Adjust the concentrate flow control valve to obtain the desired pressure and flow. A good starting point may be a feed pressure of 40 MN/m^2 and feed flow of 1.3-1.9 $x10^{-4}$ m^3/s.
4. Adjust the cooling water flow to the cooling coil to obtain the desired temperature.
5. Add sodium chloride to obtain the desired conductivity and add hydrochloric acids or sodium hydroxide to adjust pH value.

The system was commissioned successfully. The components were found to operate satisfactorily and the system sealing was found to be good. After commissioning the system

a number of modifications were made to make the system easier to work with and they are as follows:

1. ***Tank Size***: The tank capacity changed from 240-litre to 65-litre and then to 7-litre tank capacity. For pure water tests, the 240-litre tank was fine. However when oil/water test solution experiments started, it was noticed that mixing water with oil in a big tank was not efficient. To minimize oil consumption it was decided use a smaller tank (7 litre). For the 7-litre tank only 3.5 litres of oil was used. Mixing was optimized using the smaller tank.

2. ***The Mixer***: In the initial design, the tank was built without a mixer and the idea was to utilize the high circulation flow expected from the pump. However, circulation was found not to be efficient and clear separation of the oil water was observed in the tank. The introduction of the mixer solved this problem and it was then possible to achieve a homogeneous oil/water feed into the cell. To check the oil/water ratio entering the RO membrane cell frequent sampling was undertaken as shown in Chapter 8. These samples were collected from feedwater piping, just before the cell. Samples were collected in graduated cylinders left for about 20 minutes until separation was achieved. Then the oil percentage was measured. In low oil contamination experiments, TOC analysis for feedwater was required.

3. ***Flow meters***: Two flow meters were installed initially; one before the RO membrane cell and one after the cell. Both meters were reading similar reading. The purpose of installing two meters is to measure the permeation rate by subtracting feedwater flow from concentrate flow (refer to Figure 5.1). It was noticed after commissioning the system that the permeate is too low to measure by this meter. So it was measured manually (measure the time for 5 ml permeate). So the meter after the cell was removed to reduce friction losses.

4. ***5-Micron Filter***: The 5-micron filter was installed initially to filter feedwater but it was realized later that this filter is not needed since the same clean water is being circulated. Removing it reduced friction losses and simplified the system.

To evaluate membrane performance the following are recorded:

- Feedwater - flow, pressure, temperature and conductivity
- Permeate - flow and conductivity
- Feed and permeate water pH
- Oil concentration in the feed water tank and permeate

5.5 Atomic Force Microscopy (AFM)

Atomic Force Microscopy (AFM) has the ability to image the surface at atomic resolution and its primary purpose in this study is to study membrane topography and to quantitatively assess surface roughness. The AFM is used here mainly to study membrane surface morphology of tested membranes after exposure to different environments. Figure 5.3 gives a simplified drawing for AFM main components.

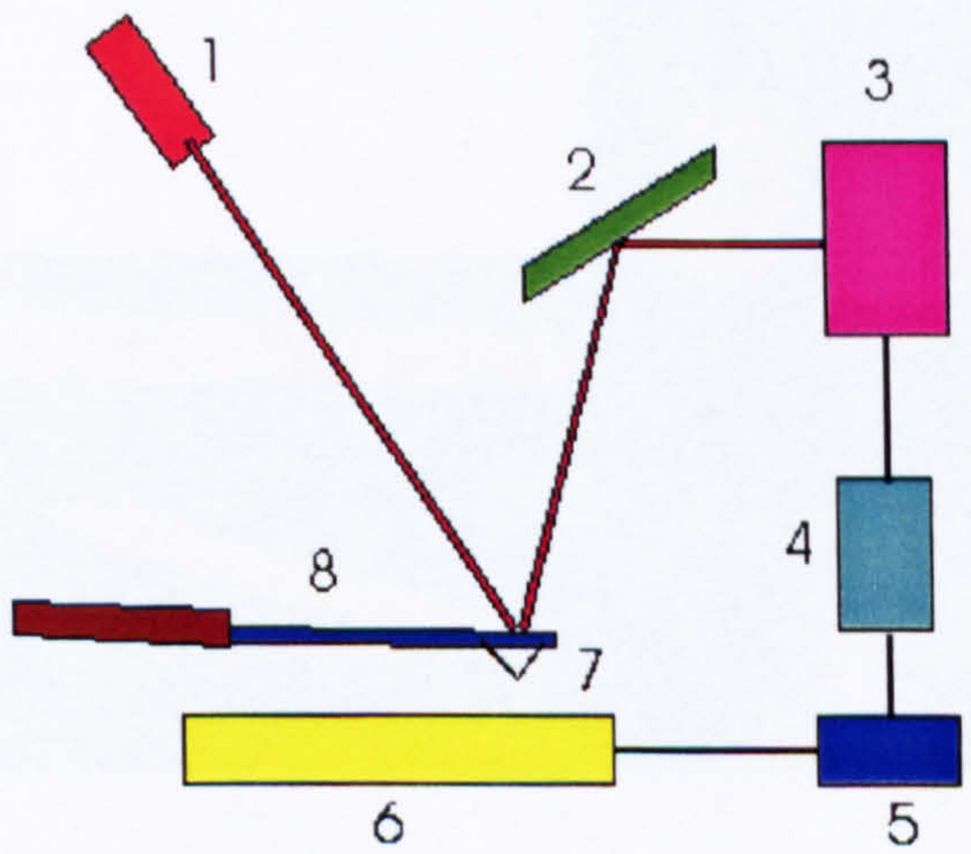

Figure 5.3. Simplified drawing for AFM: 1. Laser 2. Mirror 3. Photodetector 4. Amplifier 5. Register 6. Sample 7. Probe 8. Cantilever [21]

The principles of how the AFM works are very simple. An atomically sharp Si_3N_4 tip about 3 μm tall pyramid with approximately 10-30 nm end radius (see Figure 5.4) is scanned over a surface.

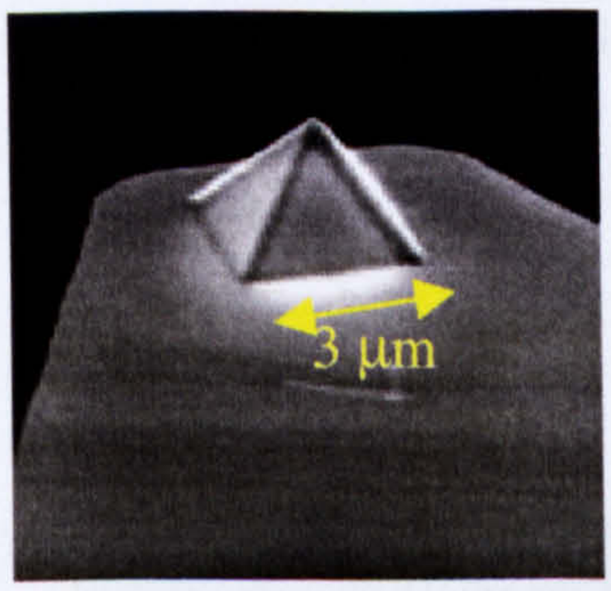

Figure 5.4. Atomic Force Microscopy sharp tip [154]

As the tip scans the surface of the sample, moving up and down with the contour of the surface, the laser beam is deflected off the attached cantilever into a dual element photodiode (see Figure 5.5).

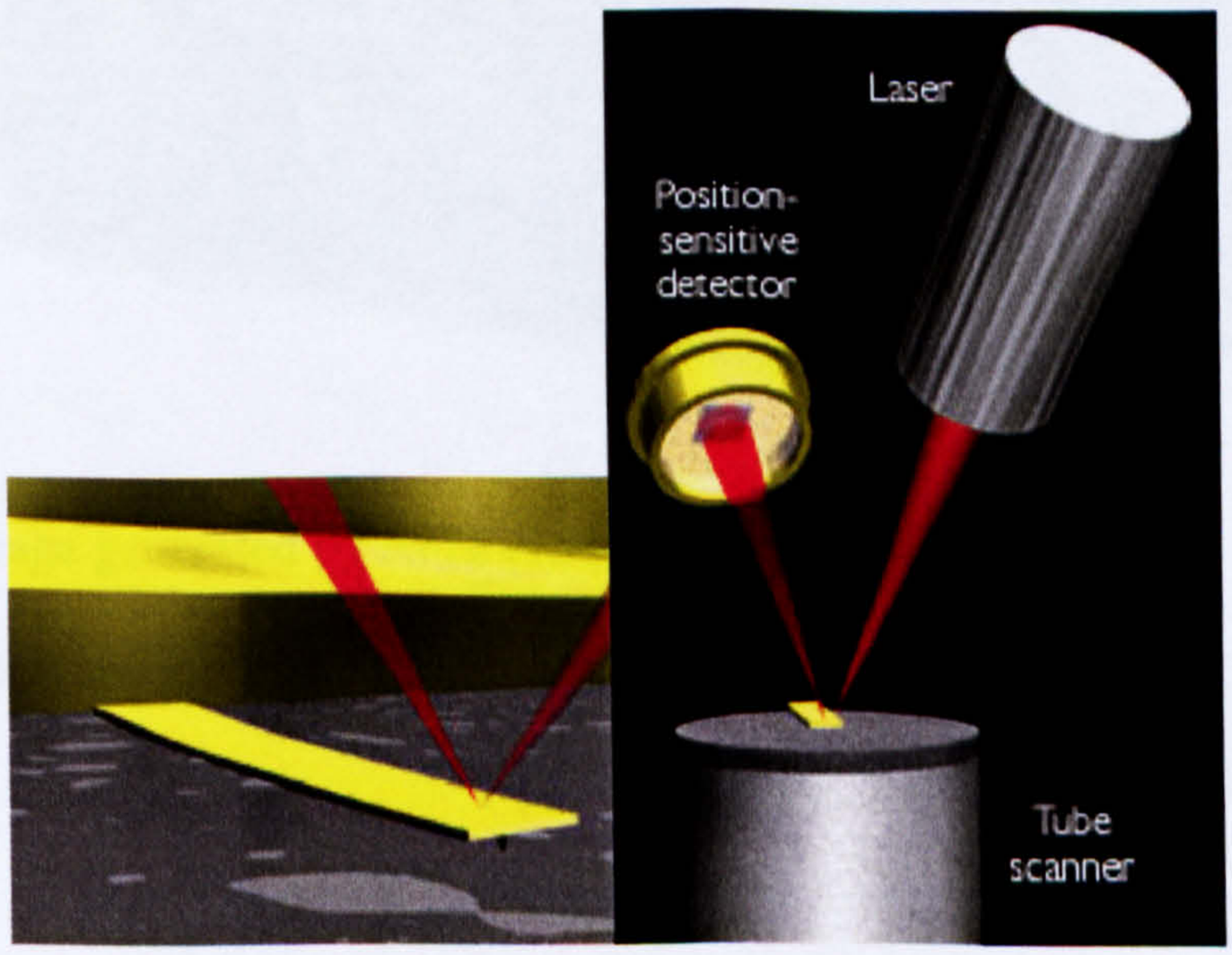

Figure 5.5. AFM and the optical lever: (left) a cantilever touching a sample; (right) the optical lever. Scale drawing; the tube scanner measures 24 mm in diameter, while the cantilever is 100 μm long [154].

The photo-detector measures the difference in light intensities between the upper and lower photo-detectors, and then converts to voltage. Feedback from the photodiode difference

signal, through software control from the computer, enables the tip to maintain either a constant force or constant height above the sample. In the constant force mode the piezo-electric transducer monitors real time height deviation. In the constant height mode the deflection force on the sample is recorded. Three dimensional topographical maps of the surface are constructed by plotting the local sample height versus horizontal probe tip position (see Figure 5.6) [154].

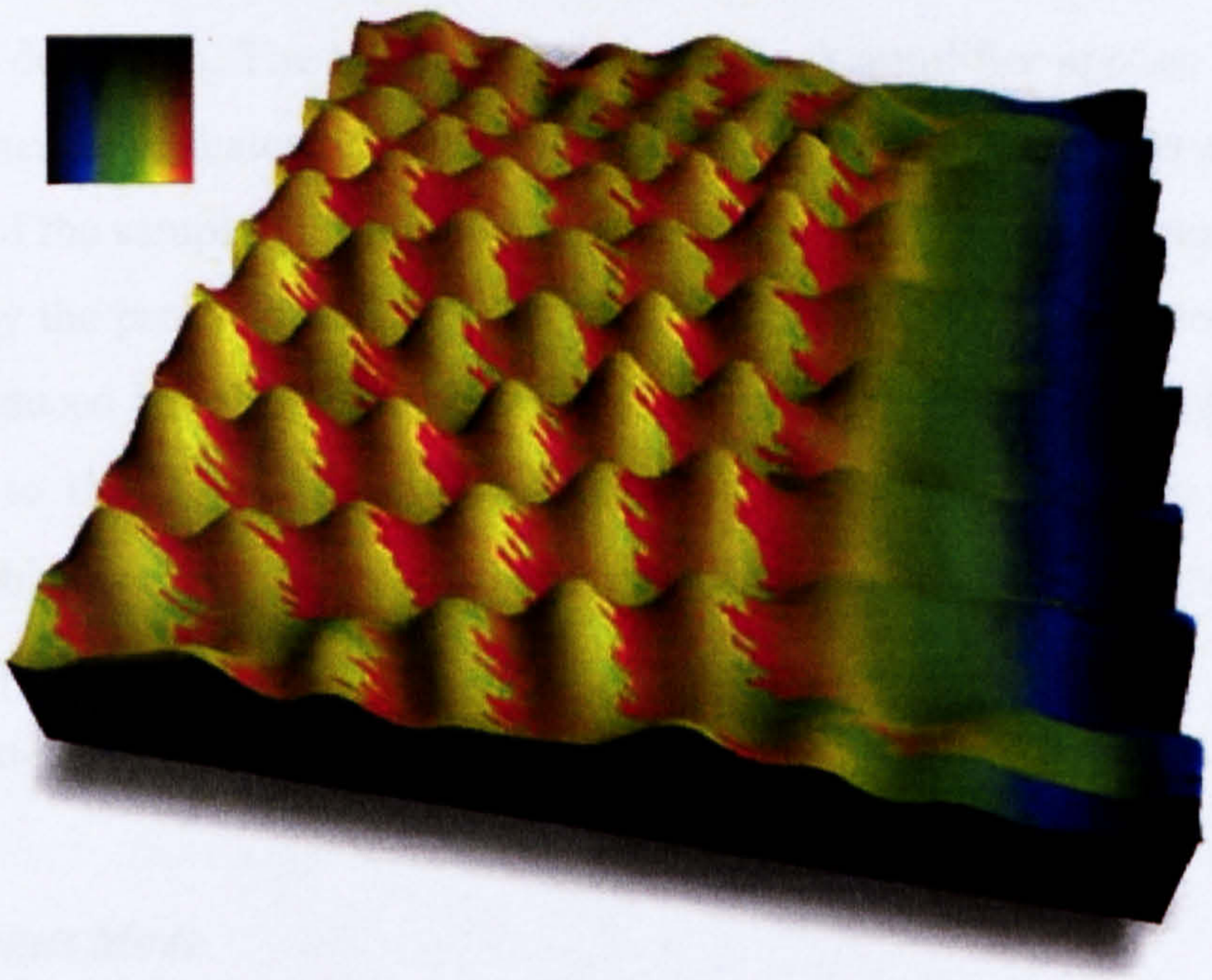

Figure 5.6. 3-D image generated by AFM [154].

There are three AFM operational modes: contact mode, non-contact mode, and tapping mode (see Figure 5.7).

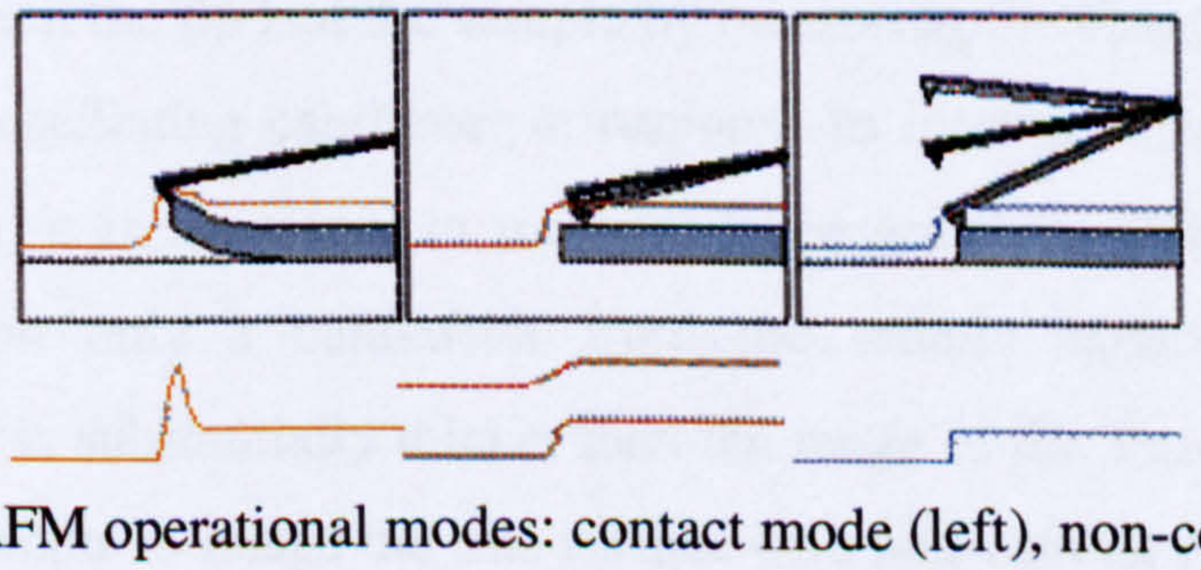

Figure 5.7. The AFM operational modes: contact mode (left), non-contact mode (middle) and tapping mode (right) [155].

5.5.1. Contact Mode

The contact mode where the tip scans the sample in close contact with the surface is the common mode used in the force microscope. The force on the tip is repulsive with a mean value of 10^{-9} N. This force is set by pushing the cantilever against the sample surface with a piezoelectric positioning element. In contact mode AFM the deflection of the cantilever is sensed and compared in a DC feedback amplifier to some desired value of deflection. If the measured deflection is different from the desired value the feedback amplifier applies a voltage to the piezo to raise or lower the sample relative to the cantilever to restore the desired value of deflection. The voltage that the feedback amplifier applies to the piezo is a measure of the height of features on the sample surface. It is displayed as a function of the lateral position of the sample. Problems with contact mode are caused by excessive tracking forces applied by the probe to the sample. These forces can be set between 0-60 nA. The effects can be reduced by minimizing tracking force of the probe on the sample, but there are practical limits to the magnitude of the force that can be controlled by the user during operation in ambient environments. In practice, it appears that these frictional forces can damage the sample, dull the cantilever probe and distort the resulting data. To avoid these problems the non-contact mode is used.

5.5.2 Non-contact Mode

In this mode the tip hovers 50-150 Angstrom above the sample surface. Attractive Van der Waals forces acting between the tip and the sample are detected, and topographic images are constructed by scanning the tip above the surface. Unfortunately the attractive forces from the sample are substantially weaker than the forces used by contact mode. Therefore the tip must be given a small oscillation so that AC detection methods can be used to detect the small forces between the tip and the sample by measuring the change in amplitude, phase, or frequency of the oscillating cantilever in response to force gradients from the sample. For highest resolution, it is necessary to measure force gradients from Van der Waals forces, which may extend only a nanometer from the sample surface. In general, the fluid contaminant layer is substantially thicker than the range of the Van der Waals force gradient and therefore, attempts to image the true surface with non-contact AFM fail as the oscillating

probe becomes trapped in the fluid layer or hovers beyond the effective range of the forces it attempts to measure.

5.5.3 Tapping Mode

Tapping mode is a key advance in AFM. This potent technique allows high resolution topographic imaging of sample surfaces that are easily damaged, loosely hold to their substrate, or difficult to image by other AFM techniques. Tapping mode overcomes problems associated with friction, adhesion, electrostatic forces, and other difficulties that an plague conventional AFM scanning methods by alternately placing the tip in contact with the surface to provide high resolution and then lifting the tip off the surface to avoid dragging the tip across the surface. Tapping mode imaging is implemented in ambient air by oscillating the cantilever assembly at or near the cantilever's resonant frequency using a piezoelectric crystal. The piezo motion causes the cantilever to oscillate with a high amplitude (typically greater than 20nm) when the tip is not in contact with the surface. The oscillating tip is then moved toward the surface until it begins to lightly touch, or tap the surface. During scanning, the vertically oscillating tip alternately contacts the surface and lifts off, generally at a frequency of 50,000 to 500,000 cycles per second. As the oscillating cantilever begins to intermittently contact the surface, the cantilever oscillation is necessarily reduced due to energy loss caused by the tip contacting the surface. The reduction in oscillation amplitude is used to identify and measure surface features.

During tapping mode operation, the cantilever oscillation amplitude is maintained constant by a feedback loop. Selection of the optimal oscillation frequency is software-assisted and the force on the sample is automatically set and maintained at the lowest possible level. When the tip passes over a bump in the surface, the cantilever has less room to oscillate and the amplitude of oscillation decreases. Conversely, when the tip passes over a depression, the cantilever has more room to oscillate and the amplitude increases (approaching the maximum free air amplitude). The oscillation amplitude of the tip is measured by the detector and input to the NanoScope III controller electronics. The digital feedback loop then adjusts the tip-sample separation to maintain constant amplitude and force on the sample [155].

Tapping Mode inherently prevents the tip from sticking to the surface and causing damage during scanning.

In our work contact mode was used. The imaged membranes samples were cut into small sections 0.5x0.5 mm^2 area. Some samples were imaged dry and other under water.

It has to be realized that RO membranes imaging by AFM is a complex task. In many circumstances, good quality images were not obtained due to the difficulty in adjusting the distance and the angle between the membrane surface and AFM tip. Such difficulty has lead to many poor quality images (see Figure 5.8). It was found that to produce a good quality image a considerable attention has to be given to surface to tip distance and angle adjustment.

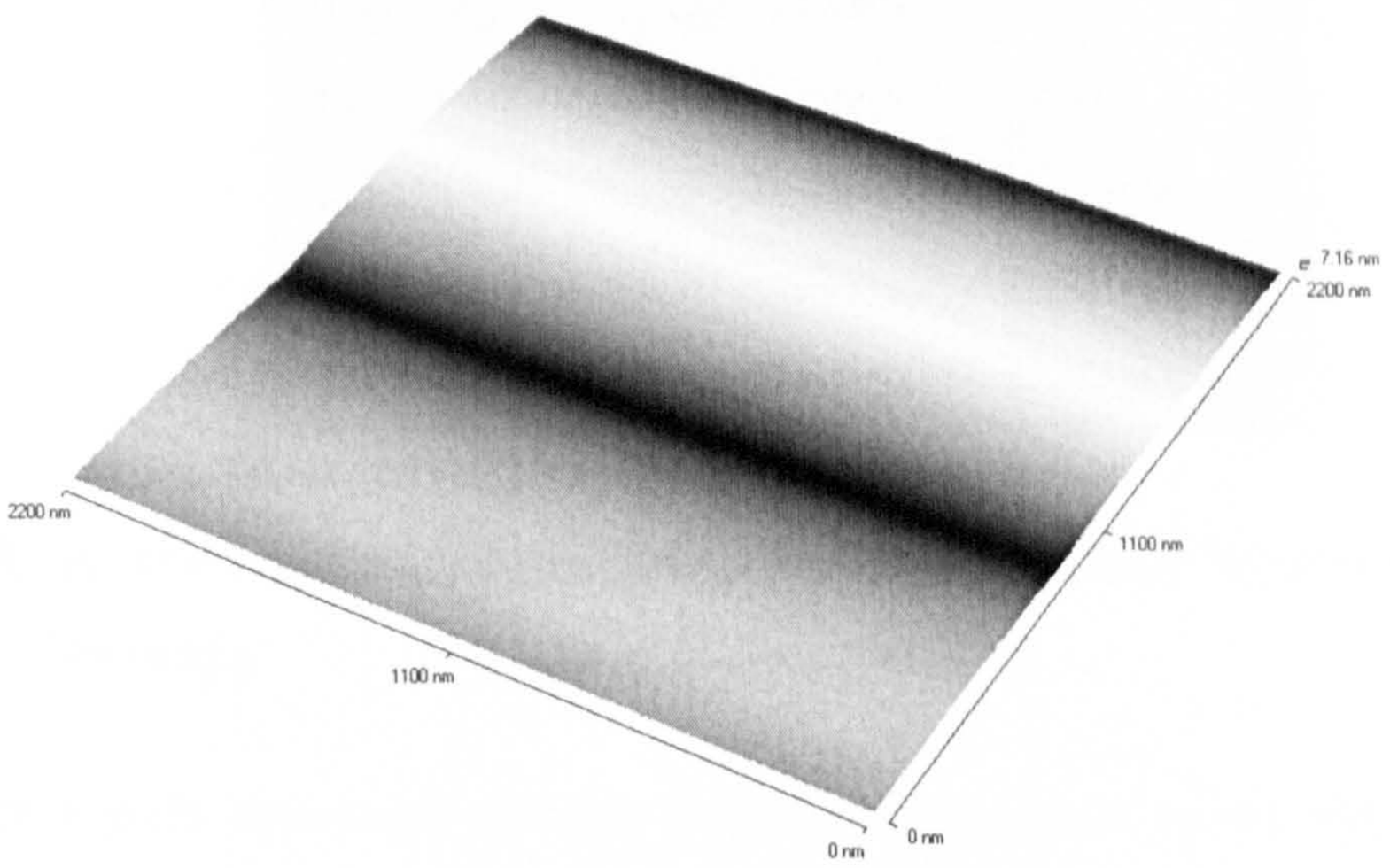

Figure 5.8. Poor quality membrane surface image

5.6 Environmental Scanning Electronic Microscopy (ESEM)

Environmental Scanning Electron Microscopy (ESEM) is most widely used for surface analytical studies (see Figure 5.9). In this study, it was used to image the membranes active and support layer and to give structural information of the tested membranes surface and cross-section. ESEM is considered a relatively rapid, inexpensive, and basically non-destructive approach to surface analysis. The ESEM used in our study is Philips XL30. It is

equipped with LaB6 gun, and is capable of operating as a conventional high-vacuum SEM, or under low-vacuum in ESEM mode for the imaging of wet and non-conductive samples utilizing the ESEM's gaseous secondary electron detector. In the study of polymeric membranes the benefit of ESEM over traditional SEM is the ability to examine the surfaces with no surface coating by conductive layers.

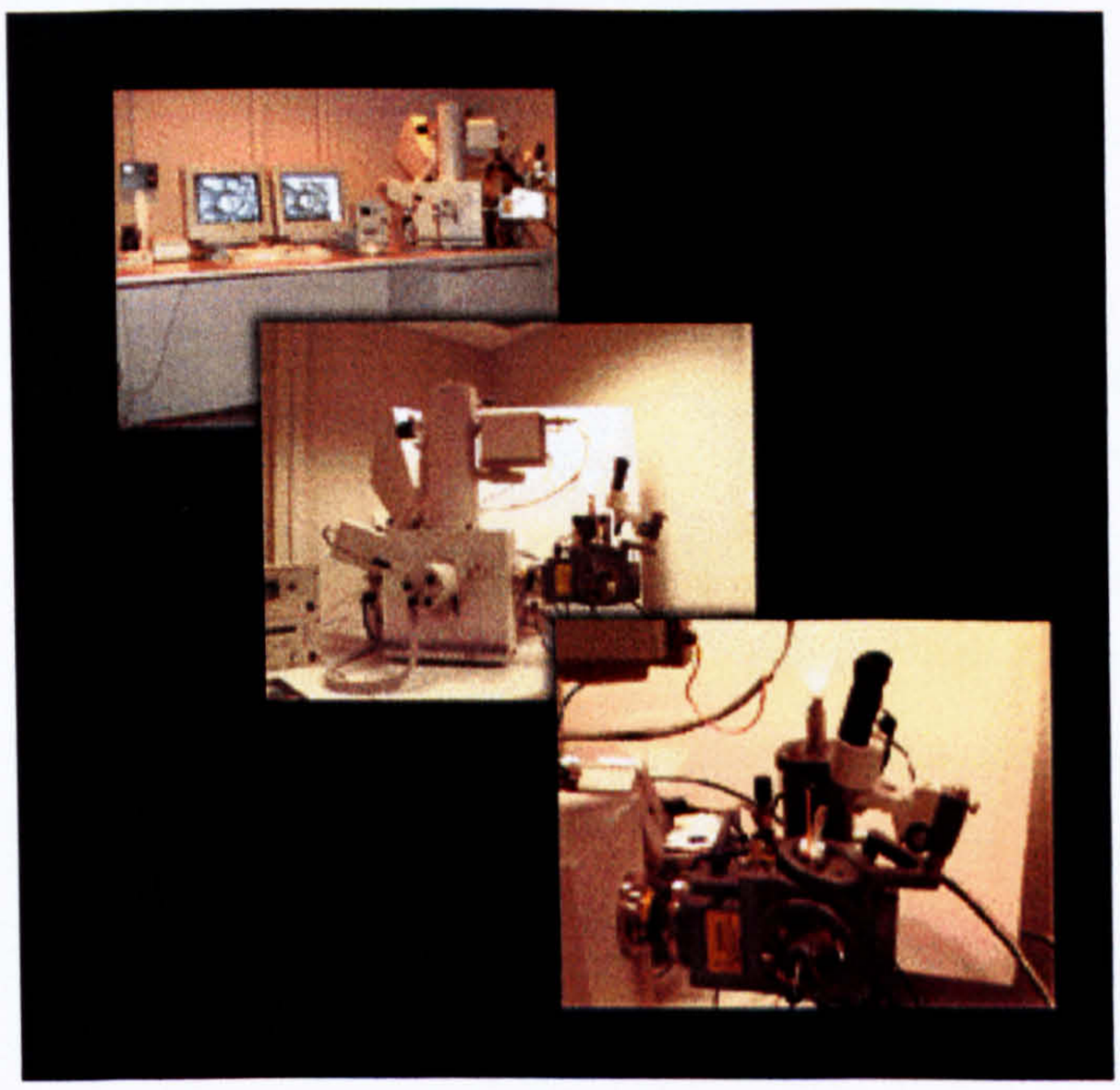

Figure 5.9. A view of the ESEM of the department of Petroleum Engineering, in Heriot Watt University

This beam travels downward through a series of magnetic lenses designed to focus the electrons to a very fine spot. Near the bottom, a set of scanning coils moves the focused beam back and forth across the specimen, row by row. As the electron beam hits each spot on the sample, secondary electrons are knocked loose from its surface. A detector counts these electrons and sends the signals to an amplifier. The final image is built up from the number of electrons emitted from each spot on the sample. The imaged membranes samples were cut into small sections (about 0.5x0.5 mm^2 area) and for SEM they were coated with gold prior to imaging.

5.7 Light Microscope

A light microscope (NIKON standard binocular) was used to analyze the membrane support layer, active layer and side thickness after exposure to water at various pH values. Amounted camera on the microscope allowed a record of each membrane surface image, which is connected to a computer that allows transferring of the images to the computer hard disk. Images are then printed for presentation.

5.8 ATR-FTIR spectroscopy

Attenuated total reflection-Fourier transform infrared (ATR-FTIR) spectroscopy was used to determine the chemical composition of the four tested membranes (TriSep X20, Osmonics SG, AD, and AG). The ATR-FTIR examines the interaction of infra-red radiation with chemical bonds between the atoms in a molecule. As a result the vibration of particular bonds and groups of atoms within the molecule are associated with characteristic infra-red frequencies. Therefore characteristic spectra are obtained for different types of molecules. ATR-FTIR is usually used to analyze inorganic and organic materials and to distinguish a variety of polymeric materials. Figure 5.10 shows Saudi Arabian Oil Company ATR-FTIR spectroscopy apparatus.

Figure 5.10. A view of Saudi Arabian Oil Company ATR-FTIR spectroscopy

The membrane support layers and active layers were analyzed at the Saudi Arabian Oil Company. It was possible to separate each membrane support layer from the active layer by fingernail. Each layer was then analyzed separately.

CHAPTER 6 - RESULTS

RO MEMBRANE STRUCTURE CHARACTERIZATION

6.1 Introduction

Understanding the relationship between RO membrane structure and their performance is a key factor in the development and manufacture of new membranes with particular performance to suit a specific treatment programme. In this chapter extensive microscopic analysis was conducted for four RO membranes using AFM, light microscopy (LM) and SEM methods. Firstly, AFM was applied to characterize the membrane active layer surface morphology and then SEM and LM were applied to characterize the membrane cross-section. Membrane surface roughness, surface area and peak height profile were examined for Osmonics SG, Osmonics AD, Osmonics AG and TriSep X20 membranes. Secondly, the flux was assessed for the four membranes under similar operating conditions to evaluate the production rate of each membrane. Then the relationship between membranes surface roughness, surface area, cross-section thickness with membrane flux was investigated. Finally, research to assess whether there is any effect of operating mode of the AFM (contact mode) on Osmonics SG and TriSep X20 membrane surfaces was undertaken. Moreover, the effect of scanning the membranes with different constant force setting was evaluated.

6.2 Assessment of membranes active layer surface

Osmonics SG, Osmonics AD, Osmonics AG and TriSep X20 membranes AFM images were examined visually to check the uniformity of the surface profile across different areas of the membrane. Such information is vital in subsequent sections to determine how membrane surface characterization should be performed. It was observed that Osmonics SG and TriSep X20 have significant differences in the active layer surface details which will be shown later in this chapter. In short, Osmonics SG was much smoother than TriSep X20. Osmonics AD and AG have similar surface features which fall between the rough TriSep X20 and smooth Osmonics SG. The full assessment of the surface was not conducted for Osmonics AG and Osmonics AD. Since the goal here

is to assess the uniformity of the membrane by applying an appropriate surface characterization procedure.

Membranes were received in flat sheets. Samples of 0.5 cm X 0.5 cm were collected. Each sample was imaged in different locations to assess the surface morphology variation.

6.2.1 Assessment of Osmonics SG active layer surface

Before quantitatively evaluating the membrane surface roughness, surface area and peak height profile, the AFM images of Osmonics SG membrane were visually assessed. AFM image sizes of 100x100 μm, 50x50 μm, 20x20 μm and 2.2x2.2 μm were chosen to cover the range of magnification values and assess the features on different scales. Figures 6.1-6.4 show the membrane surface images at each image size.

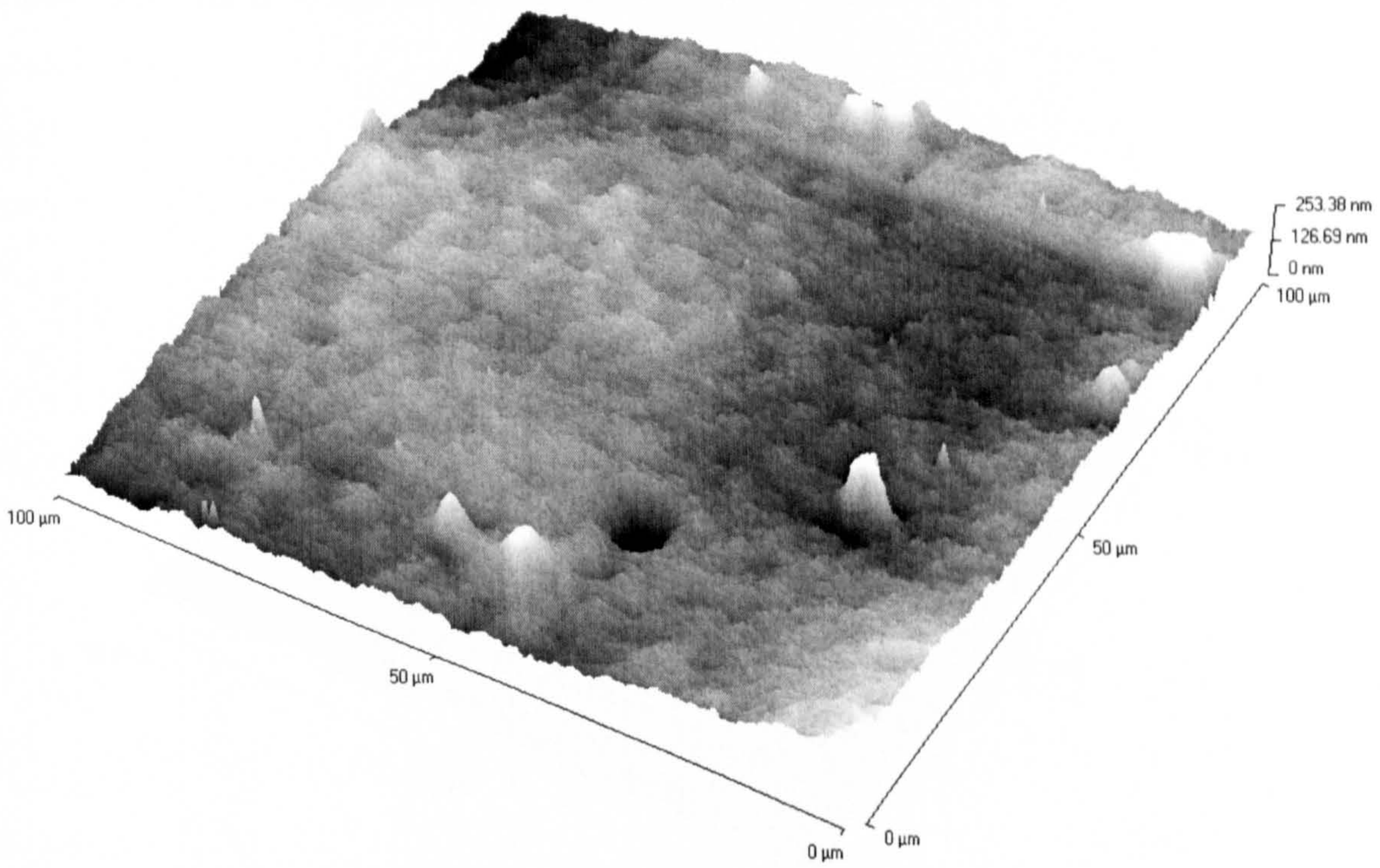

Figure 6.1. AFM image of Osmonics SG (100x100 μm)

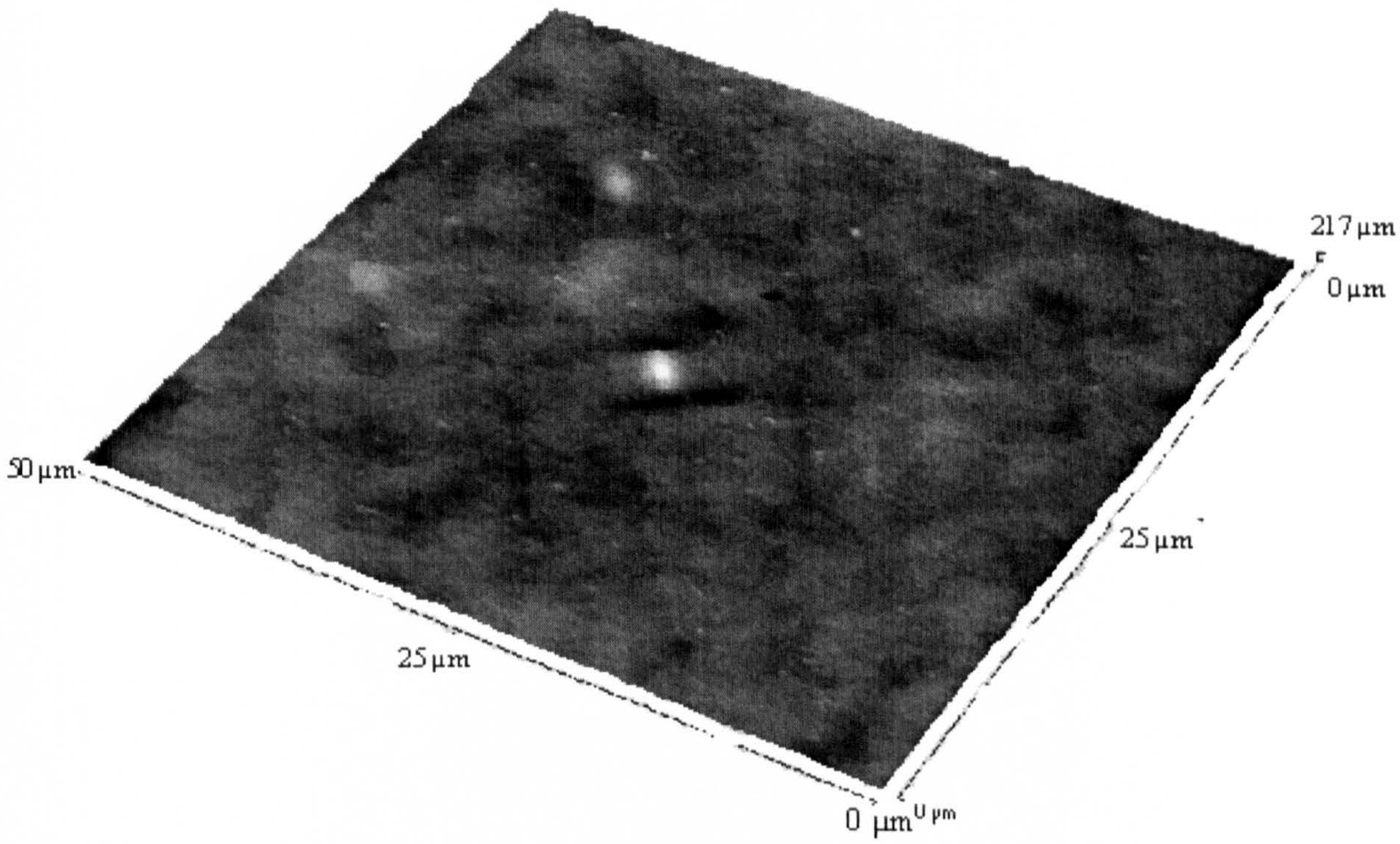

Figure 6.2. AFM image of Osmonics SG (50x50 μm)

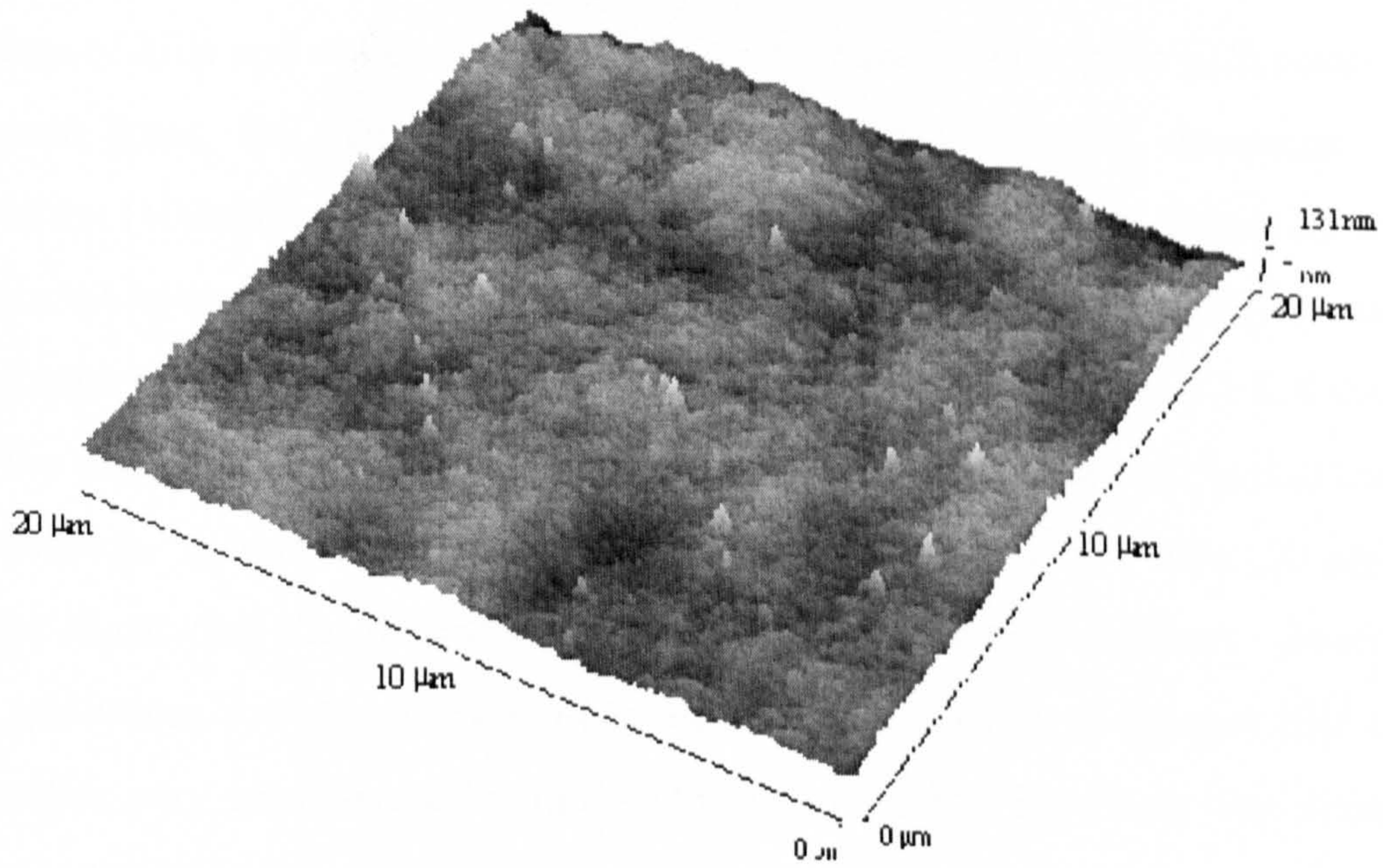

Figure 6.3. Osmonics SG AFM image, (20x20 μm)

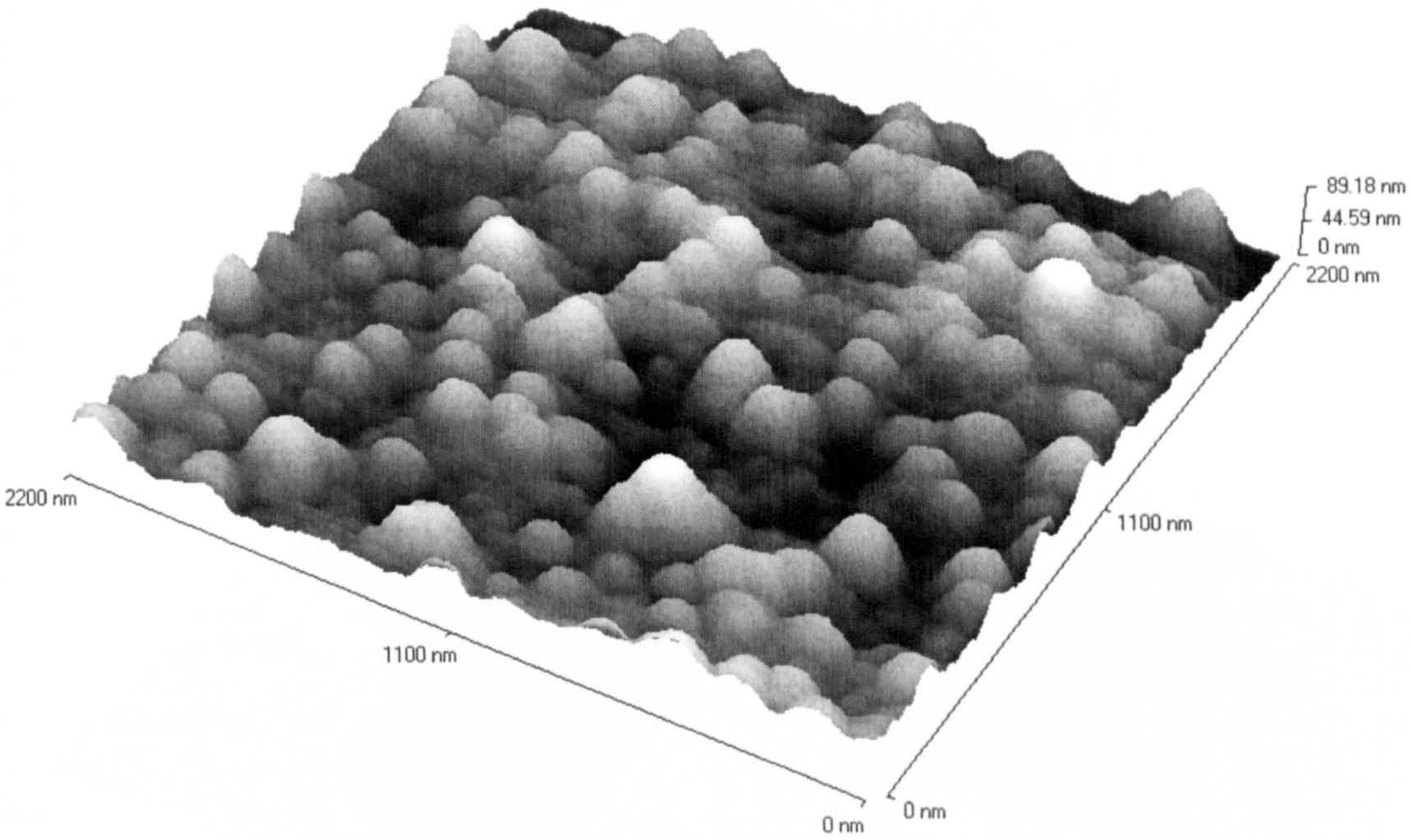

Figure 6.4. Osmonics SG AFM image, (2.2x2.2 μm)

From these figures the membrane surface details are very clear. The surface mainly consists of hills and valleys. Osmonics SG is found to have hills with rounded apexes. In some areas, the membrane surface is flat and these hills disappear. At lower resolution (100x100 μm, 50x50 μm and 20x20 μm) these details cannot be seen and the membrane overall form is seen. Also, at the lower resolution it can be seen that the membrane surface property is not entirely uniform. From Figures 6.1-6.4 it can be seen that the maximum peak height is different for these images suggesting that the surface is not uniform. A hole in the active layer was also observed in the 100x100 μm resolution image, illustrating that defects are present on the membrane surfaces. Even at 2.2x2.2 μm resolution, it was observed upon reviewing a couple of images that the surface properties vary in different locations (see Figure 6.5). However, the main structural features are uniform.

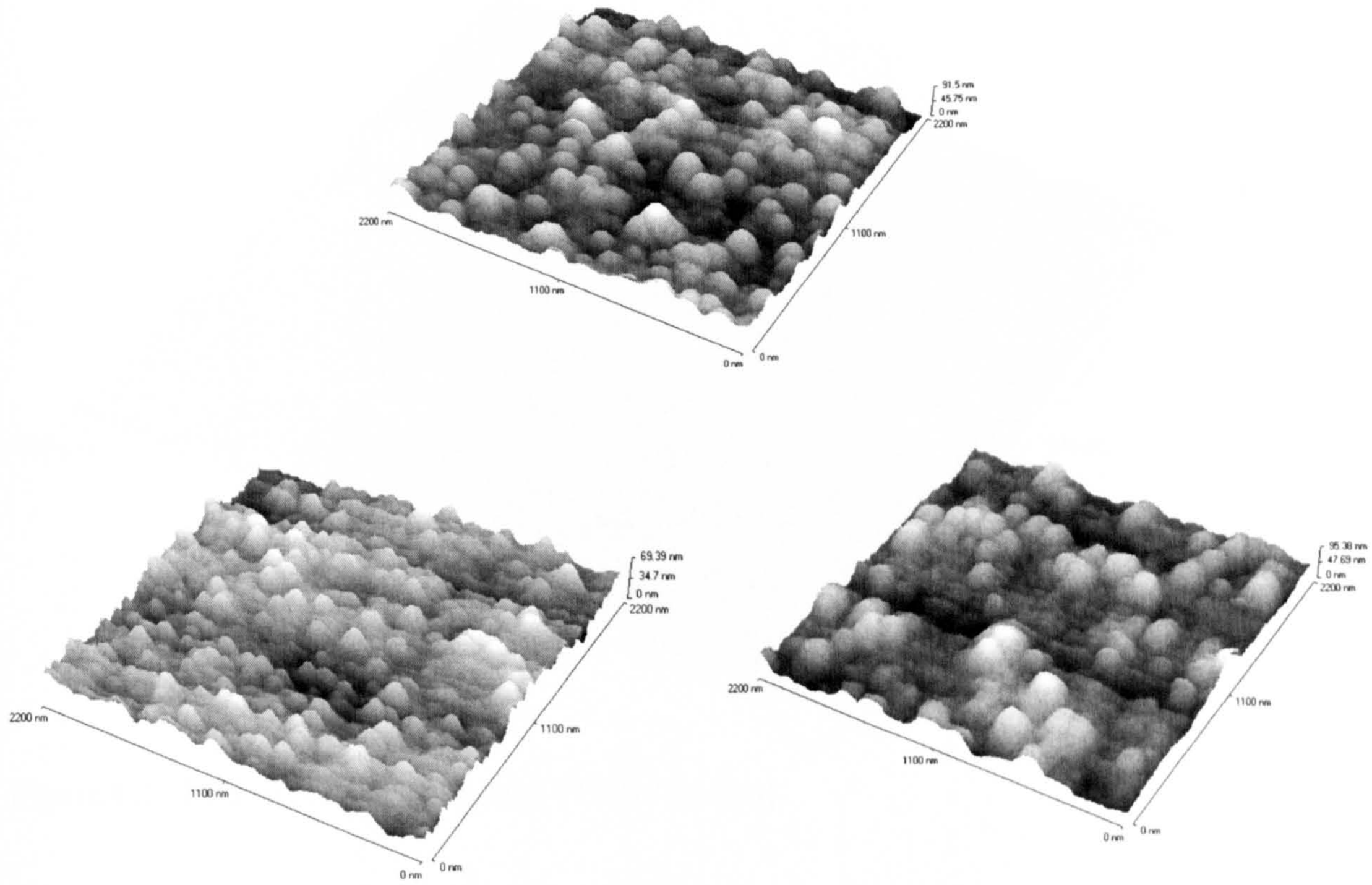

Figure 6.5. Osmonics SG images for different parts

From this initial qualitative assessment, it is important to realize that a single image is not sufficient in assessing the membrane surface morphology. However, some literature papers have reported details on the membrane surface properties based on a single AFM image.

6.2.2 Assessment of TriSep X20 active layer surface

In a similar manner to Osmonics SG the TriSep X20 AFM images were collected and compared with Osmonics SG to identify similar/unsimilar surface characteristics. The TriSep X20 membrane was imaged in the same scan range as Osmonics SG (100x100 μm, 50x50 μm, 20x20 μm and 2.2x2.2 μm). Figures 6.6-6.9 show the AFM images for this membrane.

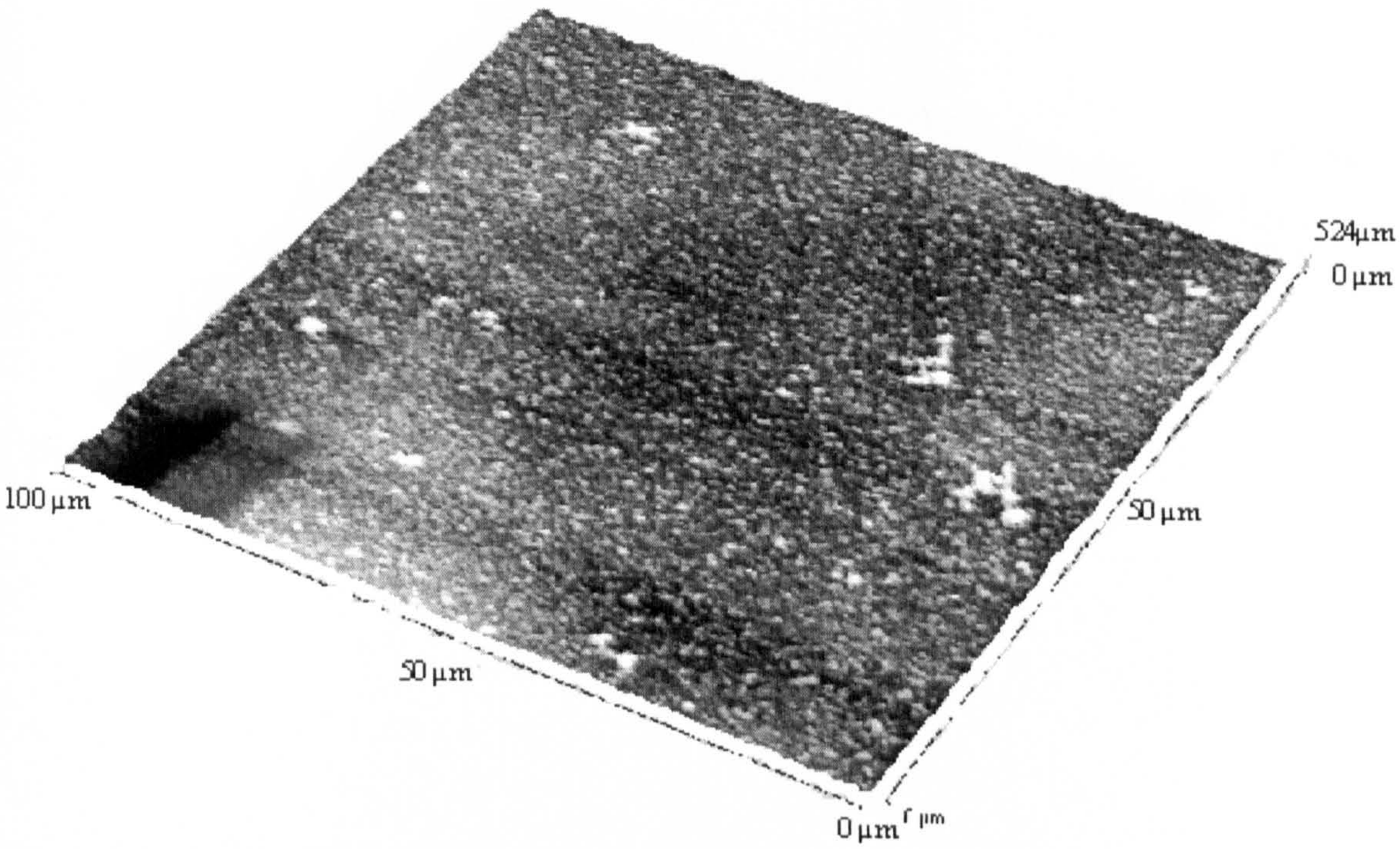

Figure 6.6. TriSep X20 AFM image (100x100 μm)

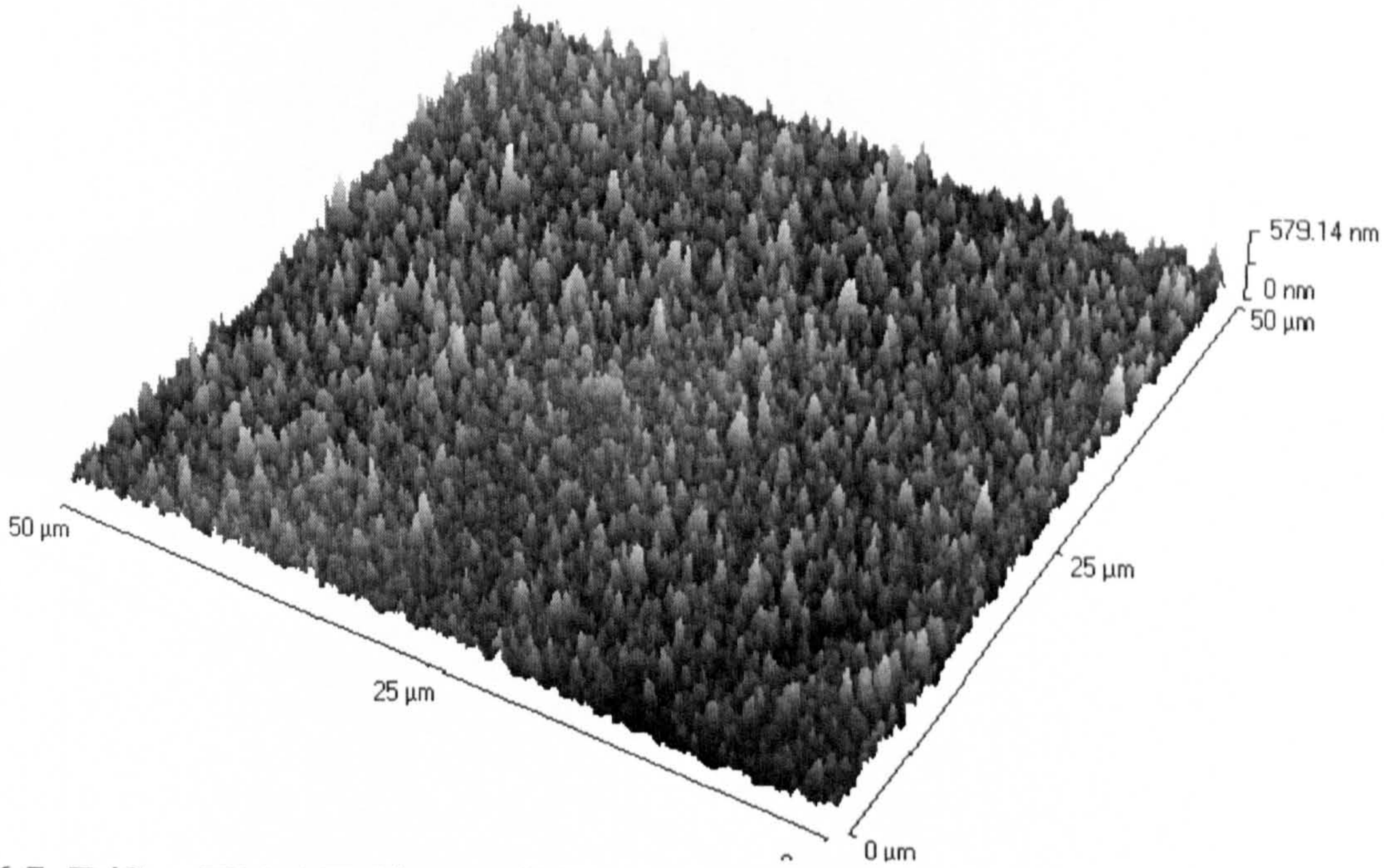

Figure 6.7. TriSep X20 AFM image (50x50 μm)

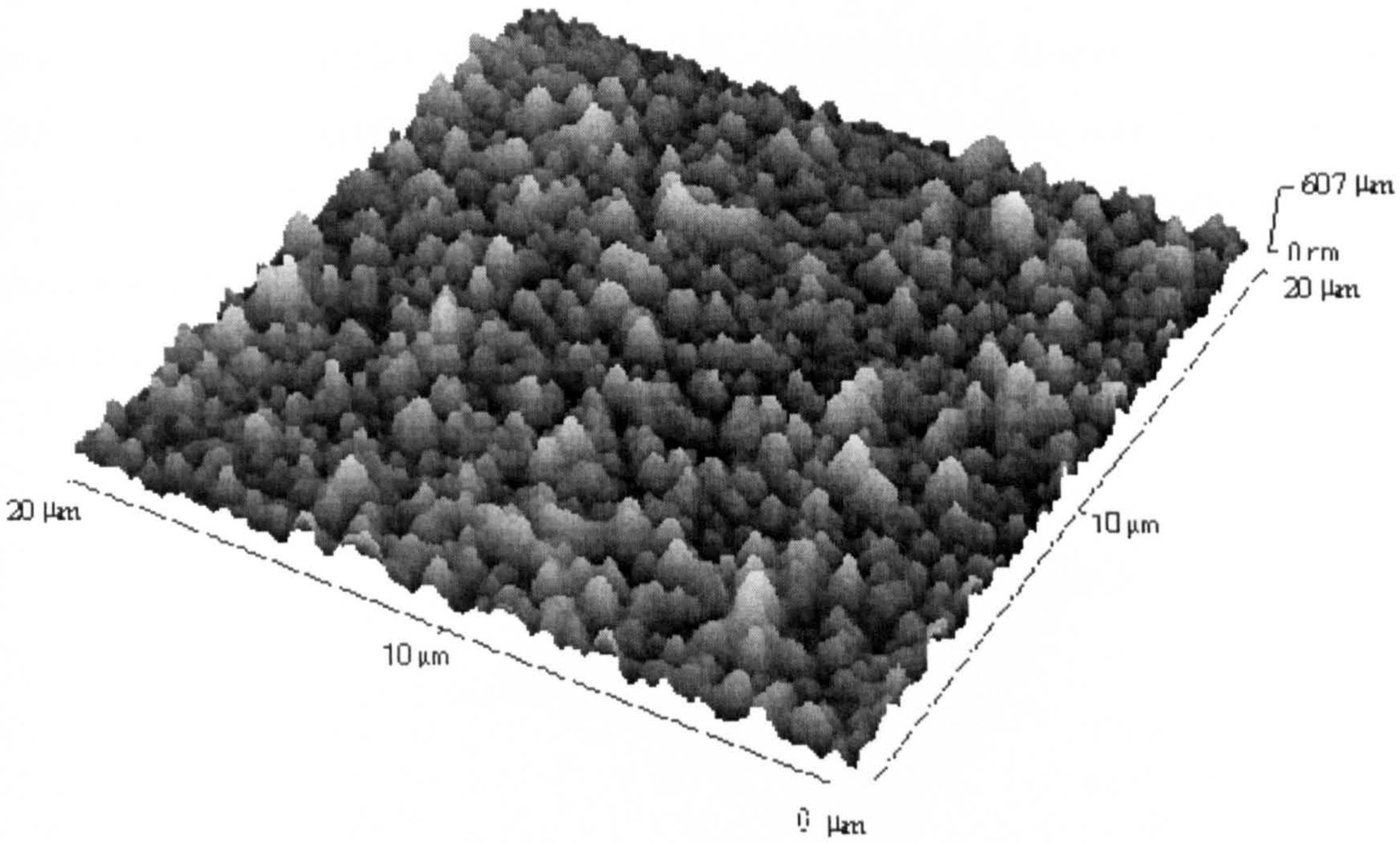

Figure 6.8. TriSep X20 AFM image, (20x20 μm)

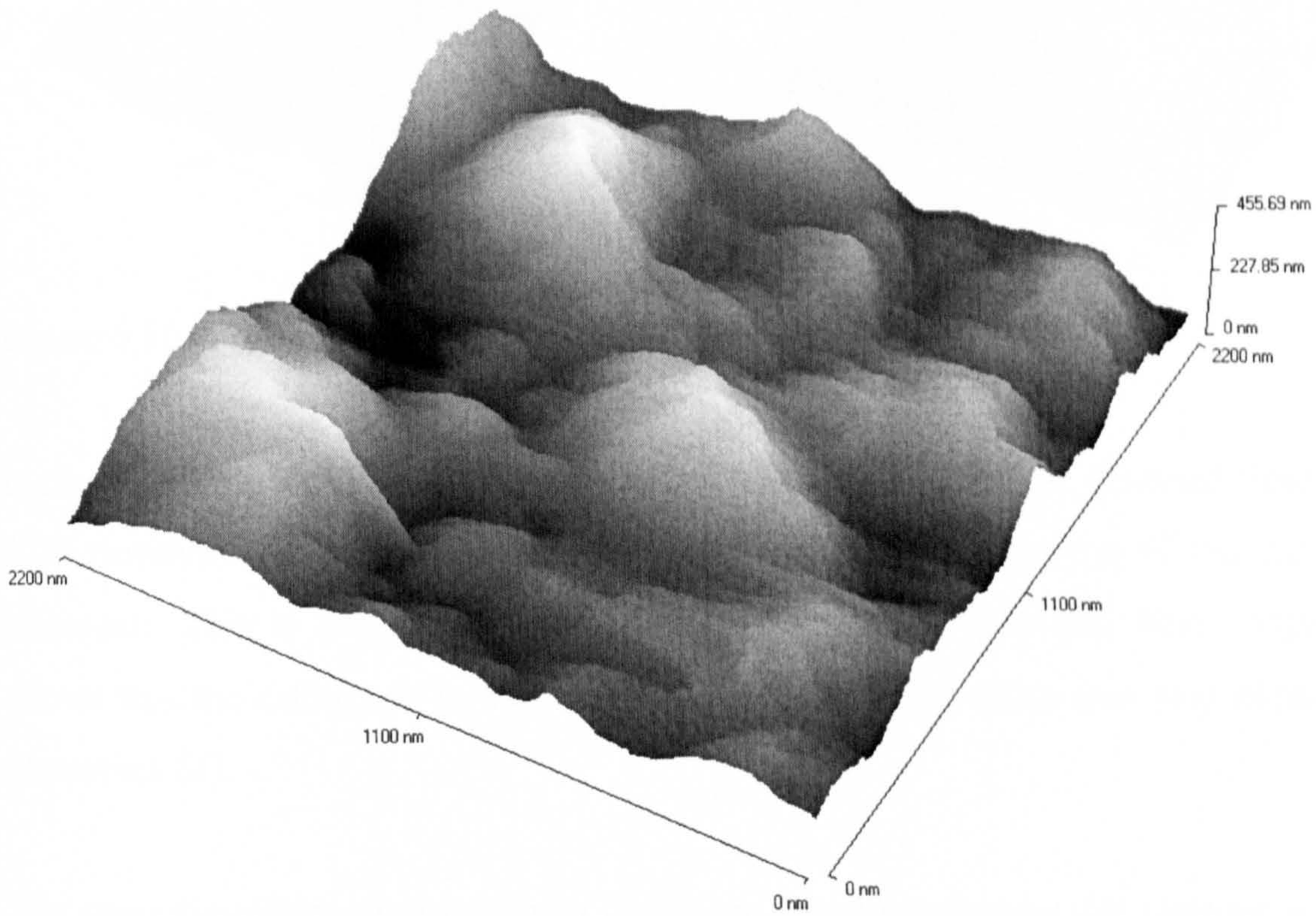

Figure 6.9. TriSep X20 AFM image, (2.2x2.2 μm)

From these figures it can be seen that TriSep X20 has a different surface morphology to Osmonics SG. It was observed that in some areas, the hill protrusions disappear and the surface is flat, which was similar to that observed in the Osmonics SG membrane. In

line scan analysis, which will be presented later in this chapter, the differences between these membranes are shown in more detail. Interestingly, it was observed that TriSep X20 images at 100x100 μm, 50x50 μm and 20x20 μm scan size, look more uniform than Osmonics SG. Different images collected from different parts at 2.2x2.2 μm resolution showed clearly that the membrane active layer surface is not uniform (see Figure 6.10).

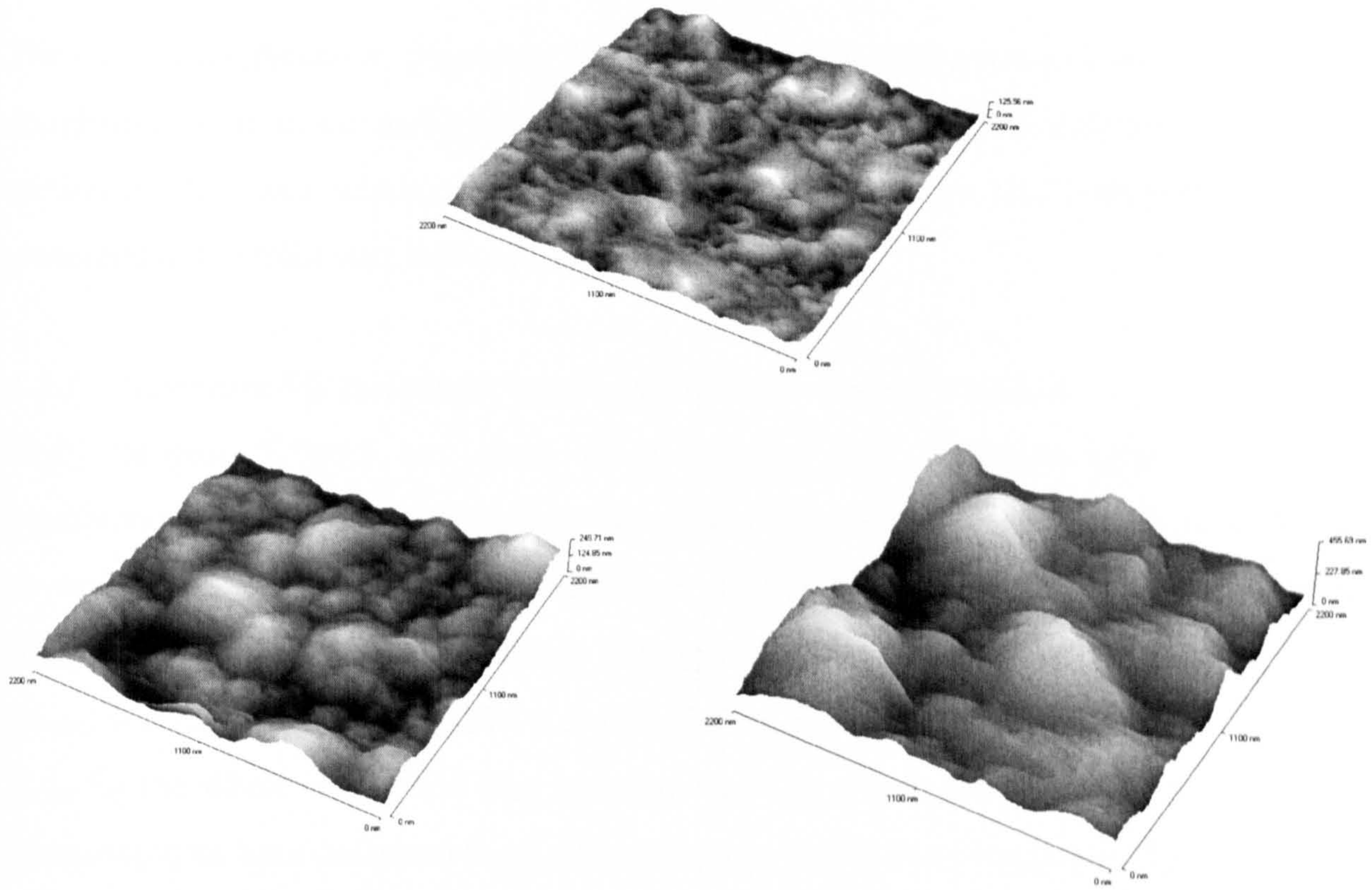

Figure 6.10. TriSep X20 membrane images (2.2x2.2 μm)

It can be seen from Figure 6.10 that although these images were obtained from TriSep X20 membrane at the same resolution, the physical characteristics of the surface are different. This is a very interesting finding and will be discussed later. Figure 6.10 shows that the difference in surface morphology is much more than that observed for Osmonics SG.

The preceding discussion has been based on visual assessment for Osmonics SG and TriSep X20 membranes. However, the goal is to assess each membrane surface according to roughness and hill height profile. Since these properties are determined based on membrane surface features, the membrane surface roughness and height profile are expected to vary at different locations. In the following section the

membrane surface roughness results for Osmonics SG and TriSep X20 will be discussed in depth to show the extent of variation in membrane surface properties for different locations. From this an assessment of the best way to assess the membrane surface properties can be made.

6.3 Membranes surface roughness characterization

The surface roughness of Osmonics SG, Osmonics AD, Osmonics AG and TriSep X20 membranes were calculated by software incorporated in the AFM instrument (refer to section 3.3 for more details). The surface roughness results for each membrane will be presented in the following sub-sections.

6.3.1 Osmonics SG membrane surface roughness characterization

Eight samples (0.5x0.5 cm^2 area) were collected from different locations on the membrane sheet to survey the membrane surface roughness. From these eight samples, several images were obtained with different resolution from several areas. From each image, the membrane average surface roughness (R_a) and root mean surface roughness (R_{rms}) were calculated. The AFM software has the ability to calculate membrane R_a and R_{rms} for the whole image and also for sections of it. From each image five roughness measurements were collected from different areas within that image (see Figure 6.11) to obtain a range of the roughness values.

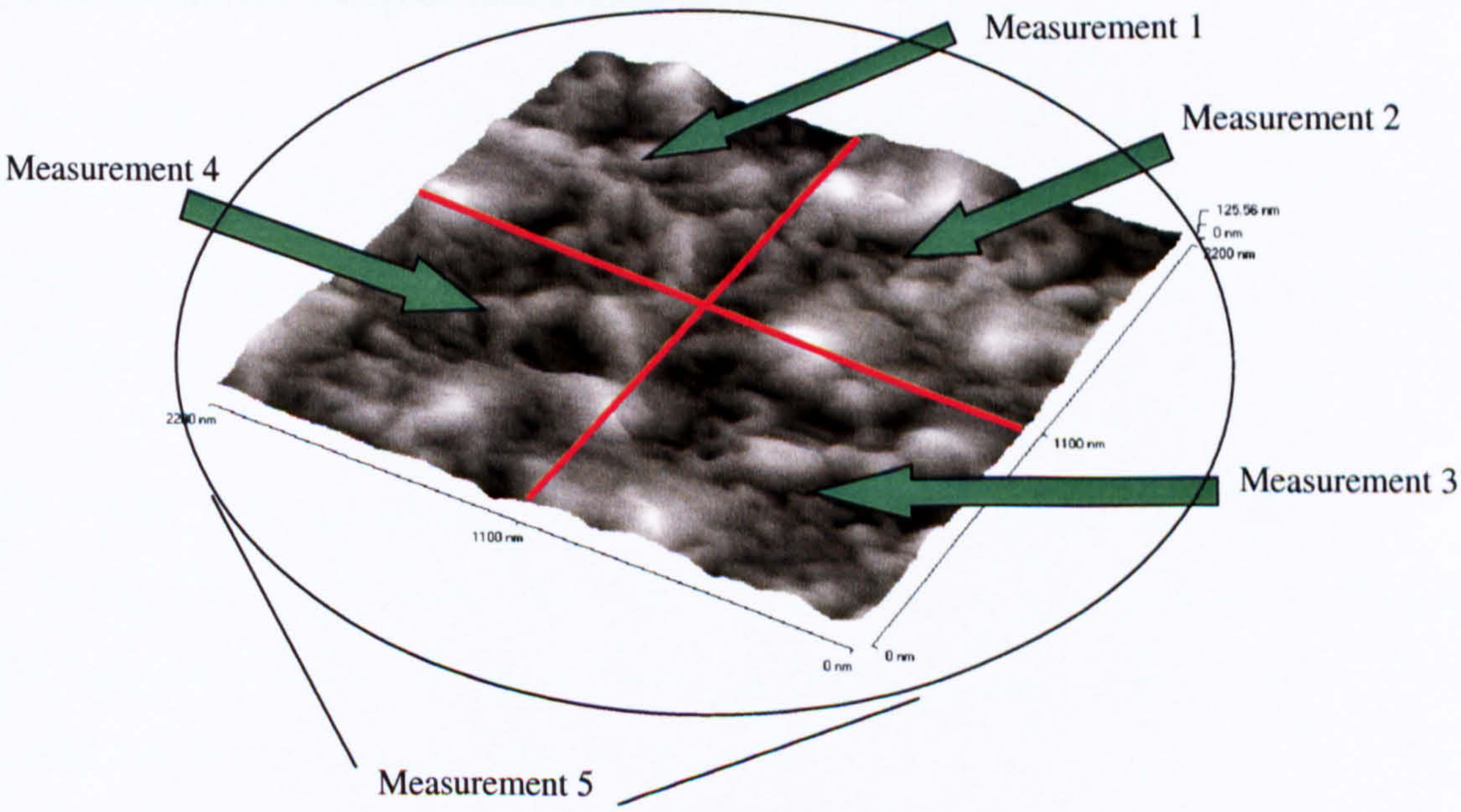

Figure 6.11. AFM image surface roughness measurement sections

It was found that the difference between R_a and R_{rms} for any imaged section (see Figure 6.12) on 20 different locations is always similar and both take the same trend. In section 3.3 definitions for R_a and R_{rms} are given and this shows that R_a and R_{rms} are based on the same measurement and different statistical analysis. Therefore R_a will be used to characterize the membrane surface roughness.

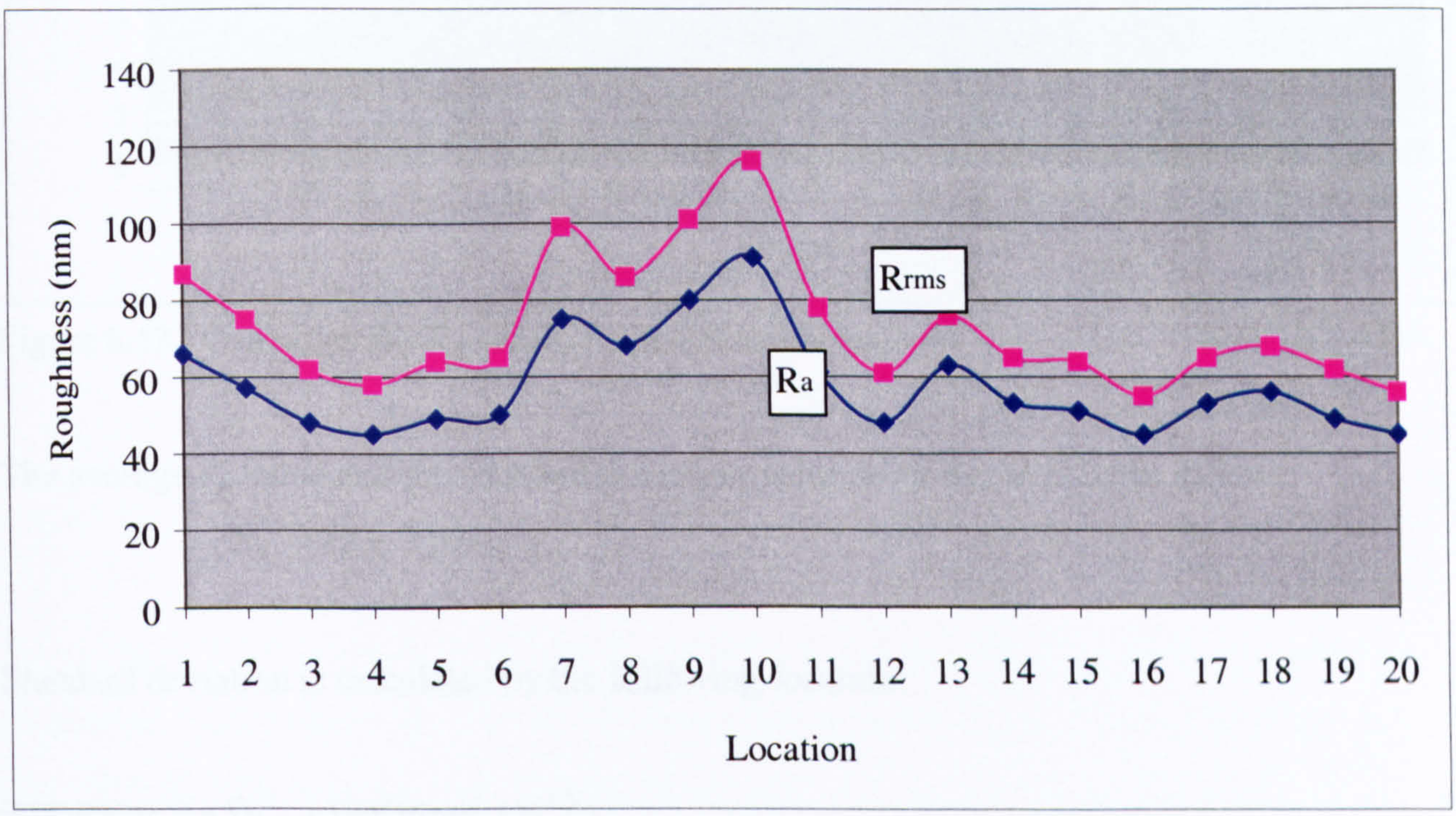

Figure 6.12. TriSep X20 membrane surface roughness in 20 different locations

Seventy-five R_a values were obtained from the 15 images, which were collected from 8 different membrane samples (see Figure 6.13).

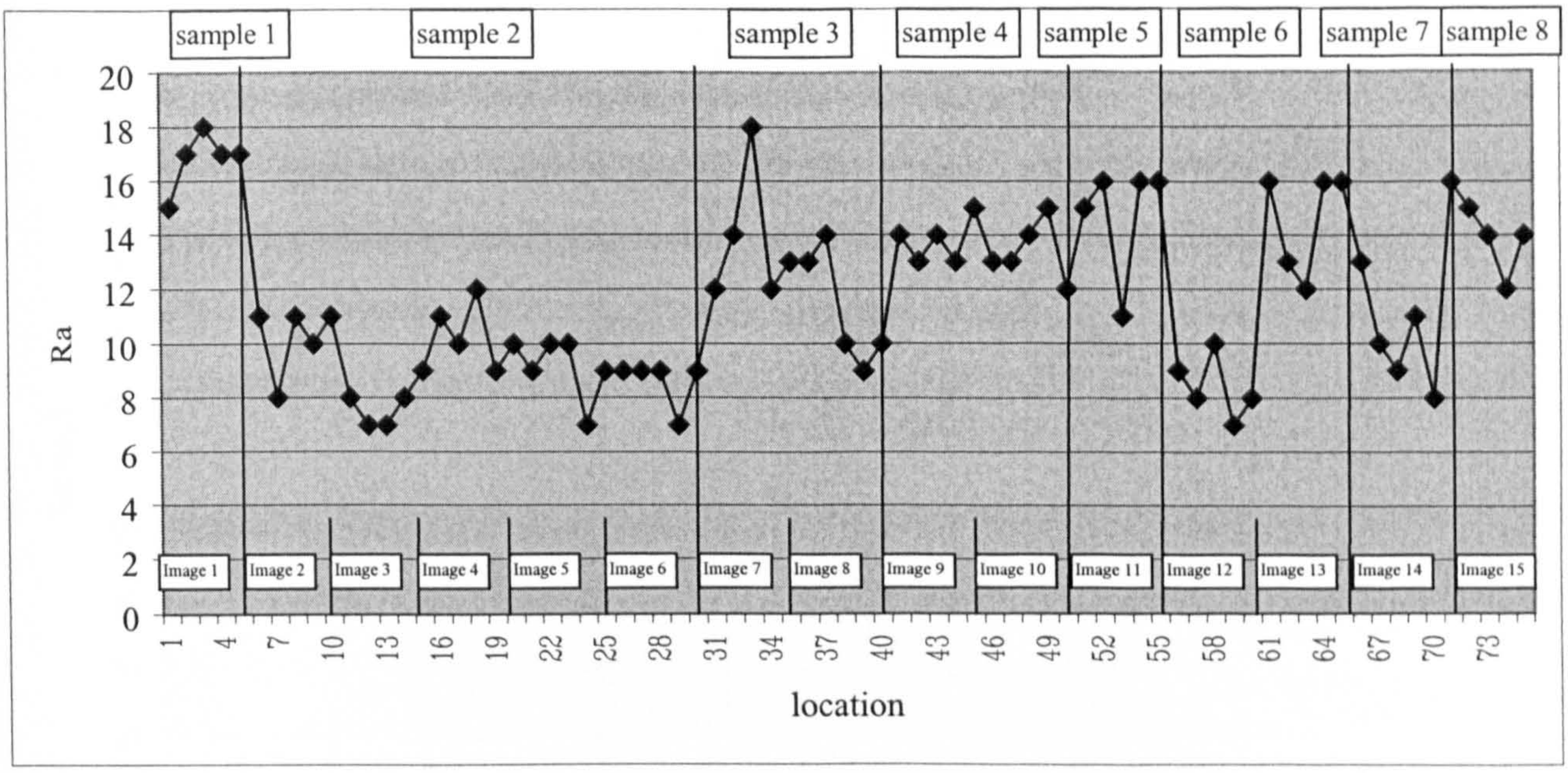

Figure 6.13. Osmonics SG R_a values from different locations

The average R_a value and the standard deviation value were found to be as follows:

$$R_a = 12 \pm 3 \text{ nm}$$

Standard deviation is calculated by the following formula:

$$STDEV = \{[n\sum x^2 - (\sum x)^2]/[n(n-1)\}^{1/2}$$

Where n is the number of roughness values used in the calculation and x is the roughness value.

Upon reviewing carefully all R_a values it was noticed that some images have lower values than others, such as image 1 and 2. For image 1, the R_a value is between 15-18 nm and for image 2, it is between 8-10 nm. It is observed also that different samples give different roughness values.

6.3.2. TriSep X20 membrane surface roughness characterization

For TriSep X20, the R_a value was evaluated based on 75 measurements collected from eight samples, which is similar to Osmonics SG (see Figure 6.14). The roughness and the standard deviation values were found to be:

$$R_a = 52 \pm 13 \text{ nm}$$

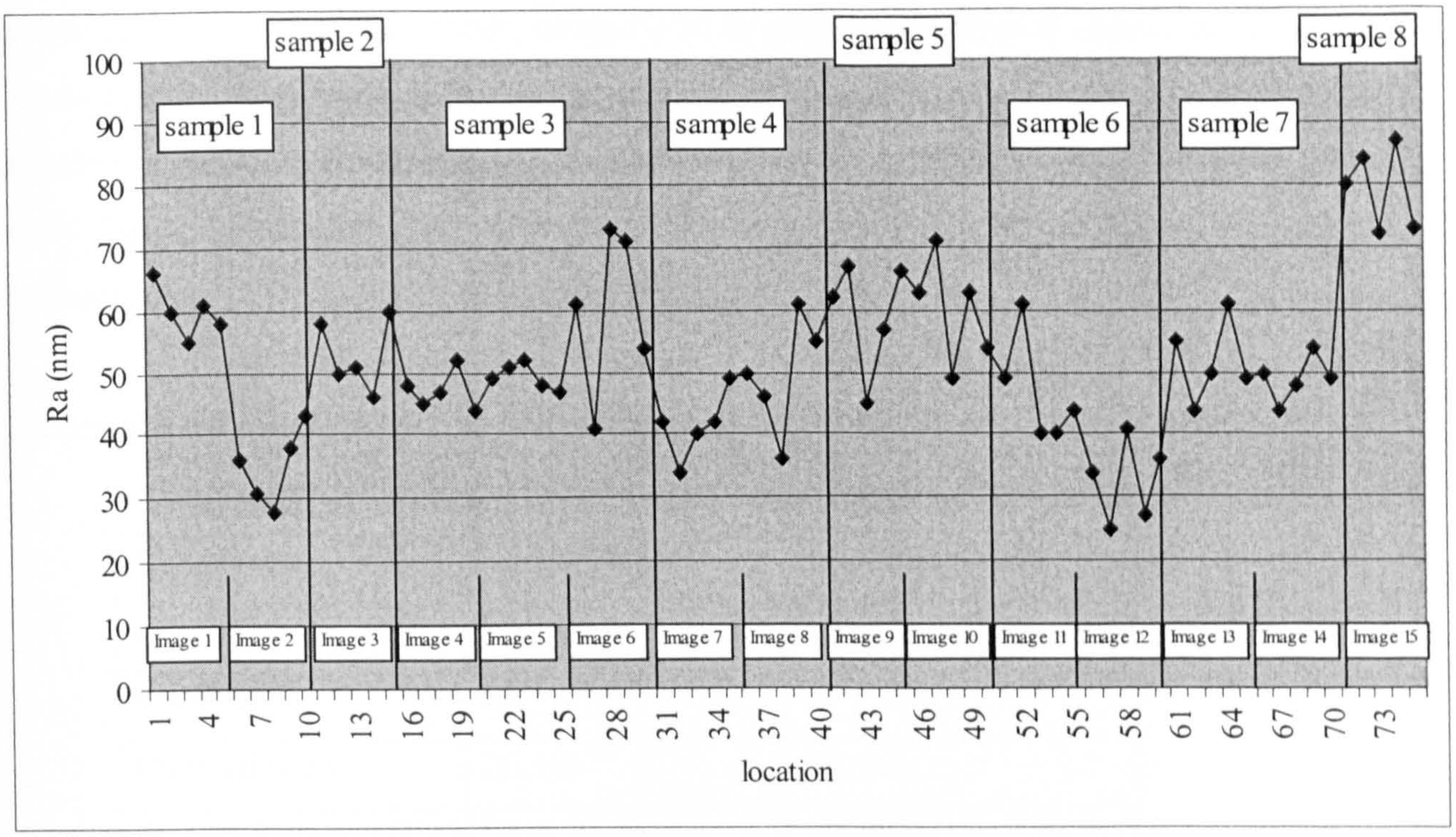

Figure 6.14. TriSep X20 R_a values from different locations

From Figure 6.14, it can be seen that R_a values can vary significantly from one section to another. In image 12, a value of 33 nm was reported for R_a, and in image 15 the R_a was 79 nm. This suggests that a single image will also not give an accurate estimation for TriSep X20 membrane and in fact the degree of variation in this membrane is significantly larger. The question therefore arises as to how many images are required to give a good representation? It is believed that a minimum of three images from different samples is required to get a reasonable estimation of the membrane surface roughness.

It has to be realized that it is important to image different samples from the membrane sheet to be confident that the images are representative of the whole surface. Based on above the following is suggested in the event of estimating membrane surface roughness:

1. At least three images should be used to estimate membrane surface roughness
2. These images should be collected from three membrane samples (the sample is the sheet required to glue on a metal for AFM imaging and it is usually 0.5x0.5 cm^2)
3. Several values from each image are required. In this work at least 5 were taken.

As the main point from this work, using AFM to assess the physical roughness it can be concluded that there is no doubt that one image is not sufficient to accurately describe a membrane surface and some progress in formulating an assessment of surfaces has been made here. Osmonics AG and Osmonics AG were evaluated based on above methodology.

The roughness values for all membranes are summarized below:

Membrane	R_a value (nm)	R_{rms} value (nm)
Osmonics SG	12 ± 3	16 ± 3
Osmonics AD	33 ± 6	43 ± 9
Osmonics AG	26 ± 4	34 ± 3
TriSep X20	52 ± 13	68 ± 17

Table 6.1. The roughness (R_a) values for the four tested membranes

Note that in Table 6.1, the root mean square surface roughness (R_{rms}) is also reported for the four membranes. In obtaining R_{rms} values a similar approach was used as was done for R_a. The AFM software gives both roughness values each time.

6.4 Membranes peak height profile characterization

The AFM software permits the measurement of height variations in the surface of the membranes along a predetermined line in the image. Figures 6.15-6.18 show the line analyses for Osmonics SG, Osmonics AD, Osmonics AG and TriSep X20 membrane surfaces. Such analysis helps to give more details about the differences in surface morphology of the membranes.

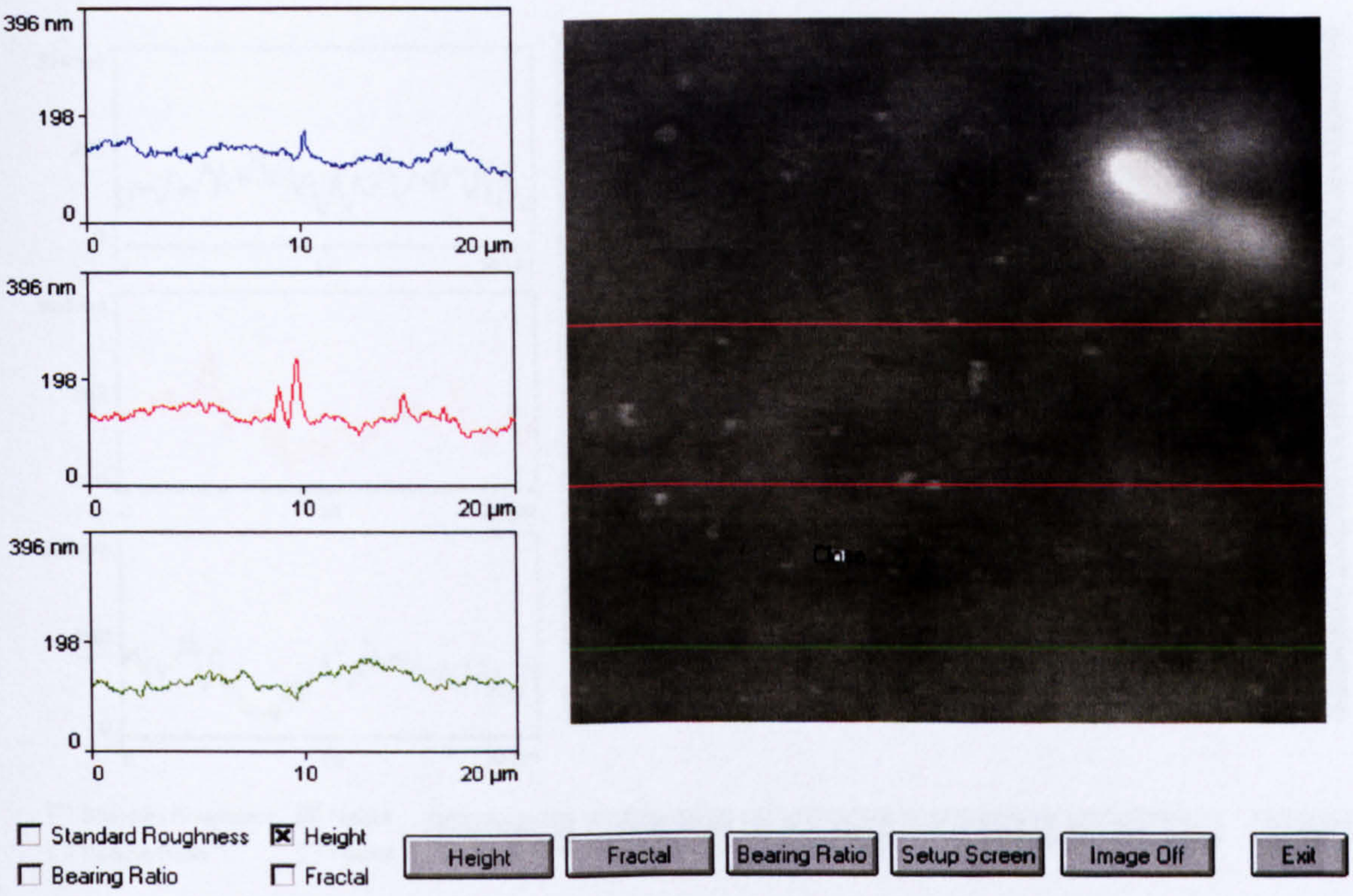

Figure 6.15. Line analysis for Osmonics SG membrane surface

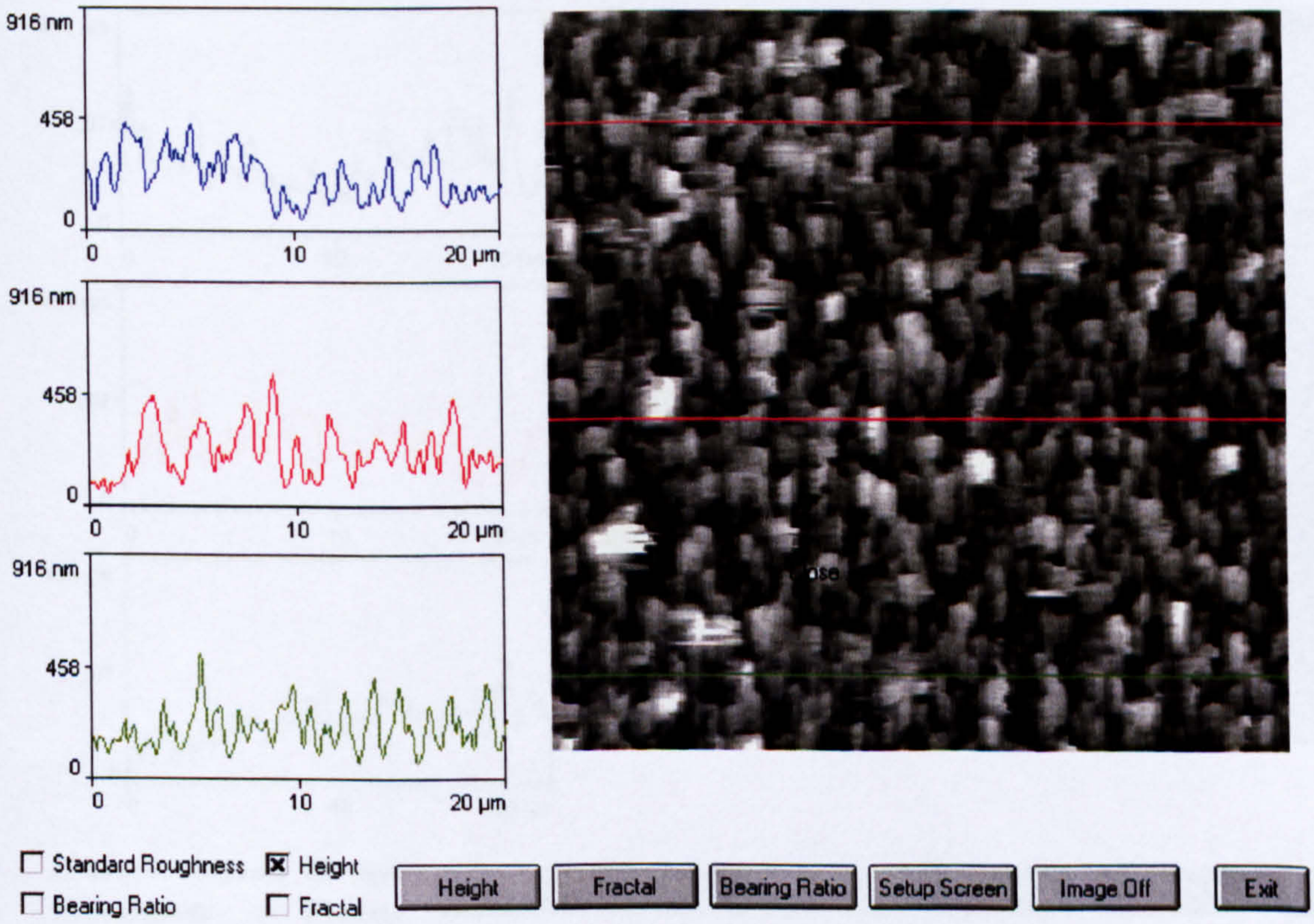

Figure 6.16. Line analysis for TriSep X20 membrane surface

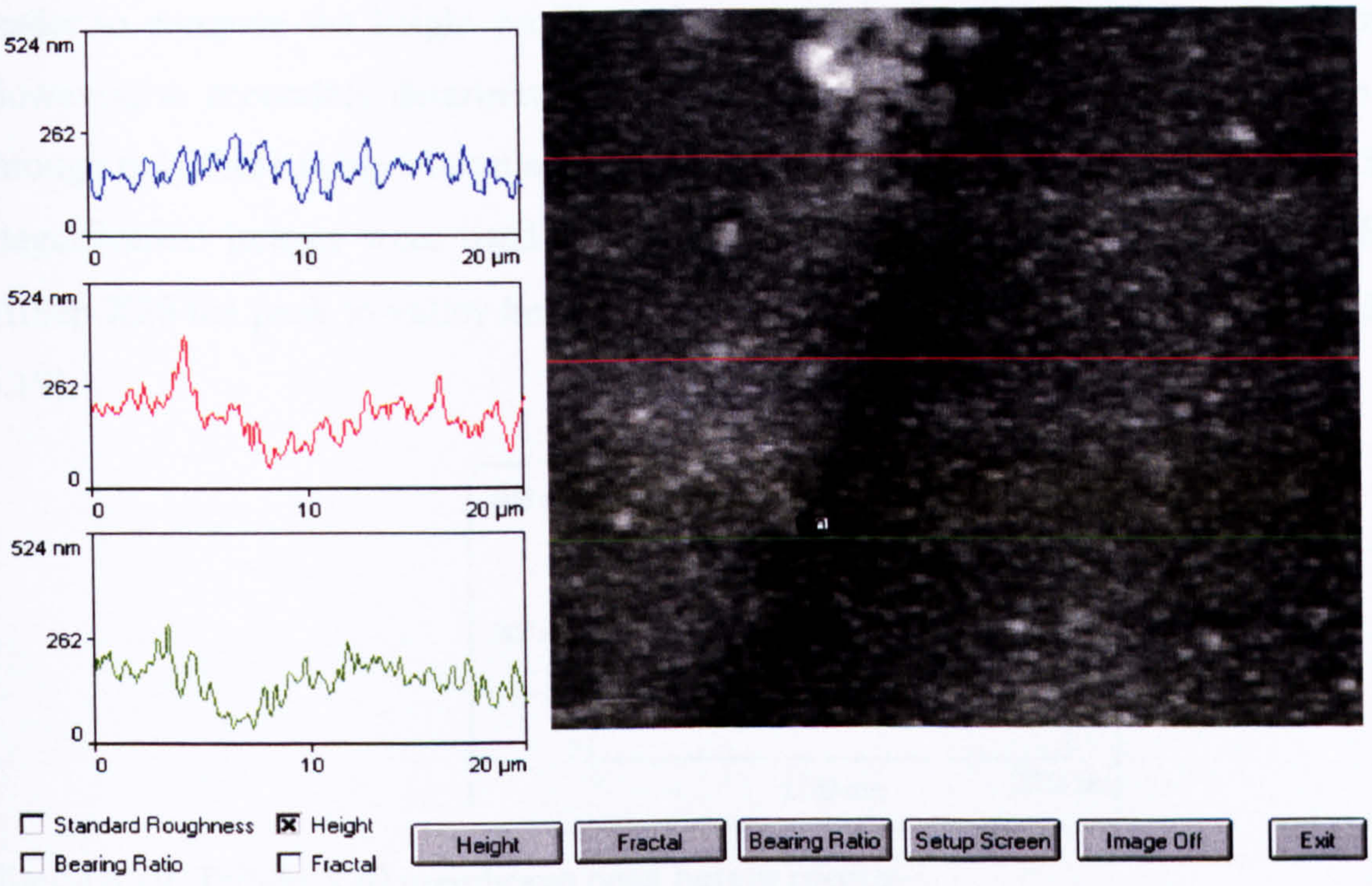

Figure 6.17. Line analysis for Osmonics AG membrane surface

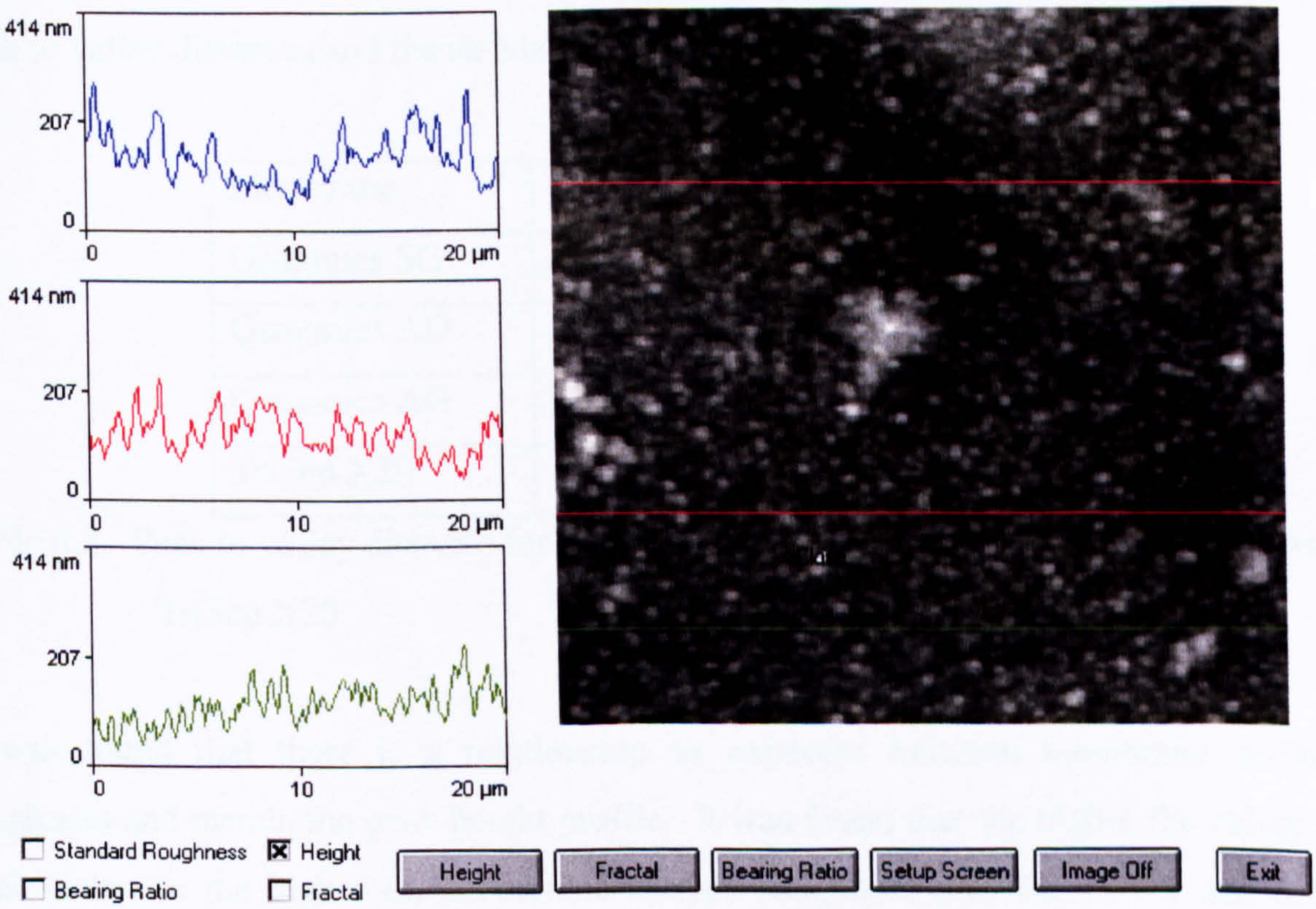

Figure 6.18. Line analysis for Osmonics AD membrane surface

All membranes in the previous images are from 20x20 μm resolution to enable the reader to compare the height profile and the overall form between these membranes. However, to accurately determine the exact height profile, it was impossible to do it through only these images because the magnification is not sufficient. Therefore, higher magnification images were used to get accurate measurements. As an example, for TriSep X20 the peak to valley height is determined from 2.2x2.2 μm image (see Figure 6.19).

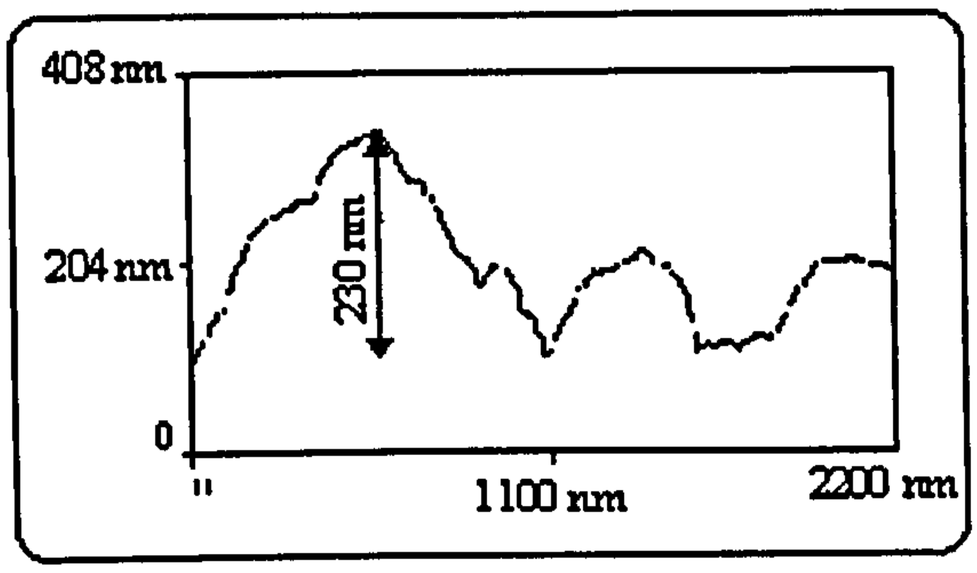

Figure 6.19. TriSep X20 membrane peak height profile

A number of peak to valley distances are obtained from different images for the four membranes to get a representative value for peak to height profile. Table 6.2 gives the peak to valley distances and the standard deviation values for the four membranes.

Membrane	Peak to valley (nm)
Osmonics SG	30 ± 10
Osmonics AD	40 ± 20
Osmonics AG	60 ± 25
TriSep X20	200 ± 40

Table 6.2. Peak to valley distance for Osmonics SG, Osmonics AD, Osmonics AG and TriSep X20

It was found that there is a relationship as expected between membrane surface roughness and membrane peak height profile. It was found that the higher the valley to peak distances the higher the membrane surface roughness (see Tables 6.1 and 6.2). The line profiles showed clearly that these images have different surface characteristics.

6.5 Membranes thickness characterization

AFM does not present the best methodology to characterize the membrane cross section. Therefore, Light Microscope and SEM were used in part of the research. The Light Microscope was employed to assess the cross-section thicknesses of Osmonics SG, Osmonics AD, Osmonics AG and TriSep X20 membranes. Figures 6.20-6.23 show Osmonics SG, Osmonics AD, Osmonics AG, and TriSep X20 membranes cross-section images. Table 6.3 shows the thickness of each membrane in 3 different locations and the average of these thicknesses.

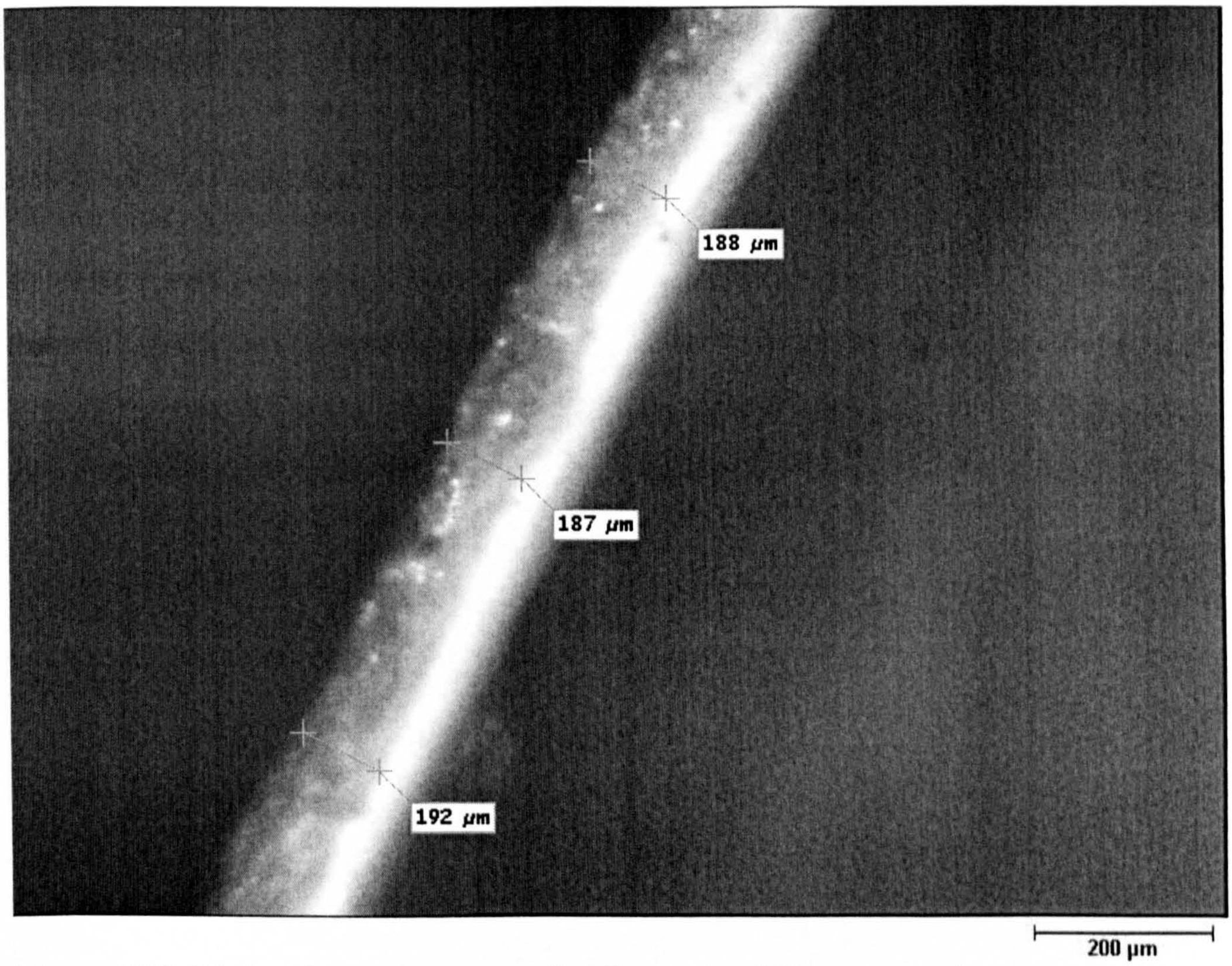

Figure 6.20. Light microscope image for Osmonics SG cross-section

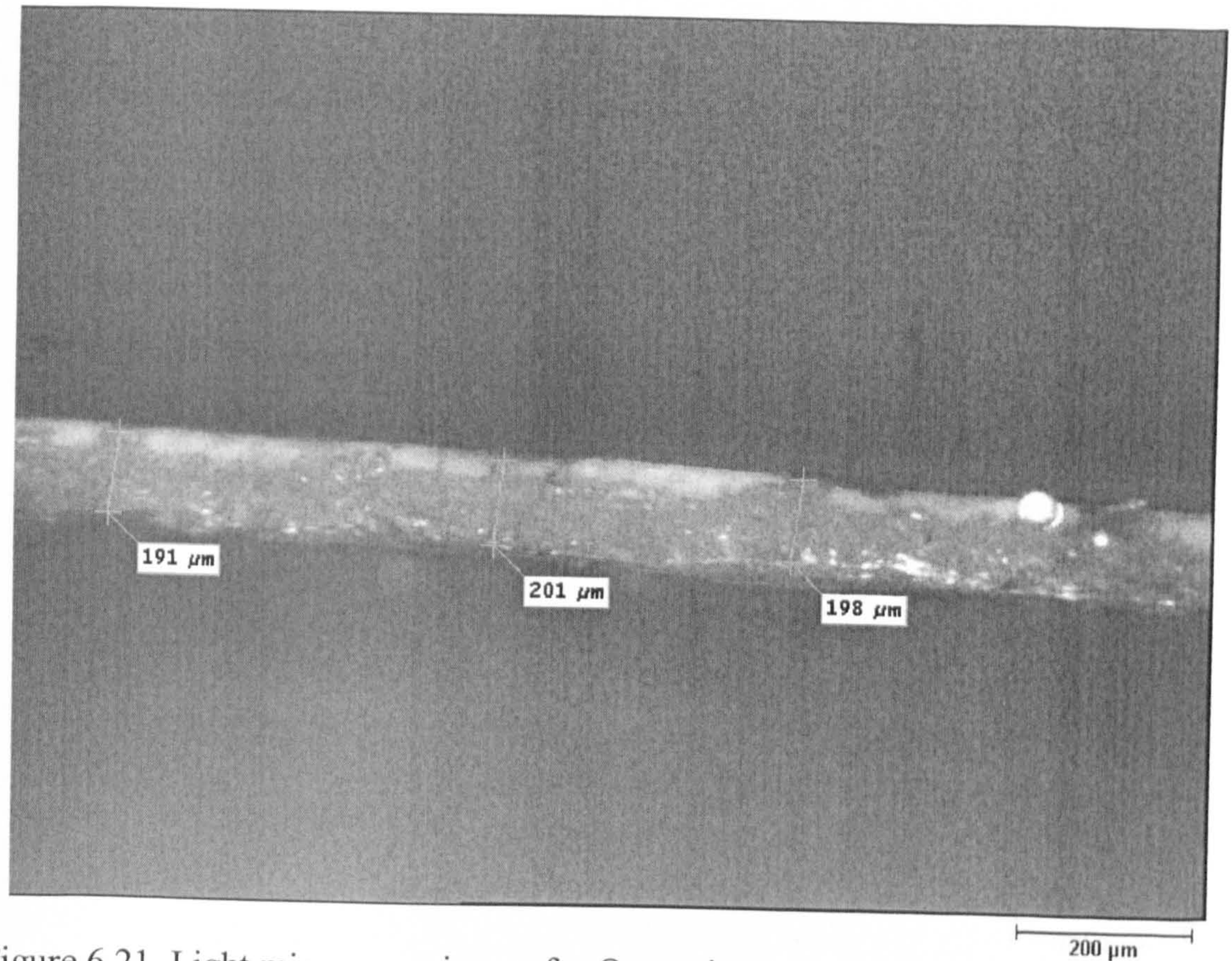

Figure 6.21. Light microscope image for Osmonics AD cross-section

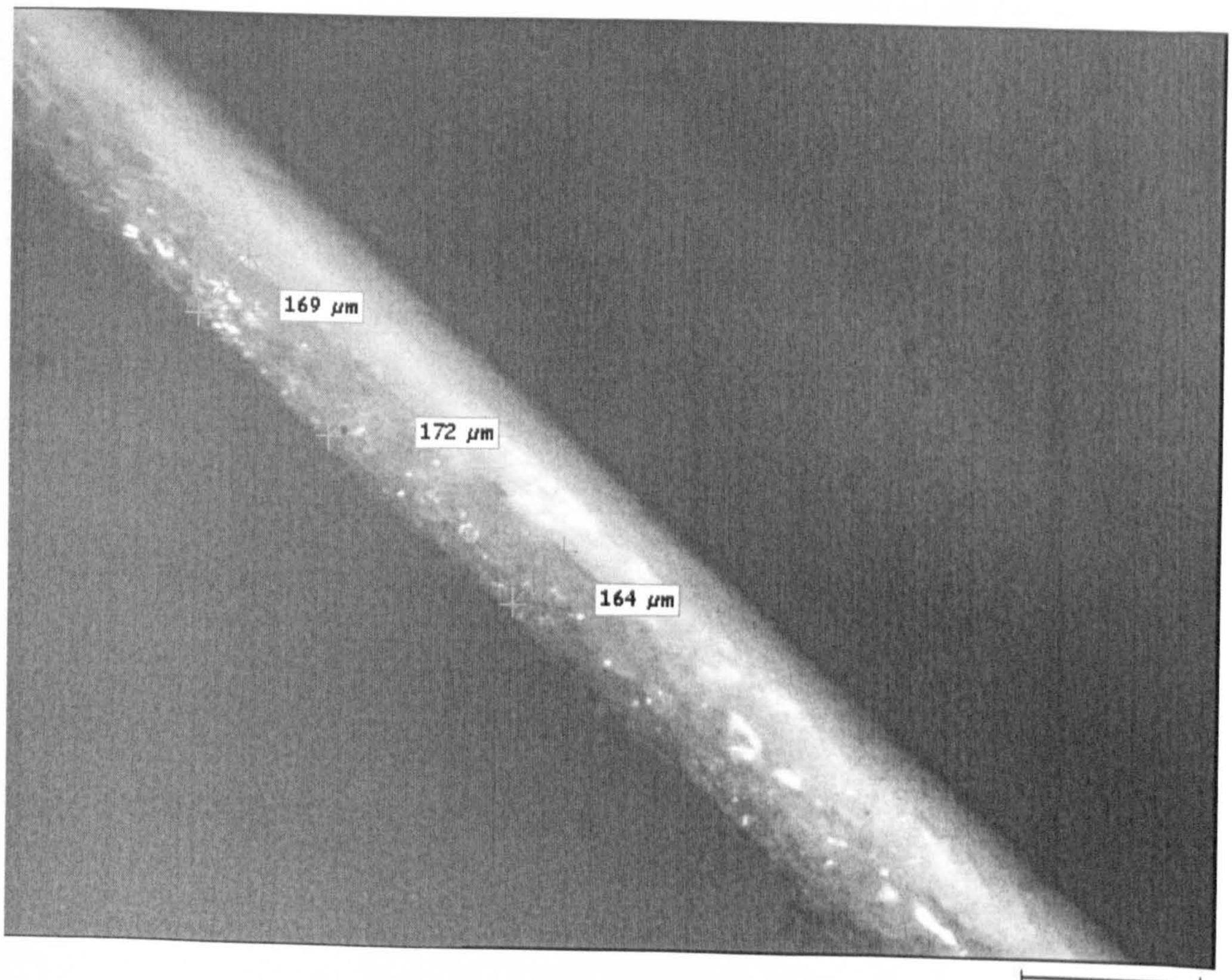

Figure 6.22. Light microscope image for Osmonics AG cross-section

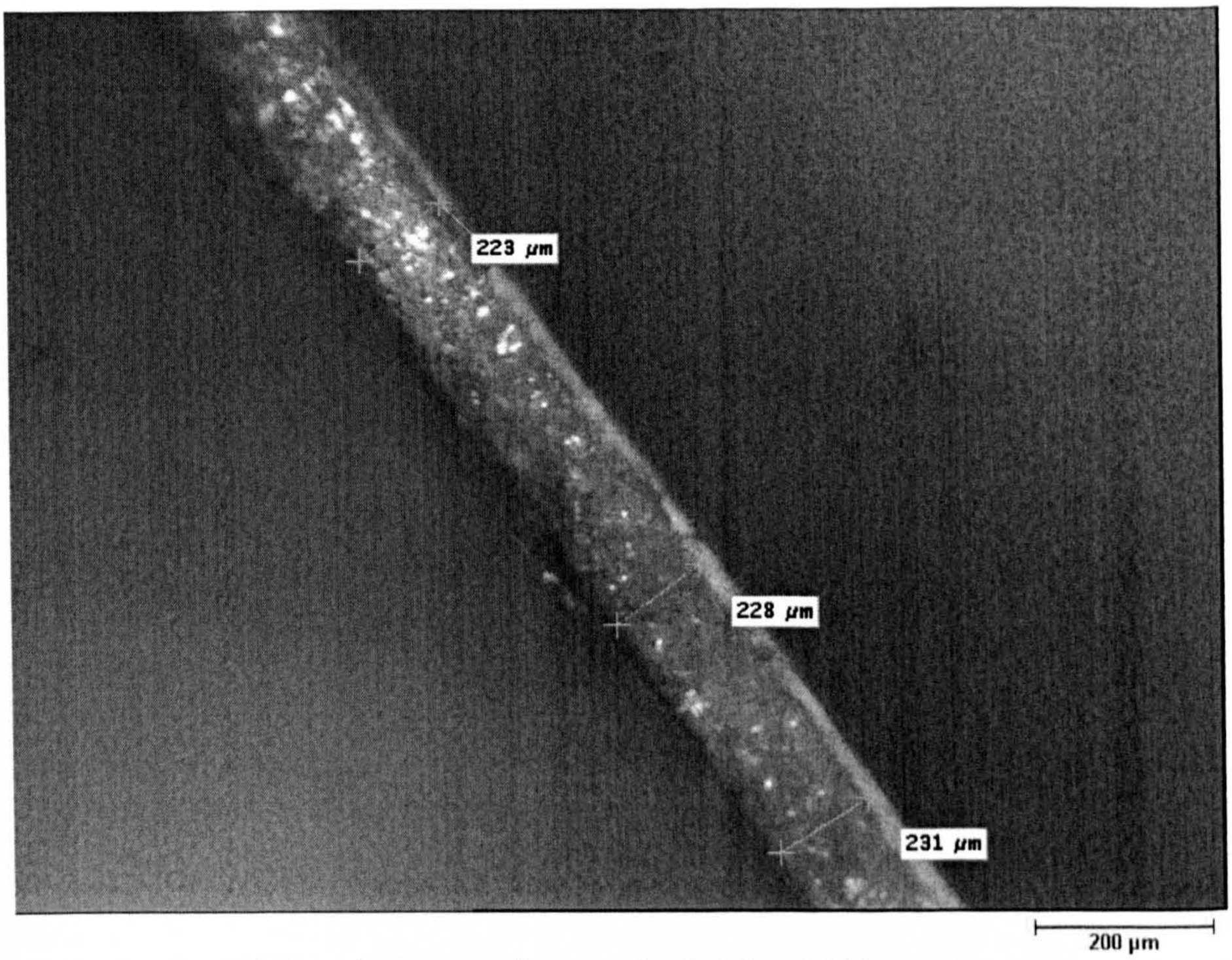

Figure 6.23. Light microscope image for TriSep X20 cross-section

Membrane	Thickness (μm) location 1	Thickness (μm) location 2	Thickness (μm) location 3	Average thickness
Osmonics SG	188	187	192	189
Osmonics AD	191	201	198	197
Osmonics AG	169	172	164	168
TriSep X20	223	228	231	227

Table 6.3. Osmonics SG/AD/AG and TriSep x20 membranes cross-section thickness

Later in this chapter the effect of membrane thickness on production rate will be assessed to determine the role of membrane thickness in membrane permeation rate.

6.6 Membrane flux characterization

In this section the membrane flux for the membrane was characterized. The purpose of this part of the study was to investigate the relationship between the physical nature of the membrane and the flux given the apparent discrepancies in the literature. In chapter 7 much more detailed study of the membranes is presented. Flux measurements of

Osmonics SG, Osmonics AD, Osmonics AG and TriSep X20 were conducted in triplicate at constant operating parameters (feedwater pressure, temperature, conductivity, flow and pH were 140 MN/m^2, 30 °C, 2800 µS, 11.7 x 10^{-5} m^3/s, and 8 respectively) and the results are given in Table 6.4.

Membrane	1st run	2nd run	3rd run	Average ± Standard deviation
Osmonics SG	65	58	54	59 ± 6
Osmonics AD	7	6	10	8 ± 2
Osmonics AG	82	77	72	77 ± 5
TriSep X20	10	9	8	9 ± 1

Table 6.4. Osmonics SG/AD/AG and TriSep X20 membranes flux in $l/h/m^2$

From Table 6.4, it can be seen that the Osmonics SG flux is significantly greater than the value for TriSep X20. Since there is a great difference in permeation rate between Osmonics SG and TriSep X20, both membranes were tested in various operating conditions to evaluate the variation in permeation rate and results are presented in Figure 6.24.

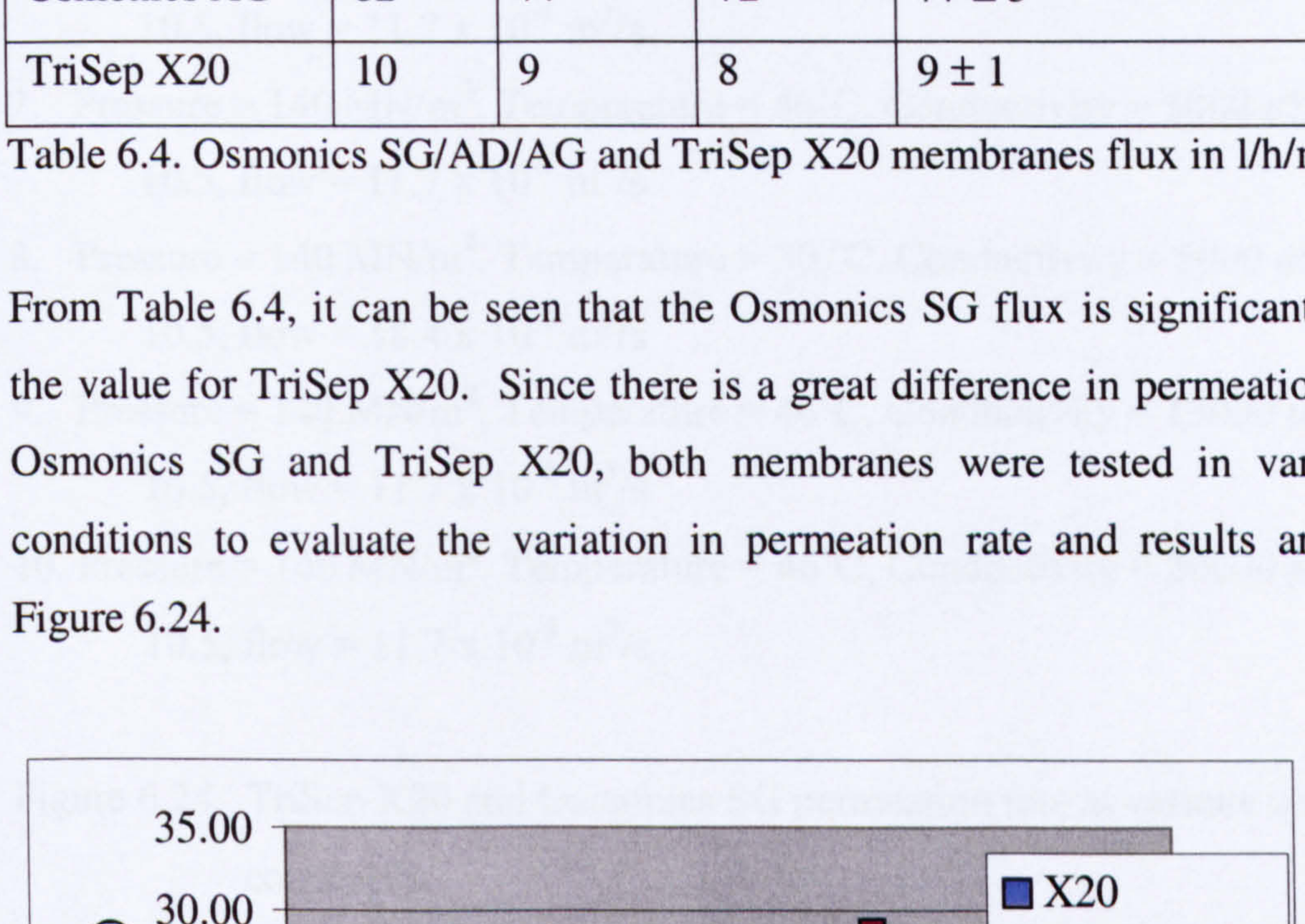

Conditions:

1. Pressure = 60 MN/m^2, Temperature = 30 °C, Conductivity = 5000 µS/cm, pH = 10.5, flow = 11.7 x 10^{-5} m^3/s

2. Pressure = 80 MN/m^2, Temperature = 30 °C, Conductivity = 25000 $\mu S/cm$, pH = 10.5, flow = 11.7 x 10^{-5} m^3/s
3. Pressure = 140 MN/m^2, Temperature = 30 °C, Conductivity = 5000 $\mu S/cm$, pH = 4, flow = 11.7 x 10^{-5} m^3/s
4. Pressure = 140 MN/m^2, Temperature = 40°C, Conductivity = 5000 $\mu S/cm$, pH = 10.5, flow = 11.7 x 10^{-5} m^3/s
5. Pressure = 140 MN/m^2, Temperature = 26°C, Conductivity = 5000 $\mu S/cm$, pH = 10.5, flow = 11.7 x 10^{-5} m^3/s
6. Pressure = 140 MN/m^2, Temperature = 38°C, Conductivity = 5000 $\mu S/cm$, pH = 10.5, flow = 11.7 x 10^{-5} m^3/s
7. Pressure = 140 MN/m^2, Temperature = 46°C, Conductivity = 5000 $\mu S/cm$, pH = 10.5, flow = 11.7 x 10^{-5} m^3/s
8. Pressure = 140 MN/m^2, Temperature = 30 °C, Conductivity = 5000 $\mu S/cm$, pH = 10.5, flow = 18.4 x 10^{-5} m^3/s
9. Pressure = 140 MN/m^2, Temperature = 46°C, Conductivity = 15000 $\mu S/cm$, pH = 10.5, flow = 11.7 x 10^{-5} m^3/s
10. Pressure = 140 MN/m^2, Temperature = 46°C, Conductivity = 20000 $\mu S/cm$, pH = 10.5, flow = 11.7 x 10^{-5} m^3/s

Figure 6.24. TriSep X20 and Osmonics SG permeation rate at various operating conditions

Figure 6.24 shows the permeation rates of Osmonics SG and TriSep X20 membranes in 10 different operating conditions, which cover a range of applicable to RO plants. It is clear that in all cases Osmonics SG permeation rate is significantly higher than TriSep X20 and they are proportional to each other (see Figure 6.25).

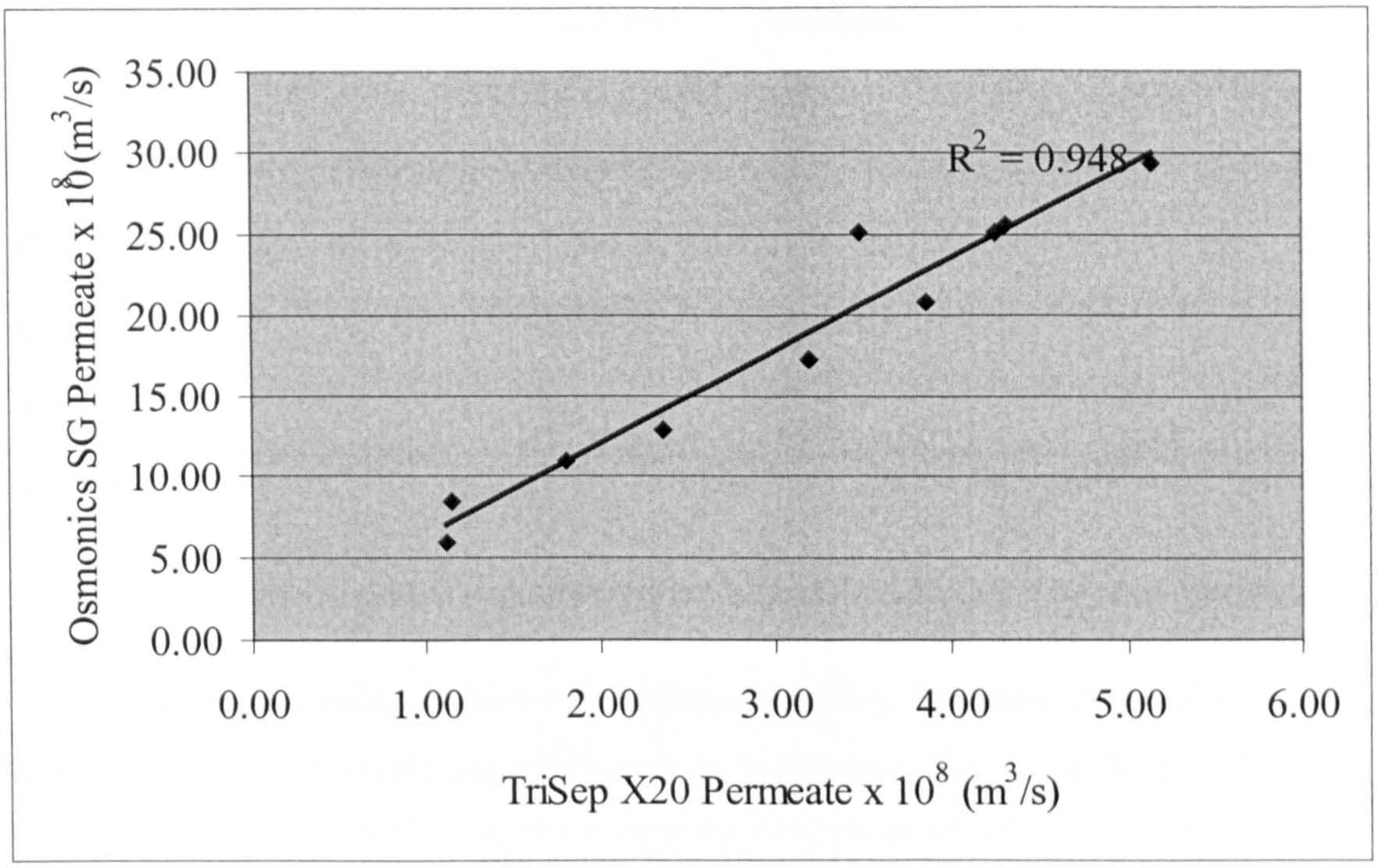

Figure 6.25. Relationship between Osmonics SG and TriSep X20 permeation

This implies that the influence of different operating parameters on Osmonics SG and TriSep X20 is not always identical possibly due to owing different surface morphology and cross-section thicknesses.

6.7 The relationship between membranes surface properties and flux

After conducting extensive characterization work on the membranes' surface morphology and in cross-section an attempt has been made to correlate, the Osmonics SG, Osmonics AD, Osmonics AG and TriSep X20 membrane properties with flux. The surface roughness (R_a), and peak height profile will be presented together to draw conclusions from this work (see Table 6.5). Then the following will be assessed:

- The relationship between membrane surface roughness and flux
- The relationship between membrane actual surface area and flux.
- The relationship between membrane thickness and flux

Membrane	R_{rms} (nm)	R_a (nm)	Thickness (μm)	Peak height profile (nm)	Flux in $l/h/m^2$
Osmonics SG	16 ± 3	12 ± 3	189 ± 3	30 ± 10	59 ± 6
Osmonics AD	43 ± 9	33 + 6	197 ± 5	40 ± 20	8 ± 2
Osmonics AG	34 ± 3	26 + 4	168 ± 4	60 ± 25	77 ± 5
TriSep X20	68 ± 17	52 + 13	227 ± 4	200 ± 40	9 ± 1

Table 6.5. Summary of membrane morphology characterization and flux for tested membranes.

6.7.1 The relationship between membrane surface roughness and flux

Figure 6.26 shows the relationship between membrane roughness R_a and flux.

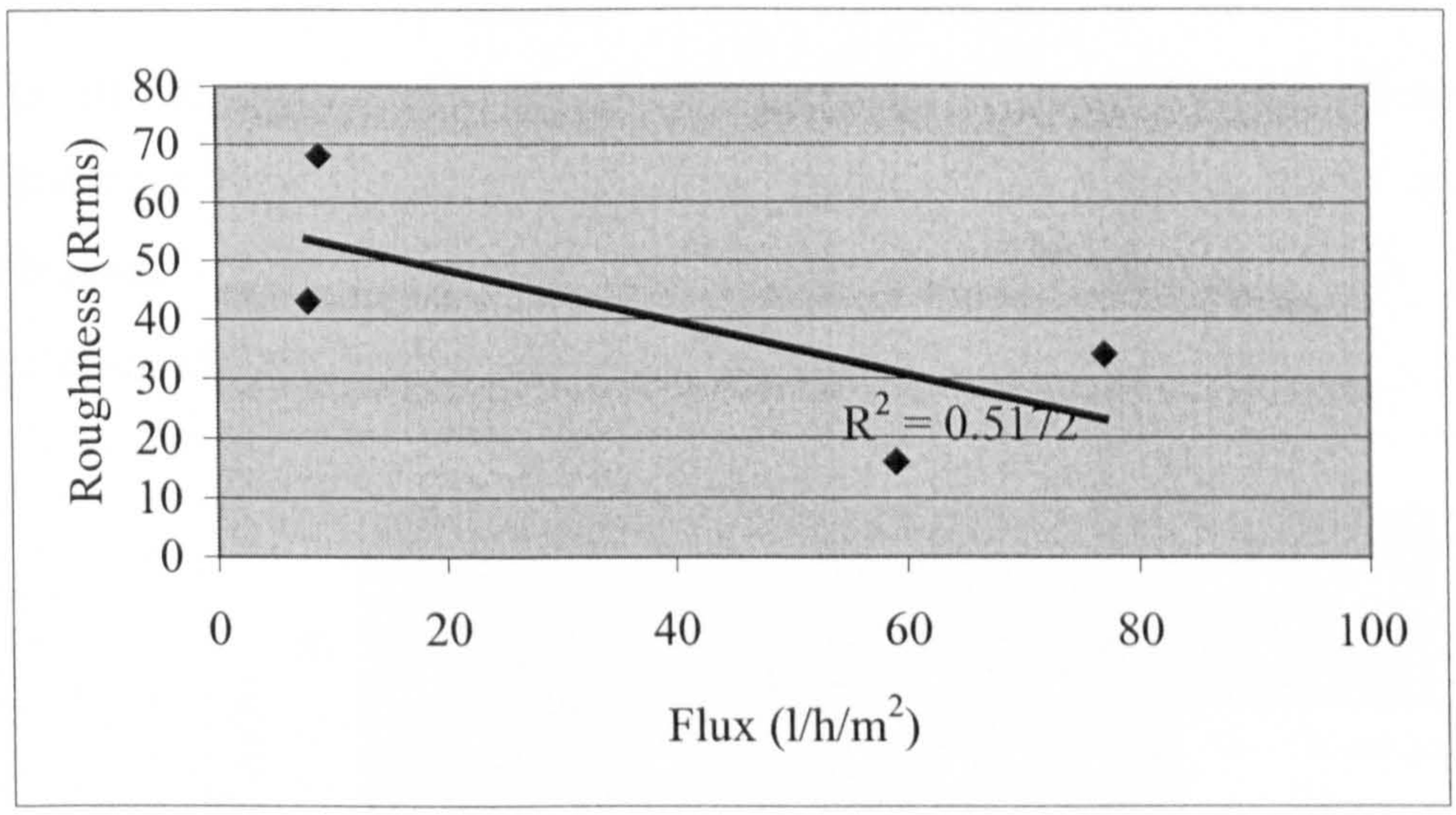

Figure 6.26. Flux versus membrane root mean square surface roughness

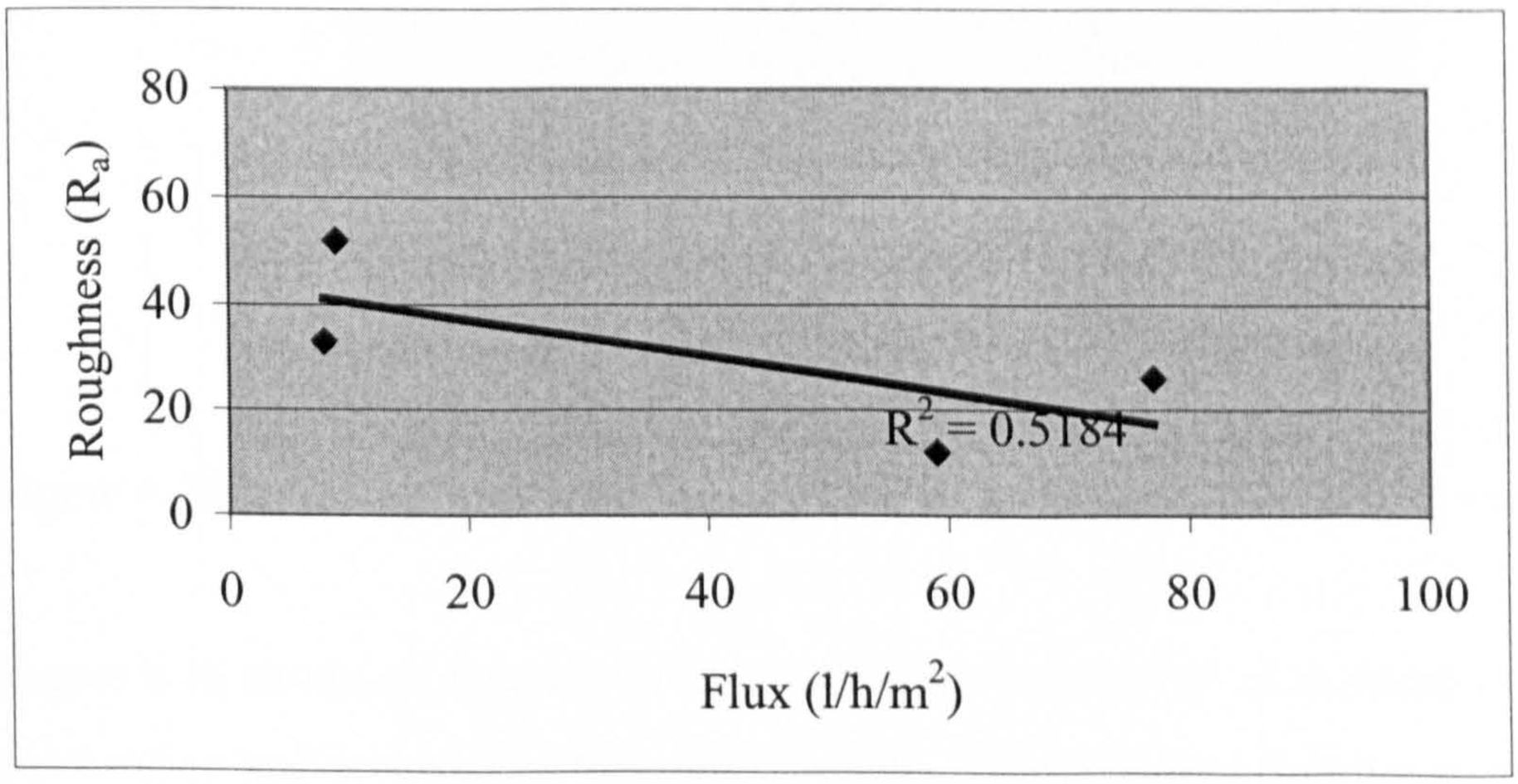

Figure 6.27. Flux versus membrane average surface roughness

Upon drawing linear trend line (see Figures 6.26 and 6.27) it is observed that the R^2 values are low. Considering root mean surface (R_{rms}) roughness values and the corresponding flux it can be seen from Figure 6.26 that the flux of TriSep X20 is similar to Osmonics AD yet surface roughness (R_{rms}) of TriSep X20 is about double of Osmonics AD. Although a general trend of decreased roughness giving increased flux is observed it is impossible to correlate flux with surface roughness for these four membranes.

The results presented in Figures 6.26 and 6.27 show that there is a very loose relationship between membrane surface roughness and flux for tested membranes. However, further experimental results analysis showed that increasing feedwater flow for smooth membranes lead to an increase in flux. On the other hand, increasing feedwater flow for rough membrane surfaces has a minor effect on flux. That was observed upon comparing the performance of Osmonics SG and TriSep X20 membranes (see Figure 6.28).

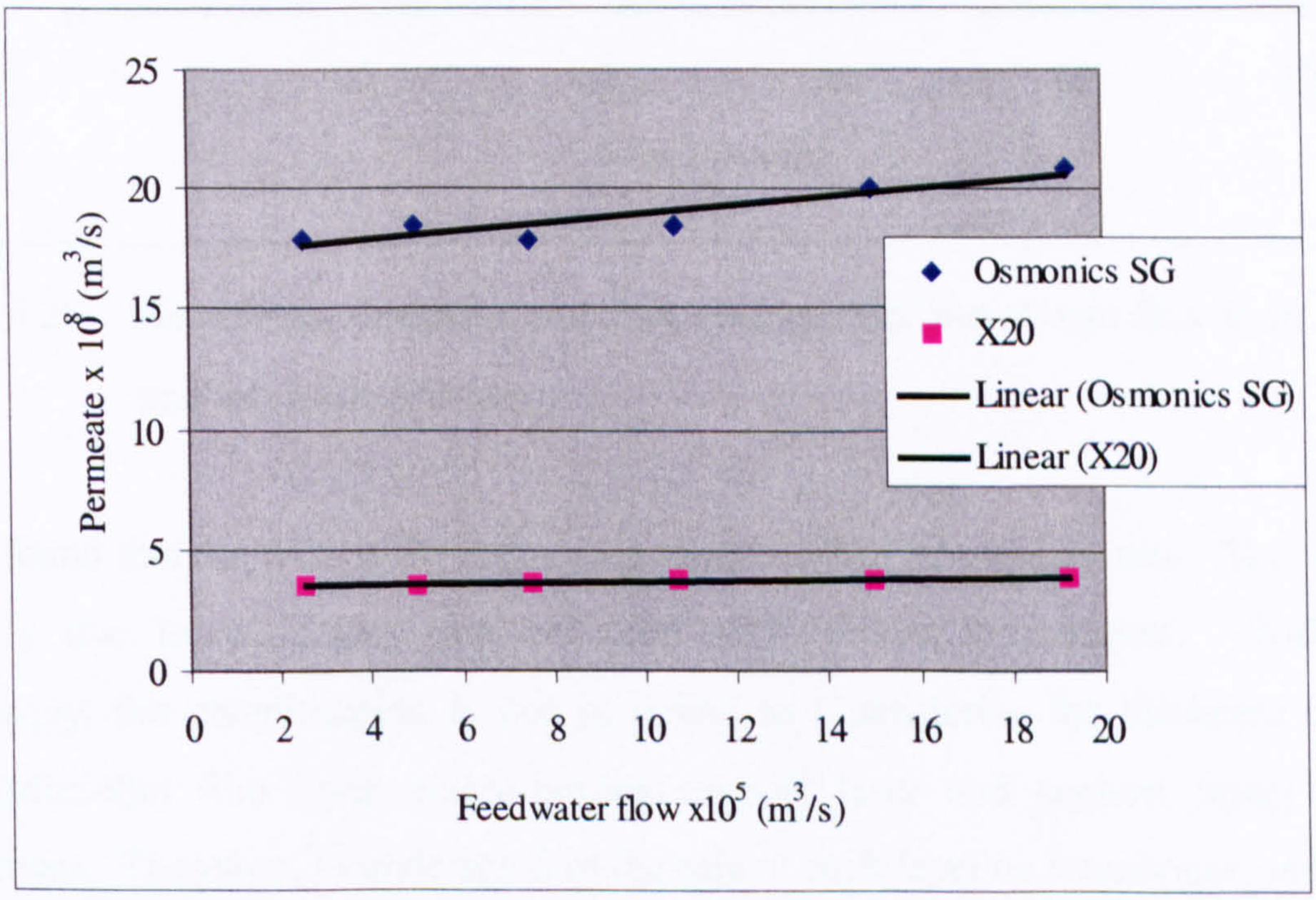

Figure 6.28. Effect of feedwater flow on Osmonics SG and TriSep X20 permeation rate

Figure 6.28 shows an increase in feedwater flow resulted in an increase in Osmonics SG permeation rate much more than TriSep X20. This indicates that the smooth membrane surface flux will increase more with feedwater flow than the rough membrane surface.

However, the increase in flux is minor suggesting that the effect of surface roughness on flux is not significant.

6.7.2 The relationship between membrane cross-section thickness and flux

Figure 6.32 shows the relationship between membrane thickness and flux. It seems to be that the flux and its relation to thickness show the strongest correlation; however that relationship is not universal. It can be seen from Figure 6.29 that similar flux is attained in the range in thickness from 195 –230 μm.

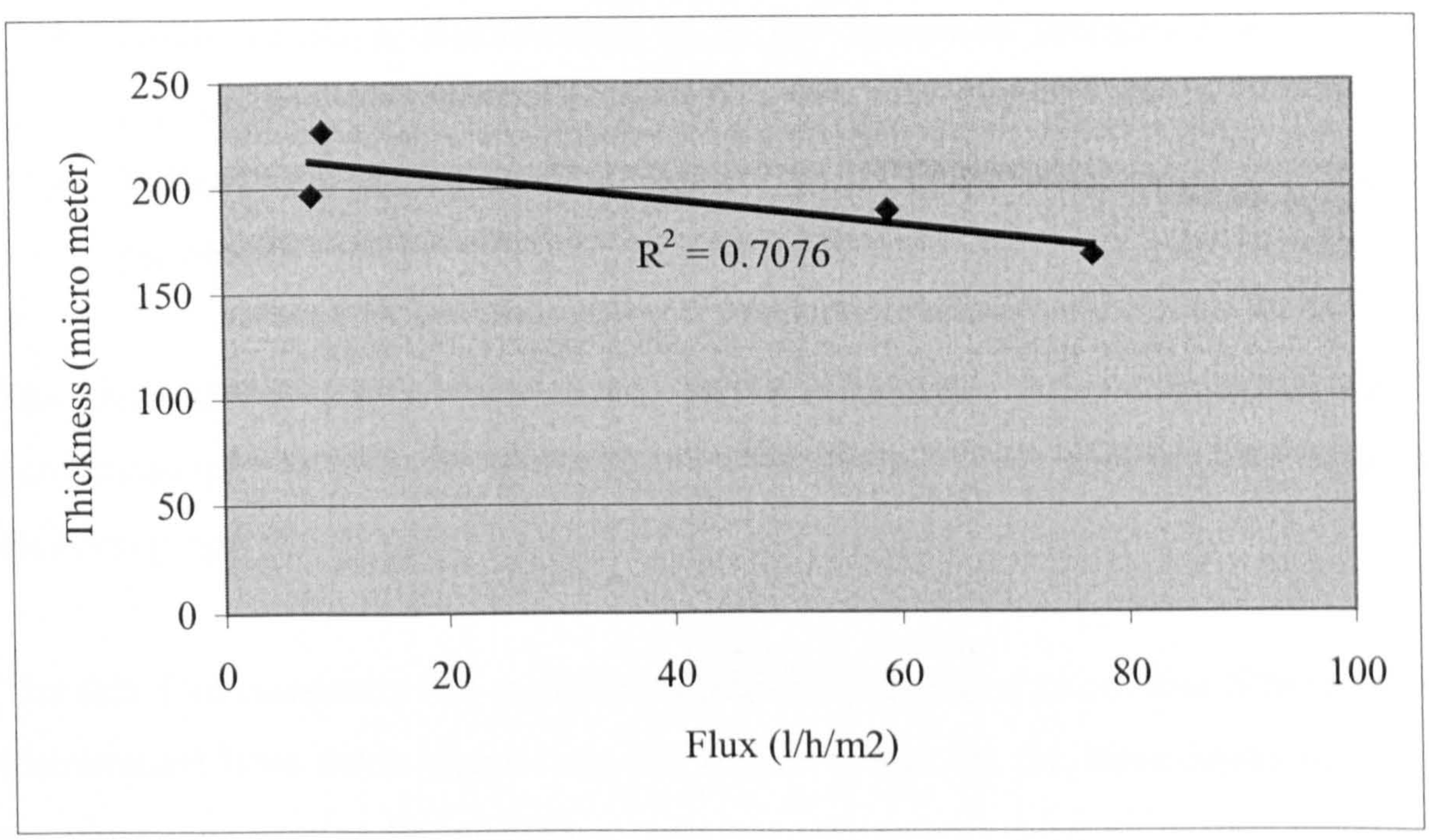

Figure 6.29. Membranes thickness and flux relationship, membrane flux is in $l/h/m^2$, and thickness is in μm

It was found that the thicker the membrane the lower the permeation rate. That is most probably due to increasing pressure drop with thicker membranes. With light microscopy, the magnification is not sufficient to characterize the thickness of each layer (ultra-thin film layer, micro-porous support layer and support layer) of RO membranes. Therefore, to understand in the role of each layer on membrane permeation rate, extensive analysis by SEM (much high magnification can be attain) was conducted, which will be presented in the following section.

6.8 RO membranes surface and cross-section analysis by SEM

In the previous section it was shown that the membrane thickness has an influence on membrane permeation rate. SEM was used to further investigate the role that the membrane cross-section thickness plays in the permeation rate. Osmonics SG and TriSep X20 were selected to conduct this investigation. The reasons for the selection of Osmonics SG and TriSep X20 are as follows:

- Osmonics SG is characterized to be the smoothest membrane with the high permeation.
- TriSep X20 is characterized to be the roughest membrane with the low permeation.

The great difference in permeation rate between these two membranes (Osmonics SG permeation rate is about 6 times higher than TriSep X20) suggests that they have different properties.

The thin film composite RO membranes (all tested membranes are thin film composite membranes) have three layers. An illustrative image for the three layers of the RO membrane is shown in Figure 6.30.

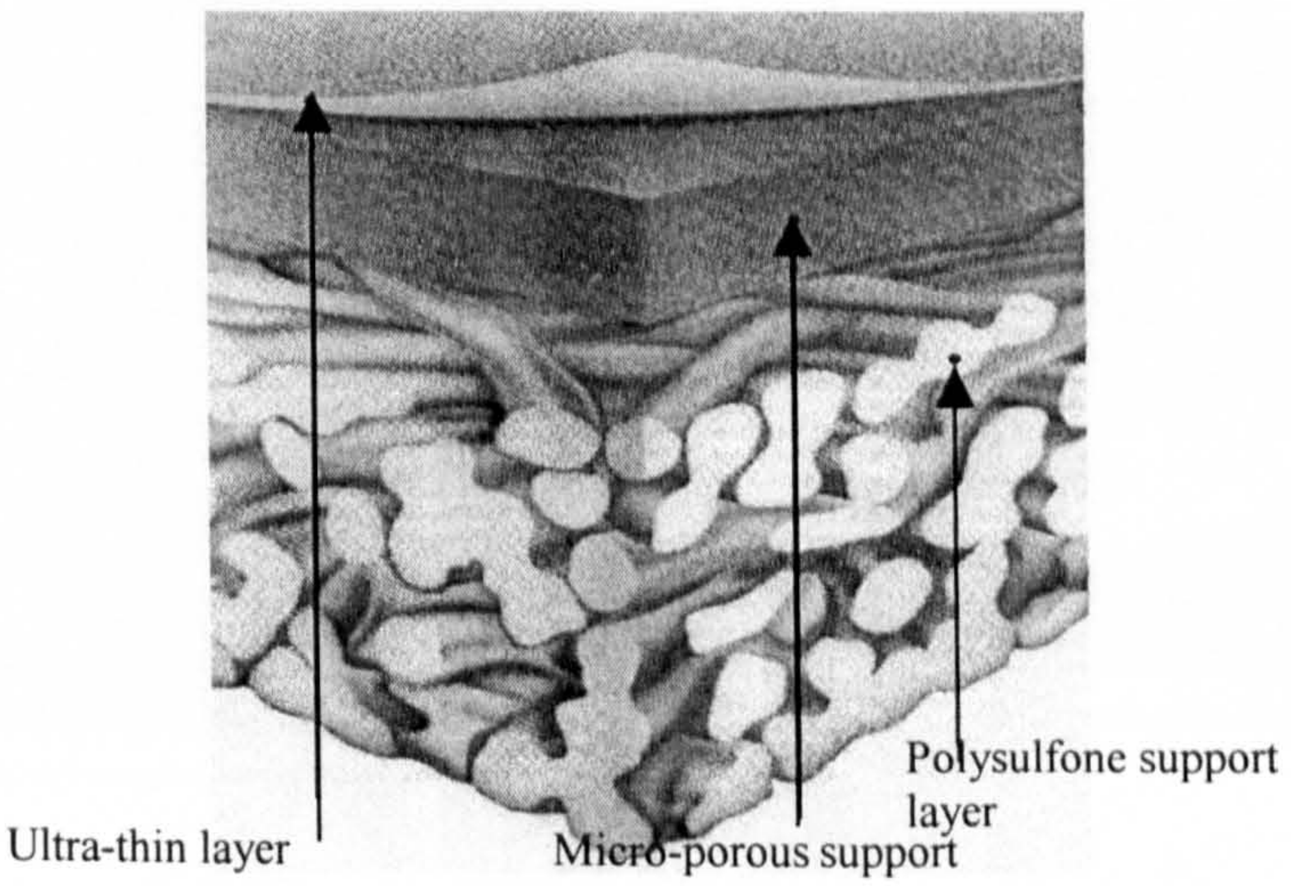

Figure 6.30. Typical cross-section image for thin film composite membranes

The membrane cross-section consists of an ultra-thin film layer, a micro-porous support layer and another support layer, which is usually polysulfone. Most researchers have reported that the ultra-thin film layer thickness plays the most important role in determining membrane flux. Therefore, SEM was used to determine the thickness of the ultra-thin film layer of Osmonics SG and TriSep X20 membranes. The polysulfone support layer was removed by hand from Osmonics SG and TriSep X20 membranes. Microscopic analysis was then conducted by SEM on the ultra-thin film and micro-porous support layers of the two membranes. Figure 6.31 shows SEM images of Osmonics SG and TriSep X20.

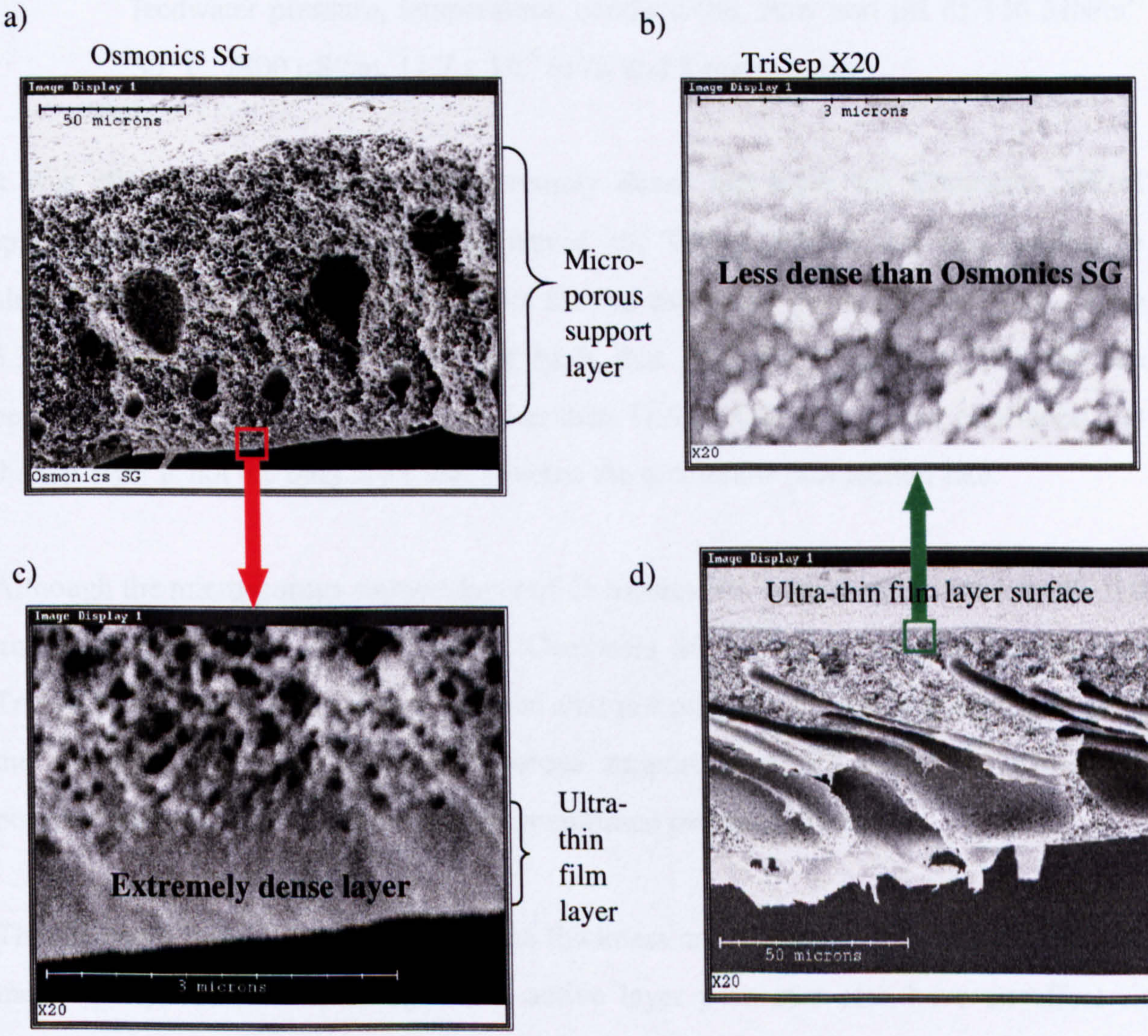

Figure 6.31. SEM cross-section images for TriSep X20 and Osmonics SG

From Figure 6.31, the TriSep X20 and Osmonics SG membrane ultra-thin film and micro-porous support layer thicknesses with their properties were determined (see Table 6.6).

Parameter	Osmonics SG	TriSep X20
Ultra-thin film layer thickness	0.8 μm	Not known
Ultra-thin film layer property, visual assessment	Very dense and not porous	Dense and porous
Micro-porous support layer thickness	89-104 μm	47-54 μm
Permeation rate ($l/h/m^2$)	59	9

Table 6.6. Osmonics SG and TriSep X20 flux and structure properties, flux measured at feedwater pressure, temperature, conductivity, flow and pH of 140 MN/m^2, 30 °C, 2800 μS/cm, 11.7 x 10^{-5} m^3/s, and 8 respectively

It was observed that there is an extremely dense top layer for Osmonics SG of approximately 0.8 μm thickness. However, for TriSep X20 it was not possible to identify such a layer. Because Osmonics SG has extremely dense top layer (see Figure 6.31c) whereas TriSep X20 does not have that layer (see Figure 6.31b) and the permeation rate of Osmonics SG is higher than TriSep X20, it has been concluded that the top layer is not the only layer that governs the membrane permeation rate.

Although the micro-porous support layer of Osmonics SG is found to be thicker (89-104 μm) than TriSep X20 (47-54 μm) yet Osmonics SG permeation rate is greater than TriSep X20. Based on this it is believed that not only the thickness and properties of the ultra-thin film layer and micro porous support layer but also the thickness of polysulfone support layer influences the membrane permeation rate.

This investigation is based on membrane thickness analysis only. It is believed that the membrane porosity of each layer and active layer pore size also have an effect on membrane permeation rate. AFM and SEM do not have the capability to measure RO membrane's active layer pore size and pore distribution.

6.9 Scanning RO membranes surfaces using the AFM - effect of operation mode

Assessing the effect of operating the AFM in contact mode on polymeric membranes has not previously been done. Literature shows that some researchers have avoided AFM contact mode operation and operated AFM in tapping or non-contact mode when scanning membrane surfaces because it is believed that soft membrane surfaces will be damaged. On the other hand, other researchers have used contact mode operation and obtained good images. Extensive membrane surface imaging for Osmonics SG and TriSep X20 membranes was conducted to evaluate the effect of the AFM operation on contact mode on the membrane surface at constant force setting of 30 nA. Interesting conclusions were found. The investigation covered the following:

- Membranes imaged dry (as received)
- Membranes imaged in water.
- The effect of scanning with different constant force settings

Since the damage degree that can takes place for the membrane in this work is based on visual analysis of the AFM image, it was decided to use as a guide an AFM image presented in the literature and characterized as an image with no damage (see Figure 6.32).

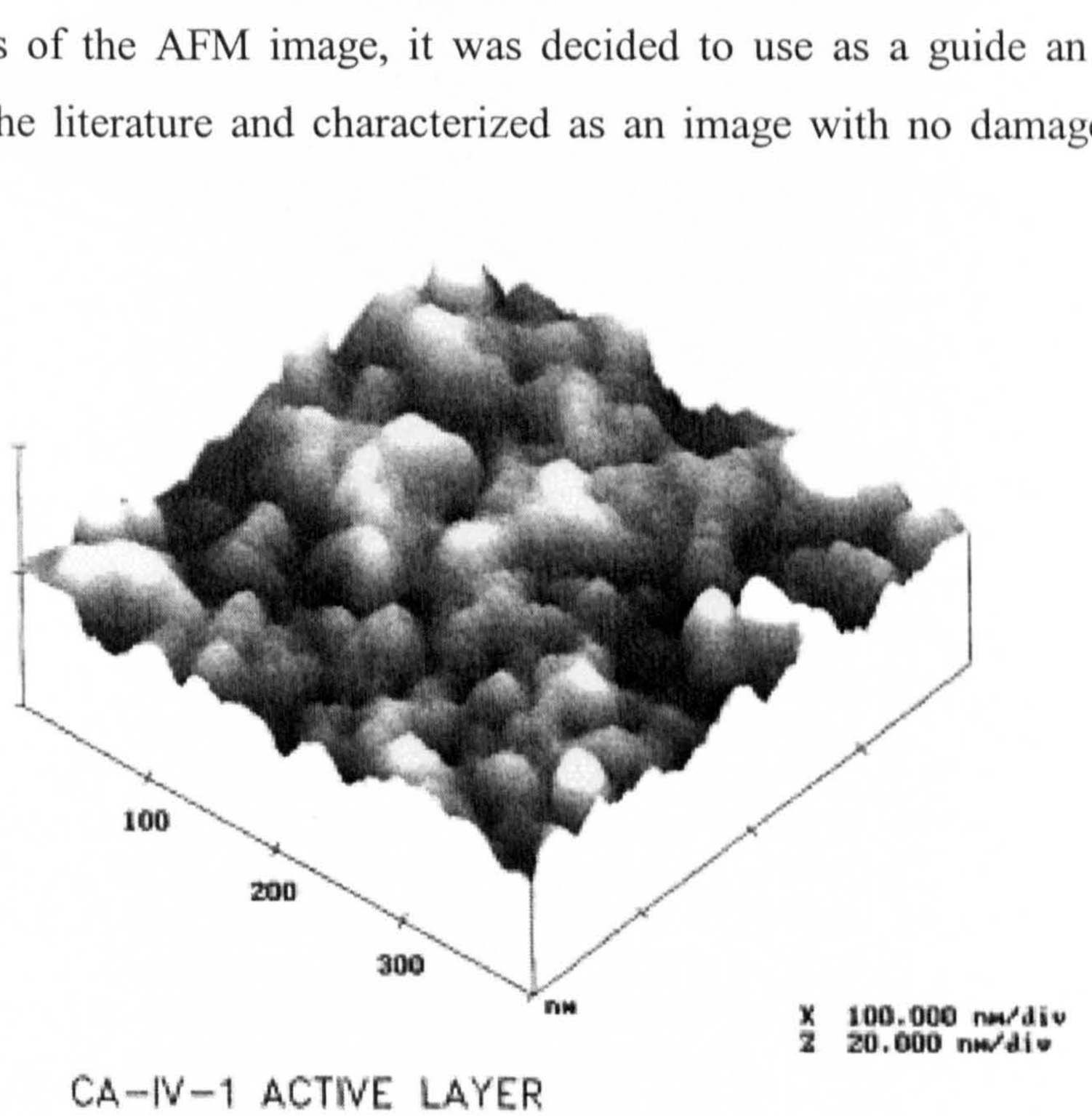

Figure 6.32. AFM image for Cellulose Acetate active layer [58]

The membrane surface will be characterized as a damaged surface upon observing directional aspect to the image, which are in the direction of the AFM tip scan.

6.9.1 Membrane imaged as received - dry

The AFM tip did not cause any damage to the as-received membranes when scanning was performed in air. This was therefore important for all the preceding images and so conclusions from these are valid. However, for literature studies where it may be important to image surfaces in a liquid experiment, the following analysis is important. The scanned membranes are Osmonics AG, AD, SG and TriSep X20 (see Figure 6.33)

a)

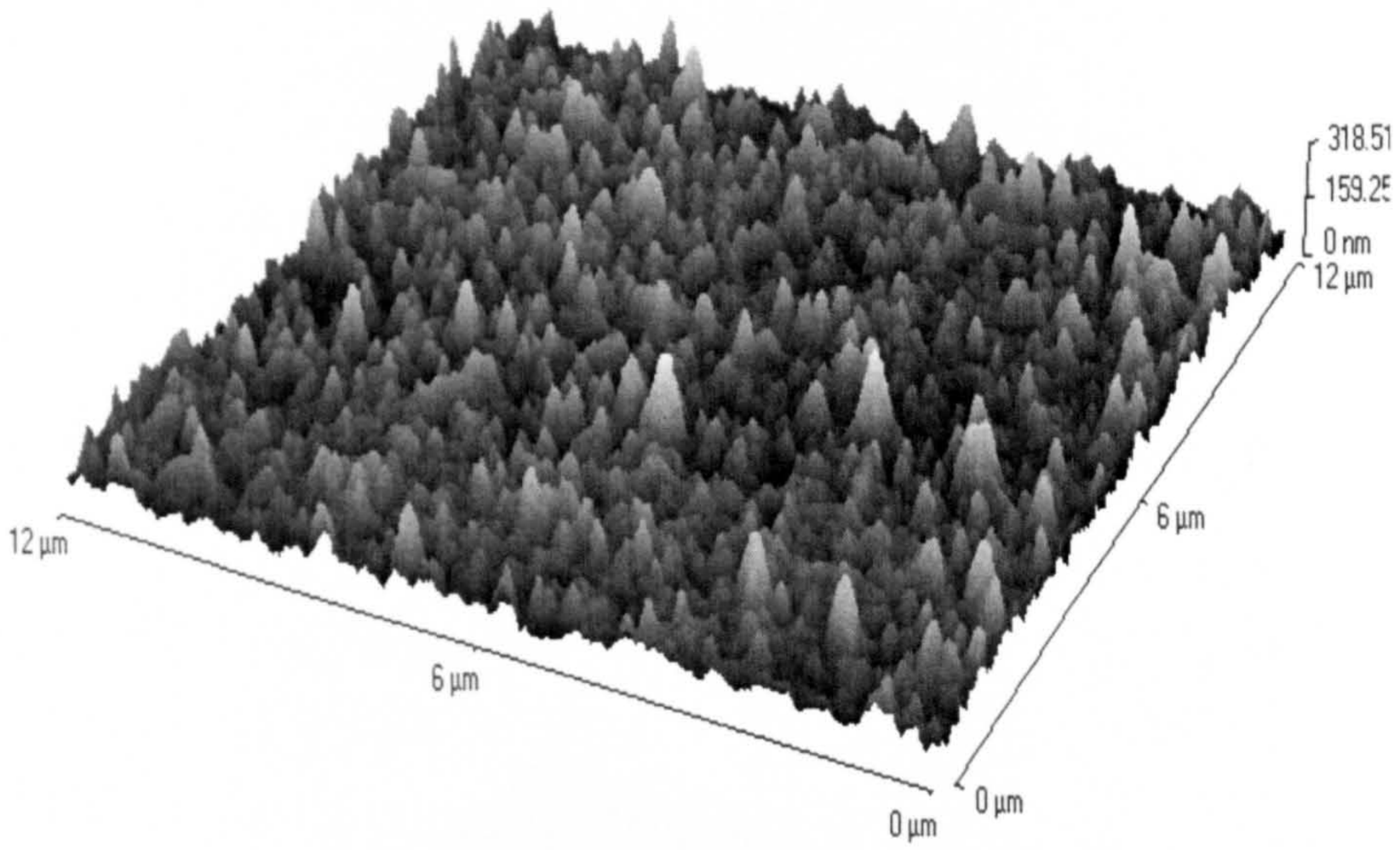

b)

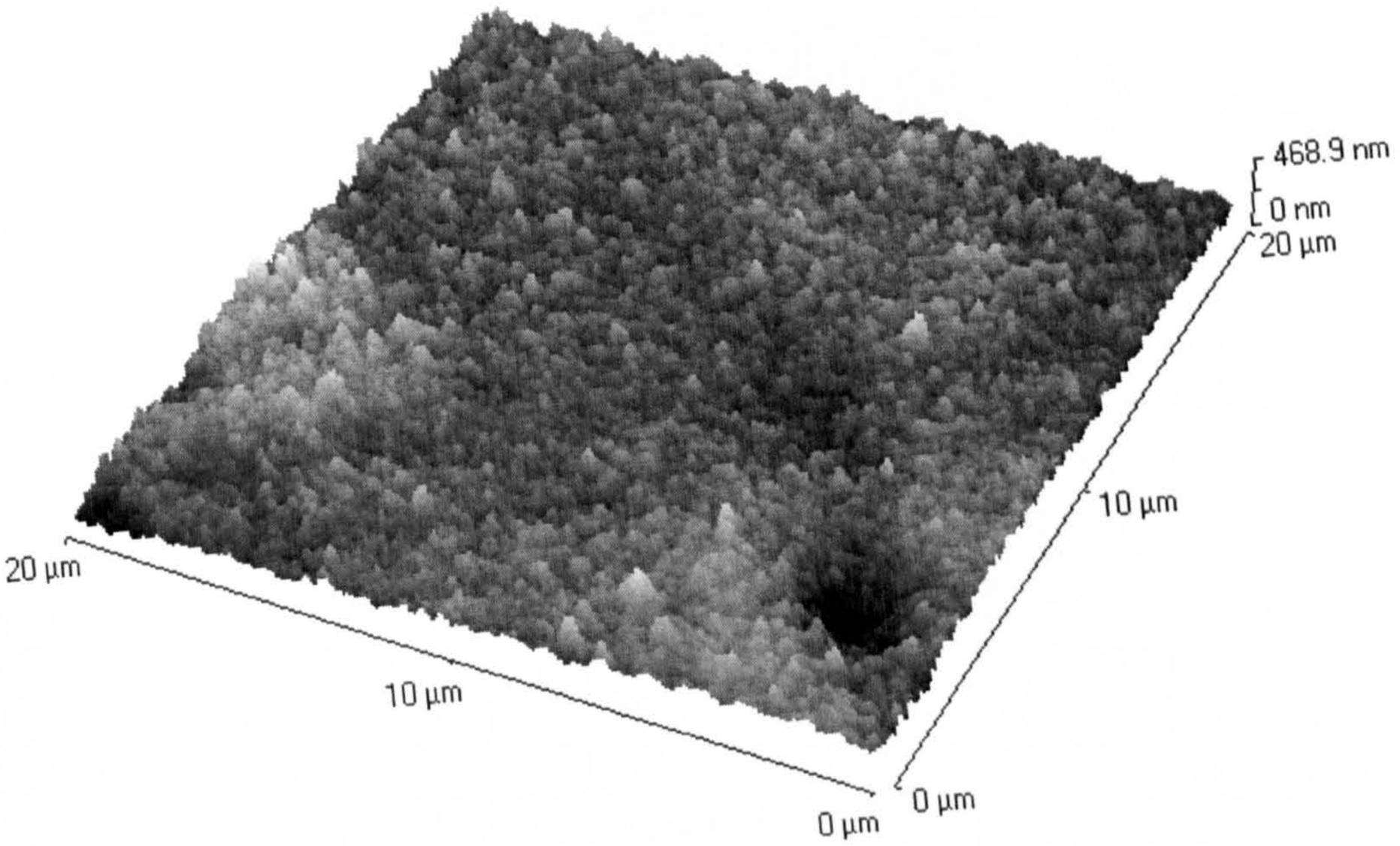
468.9 nm
0 nm
20 µm
10 µm
0 µm
20 µm
10 µm
0 µm

c)

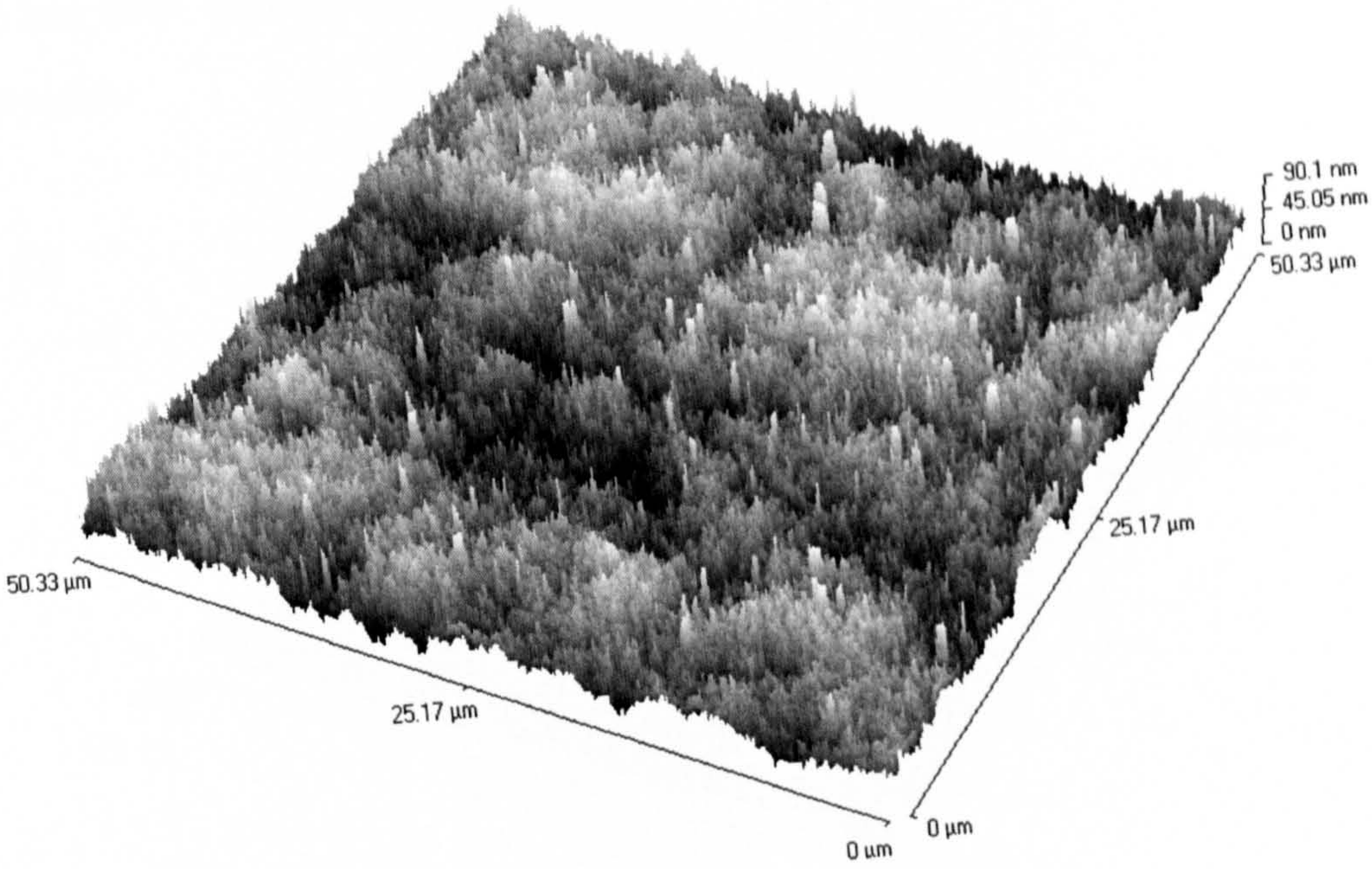
90.1 nm
45.05 nm
0 nm
50.33 µm
25.17 µm
0 µm
50.33 µm
25.17 µm
0 µm

d)

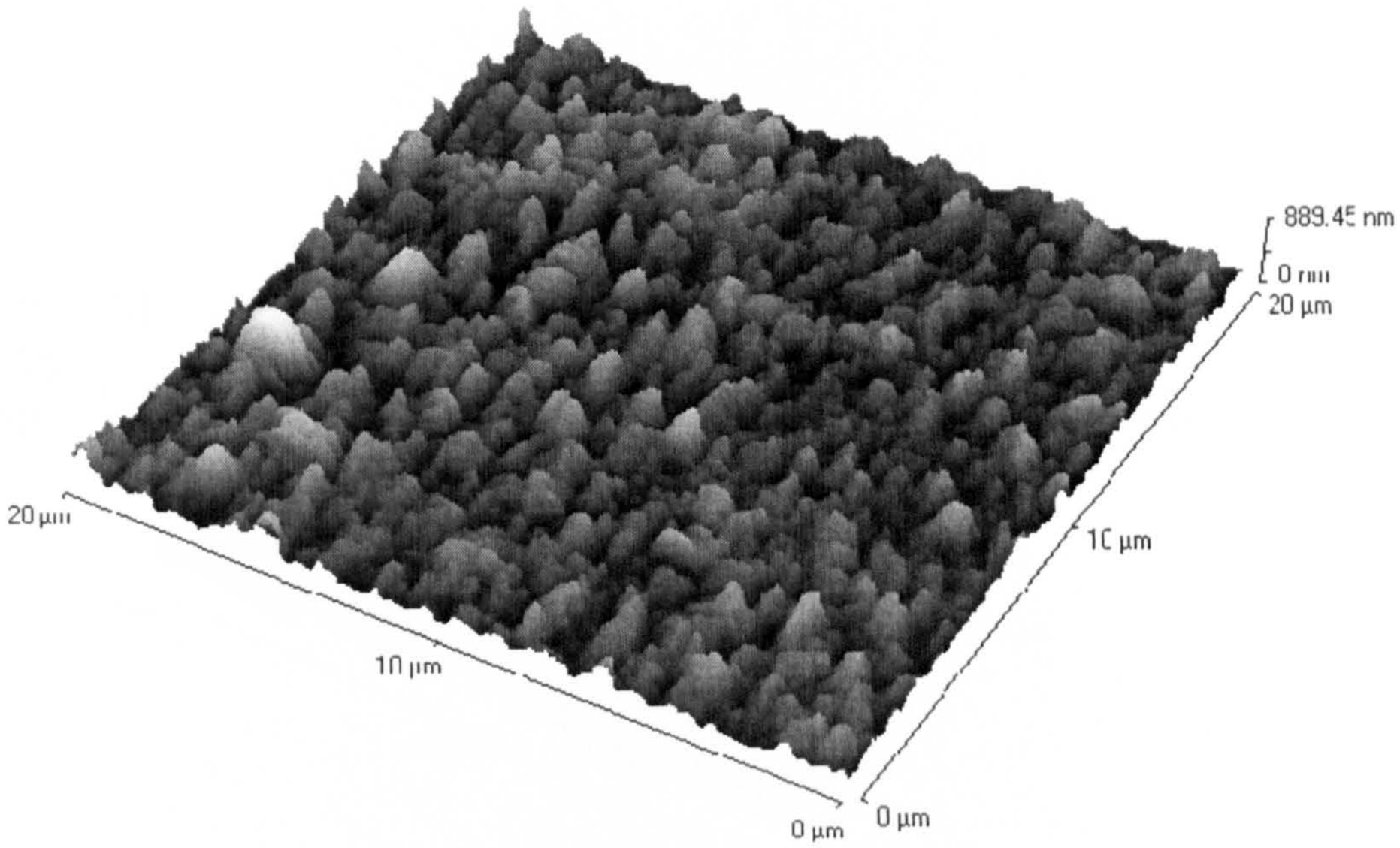

Figure 6.33. AFM images of as received - dry a) Osmonics AD, b) Osmonics SG, c) Osmonics SG, and d) TriSep X20

That implies that the tendency of RO membranes surfaces to be damaged by AFM scanning tip is very low or if the membrane is dry.

6.9.2 Membrane imaged in water

It was found that Osmonics SG membrane, which was imaged by AFM in contact mode in water has been damaged in some conditions. An assessment of this is presented in the next pages.

a)

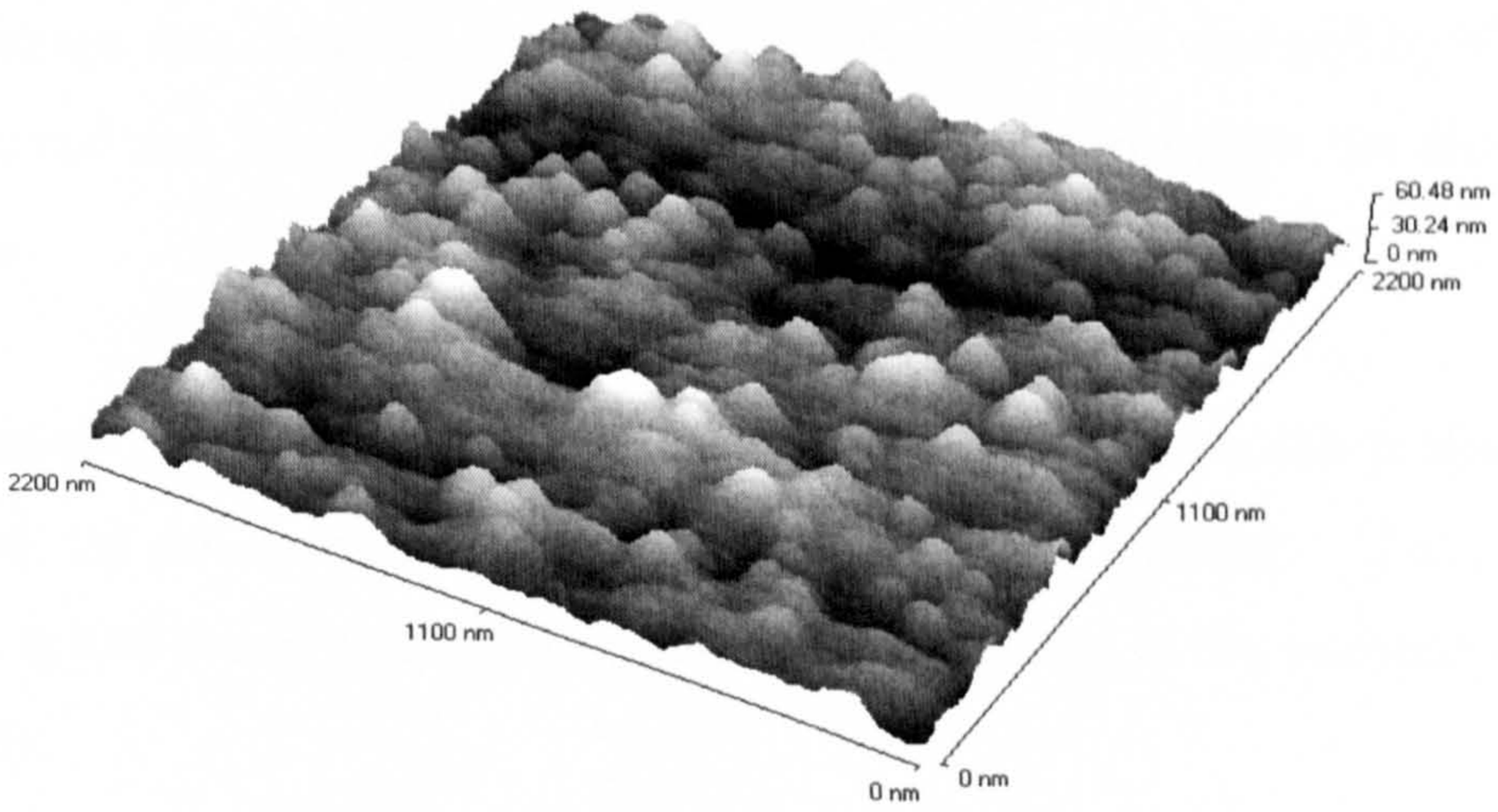

b)

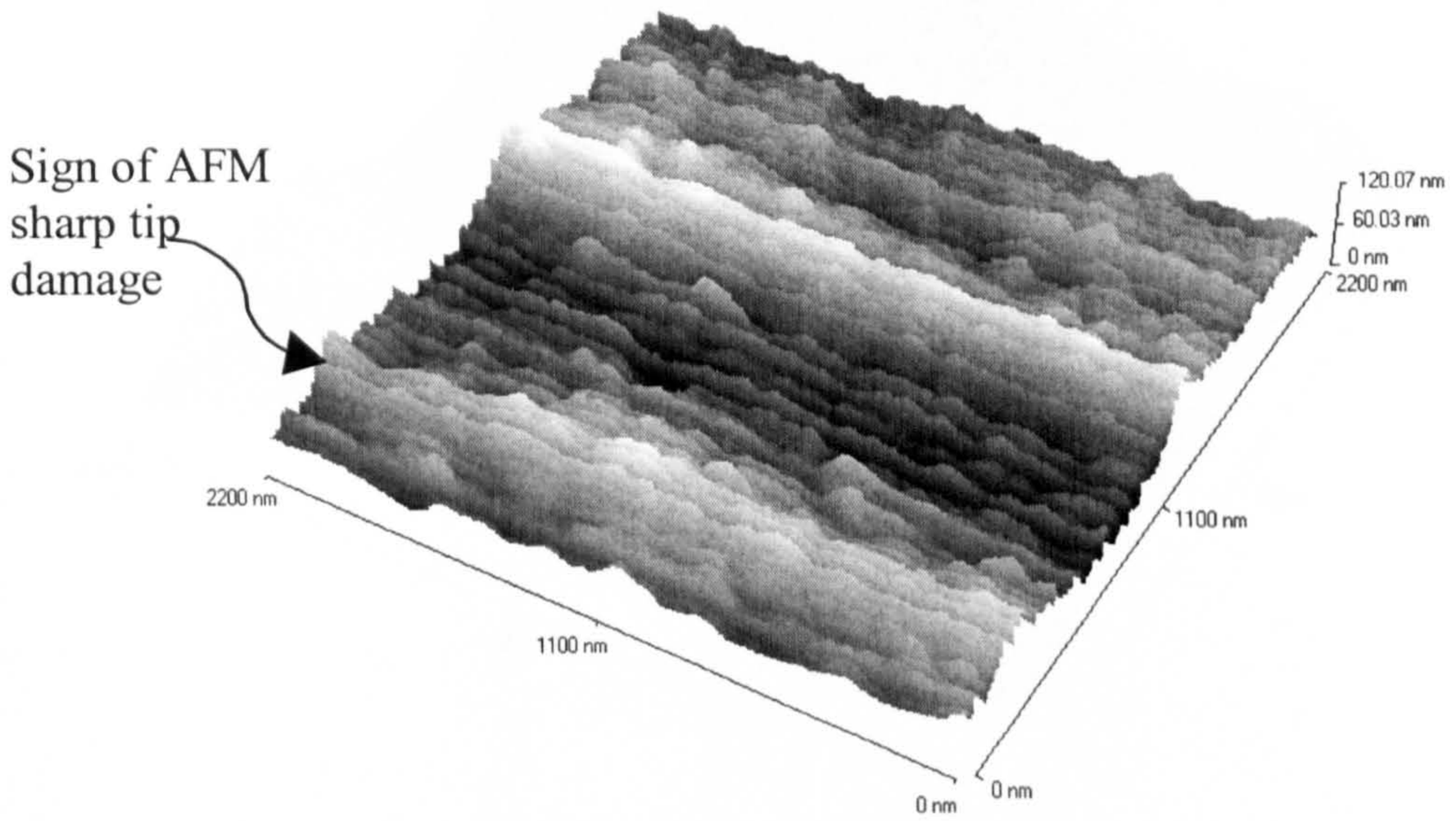

Figure 6.34. a) AFM image for Osmonics SG soaked in water at pH 2.3, b) AFM image for Osmonics SG soaked in water at pH 5

Visual comparison of images shown in Figure 6.34 to the reference image, Figure 6.32, shows that the AFM tip did not cause any damage to Osmonics SG membrane imaged in water of pH 2.3. However, when the membrane was imaged in water of pH 5, the membrane surface became sensitive to the AFM scanning tip and the tip damaged the surface.

To confirm that the image taken in water of pH 5 for Osmonics SG has been damaged by the AFM tip and that the damaged noticed did not exist in the surface morphology before the image was obtained, the tip scanning direction was changed by 90 degree and it was observed that these damage lines were seen again in follow the direction of the scanning tip.

The conclusion is that the water pH value has an influence on the probability of the sharp AFM tip to damage Osmonics SG membrane surface. For TriSep X20 membrane, it was found that AFM tip did not damage any of the scanned surfaces (see Figure 6.35).

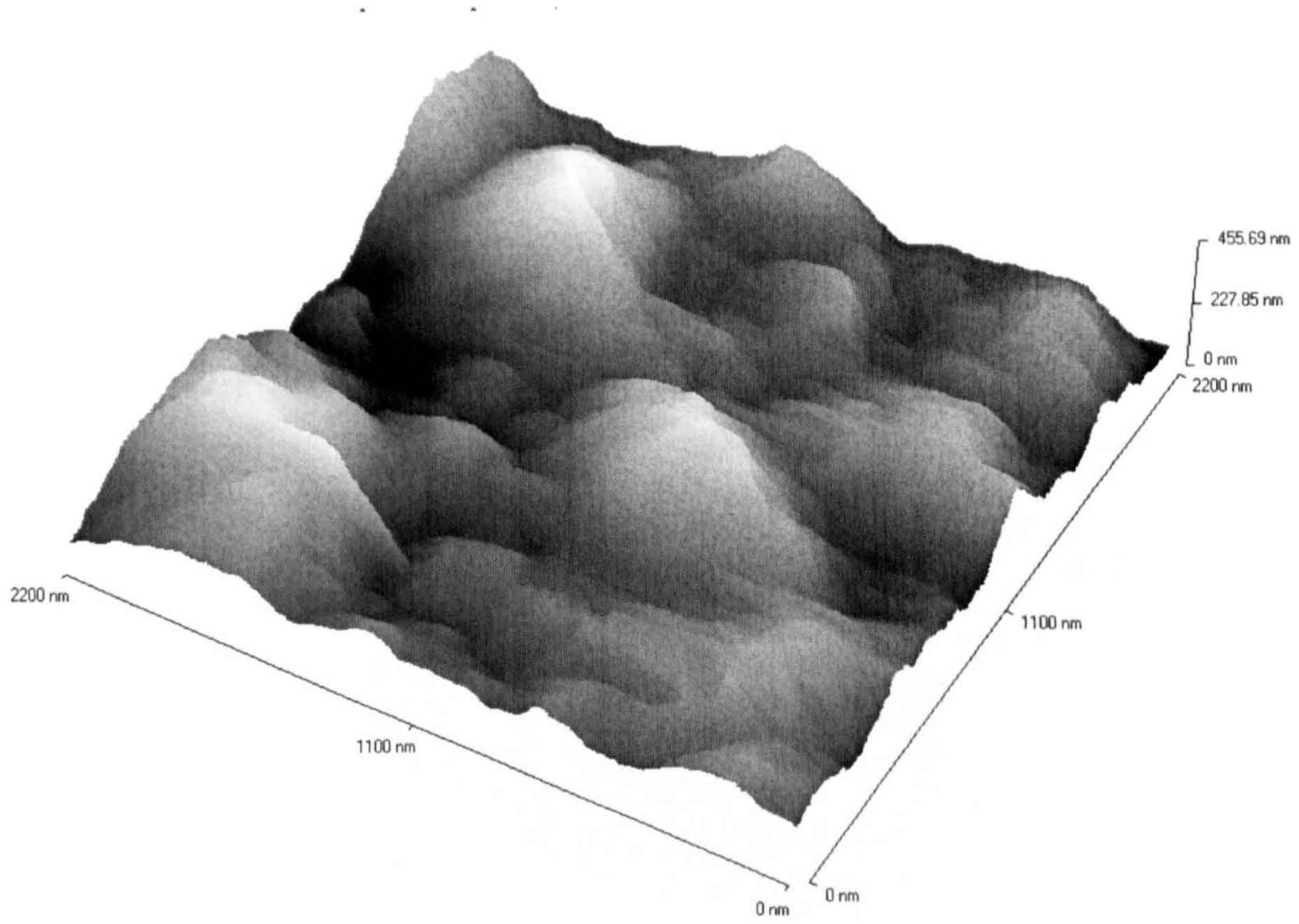

Figure 6.35. Under water AFM image of TriSep X20 which shows no surface damage

Upon scanning TriSep X20 membrane three times in the same spot to confirm this observation and prove its resistance for repeating scans minor damage was observed (see Figure 6.36).

a)

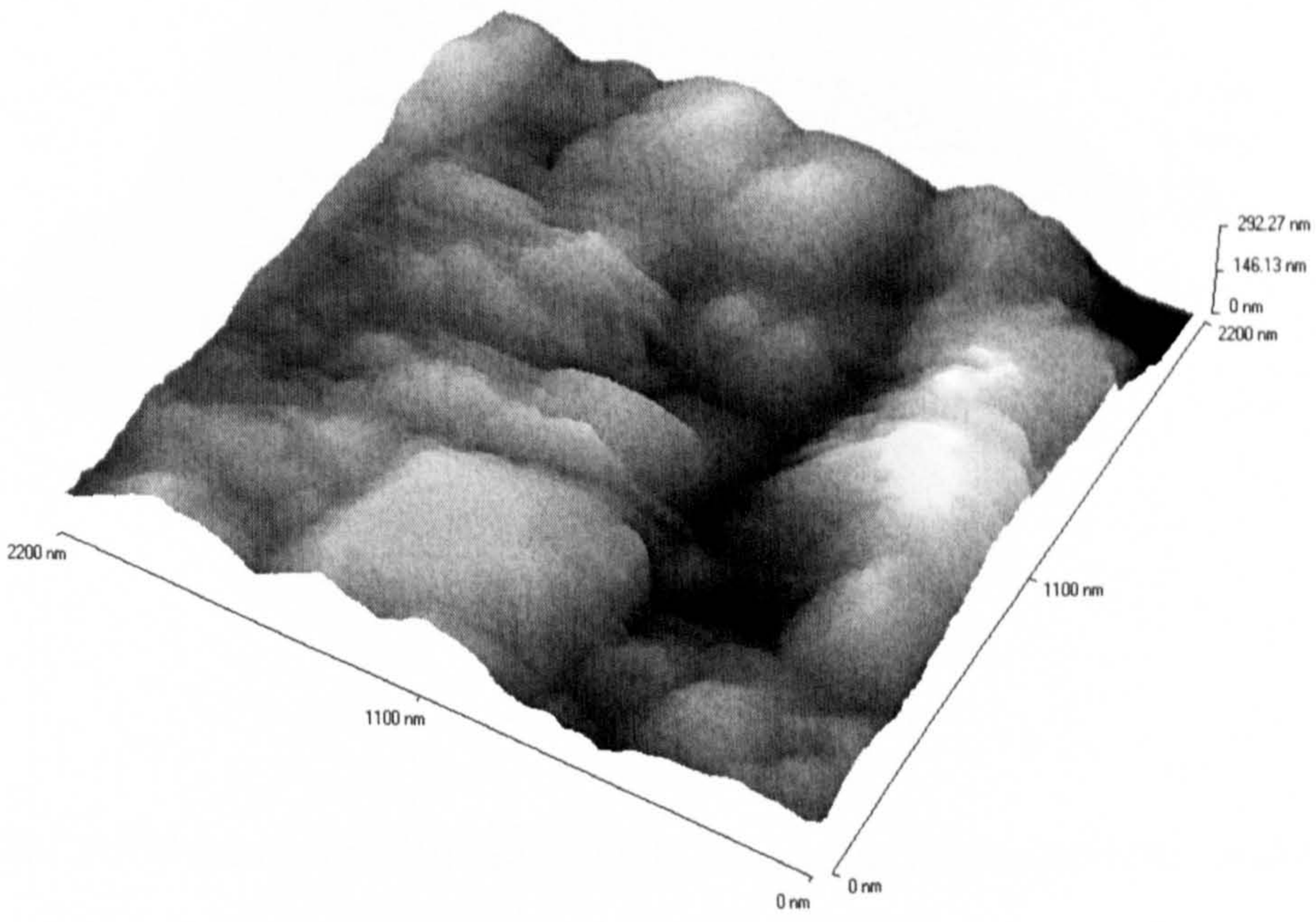

b)

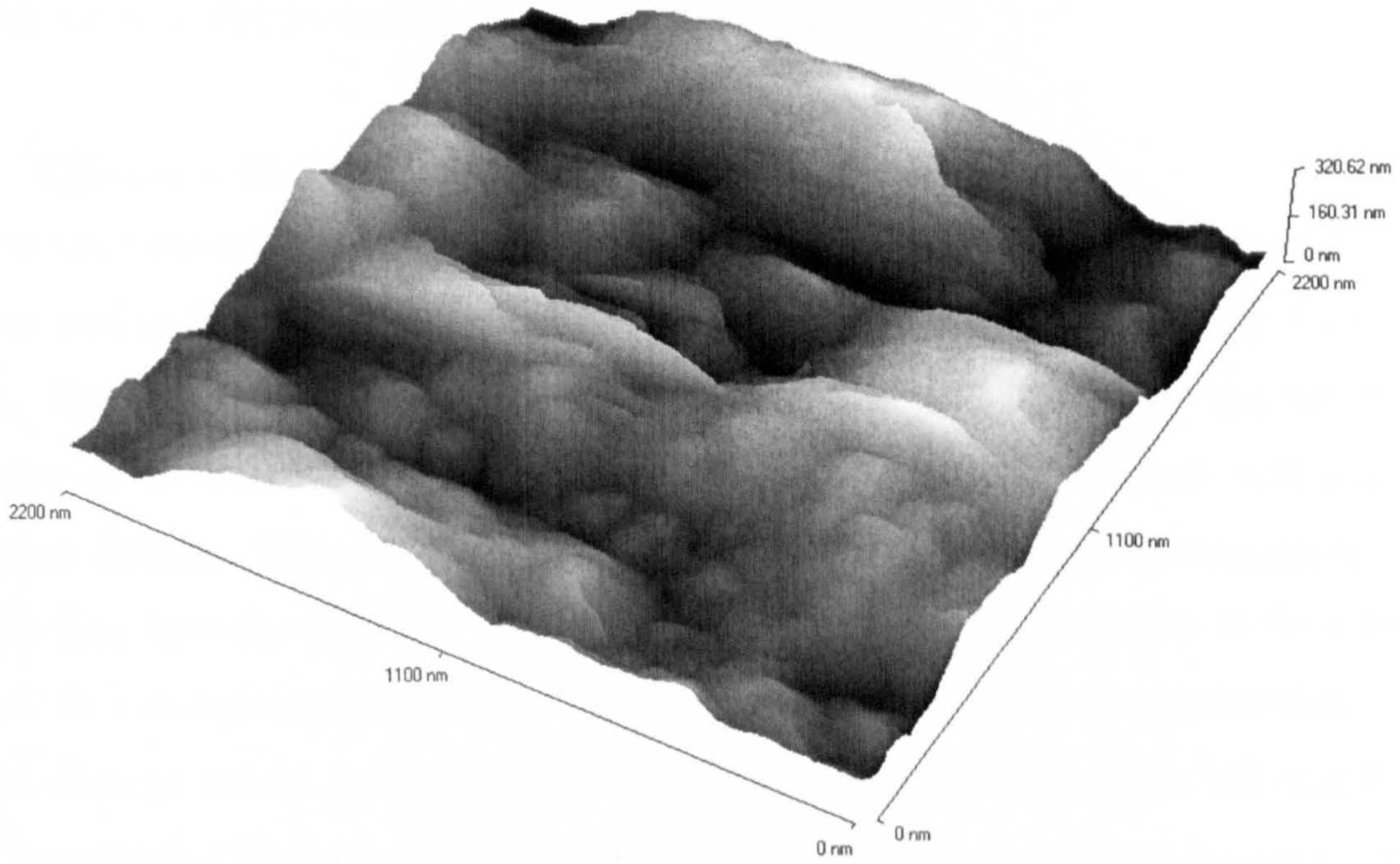

c)

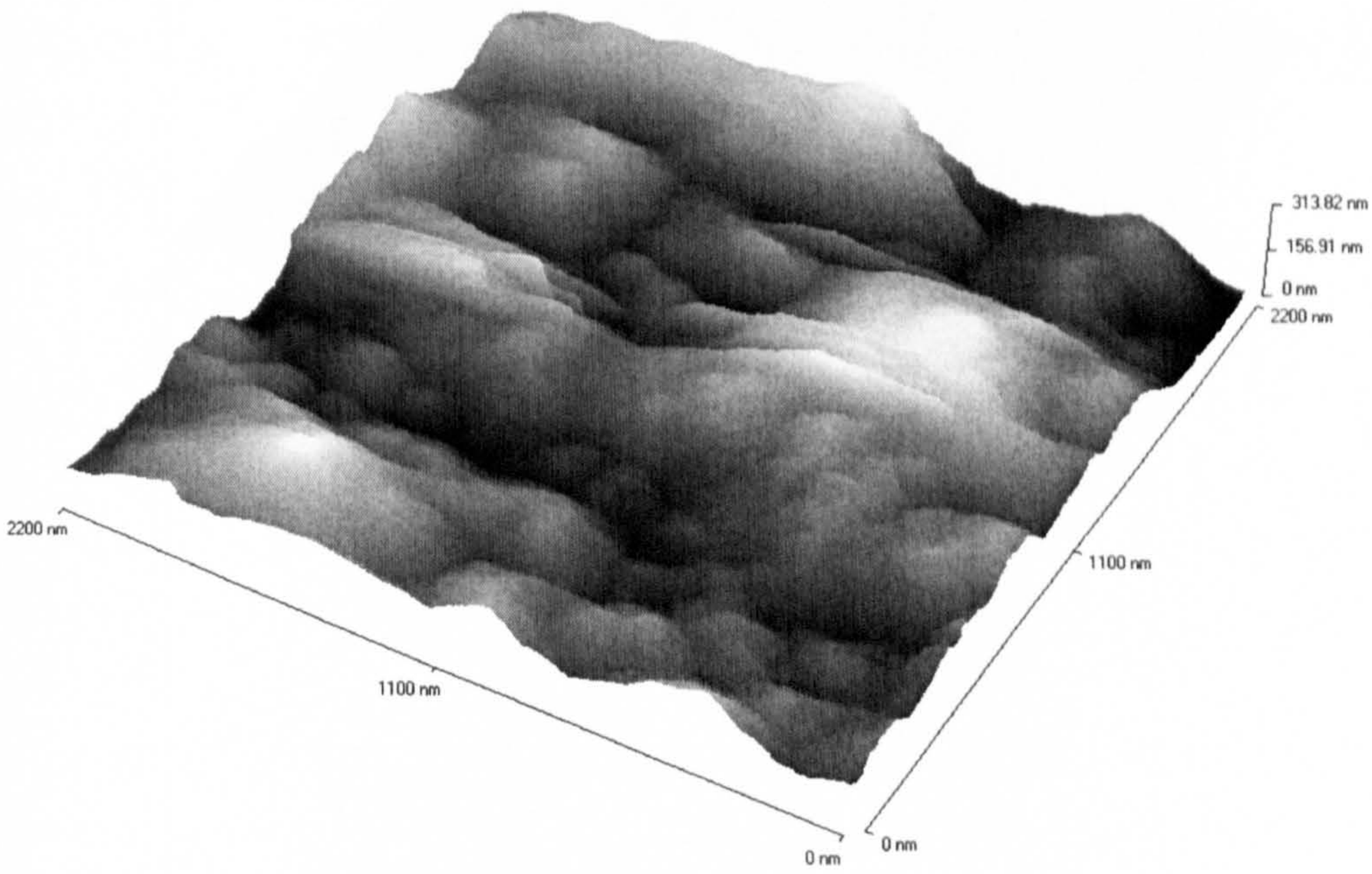

Figure 6.36. AFM images of TriSep X20, a) first scan, b) second scan, and c) third scan

So it can be concluded that different membranes have a different resistance to abrasion by the sharp AFM tip in imaging in water and membranes have different hardness properties, which vary with water pH. TriSep X20 was found to be resistant to the AFM tip whereas Osmonics SG was not in all conditions.

6.9.3 Effect of scanning with different constant force settings

An extensive investigation was conducted to understand the effect of imaging Osmonics SG and TriSep X20 with different AFM tip constant force settings namely: 0, 30, and 60 nA. Previous investigation was conducted at 30 nA force setting. In this section the objective is to determine if there is a way to image soft membrane surfaces with minimum damage. This investigation was carried out for membranes imaged in water because they have the tendency to be damaged by the AFM tip as shown in the previous section. It was expected that as tip constant force setting increase the probability for the surface damage would increase. However, Osmonics SG surface was affected by the AFM tip at 0 and 60 nA suggesting that decreasing the force setting will not minimize surface damage (see Figure 6.37).

a)

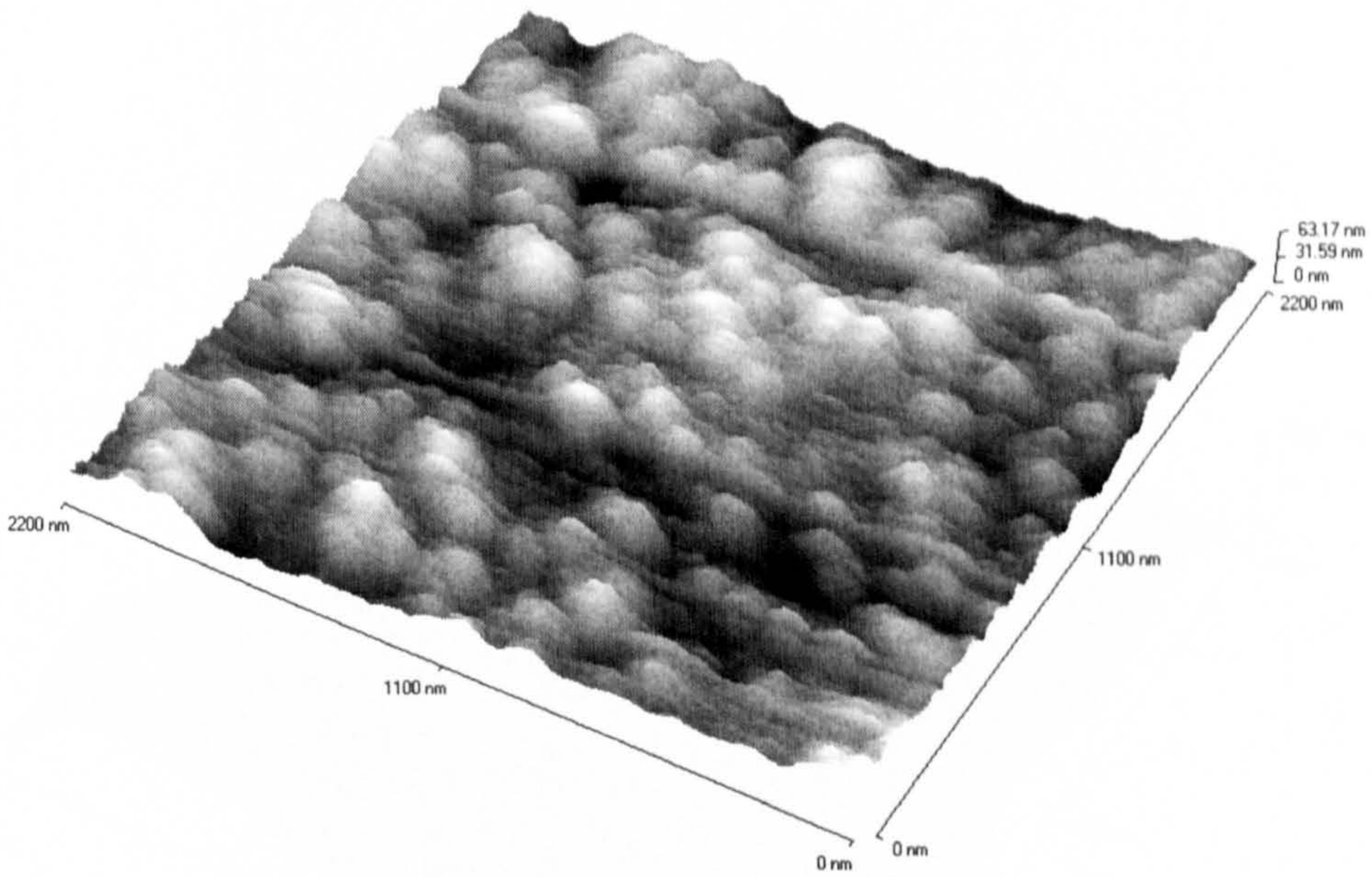

b)

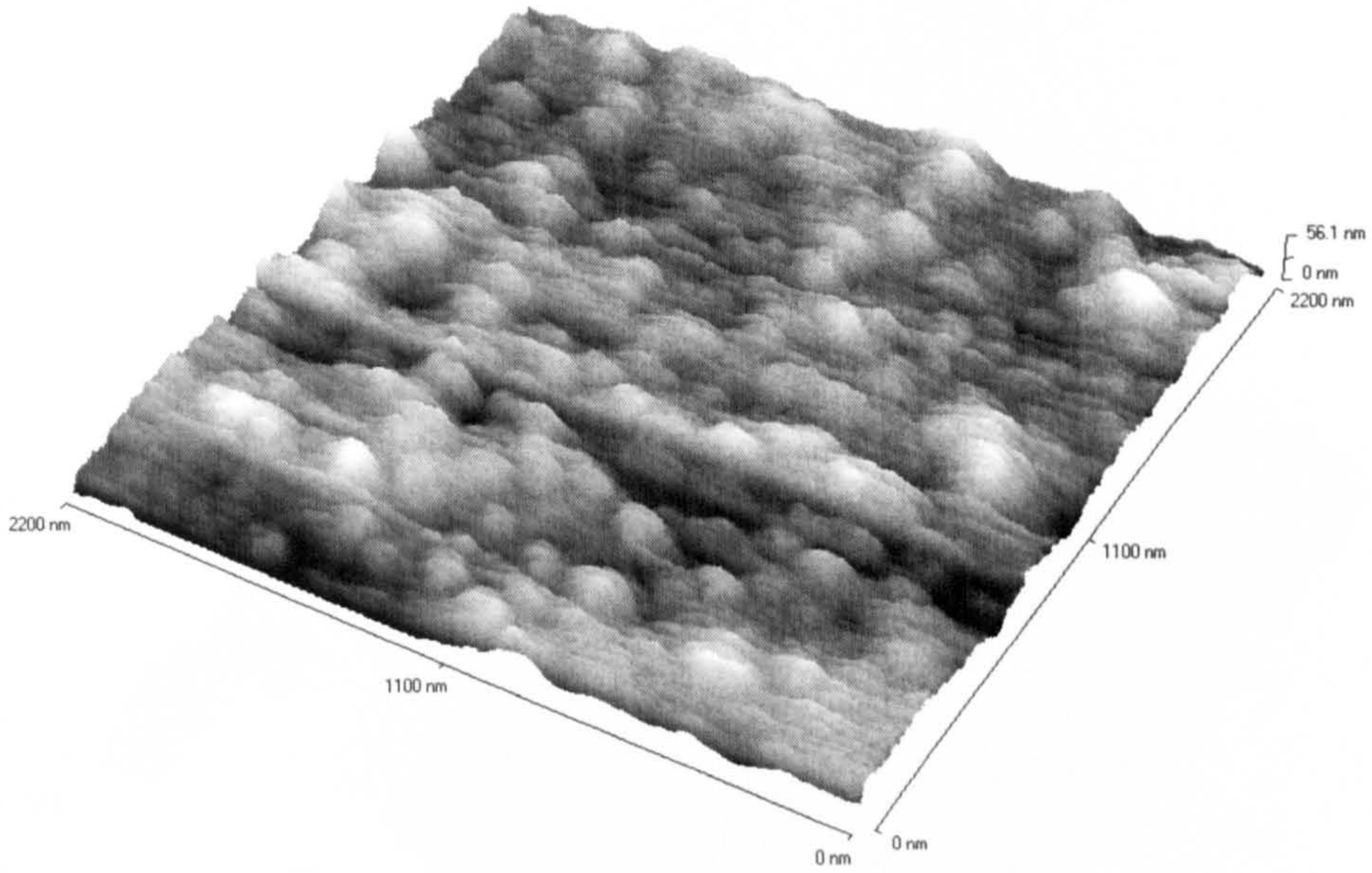

Figure 6.37. AFM image of Osmonics SG scanned at a) 60 nA force setting, b) at 0 nA setting

TriSep X20 was found to be resistant to AFM tip damage at all force settings (see Figure 6.38).

a)

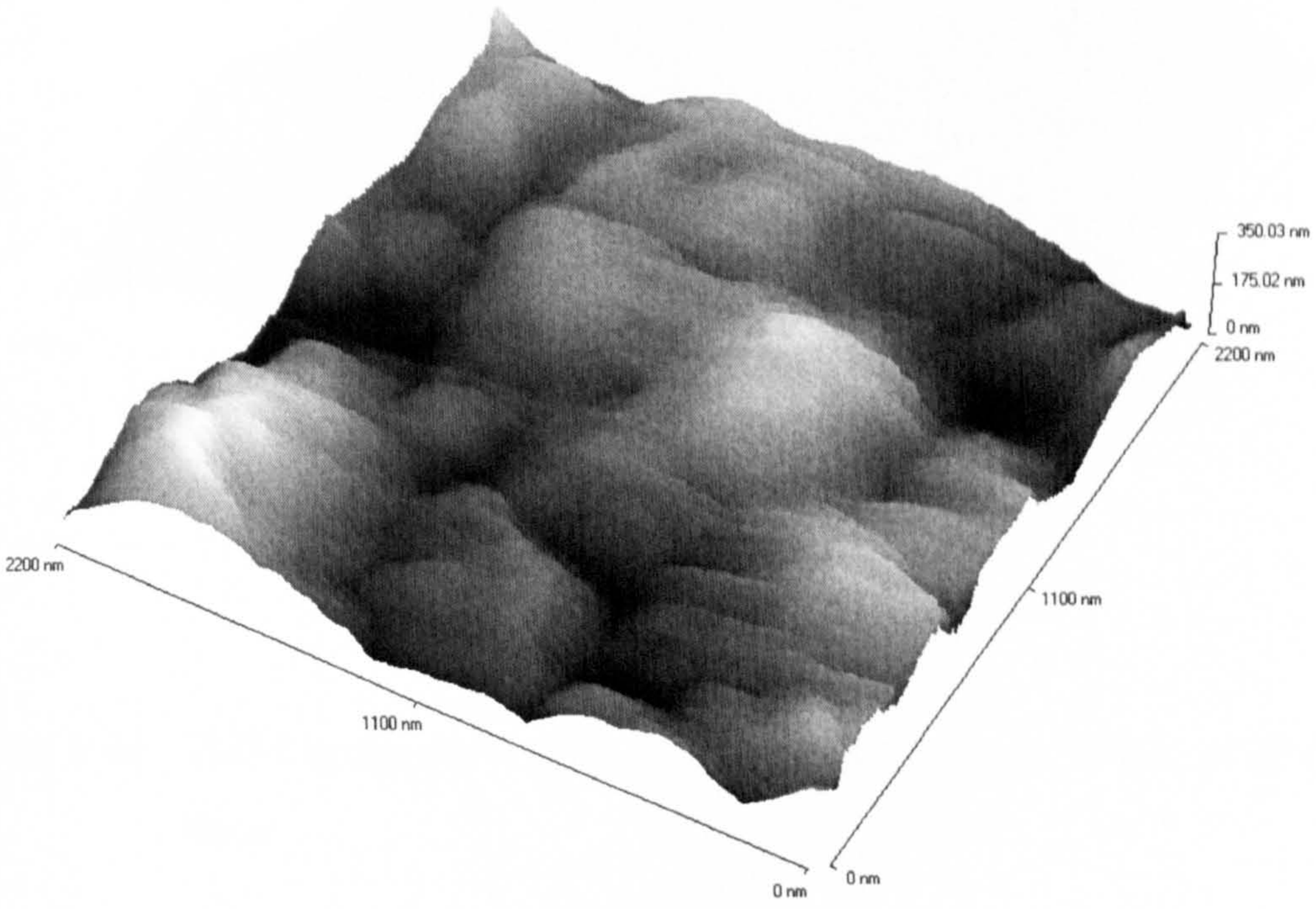

b)

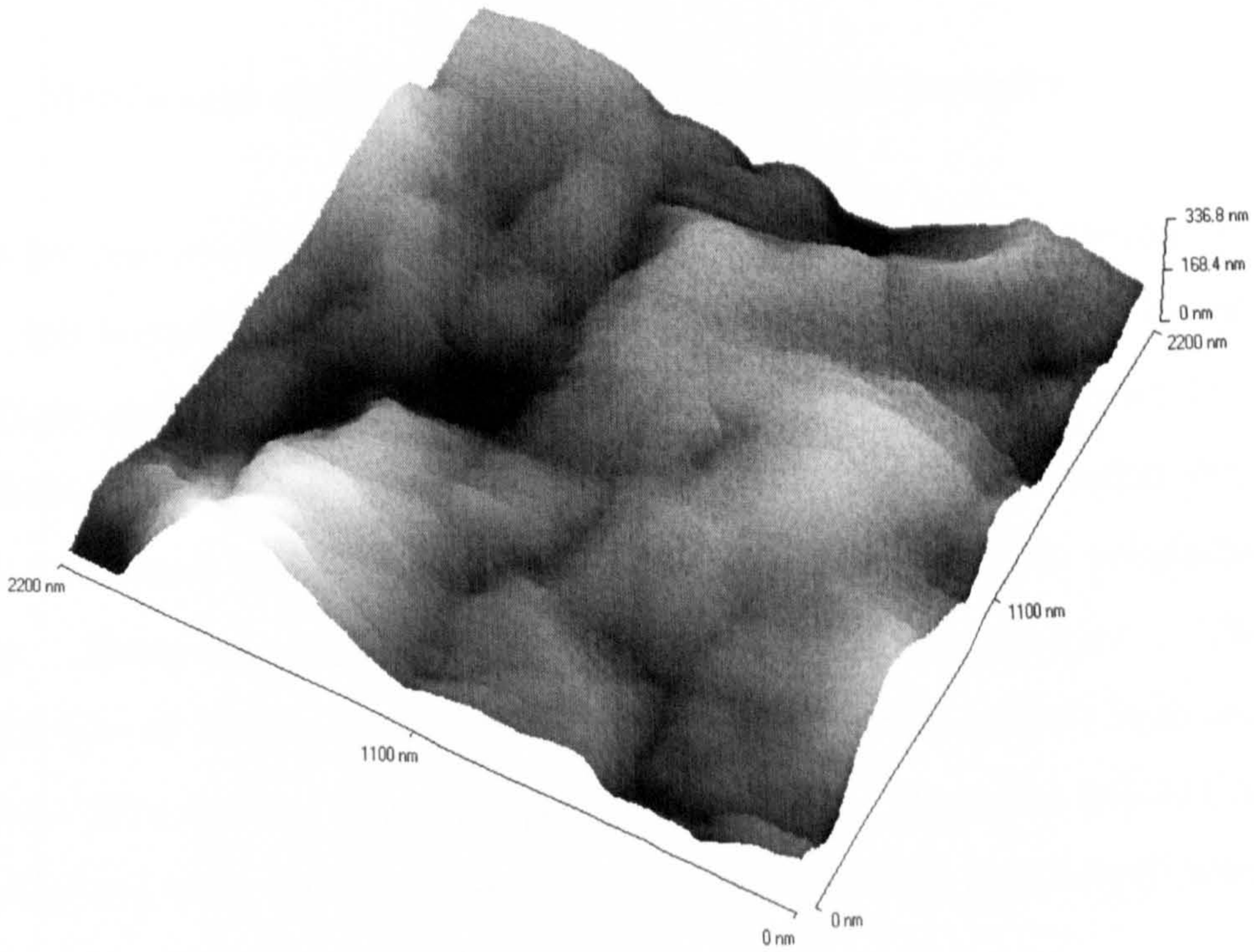

c)

Figure 6.38. AFM images of TriSep X20, a) at 0 nA, b) at 30 nA, c) at 60 nA setting force

Almost all images were not damaged and the ones with minor damage were only 3 out of 40 images. This implies that the AFM force setting has a minor effect on the degree of the membrane surface damage and other parameters such as water pH has more influence on the surface resistance to damage by AFM tip.

6.10 Membranes chemical composition and their performance

From this research it was found that the chemical composition of the membrane active layer, micro-porous support layer, and support layer has a minor or no effect on the membrane performance. Based on ATR/FTIR spectroscopy analysis for the four tested membranes (Osmonics SG, AD, AG and TriSep X20), it was found that they have similar chemical compositions (polyamide aromatic urea with polysulfone support layer). However, they show completely different performance. The chemical composition of TriSep X20 active layer and micro-porous support layer are polyamide aromatic urea and the support layer is polysulfone. Osmonics SG/AD/AG chemical compositions were not given and their composition were determined from ATR/FTIR spectroscopy analysis.

a)

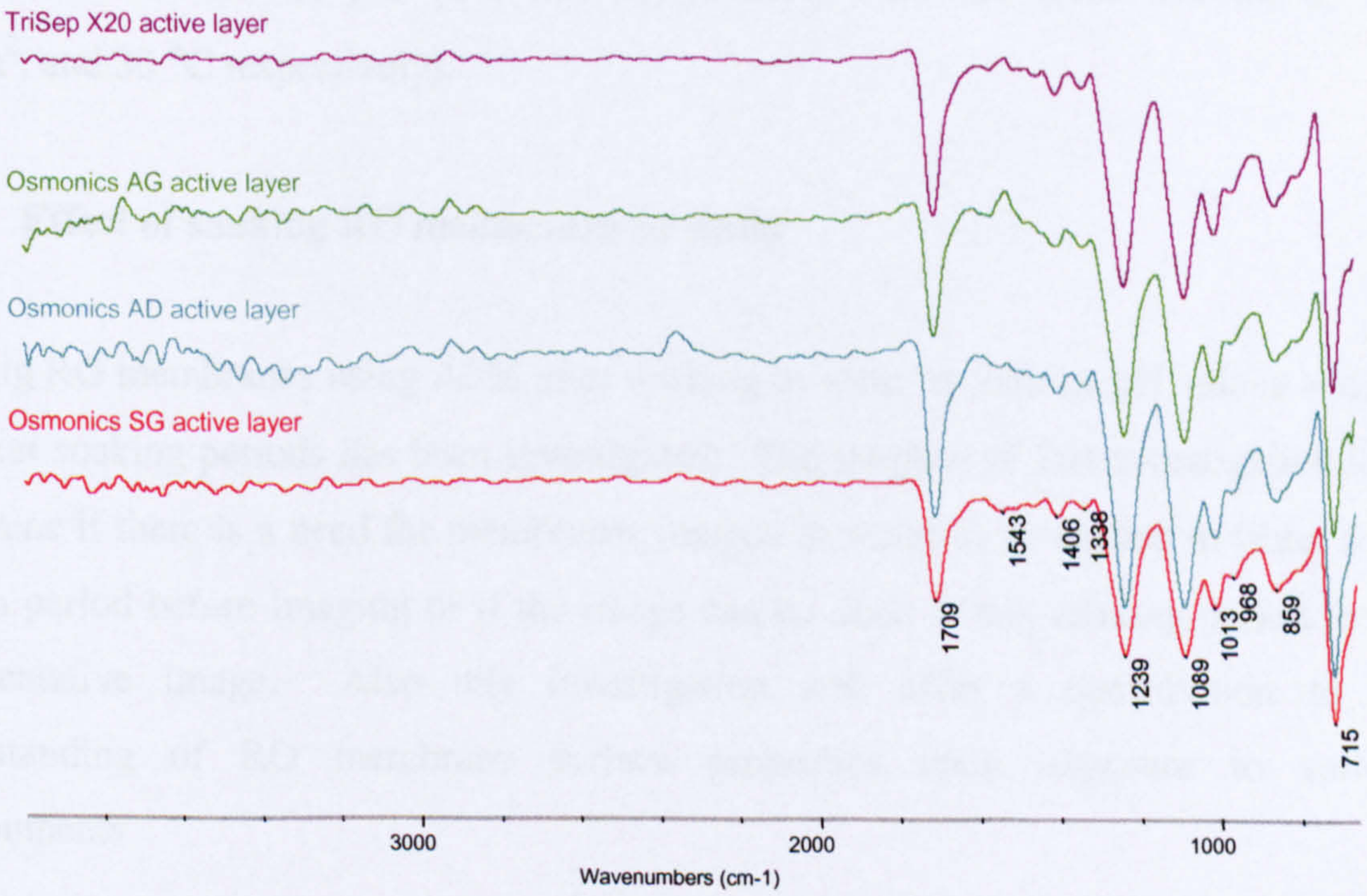

b)

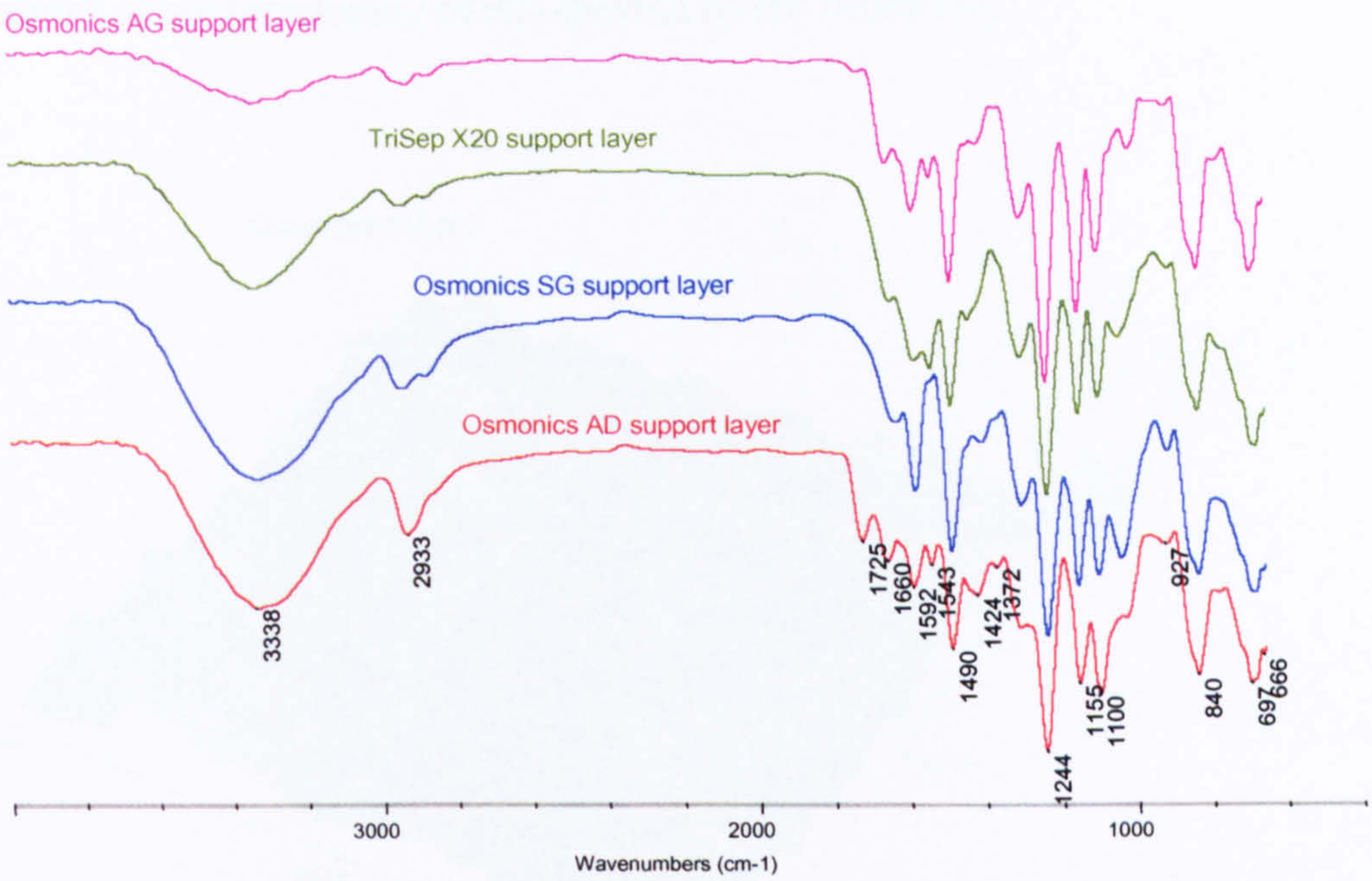

Figure 6.39. ATR/FTIR analysis of Osmonics SG/AG/AD and TriSep X20, a) active layer and b) support layer analysis

As shown in Figure 6.39, all membranes take the same curves as TriSep X20 indicating similar chemical compositions. The permeation rate of Osmonics SG, AD, AG, and TriSep X20 are 60, 8, 77, and 9 l/h/m^2 respectively at the same operating parameters (feedwater conductivity, pH, pressure, temperature, flow are 2800 µS/cm, 8, 140 MN/m^2, and 30 °C respectively).

6.11 Effect of soaking RO membranes in water

Imaging RO membranes using AFM after soaking in water at various pH values and for different soaking periods has been investigated. The purpose of this investigation is to determine if there is a need for membranes imaged in water to be soaked in water for a certain period before imaging or if the image can be done at any soaking period to get representative image. Also this investigation will offer a contribution to the understanding of RO membrane surface properties upon exposure to various environments.

It was found that RO membrane surface morphology changes and takes a different form upon exposure to different environments. Upon soaking, Osmonics SG membrane in

water at pH 2.3 shrinks in the first few minutes then expands (see Figure 6.40). This phenomenon has not previously been reported in the literature.

a)

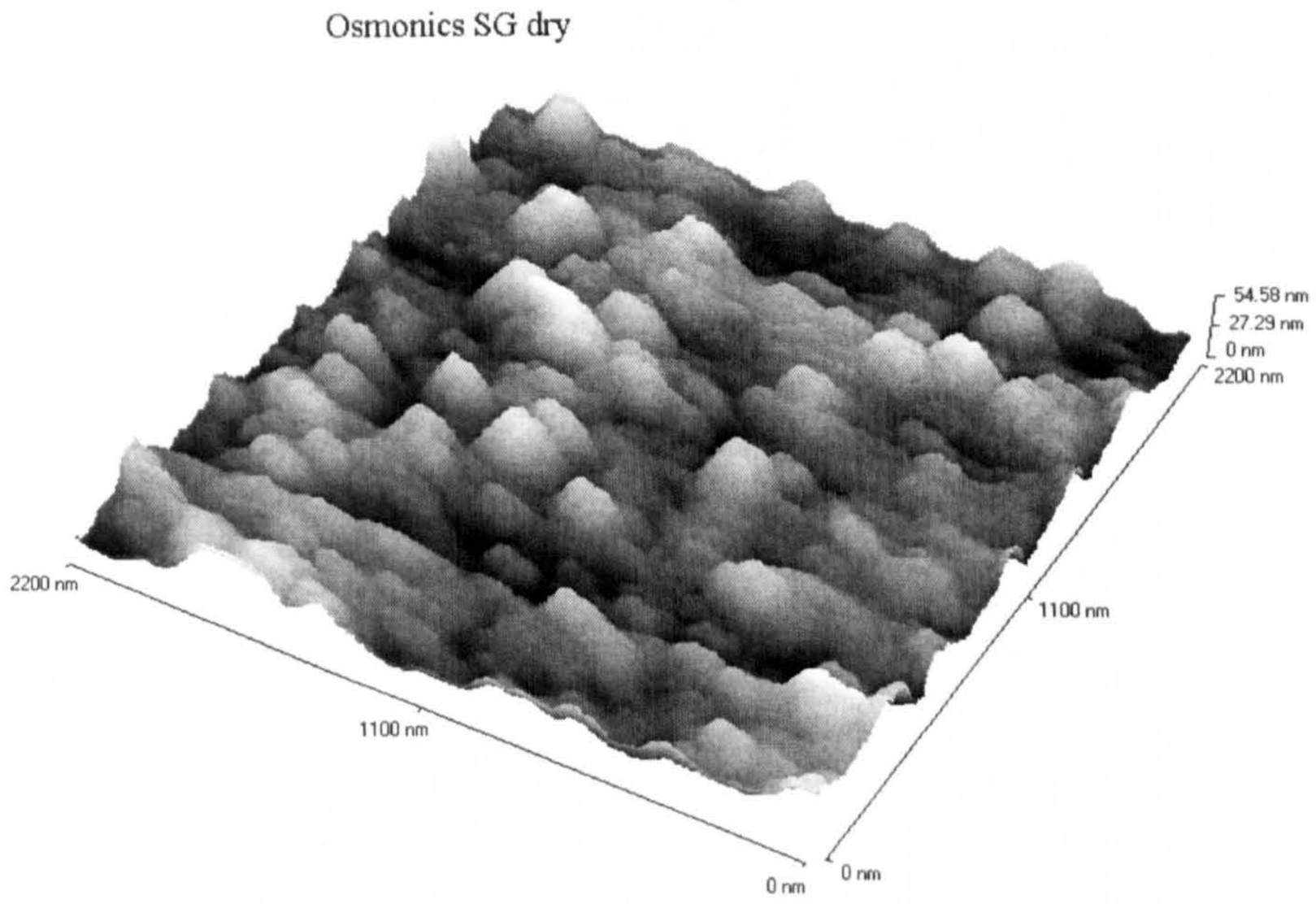

b)

Osmonics SG, wet, pH 2.3, after 15 min

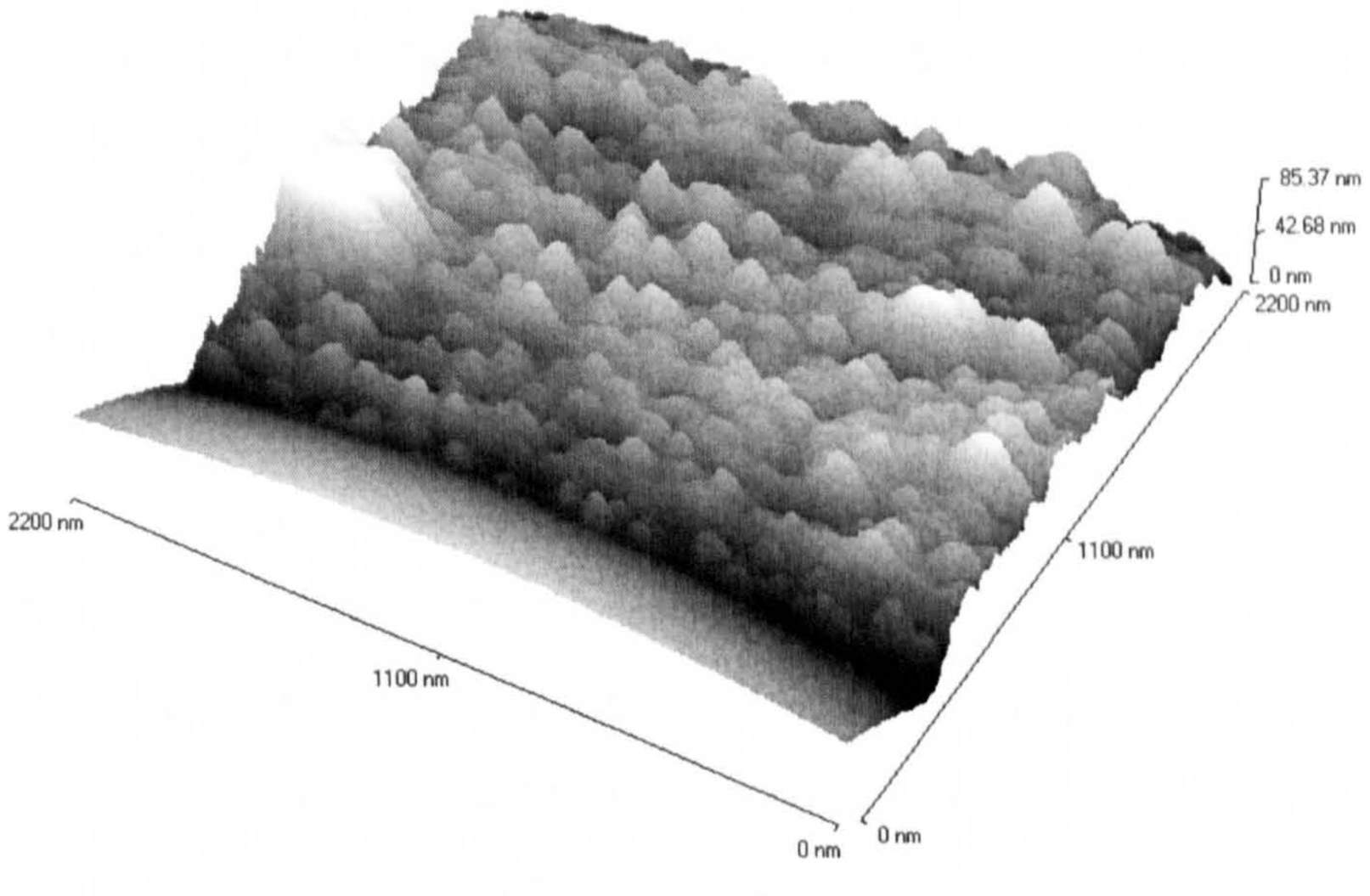

c)

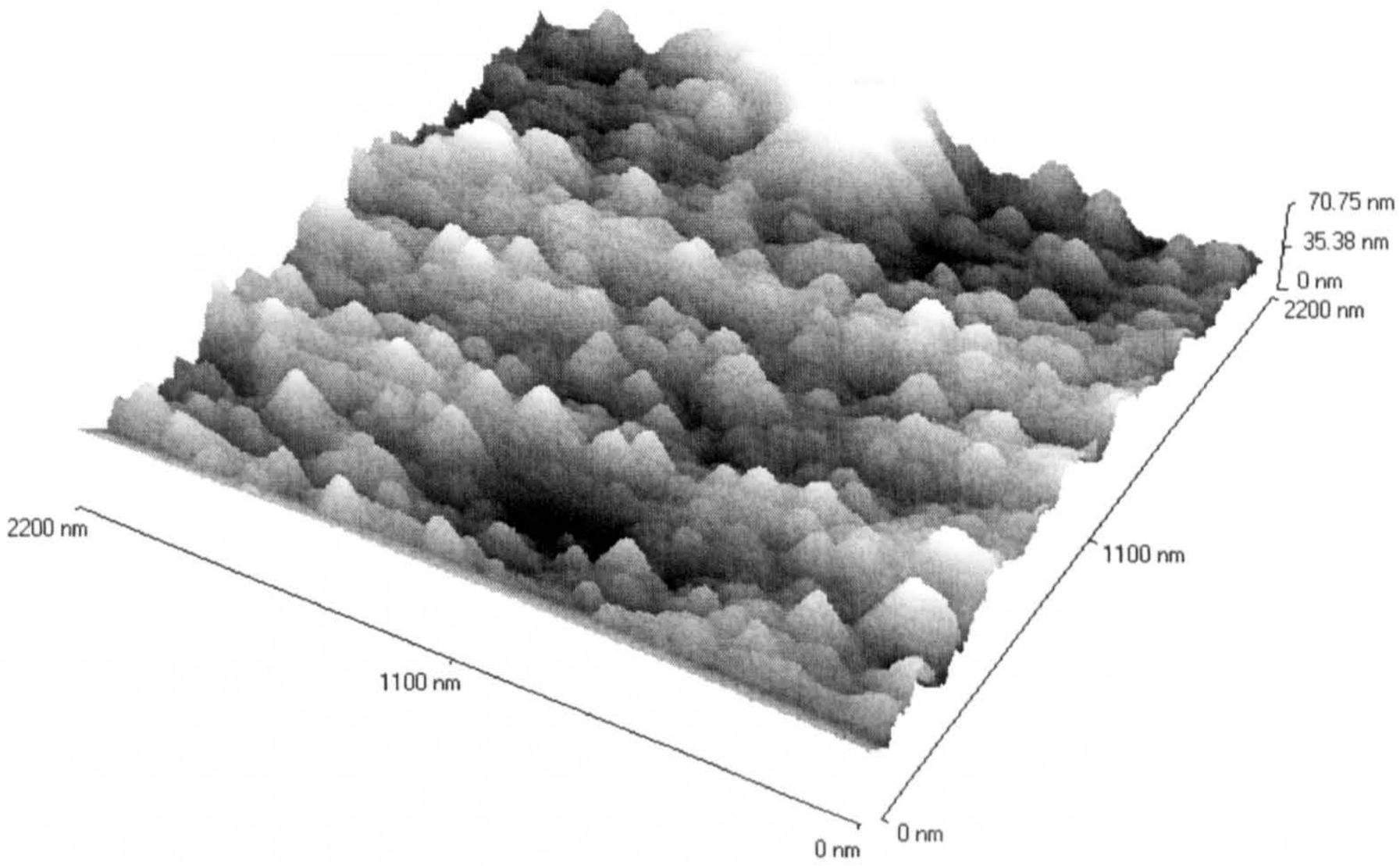

Figure 6.40. AFM image of Osmonics SG a) as received, b) after soaking in water for 15 minute in water pH 2.3, c) after soaking in water for 30 minute in water pH 2.3.

As shown in Figure 6.40, the as-received Osmonics SG membrane shrinks if soaked in water pH of 2.3 in the first 15 minutes then it expands gradually to take the original shape after 30 minutes. It is noticed that the tip has caused minor damage but the image gave the surface morphology details. This experiment was repeated two times and the observations were confirmed. It was not possible to understand the cause(s) of the shrinkage from the work done in this study. However, the purpose here is just to understand the variation that takes place for Osmonics SG upon exposure to different environments. It is found that this shrinkage is not causing any membrane structure damage because the membrane performance was tested with sudden drop in water pH from neutral to 2.3 pH and it performed very well (see Table 6.7).

Time	Water pH	Permeate conductivity (μS/cm)	Salt rejection (%)	Permeation rate (ml/min)
Zero	7.86	722	91	900
After 10 min	2.39	4020	51	818
After 20 min	7.21	730	91	900

Table 6.7. Osmonics SG performance with pH change, Test condition: Pressure = 140 MN/m^2, Temp = 28 °C, Feed conductivity = 8360 μS/cm, Feed flow = 1.1 x 10^{-4} m^3/s

As it can be seen from Table 6.7, that the membrane salt rejection was 91% at zero time and pH 7.86. The addition of acid decreased the pH to 2.39 and dropped salt rejection to 51%. Then caustic addition increased the pH to 7.21 and the membrane retained its original performance (91% salt rejection). At low and high pH the membrane salt rejection drops significantly. This phenomenon will be discussed in detail in chapter 7.

The membrane thickness also changes upon soaking in different pH solutions. The soaked sample (1x2 cm^2) from TriSep X20 membrane in water at pH 5 (water conductivity is 3000 μS/cm) for 3 hours has a thickness of 280 μm, whereas the soaked sample (pH 10 for 3 hours) has a thickness of 200 μm (see Figure 6.41a/b). Both images are the same magnification.

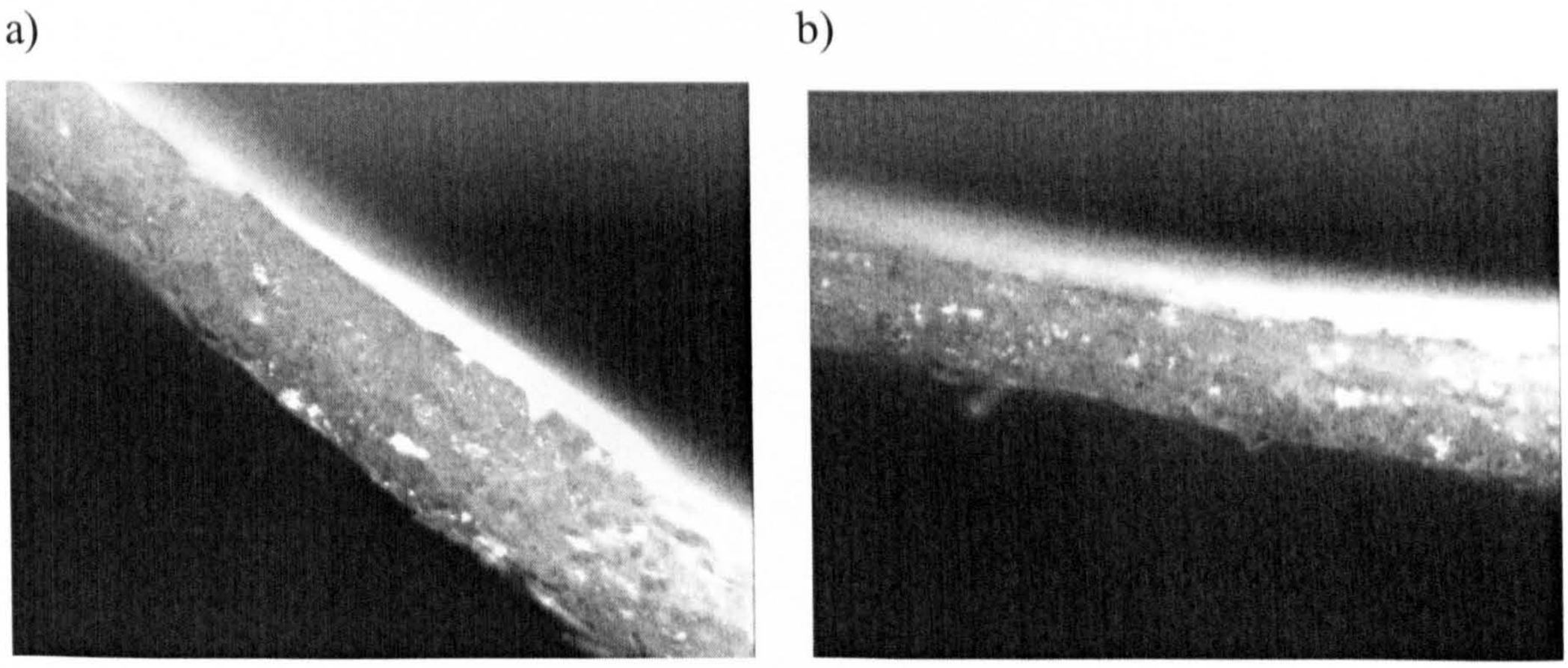

Figure 6.41. a) TriSep X20 soaked in pH 5 water (3 h), b) X20 soaked in pH 10 water.

It is noticed also that membranes expand when soaked in water. Figure 6.4 shows TriSep X20 membrane surface roughness evolution with time. The same spot (20x20 μm) was imaged at each period.

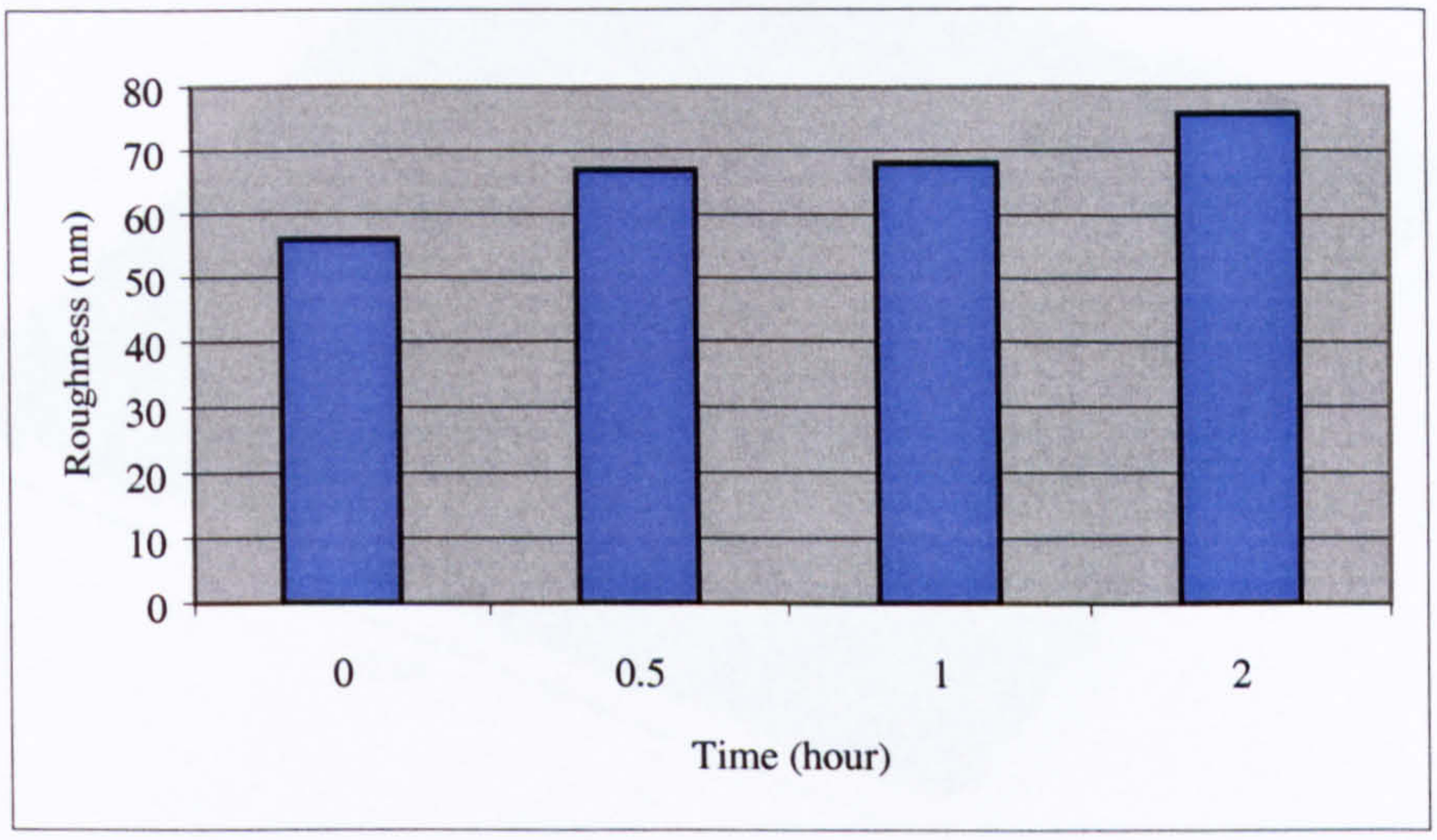

Figure 6.42. TriSep X20 membrane surface roughness changes with time

TriSep X20 membrane surface roughness increased by 35% after two hours of exposure to water indicating that water changes the surface morphology. Figure 6.43 shows how the membrane surface morphology changes with time.

a)

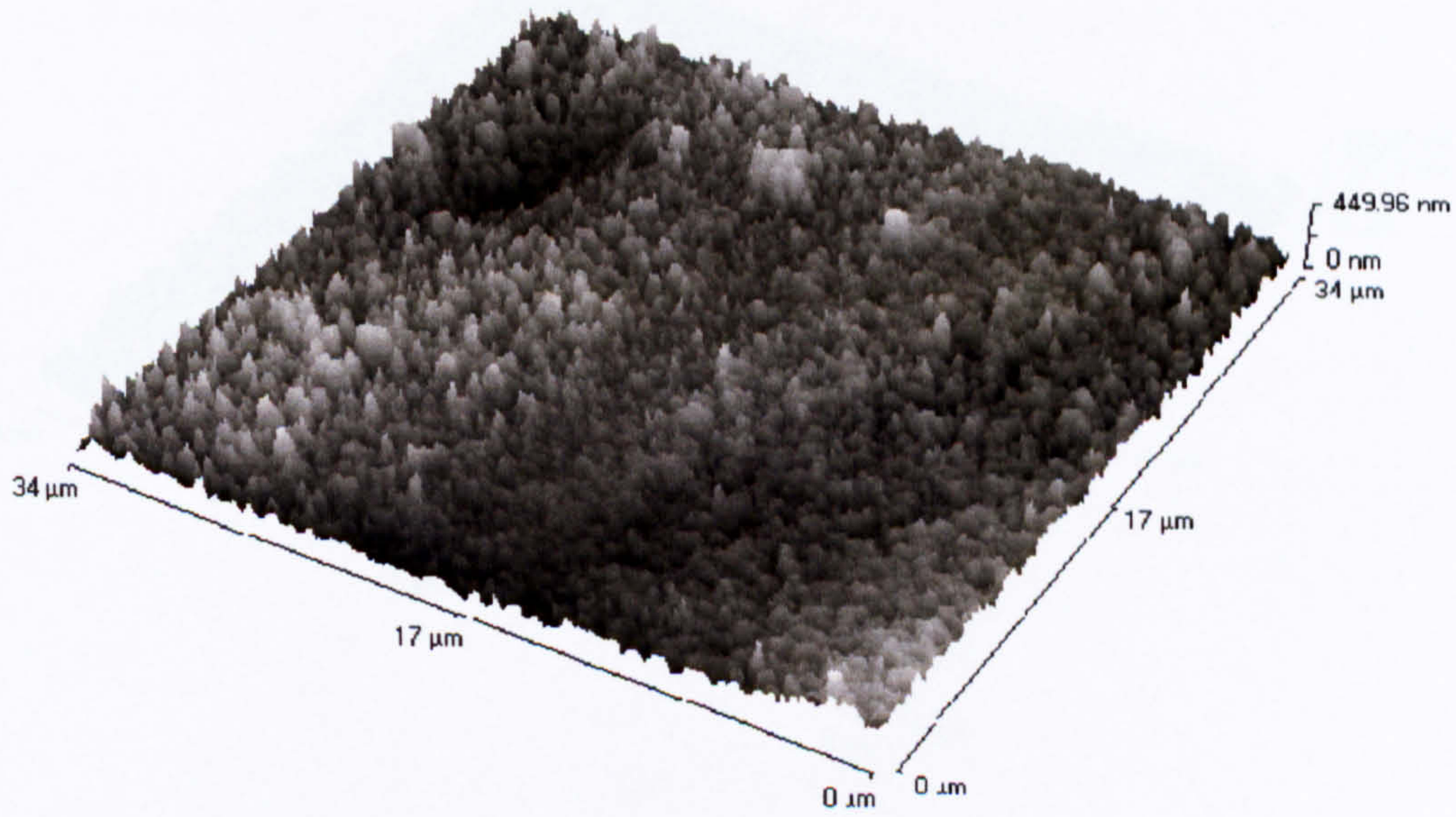

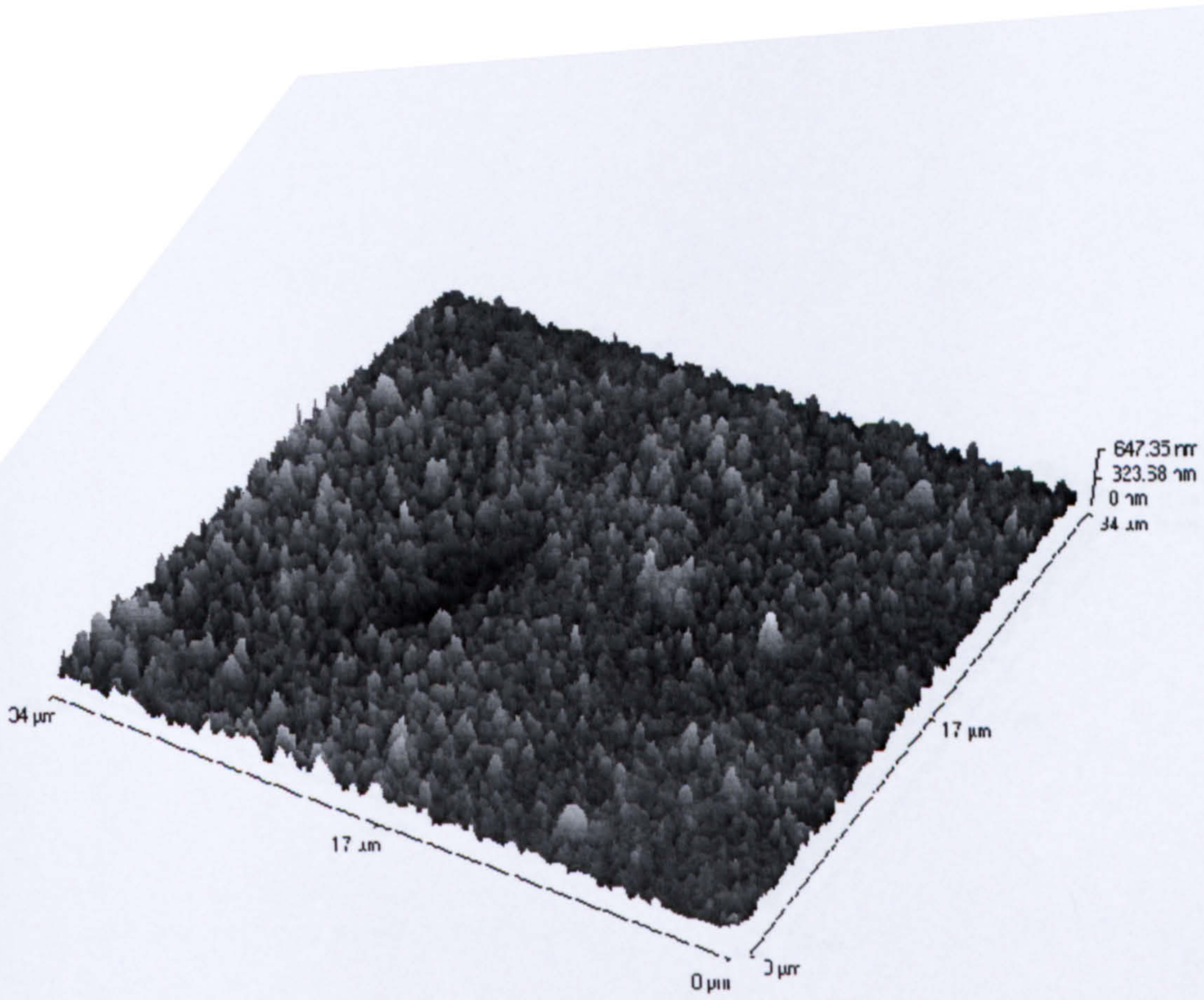
647.35 nm
323.68 nm
0 nm
34 µm
17 µm
0 µm
17 µm
0 µm

c)

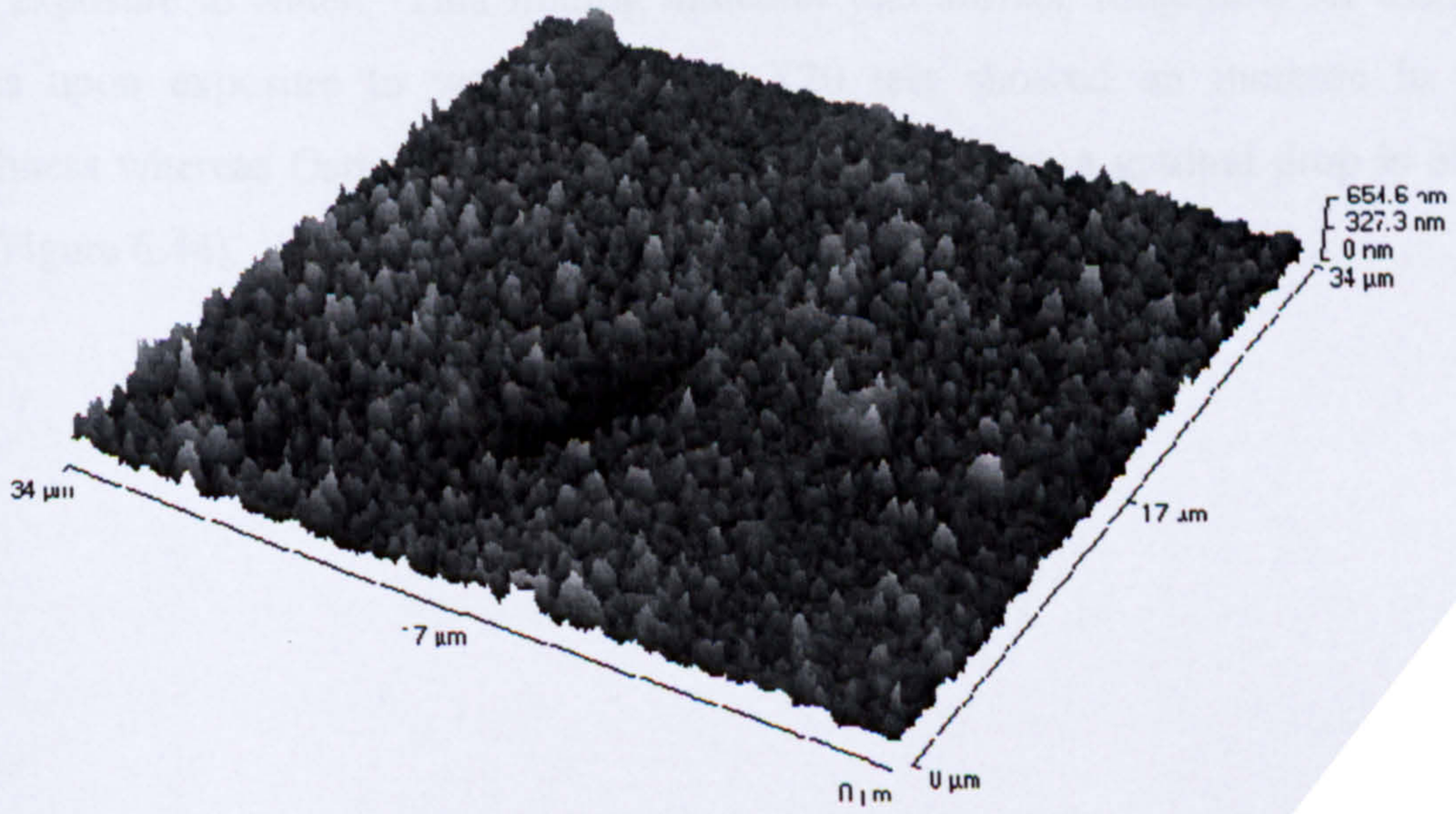
651.6 nm
327.3 nm
0 nm
34 µm
17 µm
0 µm
34 µm
17 µm

d)

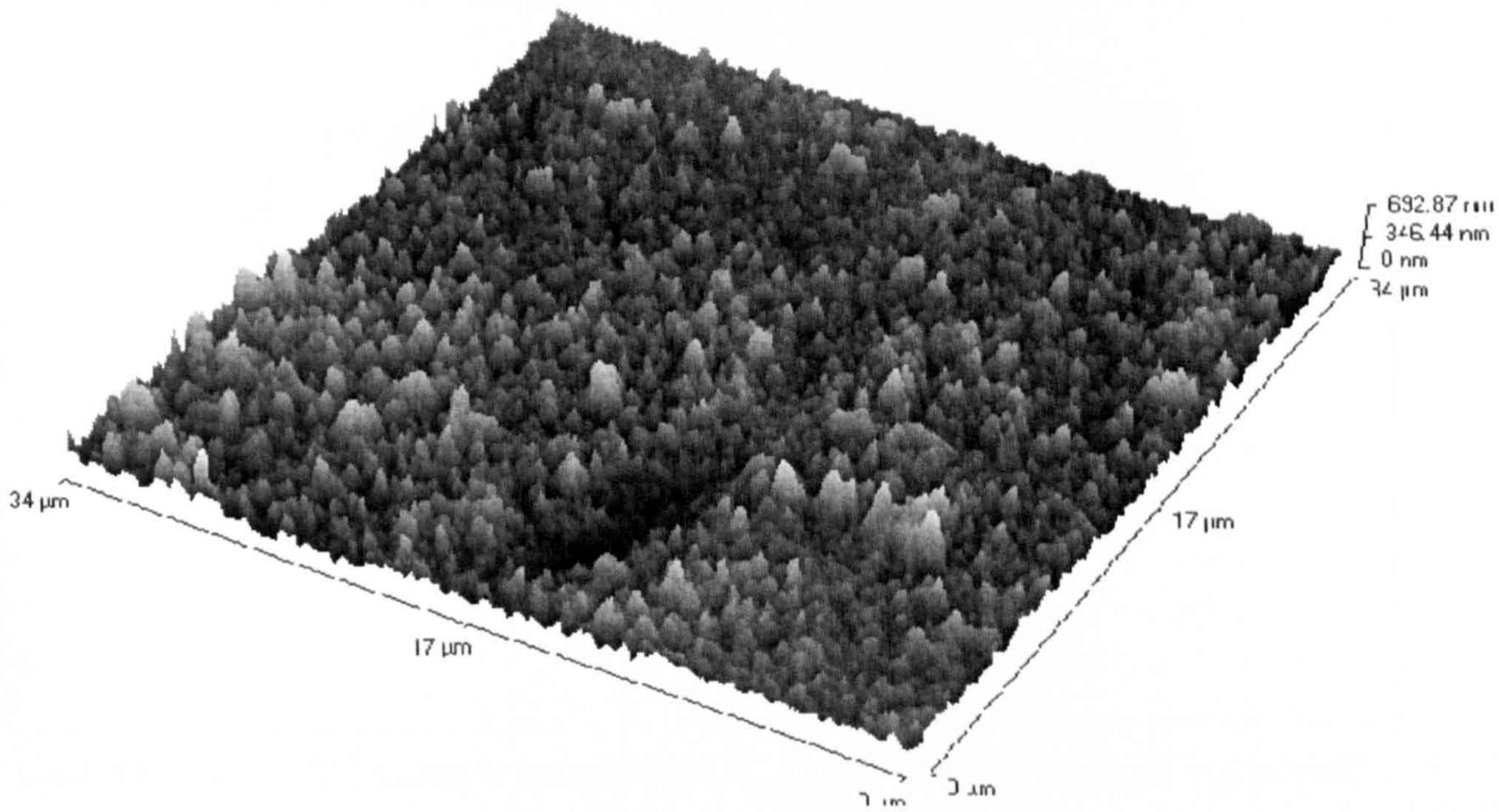

Figure 6.43. AFM images for TriSep X20 in water, a) at zero time, b) after ½ hr, c) after 1 hr, d) after 2 hr

A dip can be seen in all images, which is mainly used as a gauge for indicating that imaging is performed in the same spot. The dip will have an influence on membrane surface roughness values but the goal is not to obtain a representative surface roughness value for the entire surface but rather to check the percentage variation in roughness after exposure to water. This finding indicates that surface roughness for membranes varies upon exposure to water. TriSep X20 test showed an increase in surface roughness whereas Osmonics SG showed an increase then a gradual drop is observed (see Figure 6.44).

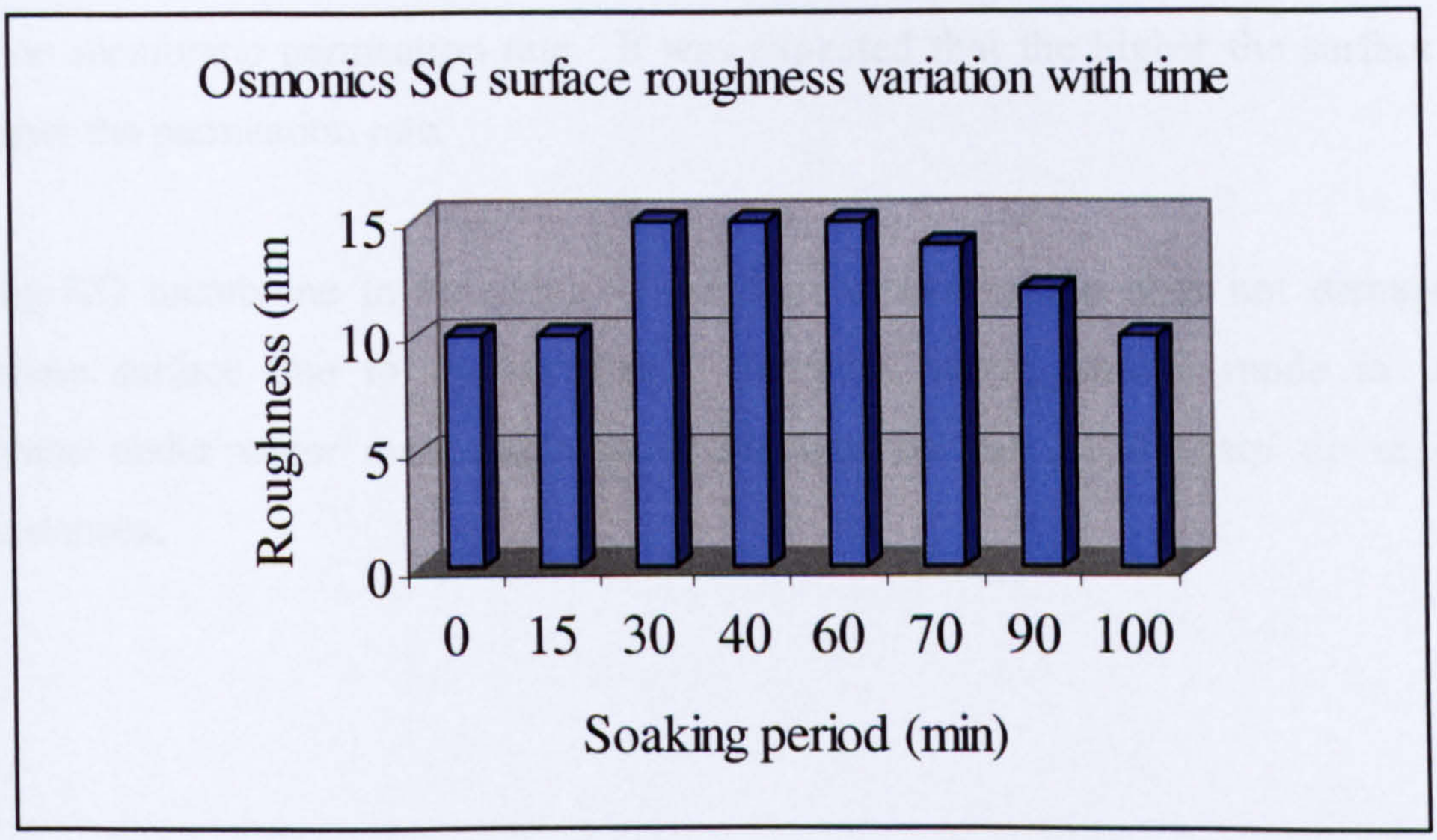

Figure 6.44. Osmonics SG surface roughness (R_{rms}) variation with soaking period

The as received Osmonics SG surface roughness was 10 nm. Upon imaging that sample under water at different periods it was noticed that surface roughness increases to 15 nm and then drops back to 10 nm, which suggest that the effect of water soaking for different membranes is different.

6.12 Summary

From analysis of RO membrane cross-section and active layer surface it was found that RO membranes are complex and simple microscopic analysis does not give information about permeation rate characteristics. Experience in AFM imaging techniques with the knowledge of the membrane representative properties are required to enable proper characterization. Images analysis has to be handled with the understanding that membrane surface morphology properties vary from one location to another within a very small section. Moreover, the environment at which the membrane is exposed to has great influence on its characteristics, which makes RO membrane microscopic characterization complex.

Based on light microscope analysis for the four studied membranes cross-section, it was found that RO membrane cross-section thickness has an influence on membrane

rate, which is possibly due higher-pressure drop across the membrane cross-section. Unexpectedly, it was found that membrane surface roughness and surface area have no effect on membrane permeation rate. It was expected that the higher the surface area the higher the permeation rate.

Imaging RO membrane in air (dry) by AFM in contact mode does not damage the membrane surface due to tip abrasive. However, using contact mode to image membrane under water may cause some damages by the AFM sharp tip in some circumstances.

CHAPTER 7 - RESULTS

RO MEMBRANE PERFORMANCE IN PURE WATER

7.1 Introduction

RO membrane performance can vary significantly not only with RO plant operating parameters but also with the feed water impurity content and type. Understanding the role of each parameter is very important in optimizing membrane performance. In this part of the research, extensive experimentation has been conducted, using pure water as a feed to the RO test unit, to understand the effects of operating parameters such as pressure, temperature, pH, conductivity and feedwater flow on membrane permeation rate and salt rejection. Pure water here refers to distilled water mixed with sodium chloride salt. The main purpose of these experiments is to establish a baseline data for the RO membrane performance using water, which is vital for the subsequent study of the influence of oil contamination on membrane performance as presented in the next chapter. Osmonics SG and TriSep X20 membranes were selected for this part of the research because they have different permeation rates, surface morphology and cross-section thickness properties as shown in chapter 6. This chapter covers the following:

- Time required to reach a steady state condition
- Selected test operating conditions
- Effect of feedwater pressure on RO membrane performance
- Effect of feedwater temperature on RO membrane performance
- Effect of feedwater pH on RO membrane performance
- Effect of feedwater flow on RO membrane performance
- Effect of feedwater conductivity on RO membrane performance
- Summary

7.2. Time required to reach steady state condition

RO membranes require time from start up before they reach steady state conditions. This is the case for not only in laboratory experiments but also in real life where RO plant manufacturers recommend collecting membrane performance data after 24 hours of operation. Establishing steady state conditions before examining RO membrane performance is a vital step, which many papers in the literature do not consider. At the beginning of each experiment, membrane salt rejection and permeation rates are low and do not reflect the real membrane performance characteristics. With time membrane performance improves (in some circumstance where the membrane is tested in severe fouling environment a drop in performance is possible) until it reaches a steady state condition. The steady state condition is defined as the state where further operation does not result in further change. The following sections present discussion about the time required to reach steady state condition from start-up and also after a change is made in one of the operating parameters while the test unit is being run.

7.2.1 Time required to reach steady state conditions from start-up

Extensive experimentation was conducted in the early stages of this research to understand the effect of the operating period on RO membrane performance. The investigation was conducted for TriSep X20 (see Figures 7.1 and 7.2). TriSep X20 was tested 3 times at different conditions, which were selected because most of the experiments conducted in oily water treatment were at these conditions. The three runs are as follows:

Run 1: Pressure 140 MN/m^2, temperature 29 °C, feed flow 11.7 x 10^{-5} m^3/s, pH 7.6, conductivity 5930 μS/cm

Run 2: Pressure 140 MN/m^2, temperature 27 °C, feed flow 6.7 x 10^{-5} m^3/s, pH 7.6, conductivity 5300 μS/cm

Run 3: Pressure 100 MN/m^2, temperature 30 °C, feed flow 6.7 x 10^{-5} m^3/s, pH 7.6, conductivity 5420 μS/cm

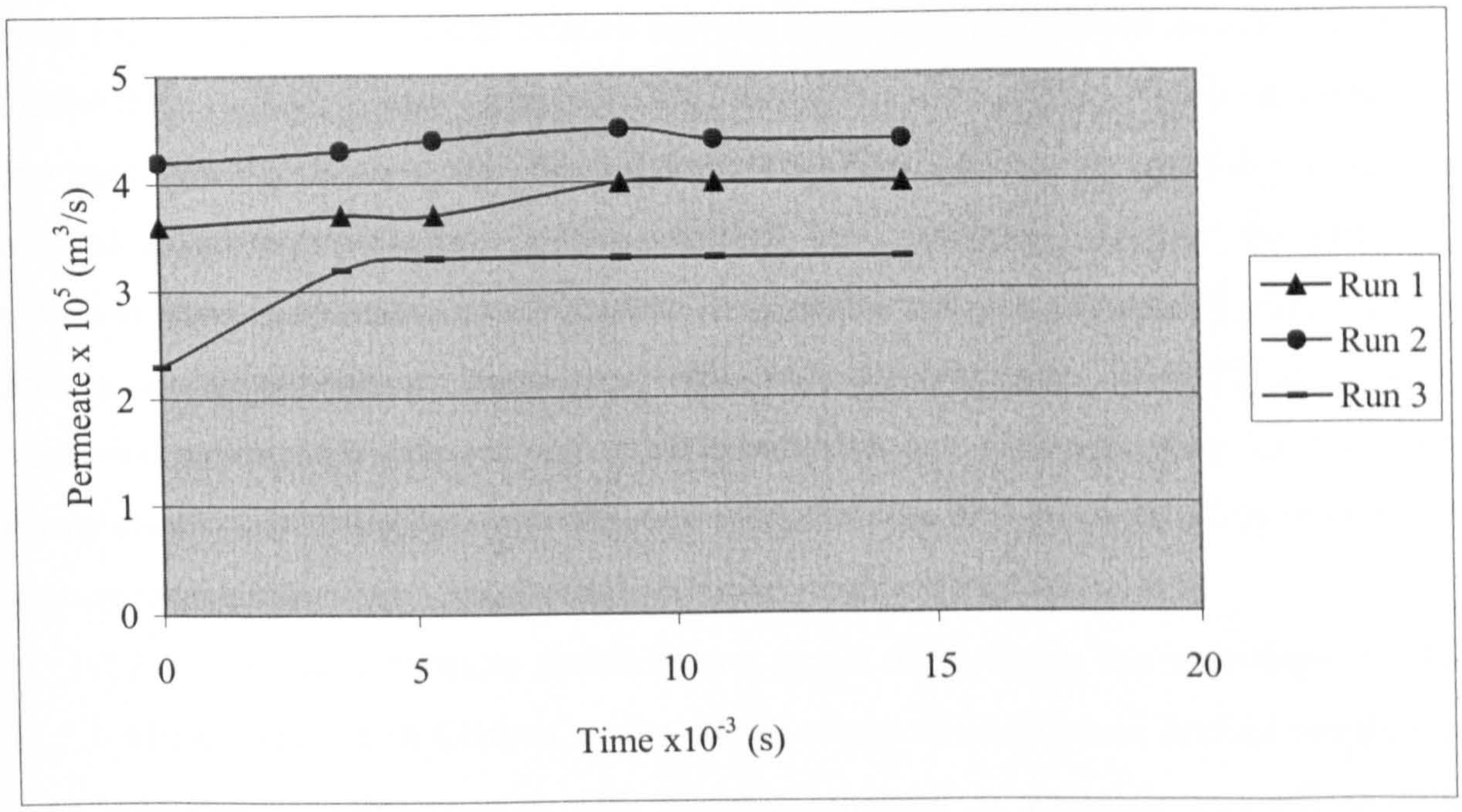

Figure 7.1. TriSep X20 permeation rate with time

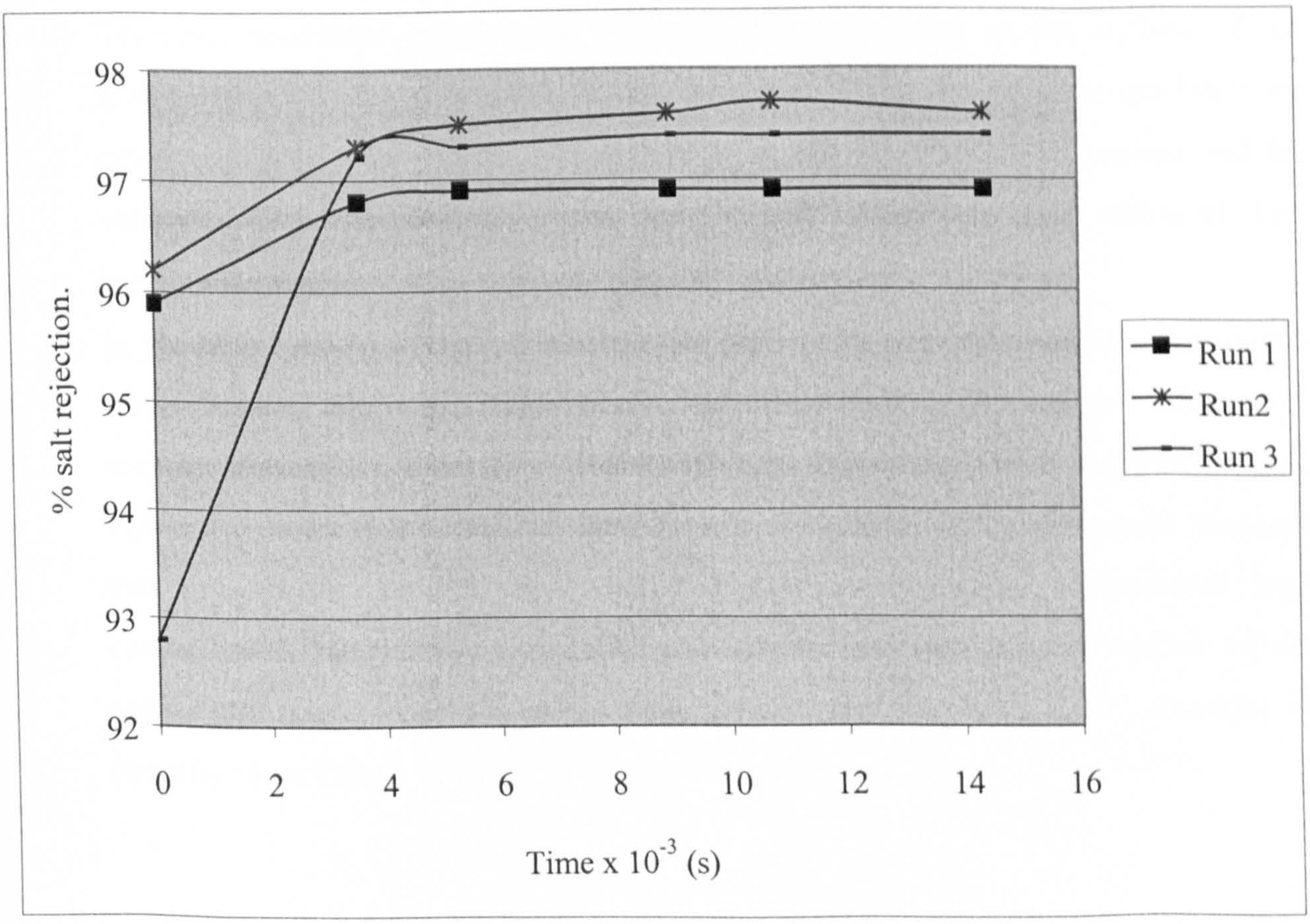

Figure 7.2. TriSep X20 salt rejection percent with time

From Figure 7.1 and 7.2, it can be seen that the membrane permeation rate and salt rejection for the three runs were increasing from the start of the test and until one hour passed. After one hour, the figures show that the salt rejection (more noticeably) and the permeation rate reached an asymptotic value. The stability of the permeation rate and the salt rejection values indicate that steady state is reached. Upon observing Osmonics SG performance with time, a similar conclusion is reached. That is in the first hour (3.6×10^3 s) of operation membrane permeation rate and salt rejection are low and with time they improve to reach steady state conditions after approximately one hour. There are two possible reasons for this phenomenon:

1) A change in membrane structure as a result of changing the environment. This is already proved in Chapter 6 that the as-received membranes surface roughness and thicknesses changes with time when submerged in water or exposed to different environments,
2) Transient conditions encountered diffusion boundary layer at the surface of the membrane. Once the concentration, the temperature and the pressure gradients are established across the diffusion boundary layer, the steady state is reached and the values of both the permeation rate and the salt rejection become stable at their maximum values.
3) In the initial stages of the experiment, the pure water passes through the membrane leaving behind rejected salt at the surface of the membrane. The rejected salt quickly accumulates and the cross-flow is not sufficient to remove it as it accumulates (see Figure 7.3a). High salt concentration at the surface leads to higher osmotic pressure that reduces flux. With time the feed flow sweeps away accumulated high concentration salt to have a constant salt concentration right at the surface of the membrane, which happens approximately after one hour (3.6×10^3 seconds) of operation (see Figure 7.3b).

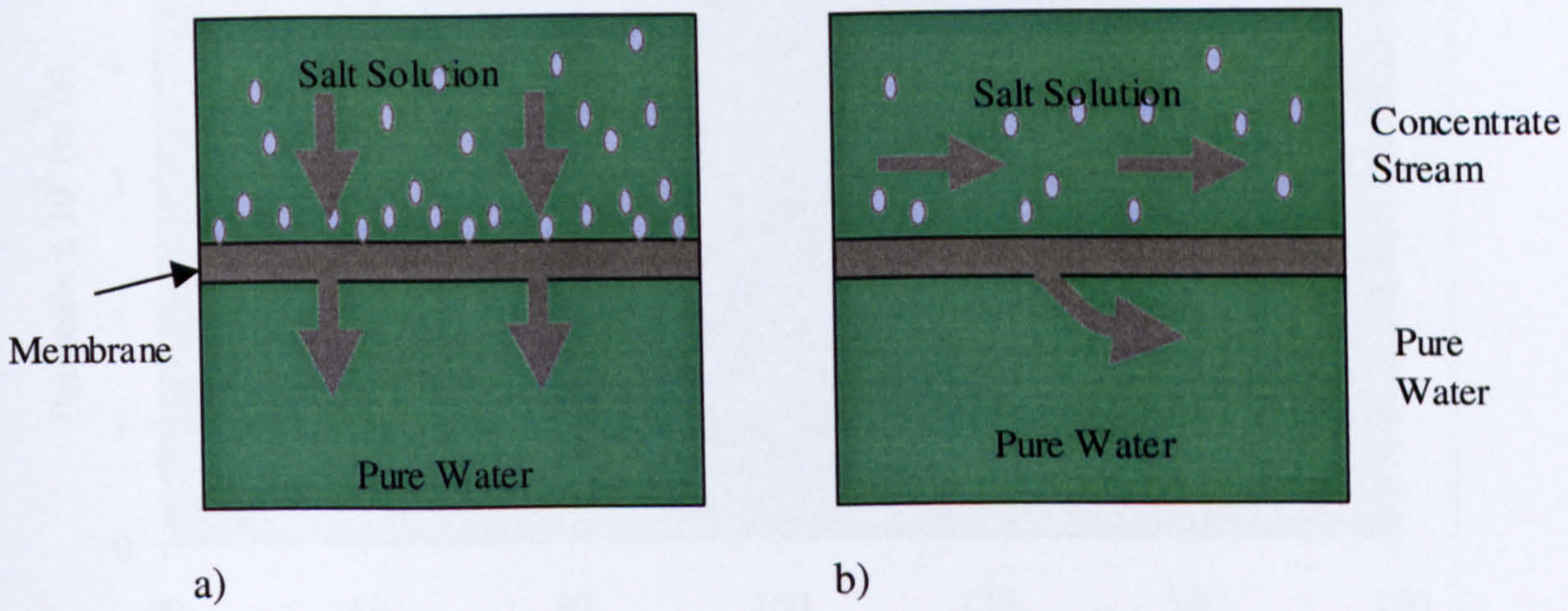

a) b)

Figure 7.3. Water permeation through RO membrane

7.2.2. Time required to reach steady state after a change in one of the operating parameters

After the steady state condition is reached, it was found that any change in one of the operating parameters results in a rapid change in the membrane performance. Unlike at the beginning of the experiment, it does not take one hour to reach a new steady state condition. This is because only one of the operating parameters is changed whereas in the beginning, all of the operating parameters in addition to membrane structure are changed. It was found that 15 minutes is enough to reach a new steady state condition

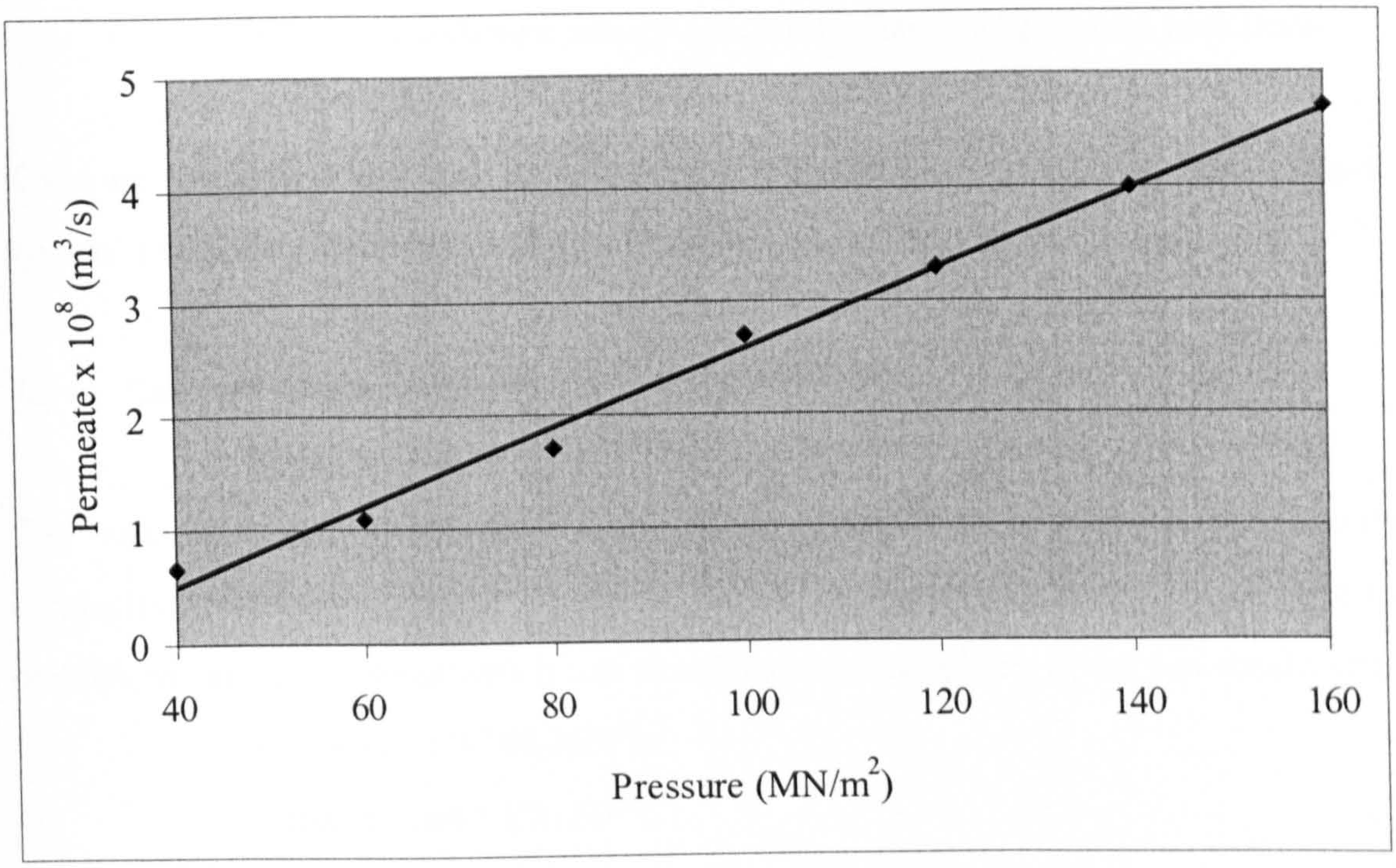

Figure 7.4. TriSep X20 membrane performance with pressure

Figure 7.4 shows the experimental results of TriSep X20 membrane permeation rate at different feed water pressure. The experiment was carried out at feed water conductivity, temperature, pH, flow of 5130 μS/cm, 30 °C, 10.7, and 11.7 x 10^{-5} m^3/s respectively. This experiment was conducted so that the experimental rig was in operation at 40 MN/m^2 feedwater pressure for one hour. Then after each 15 minutes the pressure is increased by 20 MN/m^2.

From Figure 7.4, it can be seen that the permeation rate is very sensitive to any change in the operating pressure. Within 15 minutes the permeation rate increased from 3.3 to 4 x 10^{-8} m^3/s after increasing the feedwater pressure from 120 to 140 MN/m^2. Upon testing the membrane for one hour at 140 MN/m^2 with the same operating parameters stated above (in preparation for evaluating the effect of temperature on permeation) the permeation rate is found to be 3.8 x 10^{-8} m^3/s, which is approximately similar to above result. This suggests that the membrane is very sensitive to any change for a single parameter change and 15 minutes is enough to achieve steady state condition. Based on previous discussion Osmonics SG and TriSep X20 reach steady state condition after:

- One hour from start up condition, and

- 15 minutes to reach new steady condition after changing one parameter.

Knowing the above will ensure that during collection of membrane performance data the system is in steady state and equilibrium conditions are always followed.

7.3 Selected test conditions

The variable operating parameters in this study are feedwater pressure, temperature, pH, conductivity and flow. Based on the design of the experimental rig the following operating conditions can be achieved which can simulate most RO plants operation conditions:

Pressure =10-160 MN/m^2

Temperature = 20- 50 °C

Conductivity = 0- 30,000 µS/cm and higher

Feed flow = 2.5-19.2 x 10^{-5} m^3/s

pH = 1-12

The evaluation of membrane performance using every possible operating condition with various temperatures, pressures, conductivities, flows and pH, would require a massive number of experiments. Therefore, it was decided to select operating conditions that cover a wide range of operating conditions relevant to RO plants and to devise a reasonable understanding for the effect of each operating parameter (see Table 7.1).

Parameter	Tested range	Fixed value when testing other parameters (common RO plant operating parameters)
Pressure	40-160 MN/m^2	140 MN/m^2
Temperature	26-46 °C	29-31 °C
pH	3.5-11.5	10-10.5
Flow	2.5-19.2x10^{-5} m^3/s	11.7 x 10^{-5} m^3/s
Conductivity	80-25,000 µS/cm	5000-5300 µS/cm

Table 7.1. Selected test parameters

The operating parameters were monitored by controlling bypass, cooling water and reject flow. A simplified drawing of the experimental test rig is given in Figure 7.5. Operating pressure adjustment was performed by controlling bypass and reject flow. The operating temperature adjustment was done by controlling the cooling coil flow. Feedwater flow was monitored by adjusting reject flow. Increasing cooling coil valve opening leads to higher cooling and therefore lower operating temperature. Increasing bypass flow leads to decreasing feedwater pressure. The pH adjustment was performed by the addition of hydrochloric acid or sodium hydroxide and feedwater conductivity is controlled by the addition of sodium chloride.

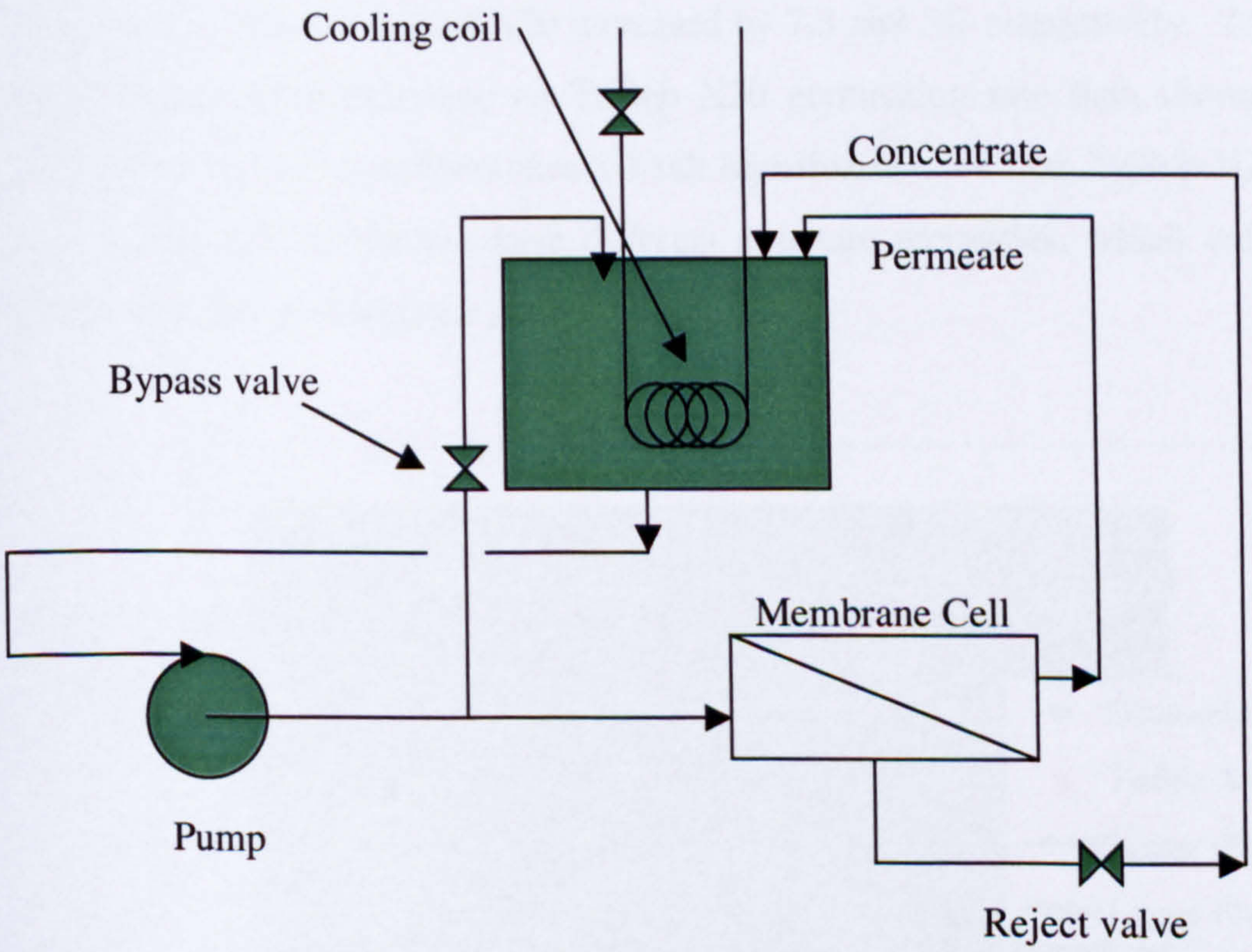

Figure 7.5. Simplified drawing for experimental rig

From the operating conditions studied in these experiments the performance in other conditions can be predicted. However, from these experiments, the expected performance from Osmonics SG and TriSep X20 can be calculated in the range of the test rig. This will be presented in the summary of this chapter.

7.4 Effect of feedwater pressure on RO membranes performance

It was found that feedwater pressure has a large effect on the RO membrane performance of the two membranes in this study. The extent of the effect was found to be membrane dependent. The general pressure effect in RO membrane performance is already reported in the literature. Experiments were conducted at feedwater conductivity, pH, temperature, feedwater flow of 5130 μS/cm, 10.7, 30 °C, and 11.7 x 10^{-5} m^3/s. Both membranes were tested at 40, 60, 80, 100, 120, 140, and 160 MN/m^2 feed water pressure. It can be seen from Figure 7.6 and 7.7 that increasing pressure from 40 to 160 MN/m^2 increased permeation rate by 5.7 times and 7.2 times for Osmonics SG and TriSep X20 respectively and salt rejection of Osmonics SG and TriSep X20 increased by 7.3 and 3% respectively. This shows that the pressure has more influence on TriSep X20 permeation rate than Osmonics SG and the influence of pressure on Osmonics SG salt rejection is more than TriSep X20. Osmonics SG and TriSep X20 membrane have different structure properties, which will be discussed in relation to their performance later.

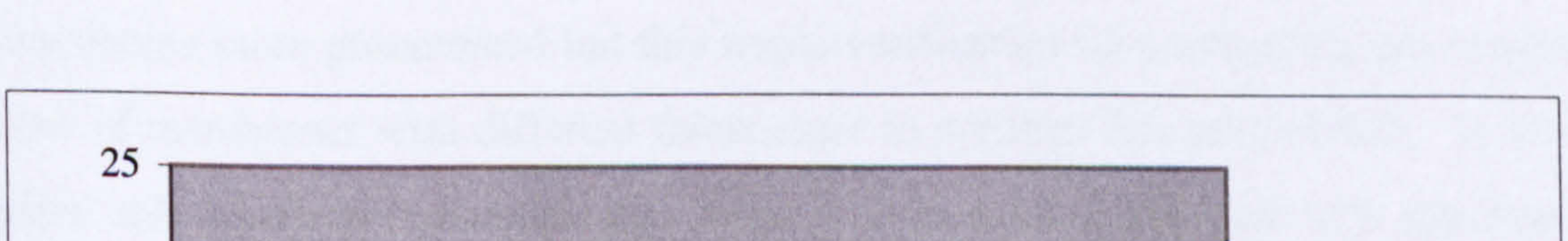

Figure 7.6. Effect of feedwater pressure on Osmonics SG and TriSep X20 permeation rate

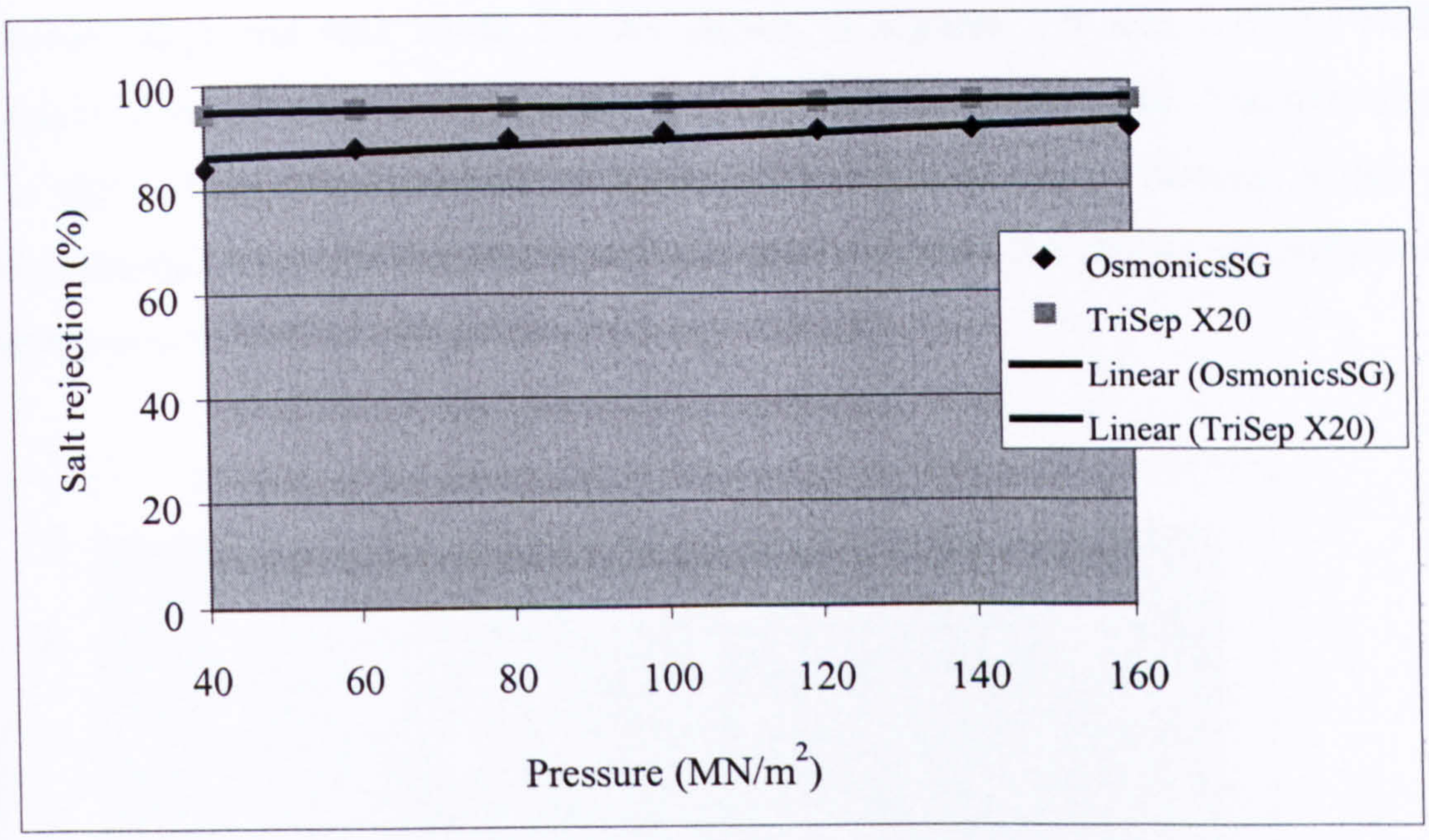

Figure 7.7. Effect of feedwater pressure on Osmonics SG and TriSep X20 salt rejection

Osmonics SG is about 20% thinner than TriSep X20 (TriSep X20 thickness is 227 μm and Osmonics SG thickness is 189 μm). This suggests that perhaps the effect of pressure on thick membrane more pronounced but this needs verification by conducting this research on a number of membranes with different thicknesses to confirm this relationship. In terms of membrane salt rejection it appears that there is a gradual increase in salt rejection with pressure increase which is possibly as a result of increasing water permeation, which dilutes permeate salts. Other than membrane thickness parameters such as membrane pore size and surface morphology could have an influence. TriSep X20 is characterized as a very rough membrane whereas Osmonics SG is considered as a smooth membrane. Surface roughness influences the dynamics of water flow in the boundary layer.

7.5 Effect of feedwater temperature on RO membranes performance

Feedwater temperature although having a significant effect on permeation rate of Osmonics SG and TriSep X20 membranes has only a negligible effect on TriSep X20 salt rejection and Osmonics SG salt rejection. Experiments were conducted at feedwater conductivity, pH, pressure, feedwater flow of 5130 μS/cm, 10.7, 140 MN/m^2, and 11.7 x 10^{-5} m^3/s. The

temperature range test was 26-46 °C. As shown in Figures 7.9 and 7.10, as feedwater temperature increases the permeation rate increases for both membranes. The most probable cause is that an increase in temperature leads to a decrease in water viscosity, which results in easier passage for water through membrane pores. Figure 7.8 shows viscosity variation with temperature.

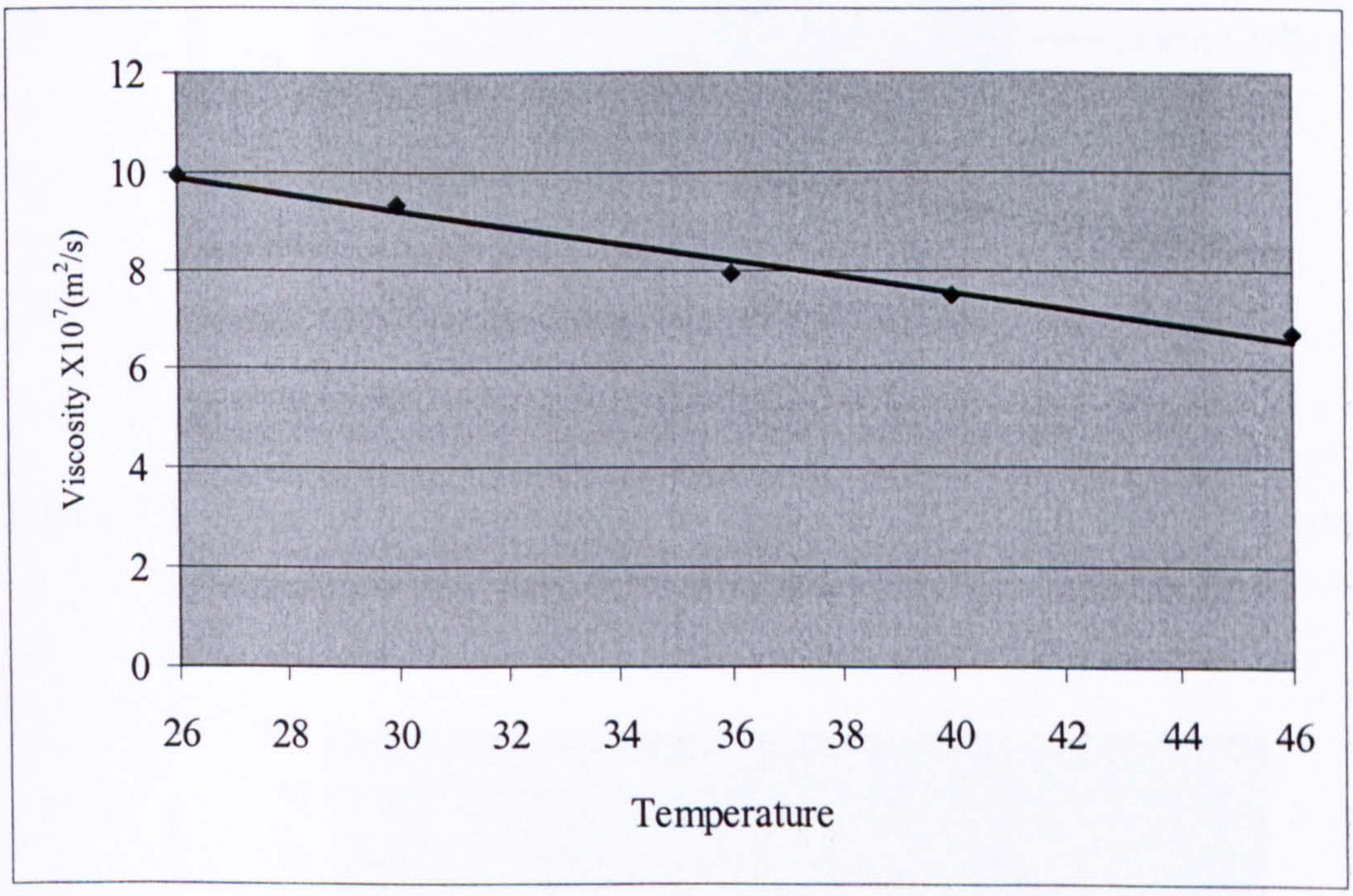

Figure 7.8. Water viscosity variation with temperature [153]

Salt rejection of both membranes was not affected by temperature change (from 26 to 46 °C). It is believed that temperature rise increases salt passage through the membrane as a result of membrane expansion, which will increase membrane pore size. However, the increase in membrane permeation rate dilutes passed salts to end up with no noticeable change in salt rejection properties.

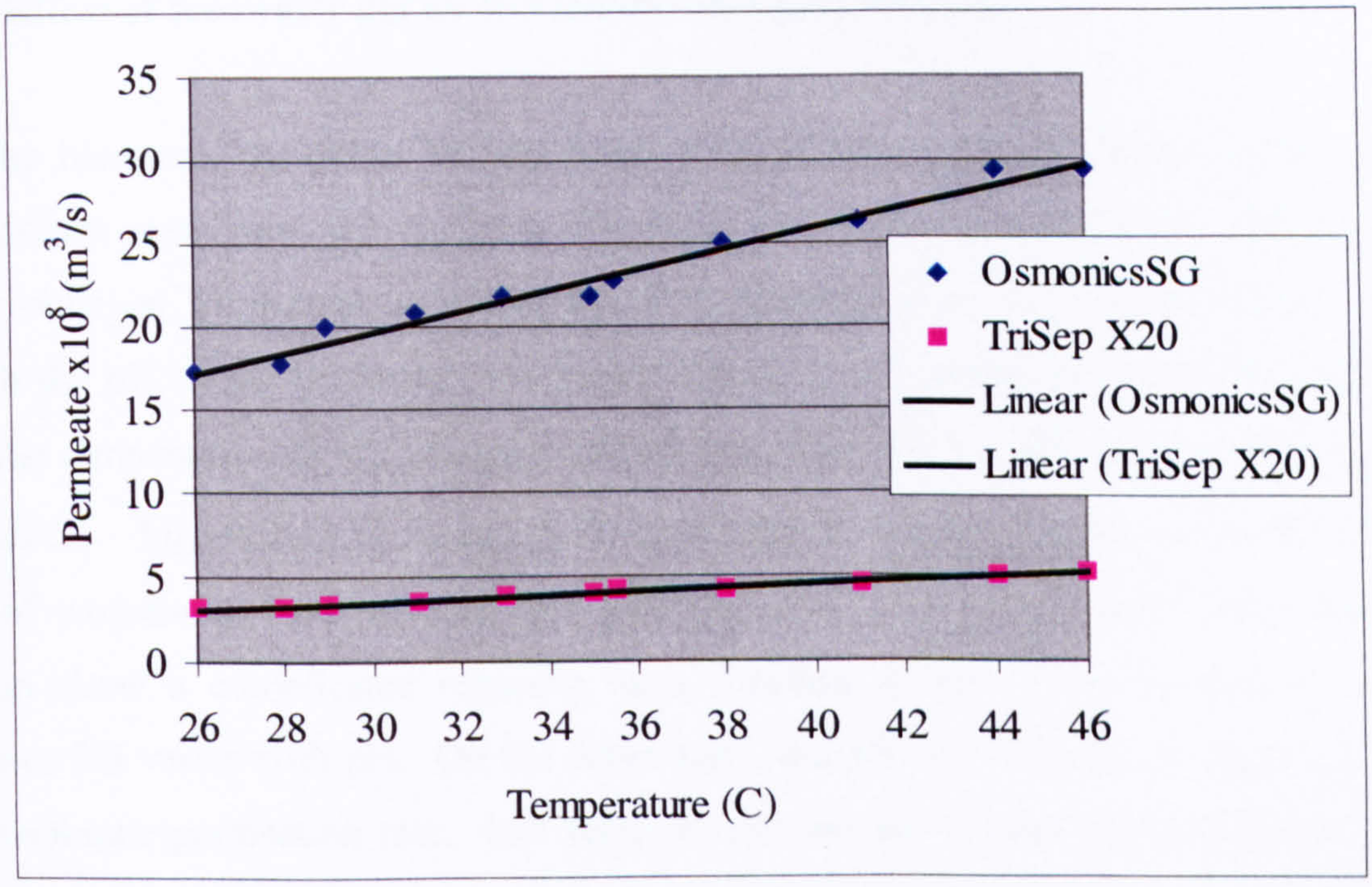

Figure 7.9. Effect of feed temperature on Osmonics SG and TriSep X20 permeation rate

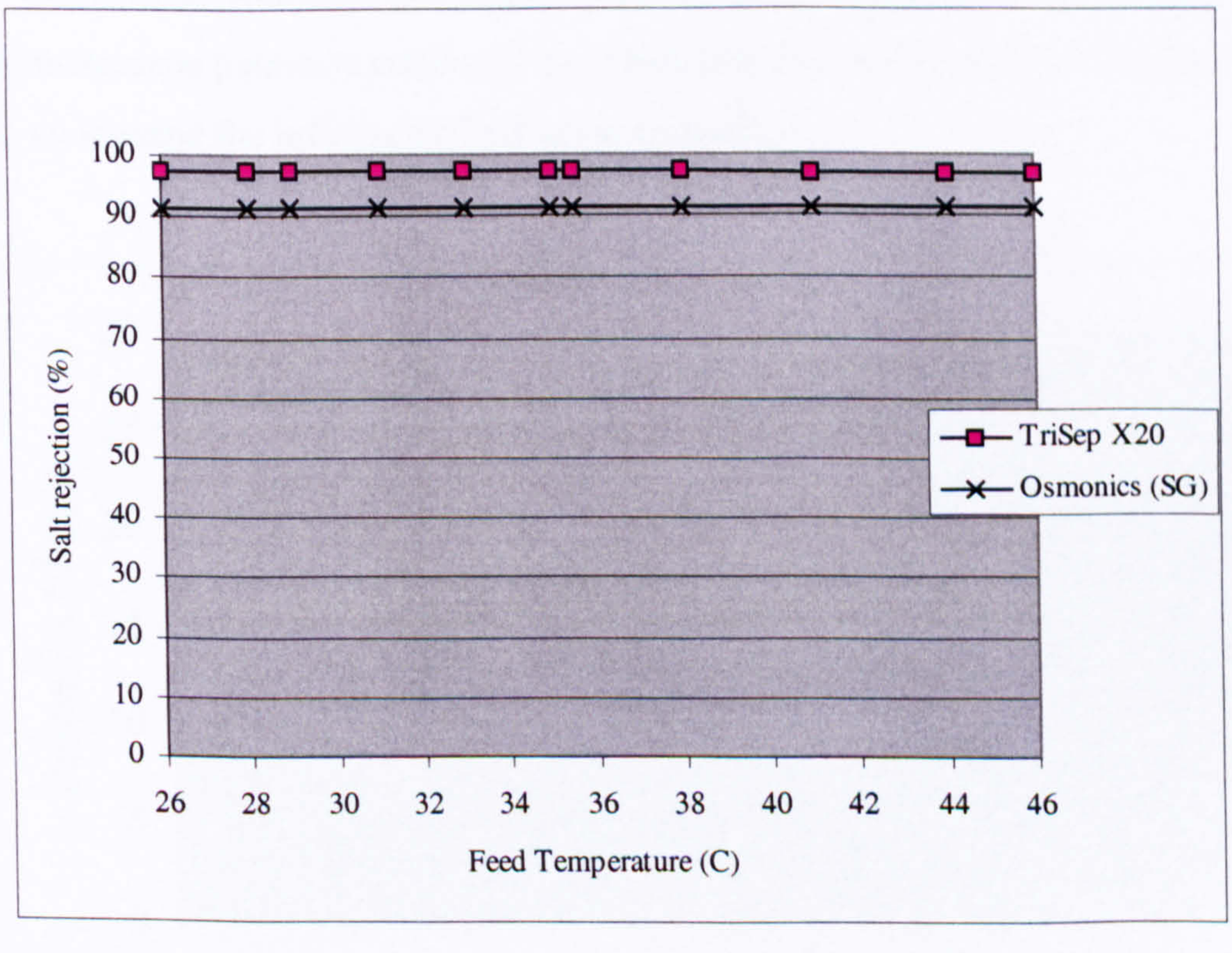

Figure 7.10. Effect of feed temperature on Osmonics SG and TriSep X20 salt rejection

7.6 Effect of feedwater pH on RO membranes performance

From the literature, the pH is known to have an influence on membrane surface charge, which affects membrane salt rejection properties and fouling mechanisms. These data are usually obtained by measuring membrane zeta potential over a wide pH range. In this research the pH of the feedwater was varied from 2 –11.8 under the following conditions: feedwater temperature 30 °C, pressure 140 MN/m^2, flow 11.7 x 10^{-5} m^3/s, and conductivity 5000 μS/cm. Figure 7.11, 7.12 and 7.13 show that, in contrast to the trends observed for effect of temperature and pressure (see previous sections), the permeate and percent salt rejection show a complicated response as a function of pH. The permeation rate for Osmonics SG varies with pH. On the other hand, the pH has virtually no effect on TriSep X20 membrane permeation rate. Salt rejection percent for TriSep x20 membrane is more than Osmonics SG membrane over all of the pH range tested. Moreover, salt rejection percent is sensitive to feedwater pH suggesting that operating pH is a crucial parameter in controlling membrane permeate conductivity. Osmonics SG was tested in extremely low and high pH to understand the influence of pH in more detail.

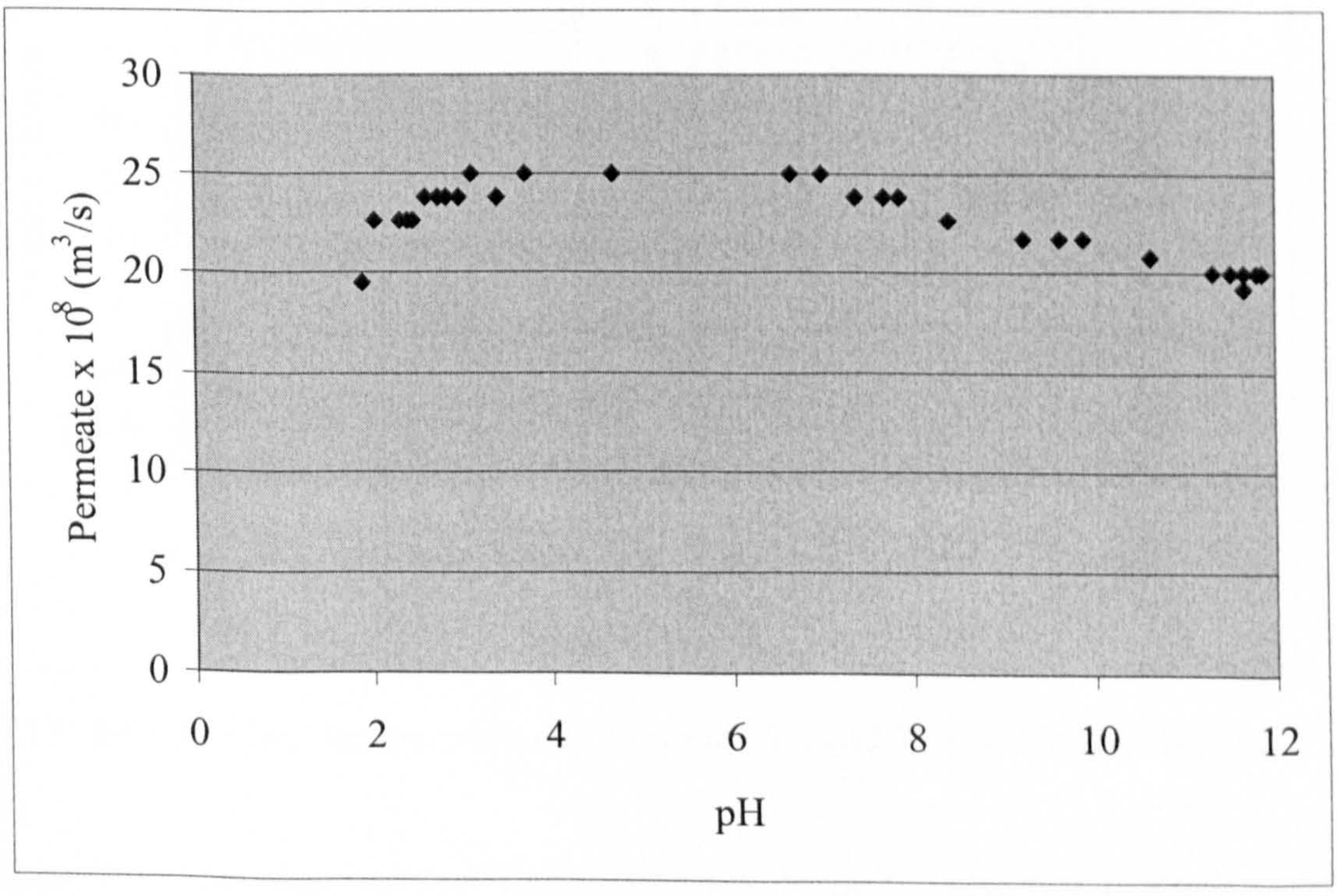

Figure 7.11. Effect of feedwater pH on Osmonics SG permeation rate

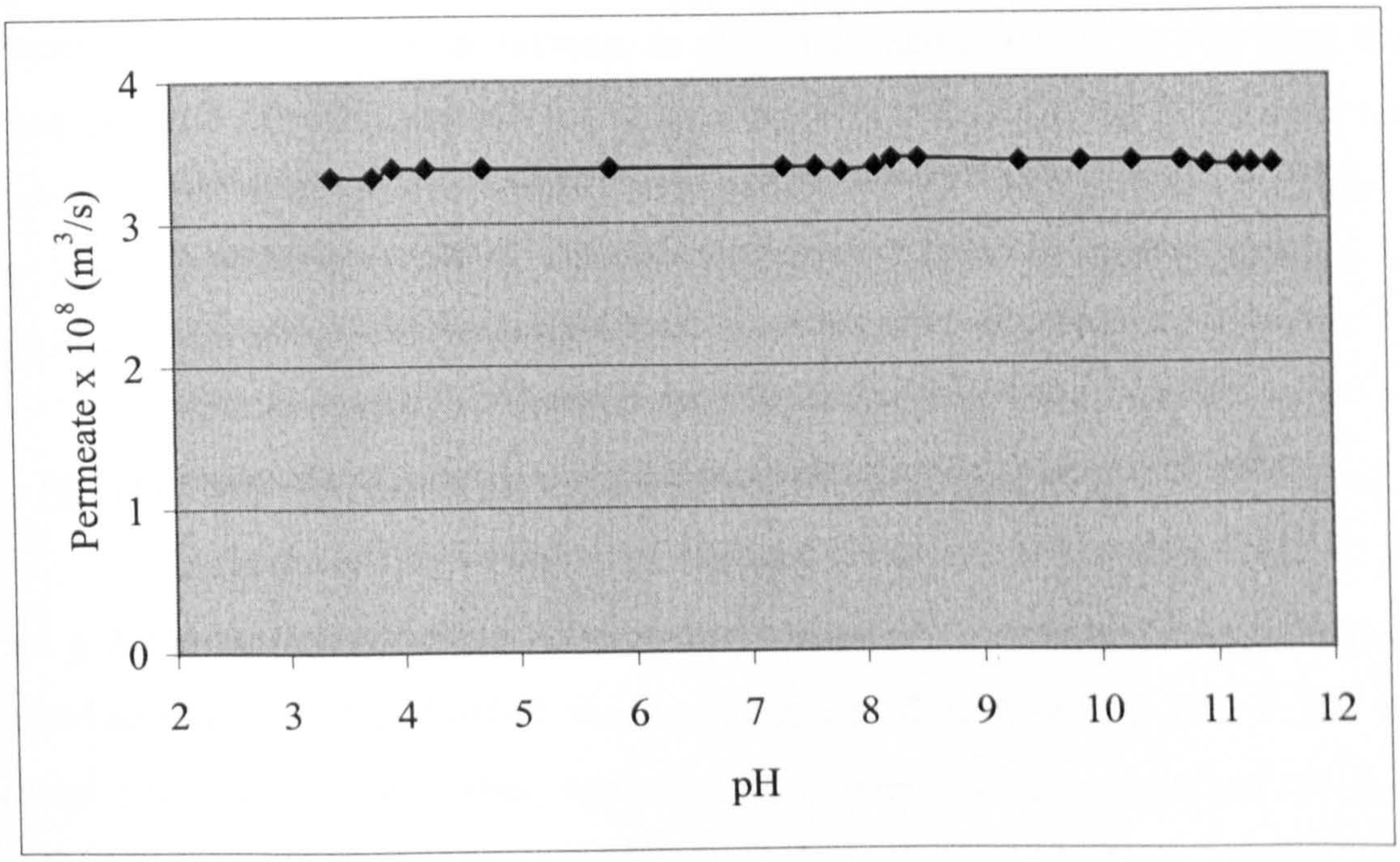

Figure 7.12. Effect of feedwater pH on TriSep X20 permeation rate

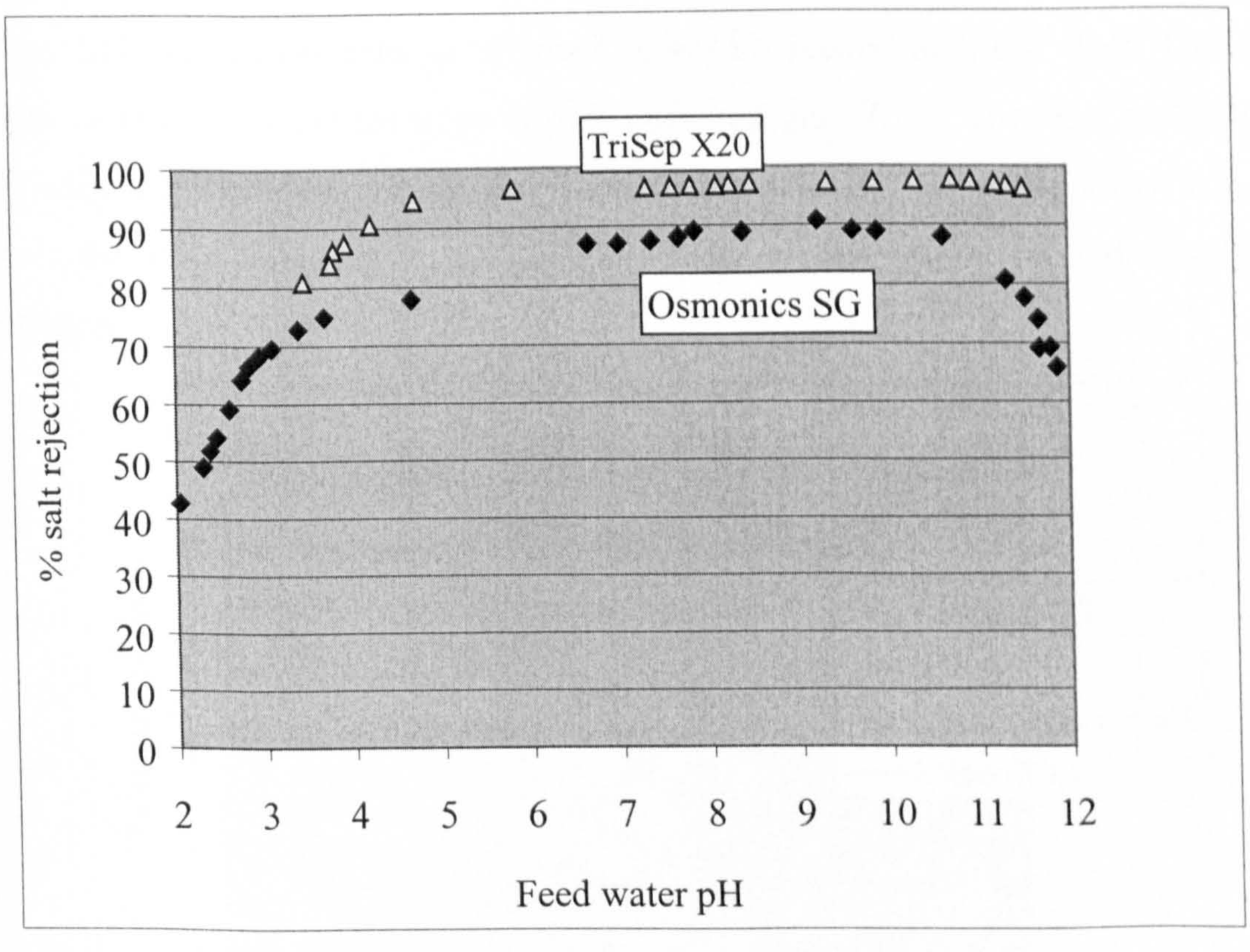

Figure 7.13. Effect of feed temperature on Osmonics SG and TriSep X20 salt rejection

From Figure 7.13, it is observed that TriSep X20 membrane salt rejection is much better than Osmonics SG but TriSep X20 permeation rate is much lower. In the literature, it is reported

that attempts which resulted in an increase in membrane salt rejection by changing ultra thin film layer properties usually leads to lower membrane flux which is similarly observed here. An increase in salt rejection for TriSep X20 is possibly due to its tight pore structure, which causes lower permeation rate. Another possible reason is the membrane surface hydrophilicity.

7.7 Effect of feedwater flow on RO membranes performance

Increasing feedwater flow leads to a minor improvement in permeation rate. Experiments were conducted to test the effect of varying feedwater flow from 2.5-19.2 x 10^{-5} m^3/s on membrane performance and other operating parameters were maintained at feedwater conductivity, temperature, pressure, pH of 5130 µS/cm, 30 °C, 140 MN/m2, and 10.5. It can be seen from Figure 7.14 and 7.15 that the effect is not significant. It is also found that Osmonics SG permeation rate is affected more by feedwater flow than TriSep X20 membrane as observed from the slope of both lines in Figure 7.14. The most probable cause is that TriSep X20 has rough surface and whereas Osmonics SG has a smooth surface, which influences the flow dynamics at the boundary layer of the membrane and therefore salt concentration.

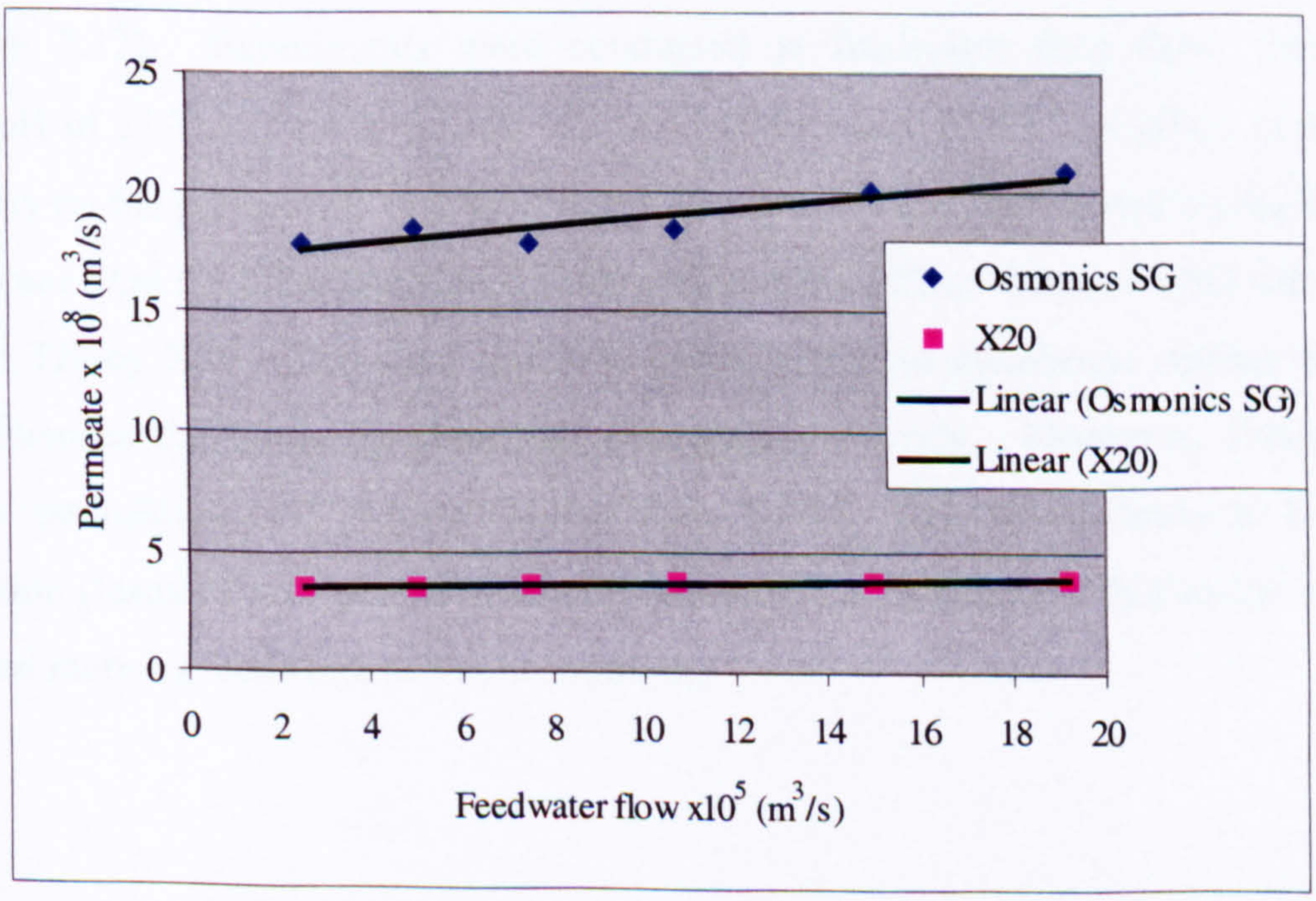

Figure 7.14. Effect of feedwater flow on Osmonics SG and TriSep X20 permeation rate

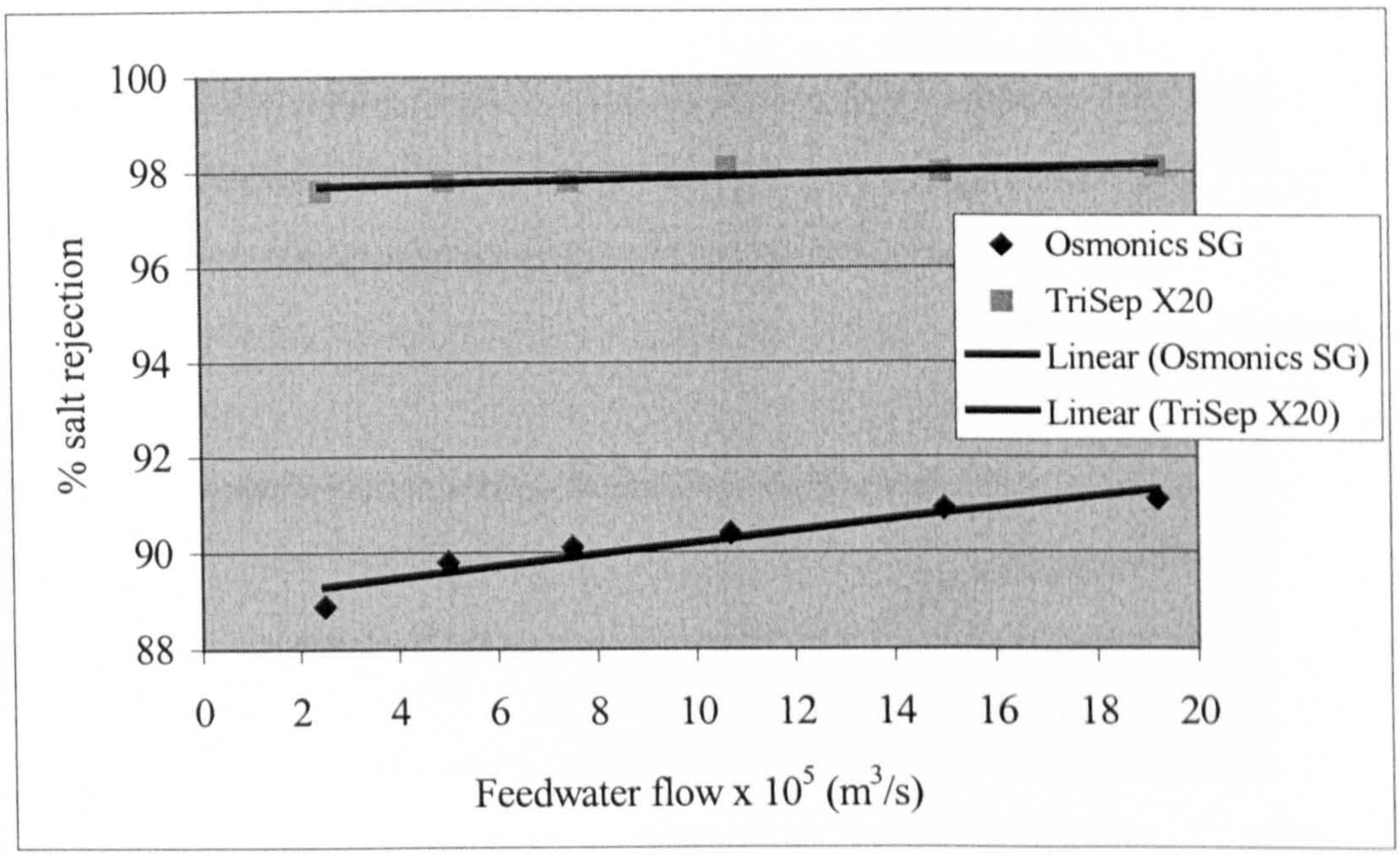

Figure 7.15. Effect of feedwater flow on Osmonics SG and TriSep X20 salt rejection

7.8 Effect of feedwater conductivity on RO membrane performance

Feedwater conductivity has a great influence on both membrane permeation rates (see Figure 7.16). The effect of feedwater conductivity is minor but more pronounced for Osmonics SG (see Figure 7.17). Experiments were conducted at feedwater feed flow, temperature, pressure, pH of 11.7×10^{-5} m^3/s, μS, 30 °C, 140 MN/m^2, and 10.5. The effect of feedwater conductivity on the permeation rate for TriSep X20 is more than that found on the Osmonics SG membrane. On the other hand, feedwater conductivity affects Osmonics SG salt rejection more than TriSep X20. The most probable cause is due to membrane surface roughness which influences the boundary layer salt concentration levels. Moreover, Osmonics SG membrane permeation rate is much higher than TriSep X20, which leads to higher salt accumulation (leads to an increase in osmotic pressure) at the surface that makes Osmonics SG affected more by feedwater salt concentration.

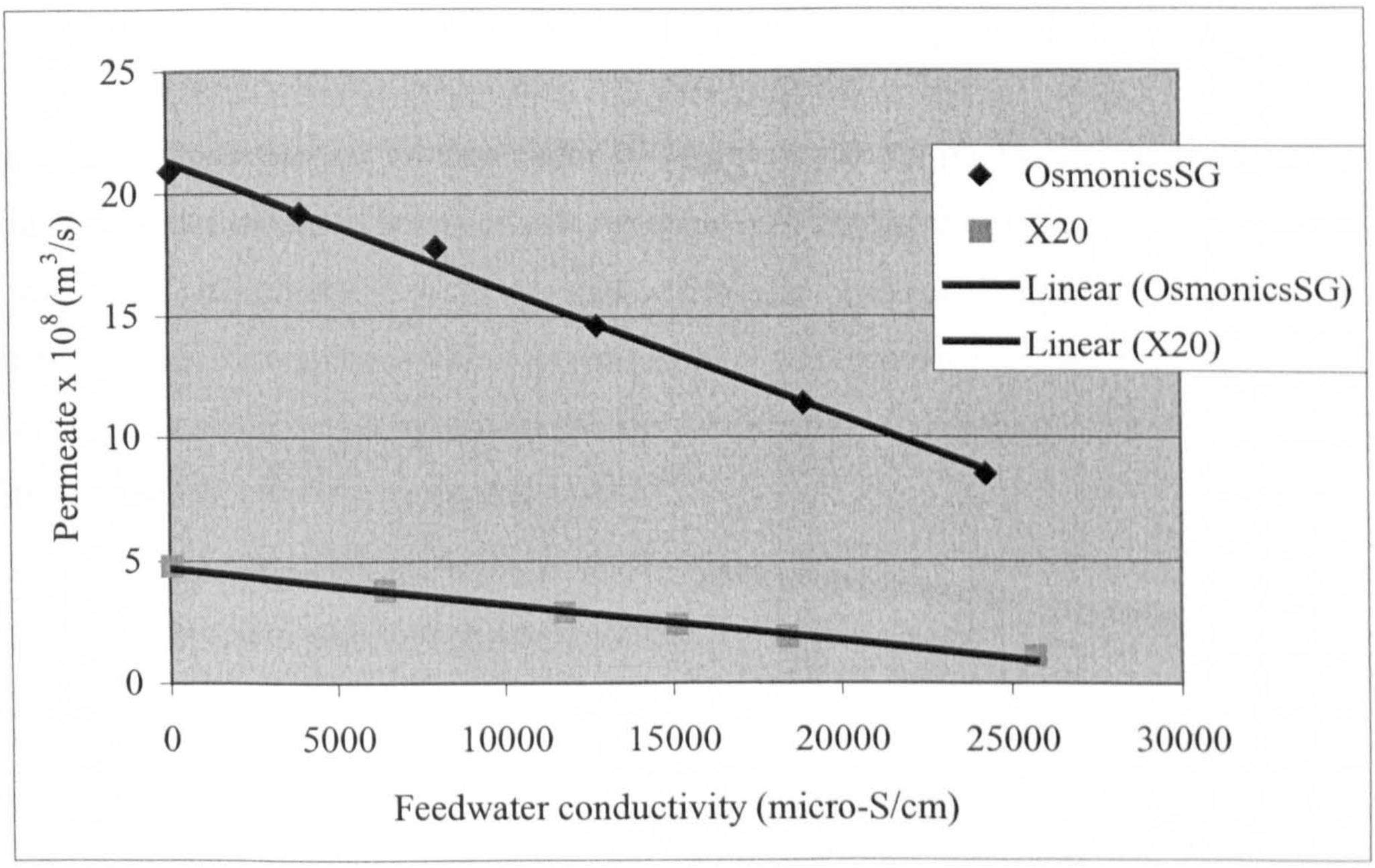

Figure 7.16. Effect of feed conductivity on Osmonics SG and TriSep X20 permeation rate

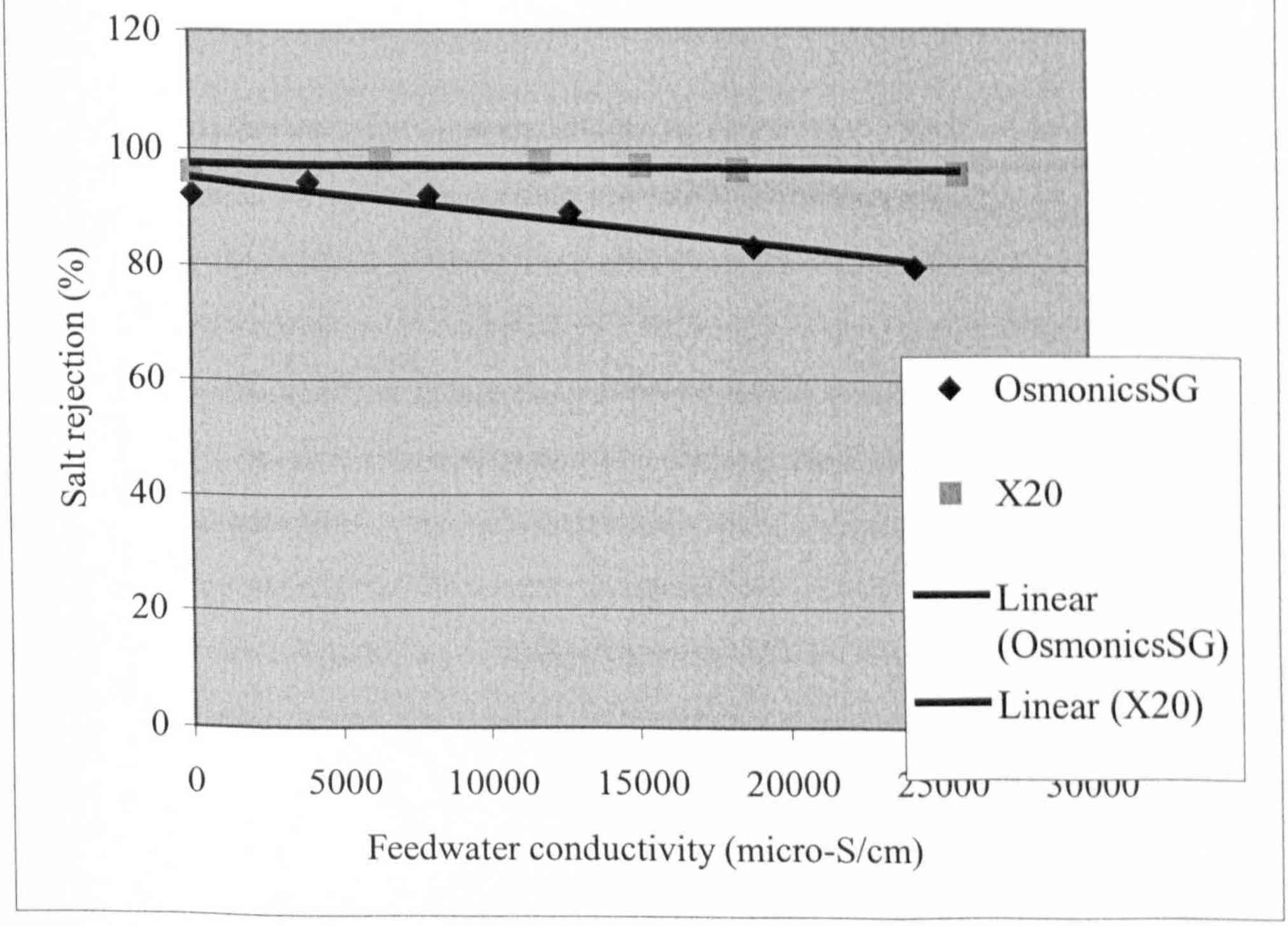

Figure 7.17. Effect of feed conductivity on Osmonics SG and TriSep X20 salt rejection

7.9 Summary of pure water experiments

From this chapter it can be concluded that all operating parameters has an effect on membrane performance in terms of salt rejection and permeation rate. However, the effect degree varies significantly from one parameter to another. Feedwater pressure and temperature have significant effect on membrane permeation rate whereas feedwater pH effect on permeation rate is minimal. On the other hand, feedwater pH has significant effect on membrane salt rejection properties.

CHAPTER 8 - RESULTS

RO MEMBRANE PERFORMANCE IN OILY WATER

8.1 Introduction

Recently many new plants and refineries have been built worldwide and existing plants are expanding and increasing their production to meet market demand, which increases the risk of releasing contaminated water with toxic material to the environment. This represents a real threat to human health. Most countries have put strict regulations to limit contaminants discharge to environment. One of these contaminants is oil. Such regulations have forced industries to look for technologies that effectively purify industrial wastewater with minimum cost. RO membrane technology has recently been applied widely in this field [3]. A thorough literature review has shown that some papers have reported that RO membranes foul in oily water treatment whereas others have reported successful application of RO membrane in the treatment of oily water [35,129,143,144,146,147]. It was also observed that RO membranes are applied to purify wastewater contaminated with only traces of oil (in ppm ranges).

In this chapter, RO membrane technology performance is assessed in the treatment of up to 50% (by volume) feedwater oil contamination in terms of fouling tendency and product water quality at various operating conditions. In addition, RO membrane permeation rate and salt rejection properties are assessed to evaluate the influence of oil on membrane performance characteristics. The oil-water mixture was prepared by mixing oil lubricant with water. The water is prepared by mixing de-ionized water with sodium chloride powder. Its conductivity is 5000 $\pm$ 200 μS/cm, which is a common RO plant feedwater conductivity. The tested membranes are Osmonics SG and TriSep X20. These two membranes were selected for this test because they have significant differences in structure and permeation properties as shown in Chapter 6. The performance of these two membranes in oily water has also been discussed in relationship to their microstructure characteristics identified and presented in chapter 6 and to that in oil-free water presented in chapter 7.

The membranes' capability in attaining less than the maximum allowable wastewater oil discharge limit (TOC = 50 ppm) and drinking water limit (TOC = 5 ppm) are examined to verify their applicability in this field.

8.2 Evaluation of Osmonics SG and TriSep X20 membrane fouling tendency in oil contaminated water

To evaluate the possibility of fouling taking place on the membranes surface by oil in oily water treatment and the impact of this fouling on the performance of RO membranes, Osmonics SG and TriSep X20 were tested for initially for 100 hours (3.6×10^5 seconds) in oily water. The test objective was to assess whether any deterioration in the membrane permeation and salt rejection occurred. When all operating parameters are constant, the deterioration in the permeation and salt rejection is an indication of membrane fouling. The test operating condition, which is one of the common RO plant operating condition, was feedwater TOC 5160 ppm, pH 10.5, conductivity 5,000 µS/cm, temperature 30 °C, pressure 100 MN/m^2 and flow 11.7×10^{-5} m^3/s. To create oily water mixture, the feedwater tank was equipped with a mixer. The mixing of the oily water was further enhanced by the feedwater pump impellers (multi-stage pump). To confirm the oil and water concentrations; samples were collected and analyzed frequently during the tests from the discharge line of the pump and just before the RO cell (see Figure 8.1).

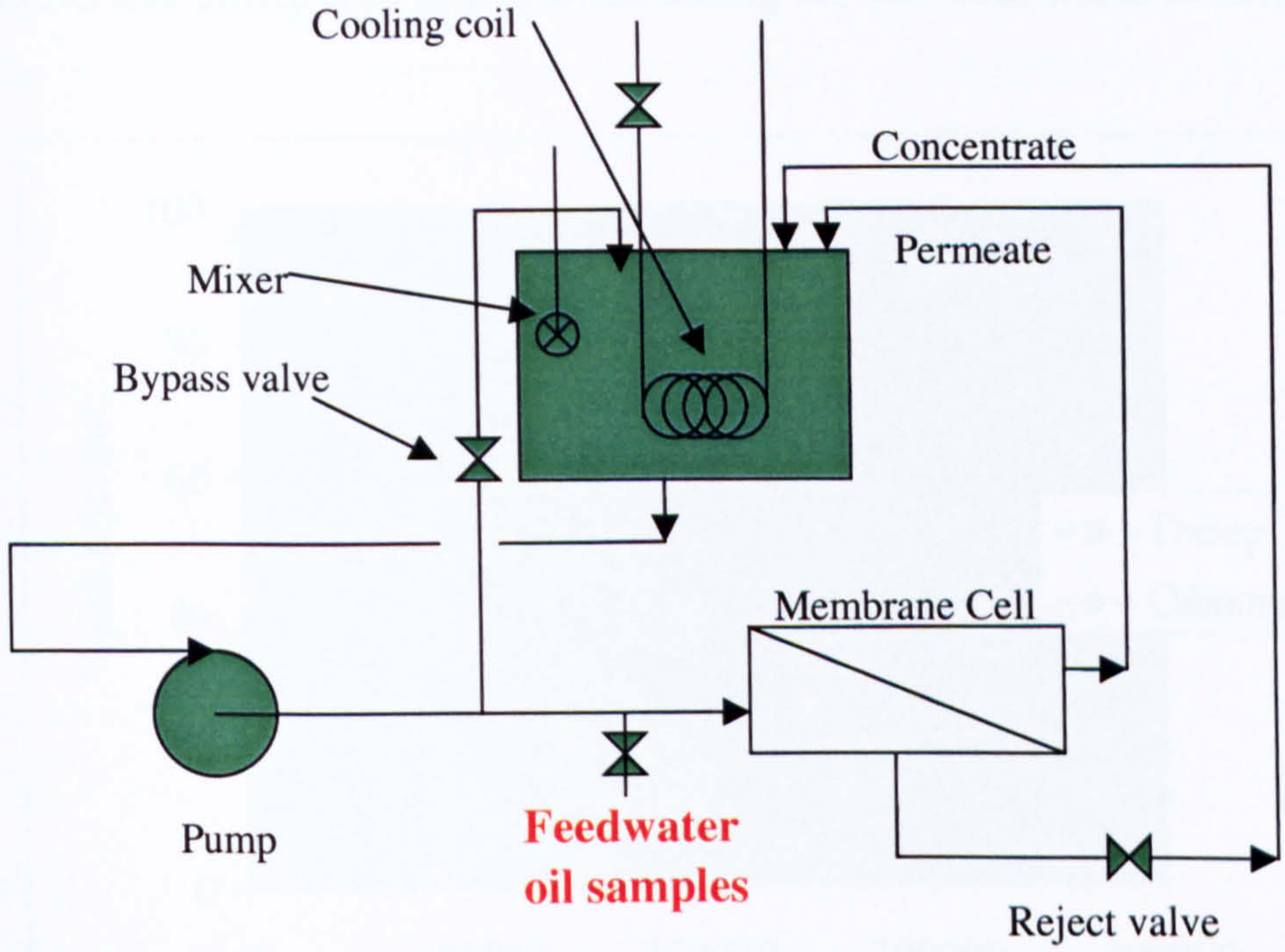

Figure 8.1. Simplified drawing for experimental rig showing feedwater oil sample point

Figures 8.2 and 8.3 show TriSep X20 and Osmonics SG permeation rate and salt rejection during the 3.6×10^5 seconds (100 hr) test period.

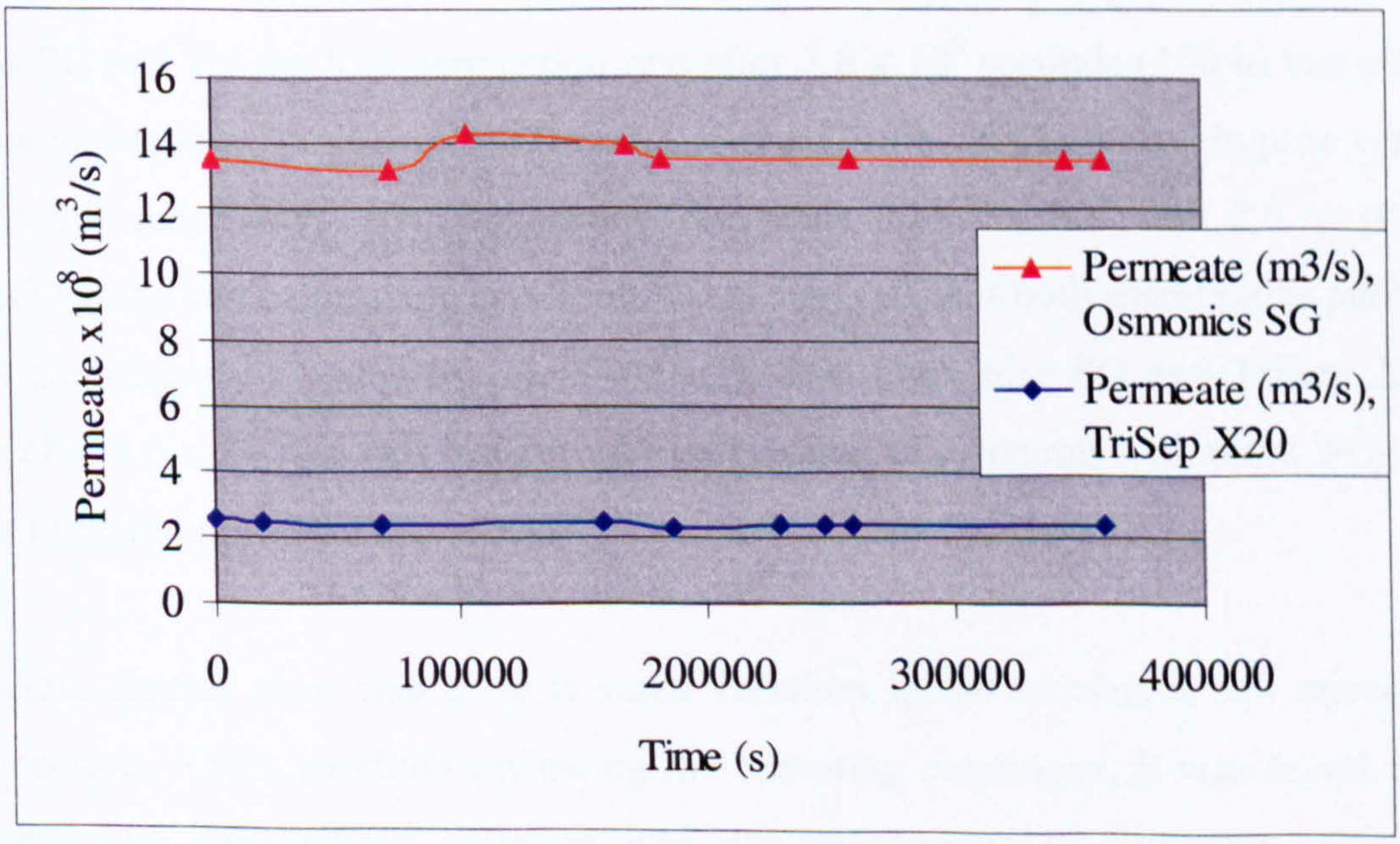

Figure. 8.2. TriSep X20 and Osmonics SG permeation in the 3.6×10^5 (100 h) test in oil contamination

Osmonics SG and TriSep X20 salt rejection during the 100-hour test is shown in Figure 8.3.

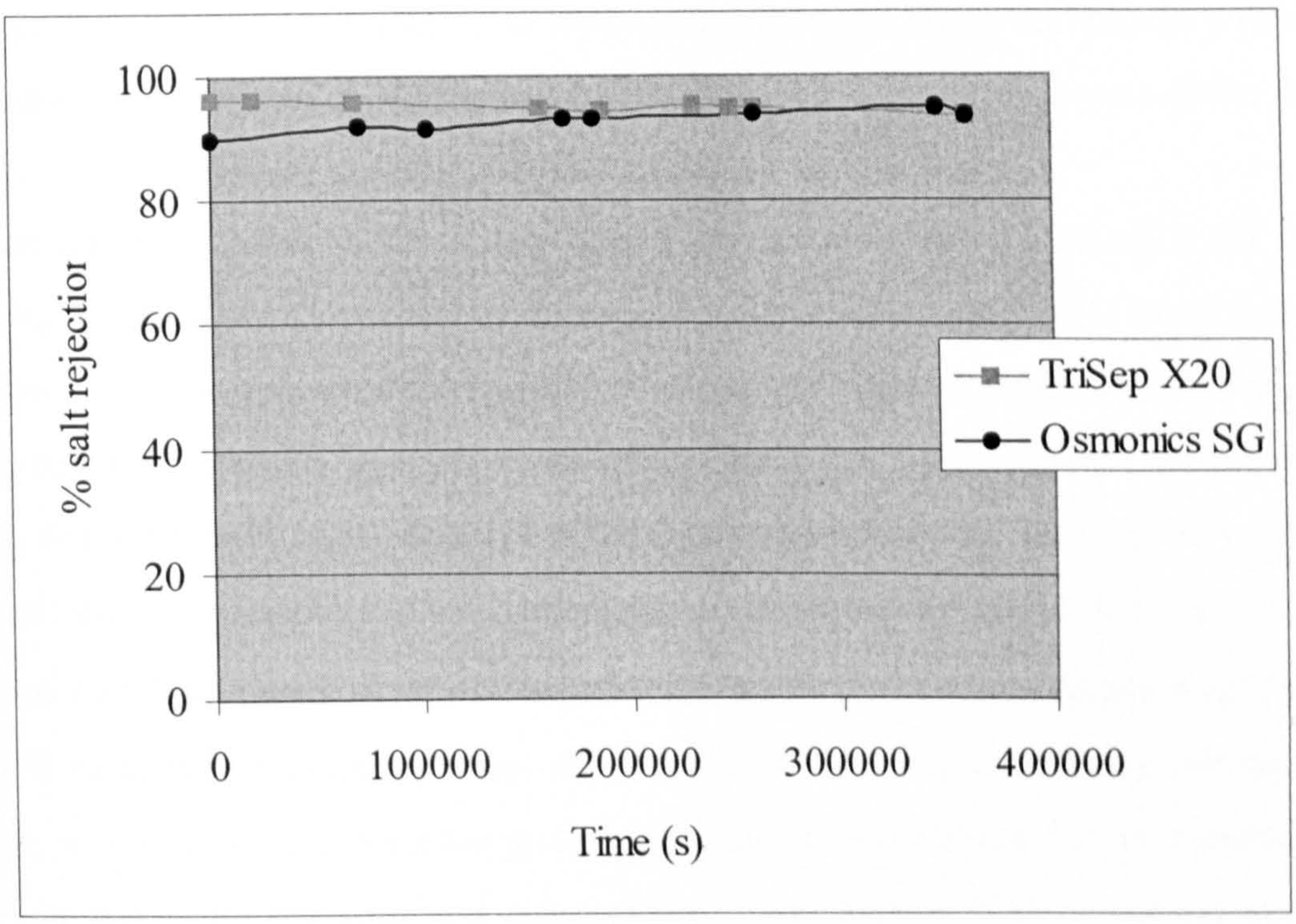

Figure. 8.3. TriSep X20 and Osmonics SG salt rejection in the 3.6 x 10^5 s (100 h) test in oil contamination

Osmonics SG and TriSep X20 permeation rate after 3.6 x 10^5 seconds (100 h) test period in oil contaminated water were 13.5 x 10^{-8} and 2.36 x 10^{-8} m^3/s respectively. In pure water test Osmonics SG and TriSep X20 permeation rate were 11.95 x 10^{-8} and 2.5 x 10^{-8} m^3/s respectively at the same operating condition. This suggests that both membranes permeation were not significantly affected by oil. Similarly, both Osmonics SG and TriSep X20 salt rejection after 3.6 x 10^5 seconds test period in oily water experiments was about 94%, which is similar to that in pure water.

The previous figures show that there is small variation in the membrane salt rejection and permeation rate. Upon carefully reviewing the operating conditions, it was found that this small membrane performance variation was due to changes in operating pressure and feedwater temperature.

The difference between day and night temperatures of the laboratory environment caused the change in the feedwater temperature. The feedwater temperature has an effect on pump performance, which leads to variation in feedwater pressure. These variations in temperature and pressure cause such small variations in membrane salt rejection and permeation rate.

From pure water test experiments, it was found that an increase in Osmonics SG feedwater pressure by 1 MN/m^2 will result in an increase by about 0.28×10^{-8} m^3/s in permeation rate (see Figure 7.7). The pressure in the experiments reported in this section was 99 ± 2 MN/m^2 so it expected to cause a $\pm$ 0.55×10^{-8} m^3/s variation in membrane permeation rate. Similarly, temperature change leads to a change in permeation rate. From pure water tests, it was found that an increase by 1 °C leads to an increase by about 0.55×10^{-8} m^3/s in permeation rate (see Figure 7.10). The temperature in these experiments was 31 ± 2 °C. Hence it is expected to cause a change of $\pm$ 1.1×10^{-8} m^3/s in membrane permeation rate. Therefore, a variation in membrane permeation rate in Osmonics SG is expected due to variation in feedwater pressure and temperature. For TriSep X20, a similar argument is applied.

Since no deterioration in salt rejection and permeation rate occurred then no fouling took place in the first 100 hours (3.6×10^5 seconds). Therefore, the membrane was further tested in higher oil contamination level to confirm that oil fouling is not taking place. Osmonics SG was tested in oil contamination (10-50%) for another 70 hour (2.5×10^5 seconds) and the membrane salt rejection was not affected (it remained above 90%). The oil levels during the 70 hour test period for Osmonics SG are given in Table 8.1.

Oil Content (%)	Tested Period (hr)
10%	10
18%	10
30%	40
50%	10

Table 8.1. Osmonics SG test in high oil contamination

The experimental results indicate that Osmonics SG has high tolerance to oil contamination.

8.3 Evaluation of Osmonics SG and TriSep X20 membrane permeate quality at various operating conditions

As discussed in section 8.2, a deterioration in membranes salt rejection and permeation rate were not observed in the tested oily water at a TOC level of 5160 ppm. However, that alone is not enough to justify the use of these membranes to treat oily water. It is very important for the product water to meet the recommended specification in terms of TOC limits (industrial effluent discharge limit is 50 ppm and drinking water limit is 5 ppm). The product water quality from Osmonics SG and TriSep X20 were examined under various operating conditions. Firstly, the product water quality from each membrane was evaluated in low oil contaminations (below 1% by volume) and then was compared to each other. Osmonics SG permeate quality was evaluated at various operating conditions in the treatment of higher oil contamination (30% by volume).

8.3.1 Osmonics SG and TriSep X20 membranes permeate quality at various operating conditions in the treatment of low oil contaminations

Osmonics SG and TriSep X20 were tested under different feedwater pressures, temperatures and pH values using oily water with 0.15, 0.25 and 0.6% oil by volume which corresponds to 1290, 2150, 5160 ppm by weight. The effect of oil presence in feedwater on membrane salt rejection and permeation rate was discussed in section 8.2. It was shown that both membranes' salt rejection and permeation rate were not affected at 5160 ppm oil contamination.

8.3.1a Effect of feedwater pressure on membrane permeate quality

Osmonics SG and TriSep X20 membranes were tested at 80 and 160 MN/m^2 feedwater pressure to evaluate the effect of pressure change on membrane permeate TOC level. The test operating condition was as follows: feedwater pH 10.5, conductivity 5,000 µS/cm, temperature 30 °C and flow 11.7×10^{-5} m^3/s. At each condition 3 samples from permeate

were collected during experiments and analyzed for TOC levels (see Figures 8.4 and 8.5). The error bar shown in the figures is a result of plotting three results at each condition.

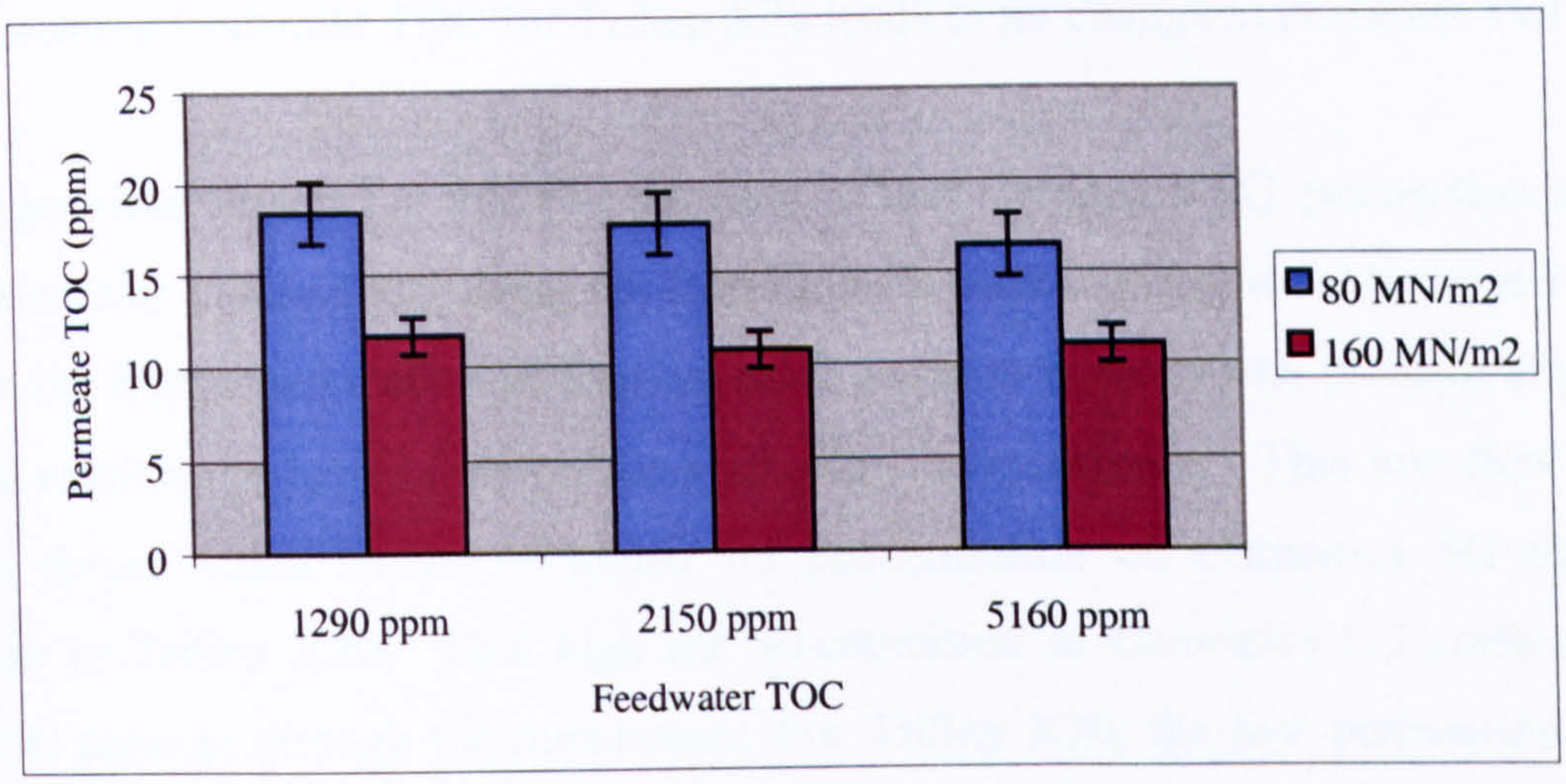

Figure 8.4. TriSep X20 membrane permeates quality with pressure

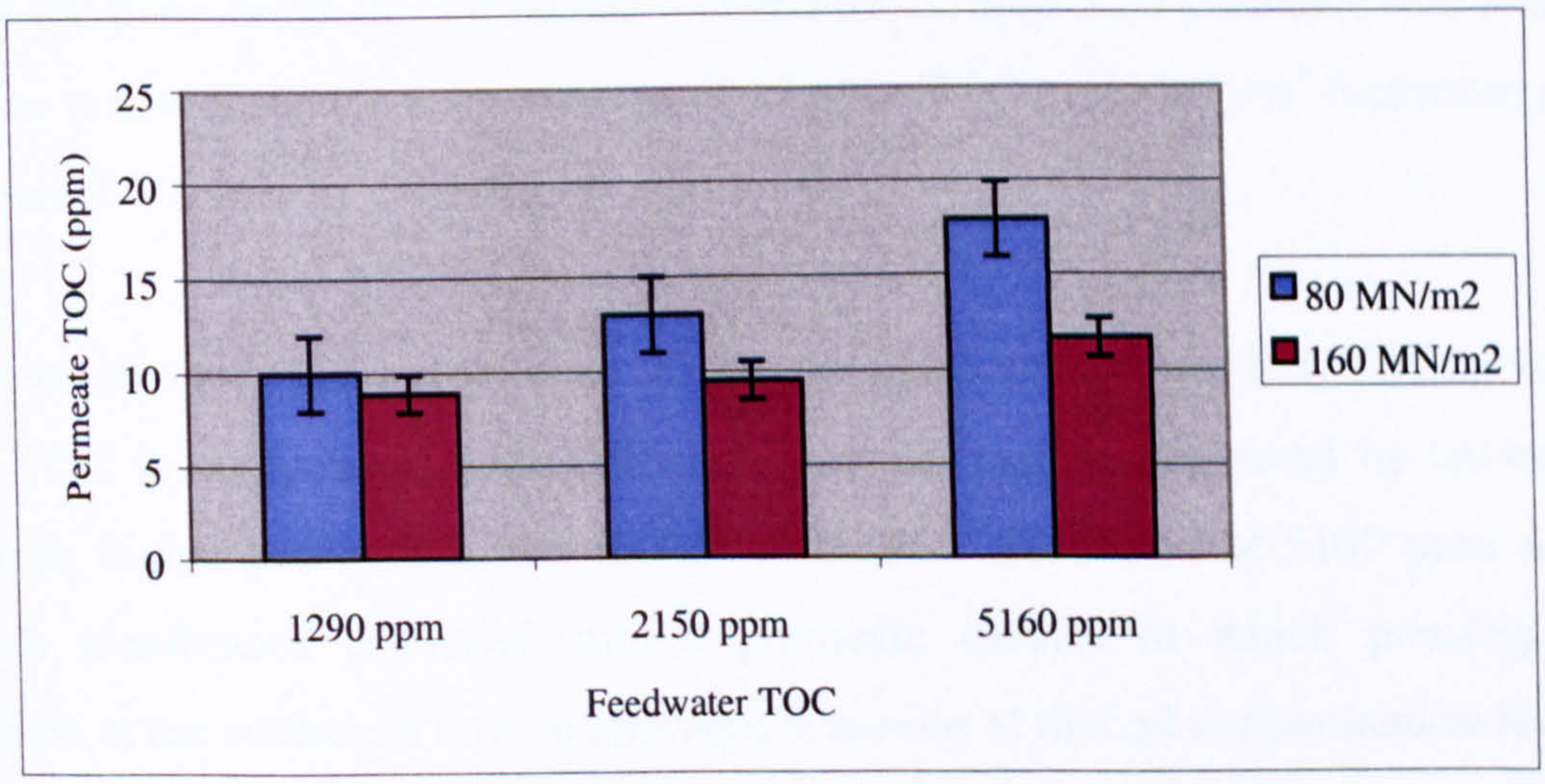

Figure 8.5. Osmonics SG membrane permeates quality with pressure

Figures 8.4 and 8.5 show that increasing feedwater pressure from 80 to 160 MN/m^2 leads to a reduction in the permeate TOC levels of both membranes. As an example for TriSep X20 at 2150 ppm feedwater TOC level the permeate TOC dropped from 17 ppm at 80 MN/m^2 to 12 ppm at 160 MN/m^2. The most possible cause for better permeate quality at higher pressure is due to an increase in water permeation rate, which leads to oil dilution. The permeation rate of TriSep X20 at 80 MN/m^2 feedwater pressure is 2 x 10^{-8} m^3/s and at 160 MN/m^2 it is 4.7 x 10^{-8} m^3/s.

It was observed at the same pressure that:

- Increasing feedwater TOC for Osmonics SG leads to higher permeate TOC and
- Increasing feedwater TOC for TriSep X20 leads to no change in permeate TOC

The most possible reason for this phenomenon is that Osmonics SG permeation rate is 6 times greater than TriSep X20. Since the feedwater for both membranes is fixed at $11.7x10^{-5}$ m3/s, then the higher permeation of Osmonics SG leads to higher water passage through the membrane resulting in lower flow on the surface of the membrane. This low flow leads to less shear force, which results in higher oil concentration on Osmonics SG surface in comparison to TriSep X20. This high oil concentration at Osmonics SG surface caused higher TOC passage through the membrane. For TriSep X20, the low permeation rate has resulted in high enough shear force that maintained low oil concentration at the membrane surface for the three feedwater oil levels. Therefore, TriSep X20 permeate was maintained for the three tested oil levels at an average of 17 ppm TOC at 80 MN/m^2 feedwater pressure and 120 ppm at 160 MN/m^2 feedwater pressure.

It was observed that Osmonics SG at 1290 and 2150 ppm feedwater TOC gives lower permeate TOC in comparison with TriSep X20 which can be explained by having higher dilution with higher permeation rate in Osmonics SG. However, at 5160 ppm feedwater TOC, both membranes produced similar permeate quality in which possibly the oil concentration at the surface of both membranes is similar at this oil contamination level.

8.3.1b Effect of feedwater temperature on membranes permeate quality

Osmonics SG and TriSep X20 membranes were tested at 30 and 40 °C feedwater temperatures. The test operating condition was as follows: feedwater pH 10.5, conductivity 5,000 μS/cm, pressure 140 MN/m^2 and flow 11.7×10^{-5} m^3/s. Three samples at each condition from permeate were collected during experiments and analyzed for TOC (see Figure 8.5 and 8.6).

It was observed that increasing feedwater temperature from 30 to 40 °C has a minor effect on the permeate quality of TriSep X20 and Osmonics SG permeate TOC at 1290 and 2150 ppm feedwater contamination levels. At higher TOC feedwater (5160 ppm) an increase in feedwater temperature from 30 to 40 °C leads to a drop in permeate quality. The most possible reason is that at higher temperature the oil viscosity is much lower which eases oil passage through the membrane. An increase in temperature will reduce not only oil viscosity but also water viscosity. However, oil is more sensitive to temperature, which leads to much lower drop in viscosity for oil than water. This leads to higher oil passage than water and therefore water dilution effects is not sufficient. This was not observed in the low feedwater oil concentration because the oil presence is not high enough to be reflected on the permeate quality.

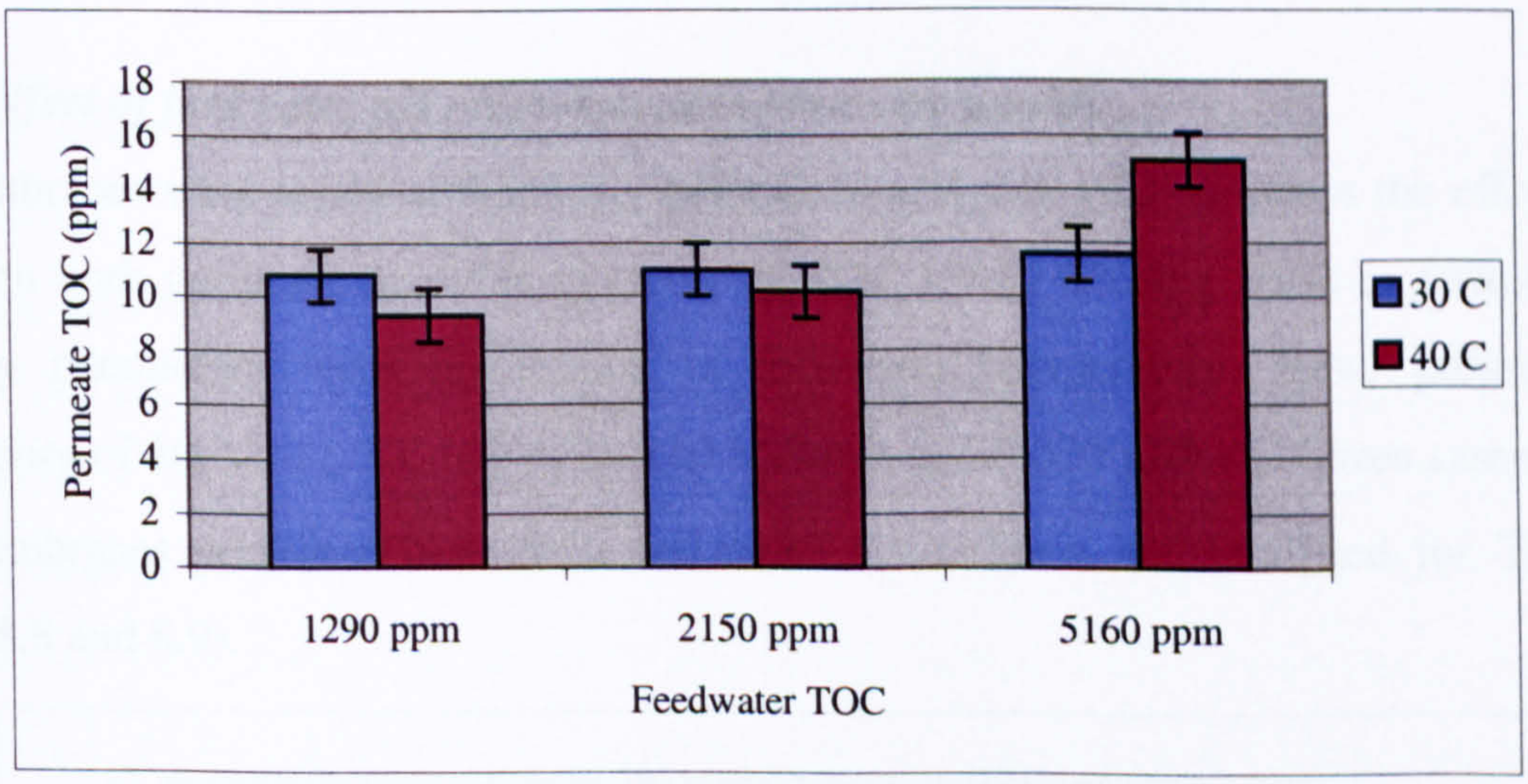

Figure 8.6. TriSep X20 membrane permeates quality with temperature

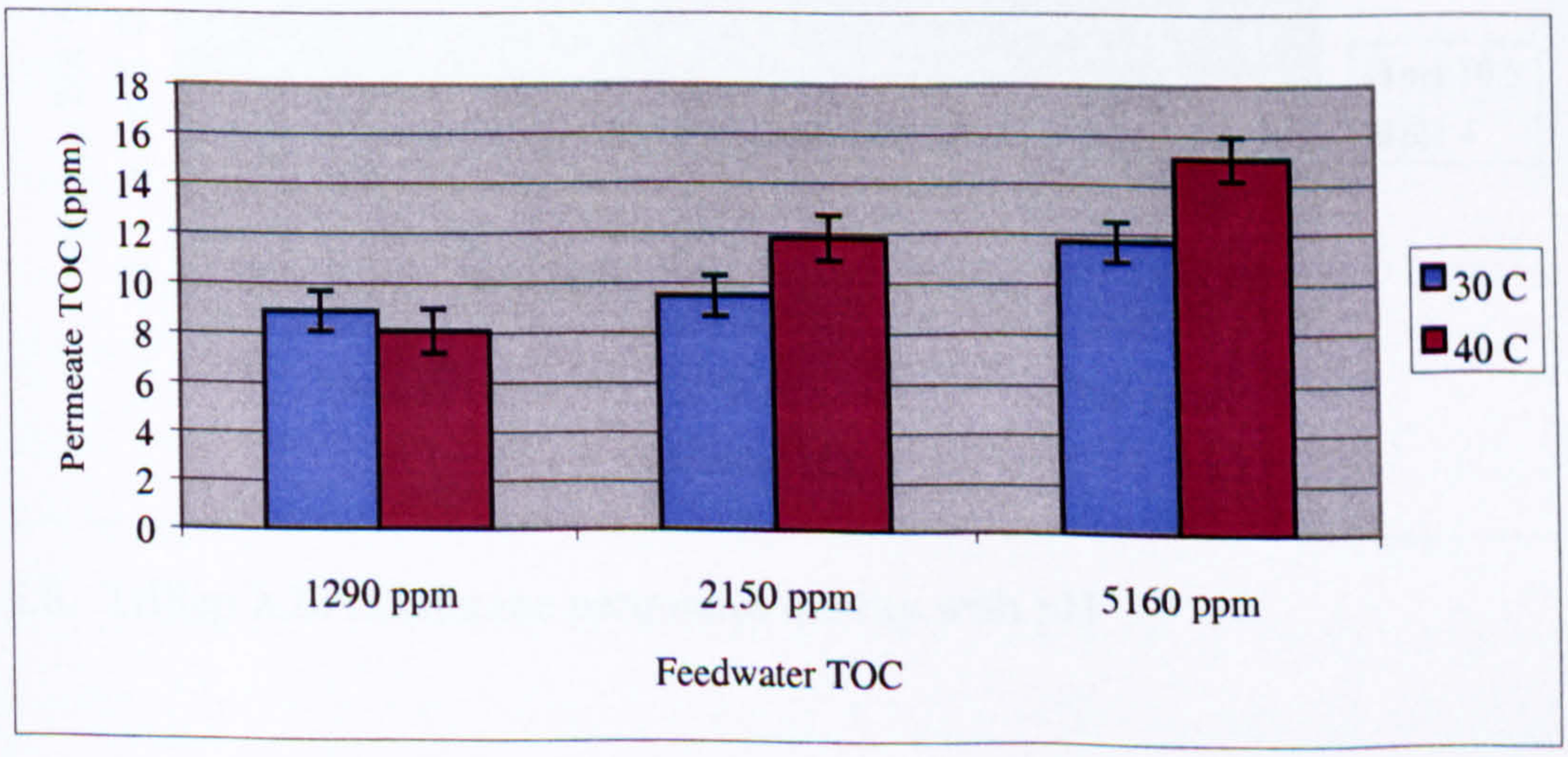

Figure 8.7. Osmonics SG membrane permeates quality with temperature

From Figures 8.6 and 8.7, it is observed that Osmonics SG permeate quality is better than TriSep X20. It is possible that the higher dilution effects with higher permeation rate has contributes to a lower permeate TOC for Osmonics SG. However, dilution effects alone are not enough to explain this phenomenon because the great difference in permeation rate between TriSep X20 and Osmonics SG suggests that TOC of Osmonics SG should be significantly lower than TriSep X20. However, Osmonics SG permeate TOC is not significantly lower than TriSep X20. This means that there are other parameters that influence membrane TOC rejection properties such as membrane pore size and surface properties. TriSep X20 membrane surface is much rougher than Osmonics SG, which makes sweeping away accumulated oil from boundary layer different from Osmonics SG.

8.3.1c Effect of feedwater pH on membranes permeate quality

The membranes were tested at feedwater pH values of 4 and 10.5 to assess the effect of pH change on both permeate qualities in terms of TOC level. During these experiments, the operating parameters were maintained at feedwater temperature, flow, pressure, and conductivity of 30 °C, 11.7 x 10^{-5} m^3/s, 140 MN/m^2, and 5,000 µS/cm. Three samples from both membranes permeate were collected at each condition and analyzed for TOC (see Figures 8.8 and 8.9).

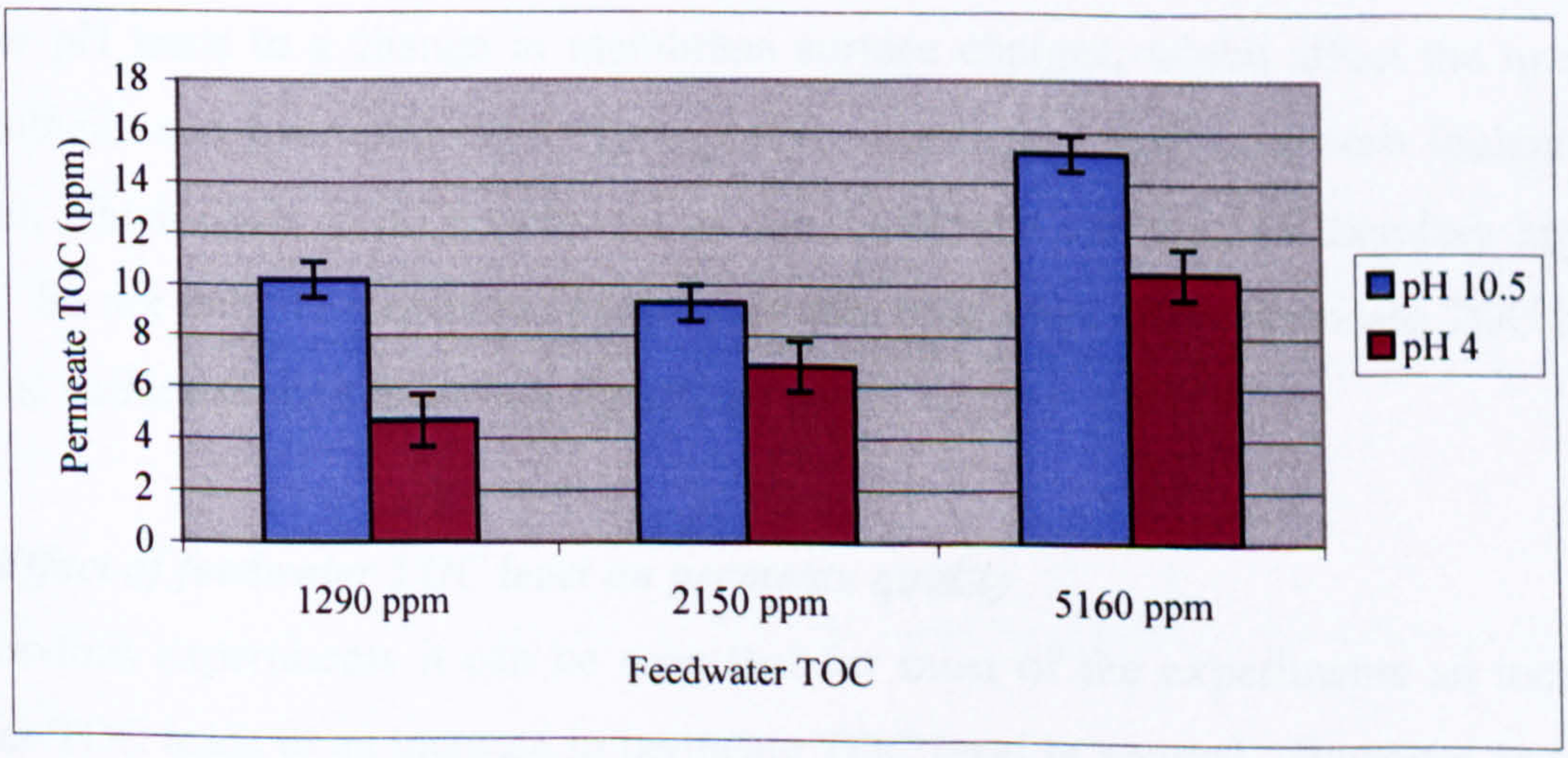

Figure 8.8. TriSep X20 membrane permeates quality with pH

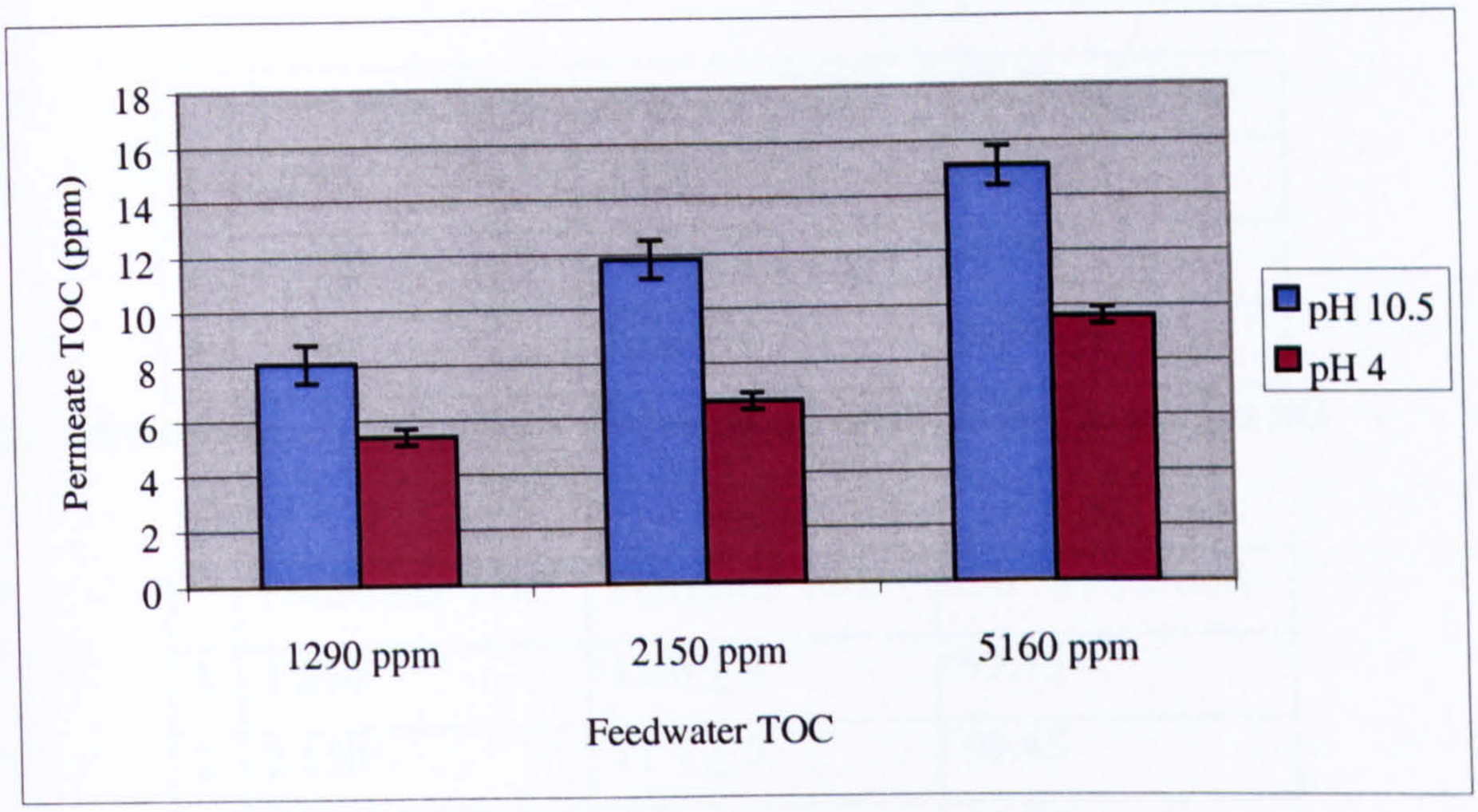

Table 8.9. Osmonics SG membrane permeates quality with pH

It was found that both membranes are sensitive to feedwater pH. A significant change in permeate quality was observed upon reducing feedwater pH from 10.5 to 4. For TriSep X20, at 1290 ppm feedwater TOC experiment, the permeate TOC dropped from 10 to 5 ppm (see Figure 8.8). In evaluating the effect of pressure on permeate quality experiments it was found that increasing water production rate increases TOC dilution, which leads to better permeate quality. The pH has a minor effect on membrane permeation rate (refer to chapter 7) yet a great improvement was observed due to pH change. From the literature [1] varying feedwater pH leads to a change in membrane surface charges, which affect the membrane hydrophobicity and hydrophilicity. Hydrophobic membranes tend to absorb foulant (oil in this case), which leads to oil attachment on the membrane surface and therefore higher oil passage. So not only do membrane permeation rate properties affect permeate TOC but also membrane surface properties have a significant role.

8.3.1d Effect of feedwater TOC level on permeate quality

From previous experiments it can be seen that for most of the experiments an increase in feedwater TOC leads to an increase in permeate TOC level in general. However, in terms of oil rejection percent, it is observed that an increase in feedwater oil concentration leads to higher percent TOC rejection. Tables 8.2 and 8.3 show the average of all experimental results presented in previous sections.

	Feedwater TOC	Permeate TOC	Oil % rejection
1	1,290	8.1 ± 2	99.37
2	2,150	10.2 ± 3	99.50
3	5,160	13.6 ± 4	99.74

Table 8.2. Permeate quality at various feedwater oil contents for Osmonics SG

	Feedwater TOC	Permeate TOC	Oil % rejection
1	1,290	11.0 ± 4	99.15
2	2,150	11.7 ± 5	99.45
3	5,160	13.4 ± 3	99.74

Table 8.3. Permeate quality at various feedwater oil contents for TriSep X20

In general both membranes performed similarly with minor differences in terms of TOC rejection percent. Interestingly, it was observed that although TriSep X20 salt rejection (96%) at these experiments is higher than Osmonics SG (92%) however, both membranes oil rejection is similar and in some circumstance Osmonics SG performed better in rejecting oil. It is believed that Osmonics SG oil rejection is lower than TriSep X20 however, higher dilution effects in Osmonics SG resulted in an improvement in permeate TOC.

Further research was conducted to test the membrane performance in higher oil contamination. Because Osmonics SG has a high permeation rate it is expected to foul faster than TriSep X20 at high oil contamination. Therefore Osmonics SG was selected to examine its performance in up to 30% (by volume) oil feedwater concentration at various operating conditions.

8.3.2 Osmonics SG permeate quality at various operating conditions in the treatment of high oil contaminations

In the previous section Osmonics SG and TriSep X20 were tested in low oil contamination conditions and their performances were compared to understand the effect of operating parameters and the effect of membrane characteristic on permeate quality. In this section,

Osmonics SG performance in high oil contamination firstly will be investigated and then it will be compared with its performance in low oil contamination to understand the role of feedwater oil concentration level on permeate quality.

It was observed that the effect of operating parameters on permeate quality in high oil contamination is different from that observed in low oil contamination conditions. The results will be presented in the following paragraphs. Note that the membrane permeation rate and salt rejection characteristics were maintained for Osmonics SG at 30% oil contamination and no deterioration was observed in all experiments. The membrane salt rejection and permeation rate results will be presented separately after the following section.

8.3.2a Effect of feedwater pressure at 30% oil contamination

Osmonics SG was tested at feedwater pressure of 40, 60, 80, and 100 MN/m^2. Three samples were collected at each pressure and analyzed for TOC. The average values with an error bar were plotted in Figure 8.10 to show the membrane performance. It was found that the highest TOC passage through the membrane was at 100 MN/m^2feedwater pressure. Note that due to pump efficiency limitation it was not possible to carry out the tests in 30% oil contamination up to 160 MN/m^2 feedwater pressure as conducted for low oil contamination experiments. In these experiments the feedwater pH, temperature, conductivity, and flow were maintained at 10.5, 30 °C, 5,000 μS/cm, and 11.7 x 10^{-5} m^3/s respectively. It is observed that:

- With high oil contamination, increasing feedwater pressure from below 80 to 100 MN/m^2 leads to significant increase in TOC passage through the membrane.
- With low oil contamination, increasing feedwater pressure leads to better permeate quality due to higher oil dilution with the increase in permeation rate.

In 30% oil contamination an increase in permeation rate with pressure results in significant increase in oil concentration at the membrane surface. The oil concentration is very high in 30% oil contamination in comparison with below 1% oil contamination. This leads to covering some part of the membrane surface with oil, which results in higher TOC passage.

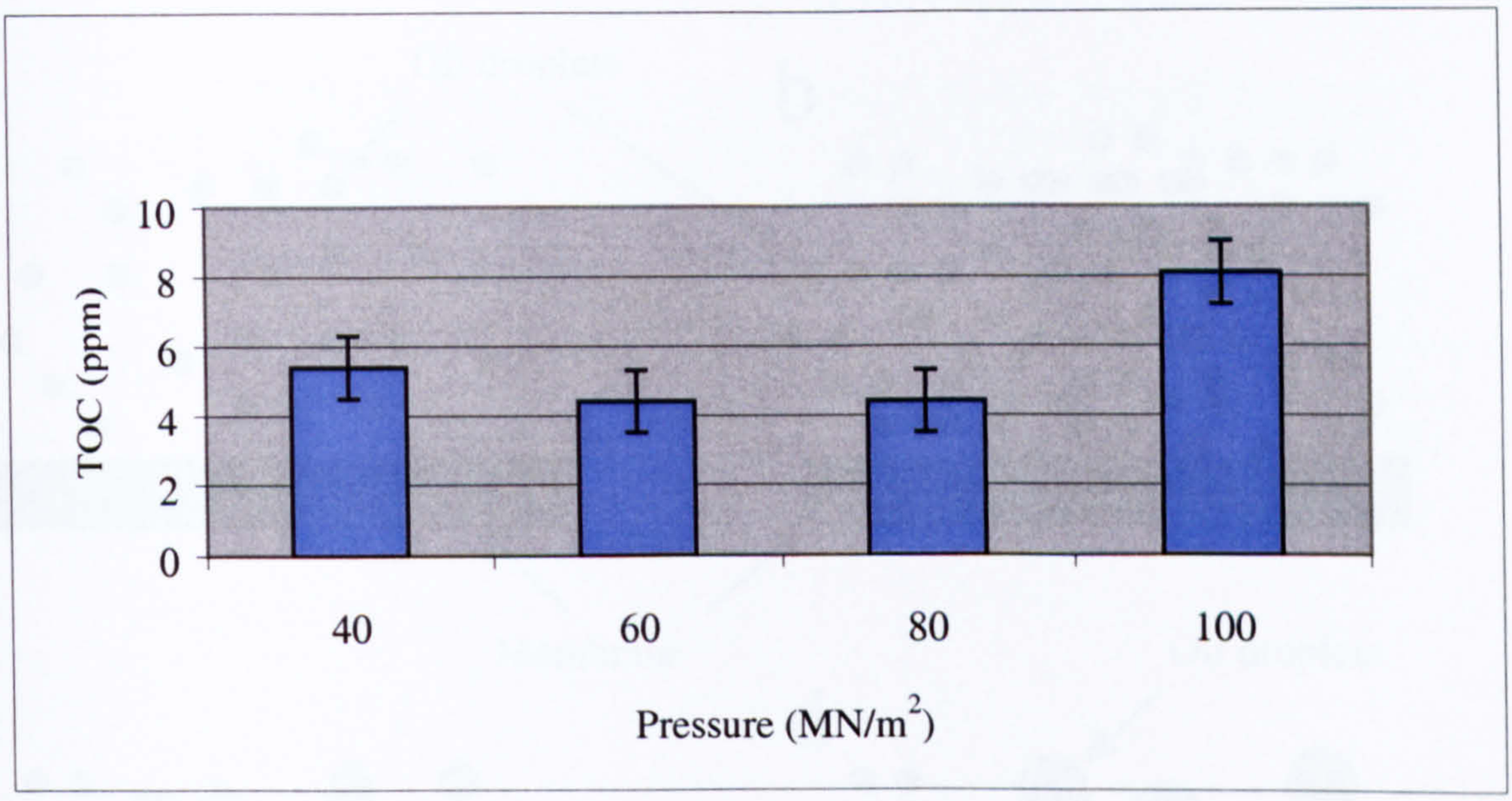

Figure 8.10. Osmonics SG performance in 30% oil contamination at various operating pressure values

At 80 MN/m^2 feedwater pressure, Osmonics SG membrane was tested with low and high oil contamination. It was observed that at 30% oil contamination permeate TOC is about 4-5 ppm whereas at low oil contamination it is about 10-18 ppm. It is strange to find out that increasing the oil concentration in the feedwater from less than 1% to 30% leads to a lower TOC passage. The most possible reason is that in low oil contamination oil droplets are dispersed in much smaller sizes and separated by water (see Figure 8.11).

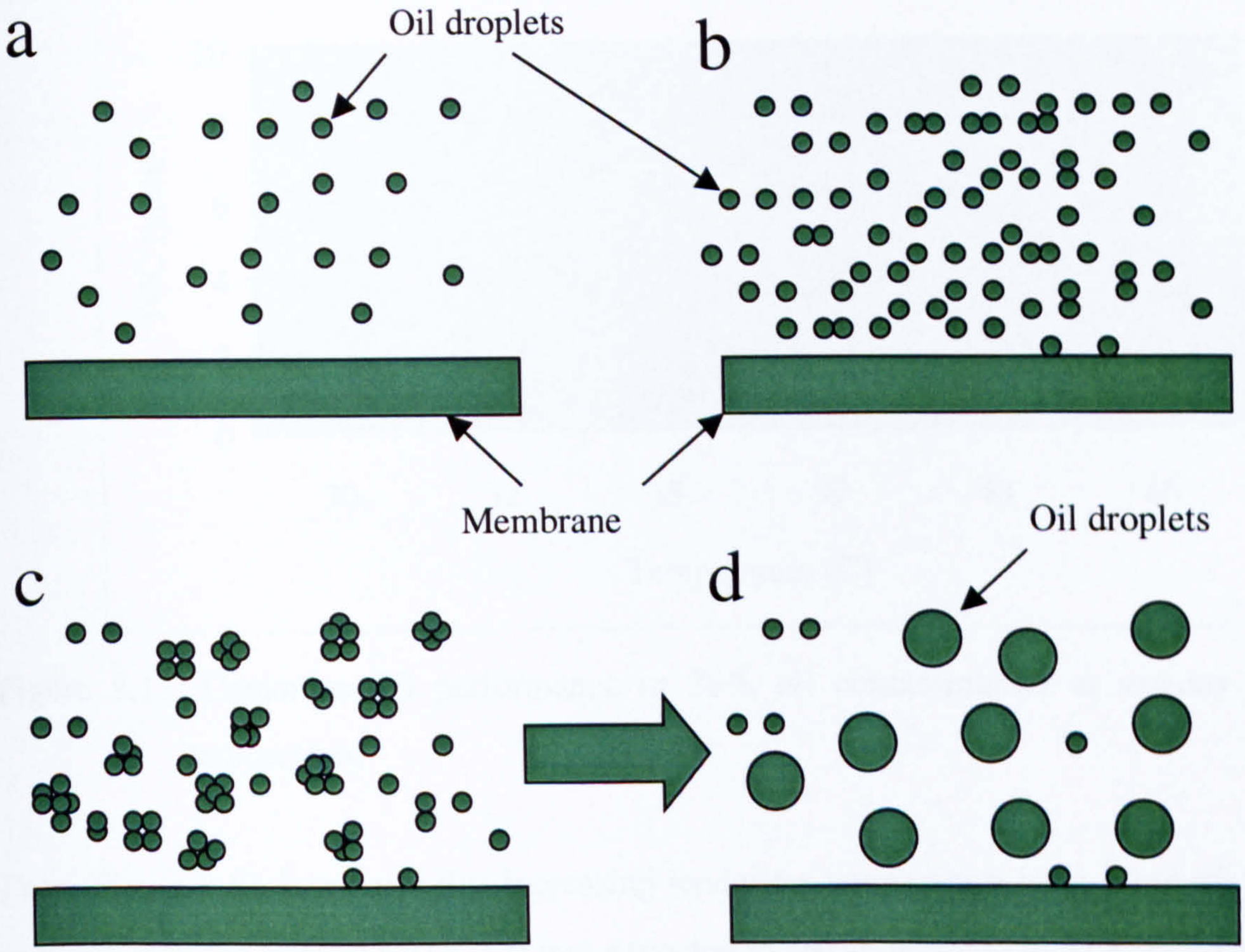

Figure 8.11. a) Shows oil droplets distribution in low oil contamination, b) shows oil droplets in high oil contamination, c) shows the process of oil droplets to come together, d) shows oil droplets coalescence to form bigger droplets.

With high oil contamination, oil droplets sizes become bigger due to coalescence of oil drops, as shown in Figure 8.11. The increase in oil droplets sizes leads to less oil passage through membrane pores.

8.3.2b Effect of feedwater temperature at 30% oil contamination

Figure 8.12 shows Osmonics SG permeate quality in 30% oil contamination in the range of 30-46 °C. At each condition 3 samples were collected and analyzed for TOC. During these experiments the feedwater pH, pressure, conductivity, and flow were maintained at 10.5, 100 MN/m^2, 5,000 μS/cm, and 11.7 x 10^{-5} m^{-5}/s respectively.

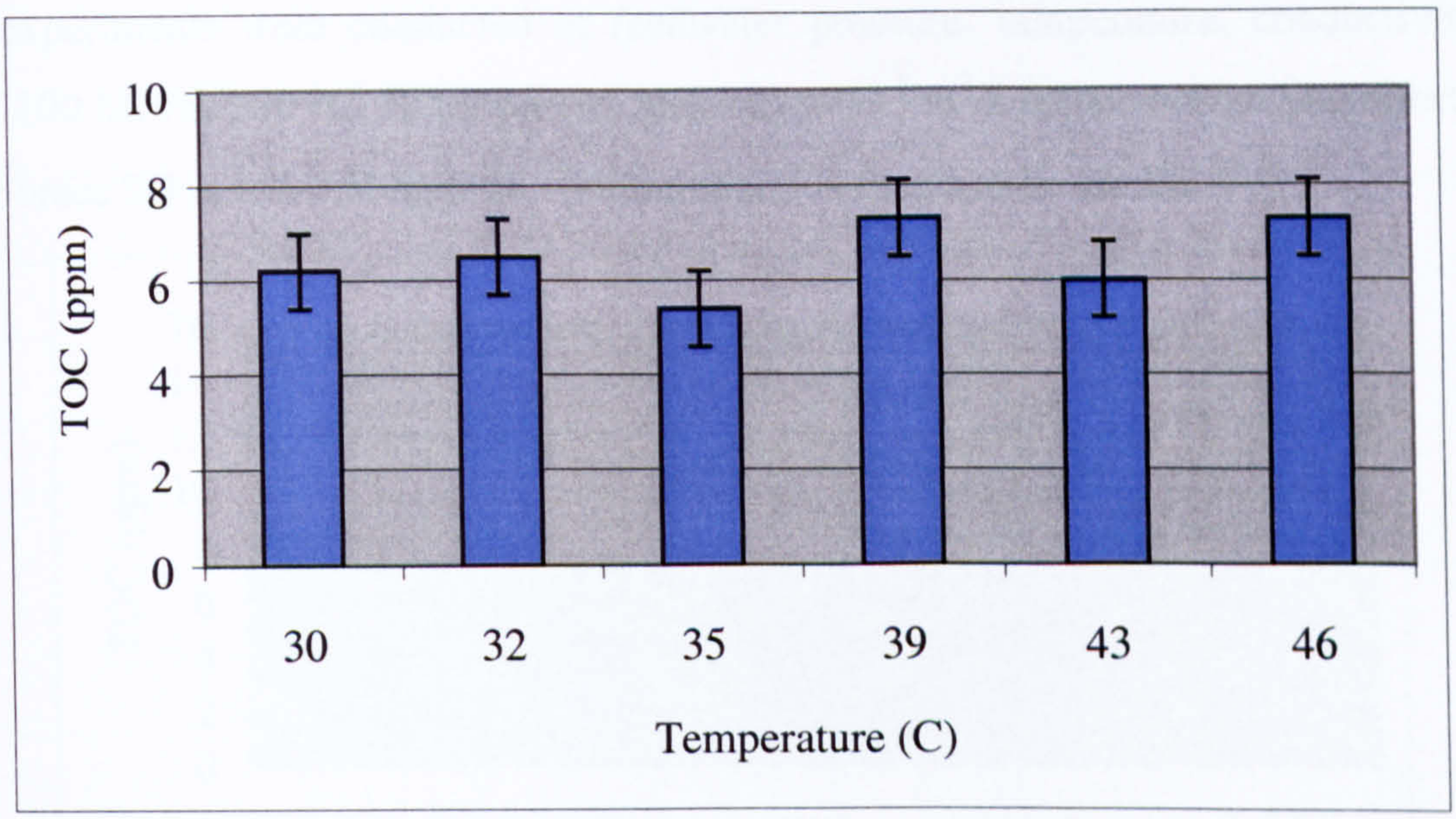

Figure 8.12. Osmonics SG performance in 30% oil contamination at various operating temperature

From Figure 8.12, it appears that increasing feedwater temperature from 30 to 46 °C has no real effect on the permeate TOC. It was expected to see an increase in TOC passage due to a decrease in oil viscosity with increasing feedwater temperature. This phenomenon can be explained as follows:

- It is believed that increasing feedwater temperature does lead to higher oil passage through the membrane due to lower oil viscosity but
- At the same time increasing feedwater temperature leads to higher permeation rate. At 30 °C feedwater temperature Osmonics SG permeation is 19.5 x 10^{-8} m^3/s and at 46 °C the permeation rate is 30.6 x 10^{-8} m^3/s.

The increase in water permeation rate with increasing temperature leads to diluting the increased oil passage, which resulted in no change in overall permeate TOC.

8.3.2c Effect of feedwater pH at 30% oil contamination

Figure 8.13 shows Osmonics SG TOC rejection results in 30% oil contamination in the range of pH from 4.3 to 10.9. Three samples were collected at each condition. The best permeate quality was achieved at low pH and the lowest permeate quality was found at pH of 10.9.

These experiments were conducted at feedwater pressure, temperature, conductivity, and flow of 100 MN/m^2, 30 °C, 5,000 µS/cm, and 11.7 x 10^{-5} m^3/s respectively. The effect of pH on Osmonics SG in low and high oil contamination is found to be similar.

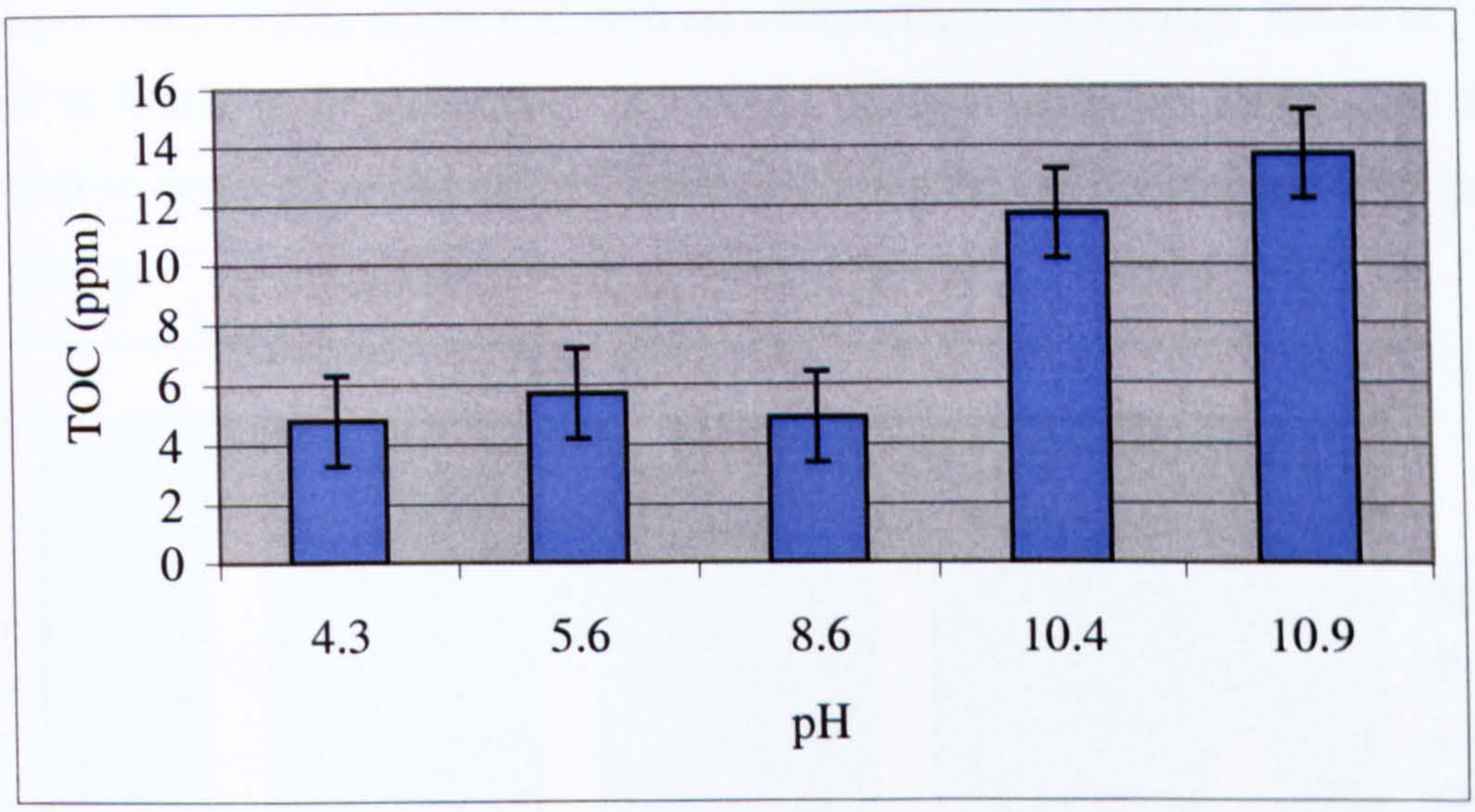

Figure 8.13. Osmonics SG performance in 30% oil contamination at various operating pH

Since the pH has influence on membrane surface changes, it appears that surface charges play significant role in membrane TOC rejection properties. Reducing feedwater pH from 10.9 to 4.3 has resulted in a significant drop in permeate TOC values (from 14 to 5 ppm). This means that pH has the greatest effect on membrane TOC rejection properties. Interestingly, Osmonics SG salt rejection at pH 4.3 is 76% and permeate TOC is 5 ppm whereas at 10.9 the membrane salt rejection is 90% and permeate TOC is 14 ppm. Hence higher membrane salt rejection properties does not imply higher TOC rejection properties. This observation can be investigated further by testing a number of membranes with different salt rejection properties in the treatment of oily water.

8.3.3 Osmonics SG performance in low and high oil contaminations

It was surprising to see that Osmonics SG permeate quality in 30% oil contamination is better than in low oil contamination (see Figure 8.14). Note that the feedwater oil contamination percent was monitored by collecting samples frequently from feedwater sample point to make sure that 30% is maintained during the test period. In low oil contamination experiments it was noticed that as feedwater TOC increases permeate TOC

generally increases. However, in high oil contamination the membrane performance in rejecting oil is much better than in low oil contamination. The limit for drinking water (5 ppm) was achieved. It was observed that the effect of operating temperature and pH on the membrane permeate quality at low and high oil contamination is similar. However, the effect of pressure is found to be different. In low oil contamination an increase in feedwater pressure leads to better permeate quality, however, in high oil contamination it leads to lower permeate quality.

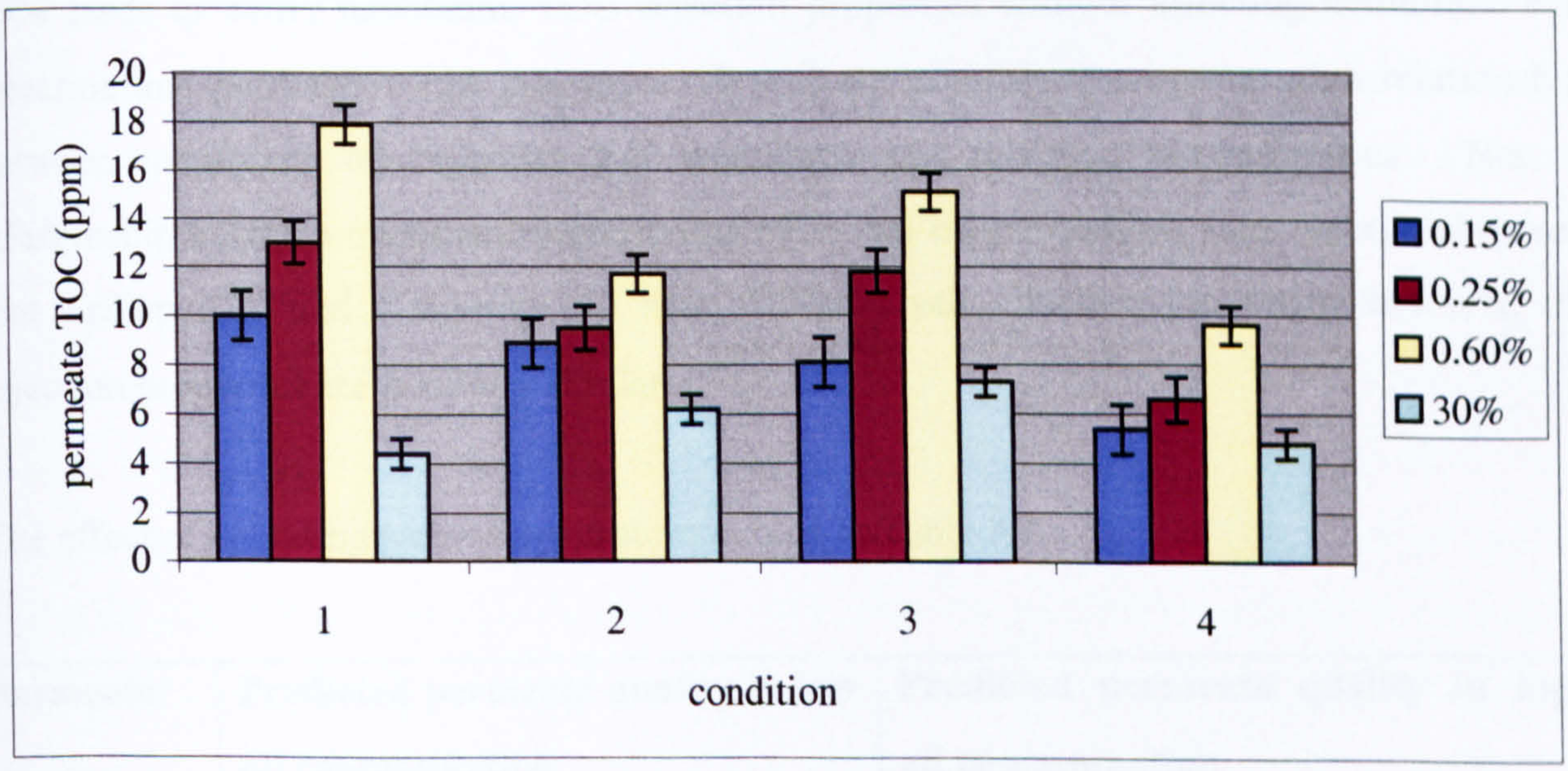

Conditions: 1. Pressure = 80 MN/m^2, Temp = 30 °C, pH = 10.5, conductivity = 5000 µS/cm

2. Pressure = 100 MN/m^2, Temp = 30 °C, pH = 10.5, conductivity = 5000 µS/cm

3. Pressure = 100 MN/m^2, Temp = 40 °C, pH = 10.5, conductivity = 5000 µS/cm

4. Pressure = 100 MN/m^2, Temp = 30 °C, pH = 4, conductivity = 5000 µS/cm

Figure 8.15. Permeate quality with feedwater TOC level

The experiments presented in Figure 8.15 show that Osmonics SG performs well up to 30% oil contamination. So, the question arises whether there is a limit to the performance of the membrane in reducing the TOC of the water. Osmonics SG was then tested at 50% oil contamination. At 50% oil contamination, it was observed that oil is evident floating in the permeate samples indicating a significant increase in permeate TOC levels. The permeate TOC level reached 80 ppm.

8.3.4 Summary

In summary, drinking water quality in term of TOC level was achieved in some operating conditions and wastewater discharge limit was achieved in all conditions except at 50% oil contamination. Osmonics SG and TriSep X20 membrane performances in oil contamination is governed by a number of parameters. It was found that feedwater pressure and pH have significant effect on membrane TOC rejection properties whereas temperature effect is minor. For Osmonics SG, increasing in feedwater oil contamination from less than 1% to 30% leads to better membrane TOC rejection properties without effecting membrane salt rejection and permeation rate properties. It was not possible to come up with relationship between membrane oil rejection and membrane salt rejection characteristics. Nor, a relationship between membrane water permeation and oil permeation rate. It was observed that TriSep X20 and Osmonics SG have different salt rejection properties however, oil rejection properties are generally similar.

The effect of operating parameters is summarized in Table 8.4.

Parameter	**Predicted permeate quality in low oil contamination**	**Predicted permeate quality in high oil contamination**
Pressure	Improves with increasing pressure	Deteriorates with increasing pressure
Temperature	Minor effect	No effect
pH	Improves with pH decrease	Improves with pH decrease

Table 8.4. Operating parameters effect on TOC level in permeate

8.4. Osmonics SG and TriSep X20 membrane water permeation rate and salt rejection at various oil contamination levels

In the previous sections it was shown that Osmonics SG and TriSep X20 are not fouled in the treatment of oily water and it was also shown that drinking water quality can be achieved by optimizing operating parameters. These findings show the suitability of both membranes in the treatment of oily water. In this section, the effect of oil on membrane permeation rate

and salt rejection will be investigated to assess the permeate quality not only in terms of TOC level but also salt rejection and production rate. Such information is important in the design stage, since plant size depends greatly on membrane permeation rate.

8.4.1. Membranes permeation rate in low oil contamination at various operating pressure

Low oil contamination here refers to 1290, 2150, and 5160 ppm TOC content in feedwater. It was expected that feedwater oil contamination leads to membrane fouling and therefore a drop in membrane permeation rate. However, it was observed that not only fouling is not taking place as shown previously in this chapter but also an improvement in some circumstances in permeation rate (see Figures 8.16 and 17). For Osmonics SG, it was observed that feedwater oil contamination leads to an improvement in membrane permeation rate by up to 20% (see Figure 8.17). The experiments were conducted at feedwater temperature, pH, flow, conductivity of 30 °C, 10.5, 11.7 x 10^{-5} m^3/s and 5000 μS/cm. At 160 MN/m^2 feedwater pressure the permeation rate was (21.68 $\pm$ 0.55) x 10^{-8} m^3/s for pure water and (26.41 $\pm$ 0.55) x 10^{-8} m^3/s in 5160 ppm TOC contaminated feedwater. However, at low operating pressure oil contamination has no real effect on membrane permeation rate. Note that in many cases data falls in much less error bar therefore error bar was almost constant.

The improvement in membrane production rate is possibly due to a drop in salt concentration at the membrane surface as a result of oil mixing with rejected salts. Low salt concentration leads to less osmotic pressure and therefore higher permeation rate. In low feedwater pressure water, the permeation rate is low which leads to relatively less turbulence right at the membrane surface. This reduces the mixing effect.

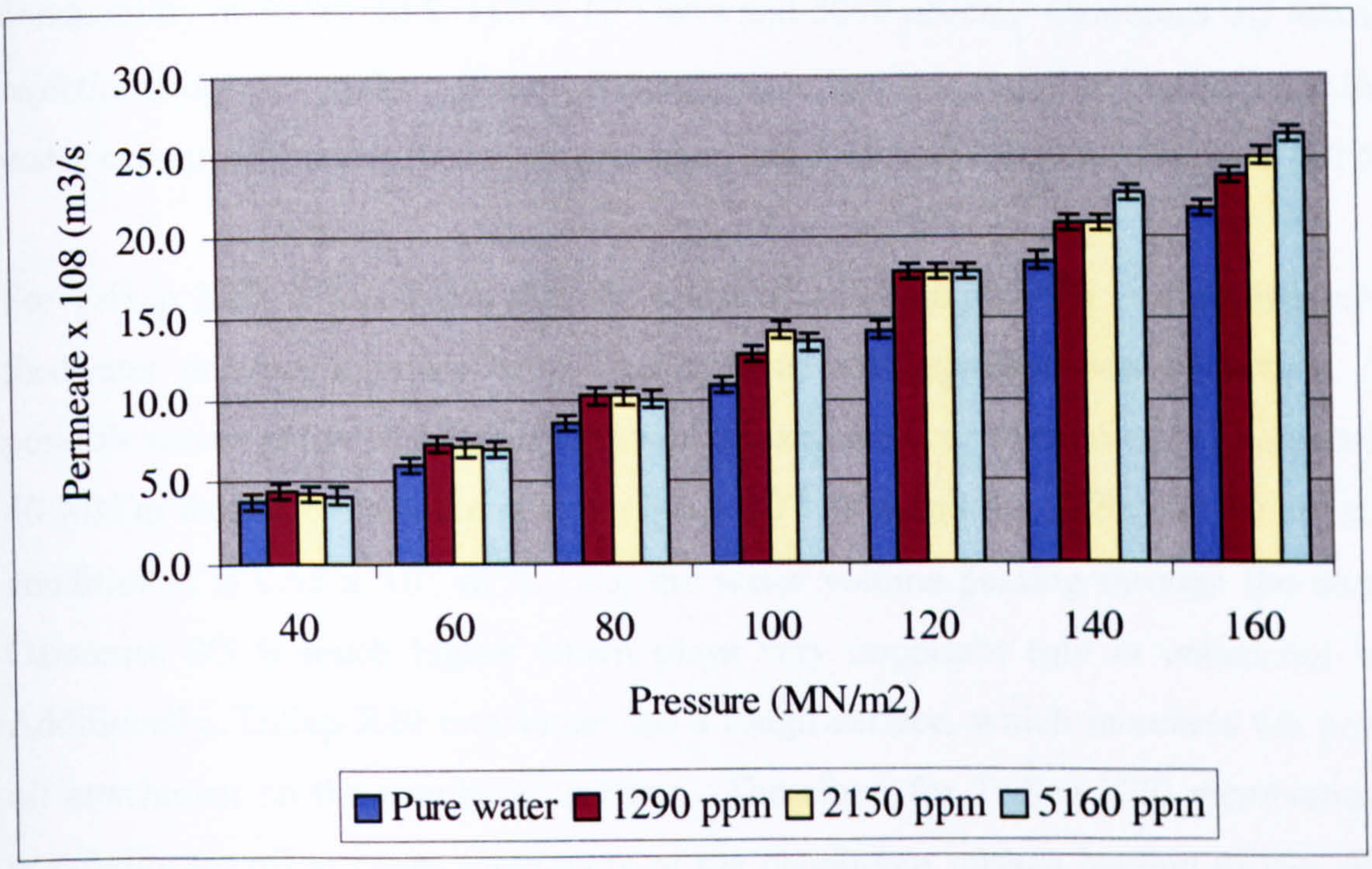

Figure 8.16. Osmonics SG permeation rate in oil contamination

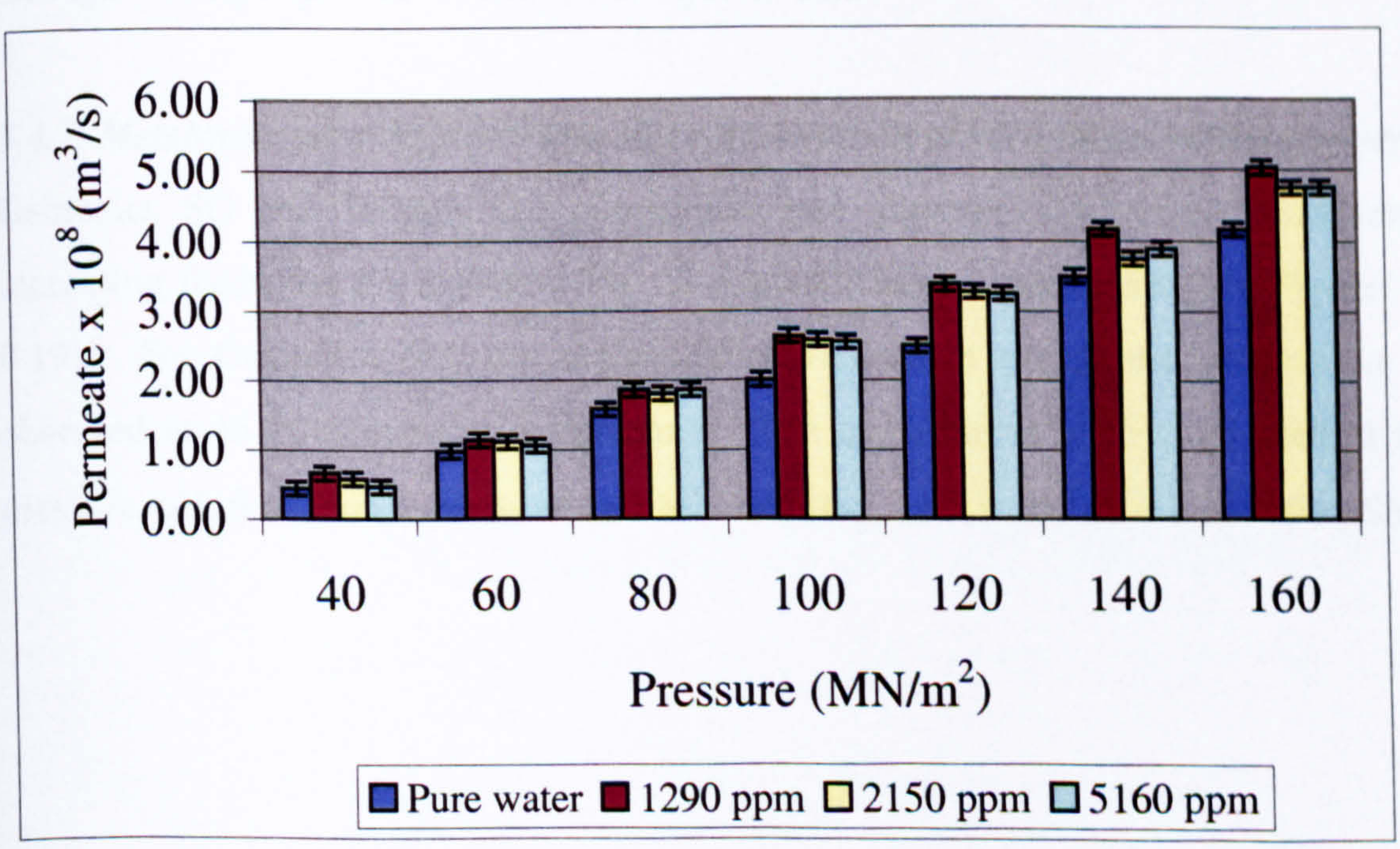

Figure 8.17. TriSep X20 membrane permeation rate in oil contamination

8.4.2. Membrane salt rejection in low oil contamination at various operating pressures

It was observed that the effect of oil on membrane salt rejection for Osmonics SG is negligible. The experiments were conducted at feedwater temperature, pH, flow,

conductivity of 30 °C, 10.5, 11.7 x 10^{-5} m^3/s and 5000 µS/cm. Osmonics SG membrane salt rejection properties in the tested oil contamination levels is found to be similar to that in pure water experiments under feedwater pressures of 40, 60, 80, 100, 120, 140, and 160 MN/m^2.

For TriSep X20, it was found that the effect of oil contamination is quit different. At low feedwater pressure a minor drop in membrane salt rejection was observed. The most possible reason is low turbulence at the membrane surface. Osmonics SG permeation rate at 40 MN/m^2feedwater pressure is about 3.6 x 10^{-8} m^3/s and for TriSep at the same operating condition it is 0.55 x 10^{-8} m^3/s. So, the water volume passing through the membrane in Osmonics SG is much higher which plays very important role in enhancing turbulence. Additionally, TriSep X20 membrane has a rough surface, which increases the possibility of oil attachment on the membrane surface. Therefore, for TriSep X20 membrane there is a possibility for oil to cover some parts of the membrane surface leading to less surface area for water to pass and therefore higher salt accumulation in the areas where water passes through leaving higher concentration of rejected salt.

8.4.3. Membrane permeation in low oil contamination at various operating temperatures

Osmonics SG and TriSep X20 permeation rate improved in some circumstances with increasing feedwater oil in below 1% oil contamination experiments (see Figures 8.18 and 8.19). For Osmonics SG, the highest improvement in membrane permeation rate was observed at 46 °C feedwater temperature. The experiments were conducted at feedwater pressure, pH, flow, conductivity of 140 MN/m^2, 10.5, 11.7 x 10^{-5} m^3/s and 5000 µS/cm.

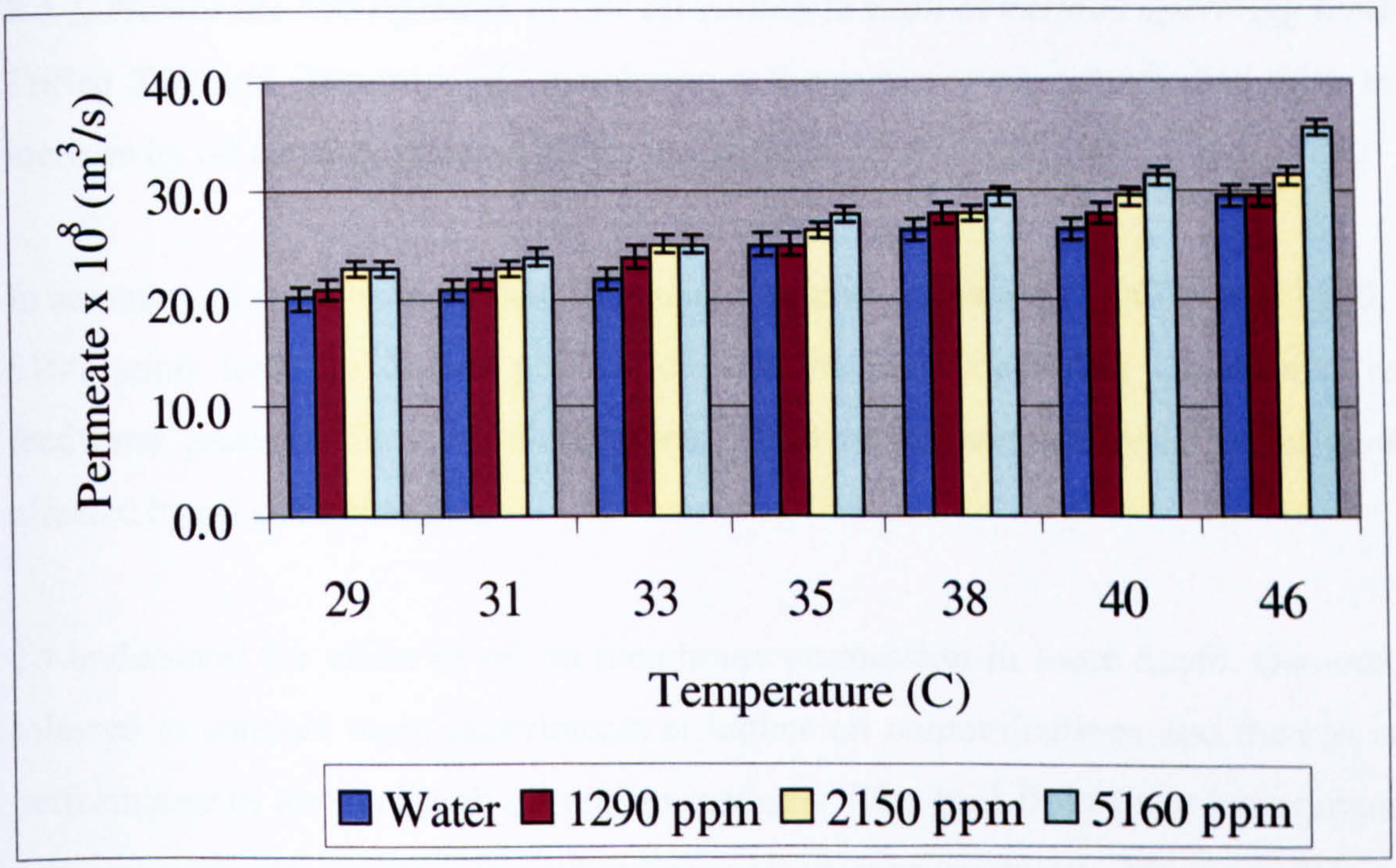

Figure 8.18. Osmonics SG permeation rate in oil contamination with temperature

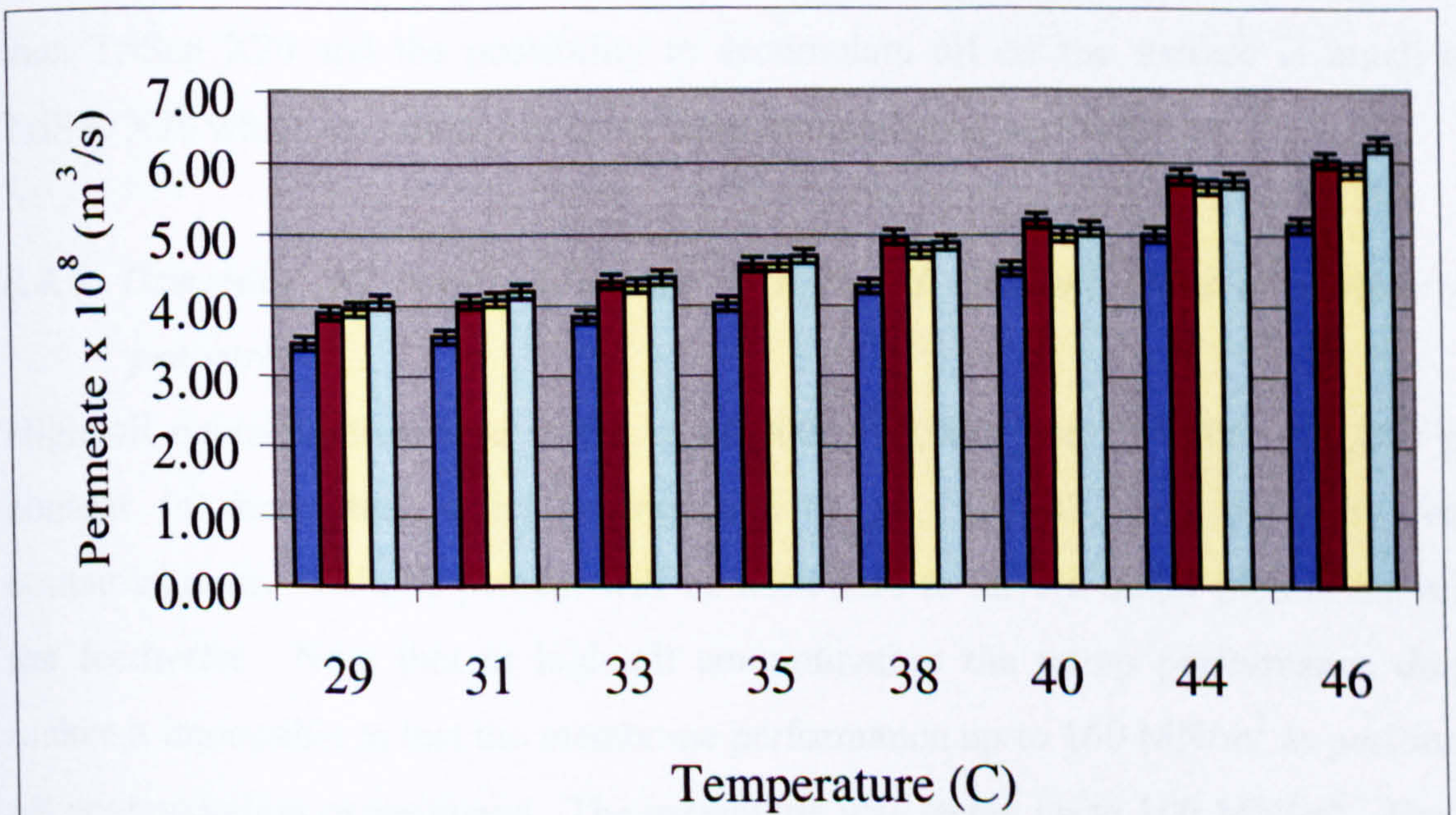

Figure 8.19. TriSep X20 membrane permeation rate in oil contamination with temperature

8.4.4. Membrane salt rejection in low oil contamination at various operating temperatures

TriSep X20 and Osmonics SG membrane salt rejection was not affected with temperature increase by oil contamination in all test conditions.

In summary, it was observed that, in general, oil contamination (TOC levels: 1290, 2150, and 5160 ppm) leads to higher permeation rate in most operating conditions (except low feedwater pressure) for both membranes. Also membrane salt rejection in general is not affected by oil contamination.

To understand the effect of oil on membrane permeation in more depth, Osmonics SG was selected to conduct more experiments at higher oil contaminations and then to compare its performance in low and high oil contaminations. The goal from these experiments is not to compare different membranes performances in oil contamination. However, it is to study the effect of feedwater oil contamination levels on membrane performance. Note that Osmonics SG was selected to conduct this part of the research because it has higher permeation rate than TriSep X20 and the possibility to accumulate oil on the surface is much more than TriSep X20 which expectedly to cause drop in membrane performance.

8.4.5. Osmonics SG permeation rate in high oil contamination at various operating pressure

High oil contamination here refers to 86,000, 155,000, and 284,000, 430,000 ppm TOC content in feedwater, which correspond to 10, 18, 33, and 50% by volume oil contaminations. Volume percent will be used here to have a better picture for oil levels in the feedwater. Note that in high oil contamination the pump performance drops, which makes it impossible to test the membrane performance up to 160 MN/m^2 as performed in low oil contamination experiments. The membrane was tested up to 100 MN/m^2. The feedwater oil contamination leads to an increase in membrane permeation rate and the highest permeation rate was at 50% oil contamination at 8 and 10 bar feedwater pressure (see Figure 8.20).

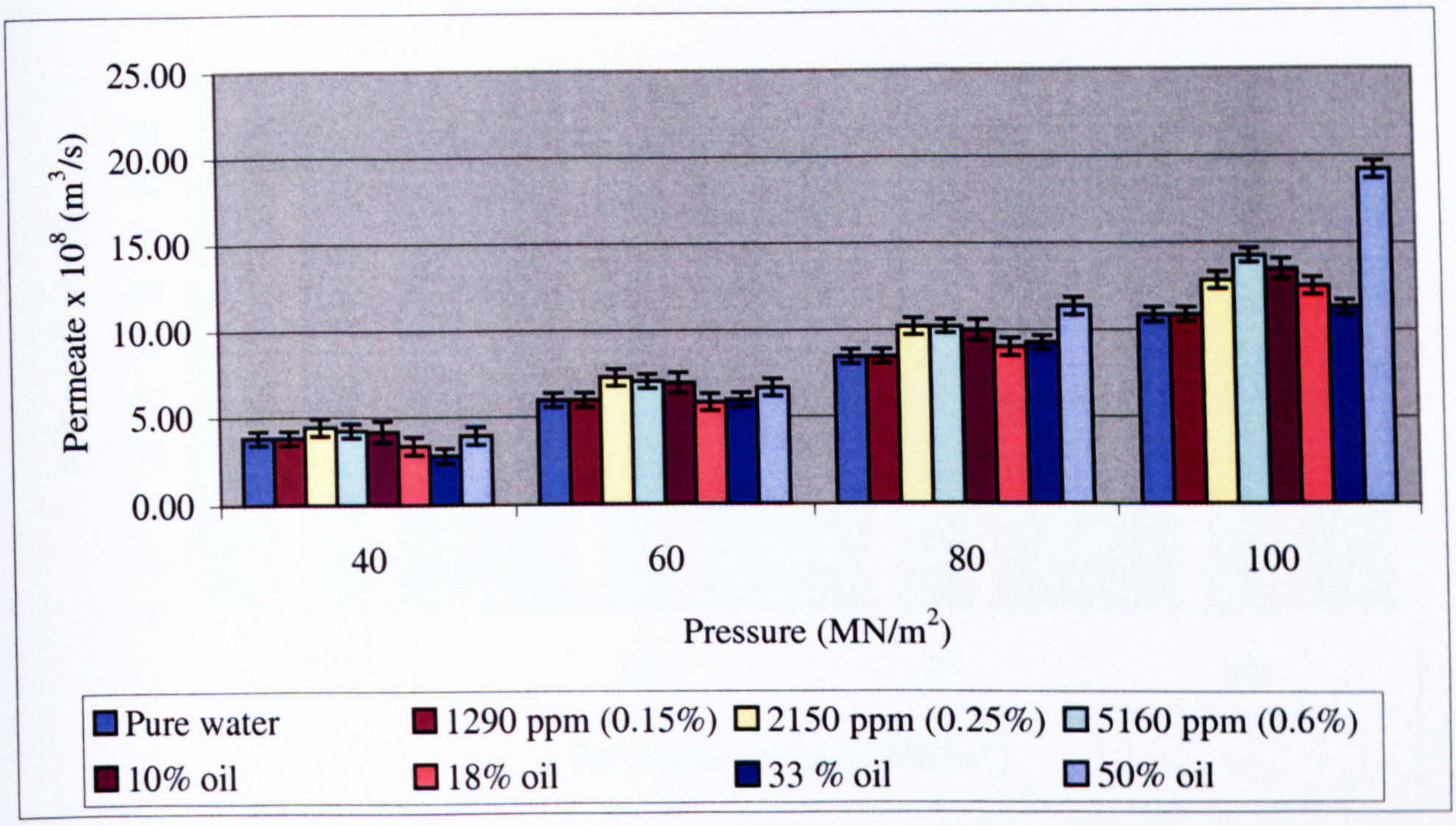

Figure 8.20. Osmonics SG permeation in oil contaminations with pressure

From literature, RO membranes permeation rate is affected significantly with osmotic pressure resulted from increasing/decreasing in salt concentration at the membrane surface. The addition of oil in feedwater has resulted possibly in diluting concentrated salts at the membrane surface, which reduced osmotic pressure. The reduction in osmotic pressure leads to higher permeation rate. However, this phenomenon (decrease in osmotic pressure with oil addition) is not linear and at some stage oil possibly covers some areas of the membrane surface, which leads to a drop in permeation rate. At 50% oil contamination a significant increase in membrane permeation rate was observed at 100 MN/m^2, which is possibly due to significant oil passage and a drop in salt concentration at the membrane surface.

8.4.6. Membrane salt rejection in high oil contamination at various operating pressure

From Figure 8.21, it can be seen that membrane salt rejection is not effect by feedwater oil contamination except at 50% oil contamination in which a minor drop was observed in salt rejection. During this experiments a floating oil was observed in the permeate samples indicating an increase in oil passage. The experiments were conducted at feedwater temperature, pH, flow, conductivity of 30 °C, 10.5, 11.7 x 10^{-5} m^3/s and 5000 µS/cm.

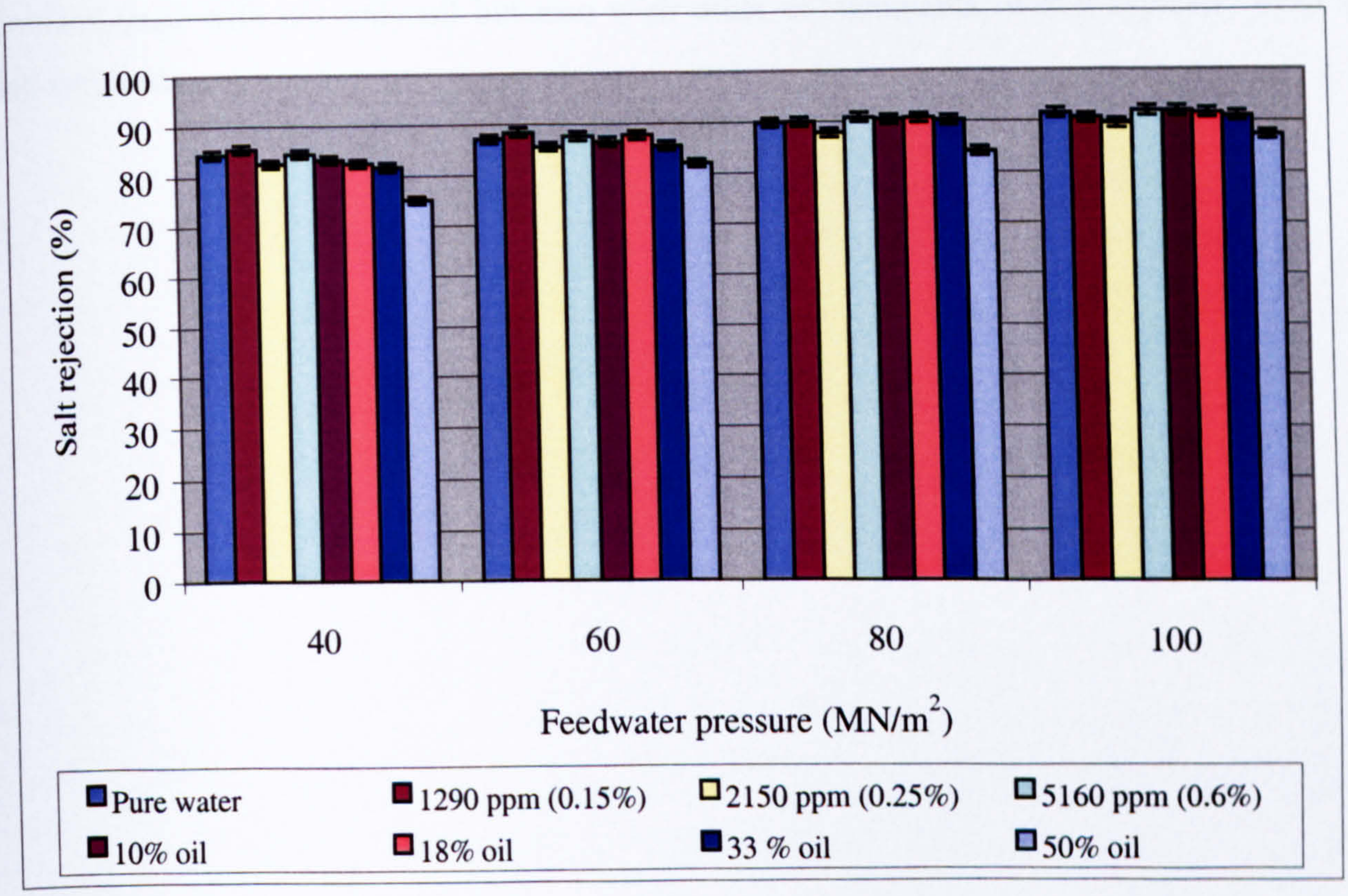

Figure 8.21. Osmonics SG salt rejection in high oil contaminations

8.5 Summary

RO membrane performance in conditions with oil contamination is not simple. Osmonics SG and TriSep X20 membranes were tested at 0.15, 0.25, 0.57, 10, 18, 33 and 50 % oil contamination levels. With low oil contamination increasing pressure lead to an improvement in permeate quality in terms of TOC level whereas in high oil contamination an increase in pressure leads to deterioration in permeate quality. The main findings here were the ability of Osmonics SG to operate up to 50% oil contamination without oil fouling and the high quality of permeate achievable in up to 30% oil contamination. Interestingly the permeate quality in the treatment of 30% is better than that at below 1% oil contamination. Moreover, the observed improvement of membrane permeation rate suggests that Osmonics SG and TriSep X20 wouldn't foul in further operation. In this research Osmonics SG and TriSep X20 were tested up 100 hours in the treatment of oily water. Therefore, it can be stated that Osmonics SG and TriSep X20 are suitable for the treatment of oily wastewater. However, it has to be realized that both membrane have to be tested in effluent water

contaminated with not only oil but also with other contaminants, which typically exist in industrial waste.

CHAPTER 9 – DISCUSSION

9.1 Introduction

In this chapter, the RO membranes' microscopic structure characterization, membrane performance in pure water and in oil-contaminated water results will be presented and discussed in relation to the current literature to draw conclusions and identify the key new findings and main contributions made by the work in this thesis.

9.2 RO membranes structure characterization

From this research it has been found that AFM is a good tool to analyze the morphological structure of RO membranes, however from this work the results obtained from AFM contribute slightly in RO membrane performance enhancement in term of permeation rate and salt rejection. This is because it was found that surface morphology characteristics have no effect on membrane salt rejection and permeation rate properties. On the other hand, AFM can contribute in membrane fouling research because some papers showed that the surface morphology characteristics play an important role in particles accumulation on the membrane surface [79].

AFM was applied in this study to measure RO membrane surface roughness and peak height profile. Important findings were drawn from this area of research. RO membranes surfaces were found to be non-uniform and different locations for the same membrane surface can have quite significantly different surface properties. Over the years, many papers have been published based on the understanding that RO membranes surfaces are uniform and a single AFM image, in the dimension of micrometres, is sufficient to characterize membrane surface properties. It is believed that this understanding has led to many contradictory findings reported in the literature in terms of the relationship between membrane surface roughness and flux [54,55,58,72].

From this work the variation in surface roughness at different locations from the same membrane surface has been quantified. This is the first study conducted to give a comprehensive understanding for membrane surface properties variation. The range of

RO membrane surface roughness can be estimated and a single value is not sufficient to characterize the membrane surface. The lowest TriSep X20 surface roughness (R_a) value obtained was found to be 25 nm and the highest was 87 nm, which makes it impossible to make correlations between membrane properties and performance using a single measurement. Vrijenhoek *et al* [79] characterized TriSep X20 by AFM and reported one reading for R_a, which is 33.4 nm and used that value to compare TriSep X20 with other two RO membranes whose R_a values of 43.2 and 52 nm. From this work, these three membranes possibly have similar roughness values.

Although the membrane surface properties vary from one location to another a reasonably accurate estimation can be obtained using a number of AFM images to fully characterize the spatial variations in roughness and topography.

The analysis in this study showed that the four RO membranes studied in this research have different surface morphologies, and cross-section thicknesseses. The effect of various membrane properties on flux was assessed and it was found that there is no universal relationship between membrane surface roughness and flux. In the literature, the effect of surface roughness on RO membrane flux is not yet clear.

Hirose [80] and based on one AFM image for each studied membrane suggested an approximately linear relationship between membrane surface roughness and flux for cross-linked aromatic polyamide RO membrane, where permeability increased with increasing surface roughness. Stamatialis *et al* [58] investigated the surface structure of dense and integrally skinned cellulose acetate (CA) and cellulose acetate butyrate (CAB) membranes by using tapping mode AFM. It was observed that the surface morphology is associated with permeation properties, the lower values of roughness the lower the flux and the higher the rejection but the relationship was not linear.

Kwak and Ihm [55] used AFM to study the performance of four commercially available RO membranes. A linear relationship between membrane surface roughness and flux was not found. However, the roughest membrane did have the highest flux. Madaeni [59] showed that the rougher the membrane the lower the permeation rate due to the adsorption and trapping of the ions on the rough surface membrane.

Contradictory findings have been reported; higher RO membrane surface roughness can mean higher flux [80], lower flux [59] or have no effect on flux [55,58]. One of the reasons for these contradictory results is believed to be due to the difficulty in properly assessing surface roughness.

The AFM images of Osmonics SG and TriSep X20 showed that peak to valley distance for TriSep X20 (400 nm) is about 4 times greater than Osmonics SG (100 nm) and the distance between each hill for TriSep X20 was found to be about 10 times greater than Osmonics SG. This makes that the probability of trapping significant amount of ions in the valleys of TriSep X20 is much more than for Osmonics SG. Hence sweeping away trapped ions in Osmonics SG (smooth surface) is much easier (see Figure 9.1). Observing an improvement in flux with increasing feed flow for Osmonics SG more than TriSep X20 confirms that this is perhaps the case.

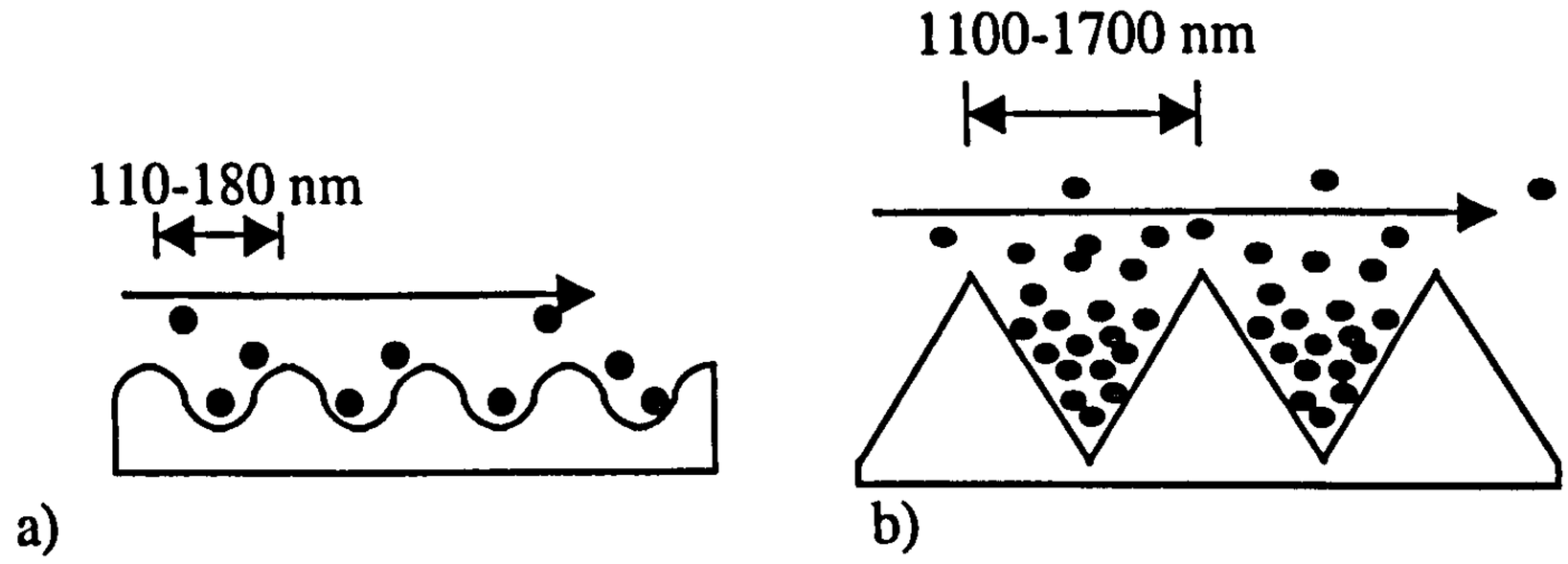

Figure 9.1. a) Osmonics SG surface morphology, b) TriSep X20 surface morphology. The arrow refers to feedwater direction and the circles represent ions.

The accumulation of ions decreases membrane performance due to an increase in osmotic pressure but that effect is minor. It is preferable to have a smooth surface not only because of the minor improvement observed in permeation rate and salt rejection but because rough surfaces showed higher fouling rate tendency in comparison with smooth membranes [79].

It appears from this research that a correlation from parameters in this study exists between membrane cross-section thickness and flux. It was found that the thicker the membrane the lower the permeation rate, in agreement with reports in the literature [7,71,80,]. The interesting part of this investigation is that the active layer thickness is not playing as important role as is sometimes reported in the literature [20,58,82].

Osmonics SG has an extremely dense active (ultra-thin film) layer and TriSep X20 layer is much less dense while Osmonics SG flux is about 6 times greater than TriSep X20. This is an interesting finding, which suggests that the effect of other layers (micro-porous support layer and support polysulfone layers) cannot be ruled out. More research needs to be conducted in this area to study the role of each layer on membrane flux by conducting extensive membrane cross-section analysis by SEM. Many papers have stated that the polysulfone support layer thickness has no effect on membrane flux [58,76].

From this work it is found that not only the thickness and properties of the ultra-thin film layer and micro porous support layer but also the thickness of polysulfone support layer influences the membrane permeation rate. This investigation is based on membrane thickness analysis only. It is believed that the membrane porosity of each layer and active layer pore size also have an effect on membrane permeation rate.

It is believed that most probably there is a high-pressure drop across the ultra-thin film layer and micro-porous support layer, which leads to very low driving force (pressure) after these two layers and any restriction in the support layer will affect the permeation rate. This conclusion is based on comparing Osmonics SG and TriSep X20 permeation rates (Osmonics SG permeation is 6 times higher than TriSep X20). Osmonics SG support layer is thin whereas TriSep X20 support layer is thicker. More research is required in this area by applying SEM extensively in characterizing membrane different layers and relating that to their performances.

9.2.1 Scanning RO membranes surfaces using AFM operation in contact mode

AFM contact mode operation was found to be suitable to image RO membranes in dry conditions and excellent images with high resolution were obtained. For membranes imaged in water, there is a possibility for surface damage to occur. The effect of scanning RO membranes by AFM in contact mode has not previously been reported in the literature although there has been a lot on imaging polymer in general [156, 157].

It appears that in much of the literature investigators presume that RO membranes have soft surfaces and will be damaged by the AFM tip and have avoided using contact mode operation [18,55,58,73,75]. Other investigators have used tapping or non-contact mode presumably for this reason [61,72,76]. Some have reported the use of contact mode and

produced high quality images without experiencing any surface damage [80,152]. A comprehensive study that shows the effect of contact mode AFM operation on membrane surfaces is not reported in the literature. This is the first study conducted to investigate the limitations of contact mode AFM operation in imaging RO membranes surfaces.

9.2.2 Effect of scanning RO membranes with different AFM constant force settings

The constant force setting used to scan the membrane surface for AFM can be adjusted between 0 and 60 nA. It was found that varying AFM tip constant force settings has a negligible effect on RO membrane surface damage. The objective of this work was to determine if there is a way to image sensitive RO membrane surfaces (in water) without damage.

Such investigations have not previously been performed or reported. Many investigators have used AFM in their research and have not reported the force setting value [18,55,57,58,63,73,76,77,78,149,151]. Some researchers have reported the force setting value but have not mentioned the reason for selecting that value [61,62,152]. This indicates that the effect of membrane force setting on RO membrane surface imaging is not known. From this work the role of AFM constant force settings was determined.

9.3 RO membranes performance in pure water

From the literature it is well known that operating parameters have a significant effect on membrane permeation rate and salt rejection properties. RO membranes are sensitive to any change in feedwater operating temperature, pressure, pH, flow and/or conductivity. One accomplishment in this research has been the development of an empirical relationship to enable the TriSep X20 and Osmonics SG performances to be calculated by knowing the operating conditions.

It was observed that pressure, temperature, feed water flow and conductivity are linearly related to membrane permeation rate and salt rejection percent. The relationship between pH and permeation rate and salt rejection is not linear for the range from 2-11.7 (see Figure 7.13 and 7.14). However, it can be approximated to linear relationship if extremely low and high pH are excluded. In the range from 3.5-11 a linear relationship can be suggested for simplicity. Based on that, a single expression to include all

operating parameters was produced to be used in calculating the membrane performance at every possible operating condition since experimental data does not cover that.

In the literature, there are papers that include computer software used to calculate membrane performance which are similar to developed expression here but using different theories [1,7]. However, the equations developed in this study can be further expanded in the future to include membrane performance in not only pure water but also in oily water and for different membranes. The permeate TOC level can be also calculated. In the oily water experiments the effect of operating parameters on membrane permeation rate and permeate quality were determined at different oil contaminations. However, the experiments do not cover a wide enough range of operating conditions to enable establishment of similar equations, which were produced for pure water. So, for future research in oily water it will be possible to expand this work to include oil contamination percentage in addition to membranes thicknesses since membrane thickness is correlated with flux and an equation can be established.

In terms of the effect of feedwater pH value on membrane performance, it was found that at extremely low or high pH values, membrane salt rejection drops significantly but the effect of pH on membrane flux is minor. Mohammedi *et al* [36] found that lower flux for FilmTec polyamide FT30 RO membrane is attained in the pH 4-7. From this study it was found that higher permeation is attained at these pH values for Osmonics SG whereas the pH value has no effect on TriSep X20 permeation rate. The most possible reason is that Osmonics SG is more porous (Osmonics SG flux is 6 times higher than TriSep X20) and therefore it expands and shrinks more freely than TriSep X20 as pH changes as a result of absorbing water or being hydrophobic membrane. It has been shown in chapter 6 that membranes expand/shrink as pH changes. From this work it can be said that the effect of pH varies from one membrane to another and generalizing the effect of pH on membrane permeation rate is not possible.

The flux is found to be very sensitive to feed pressure. Many authors have reported this [4,42,44,46,59]. For the effect of pressure on RO membrane salt rejection, Amjad [4] reported that increasing pressure results in an increased water flow per unit of membrane area and salt transport across the membrane is not affected by pressure, but the increased water flow with pressure dilutes the salt passing through the membrane, which results in

lower permeate salt concentration. Ho [15] disagrees with this interpretation and has reported that salt rejection is generally increased with pressure up to a certain value then reaches a plateau. The experimental results from this research agree with the finding by Ho (see Figure 9.2).

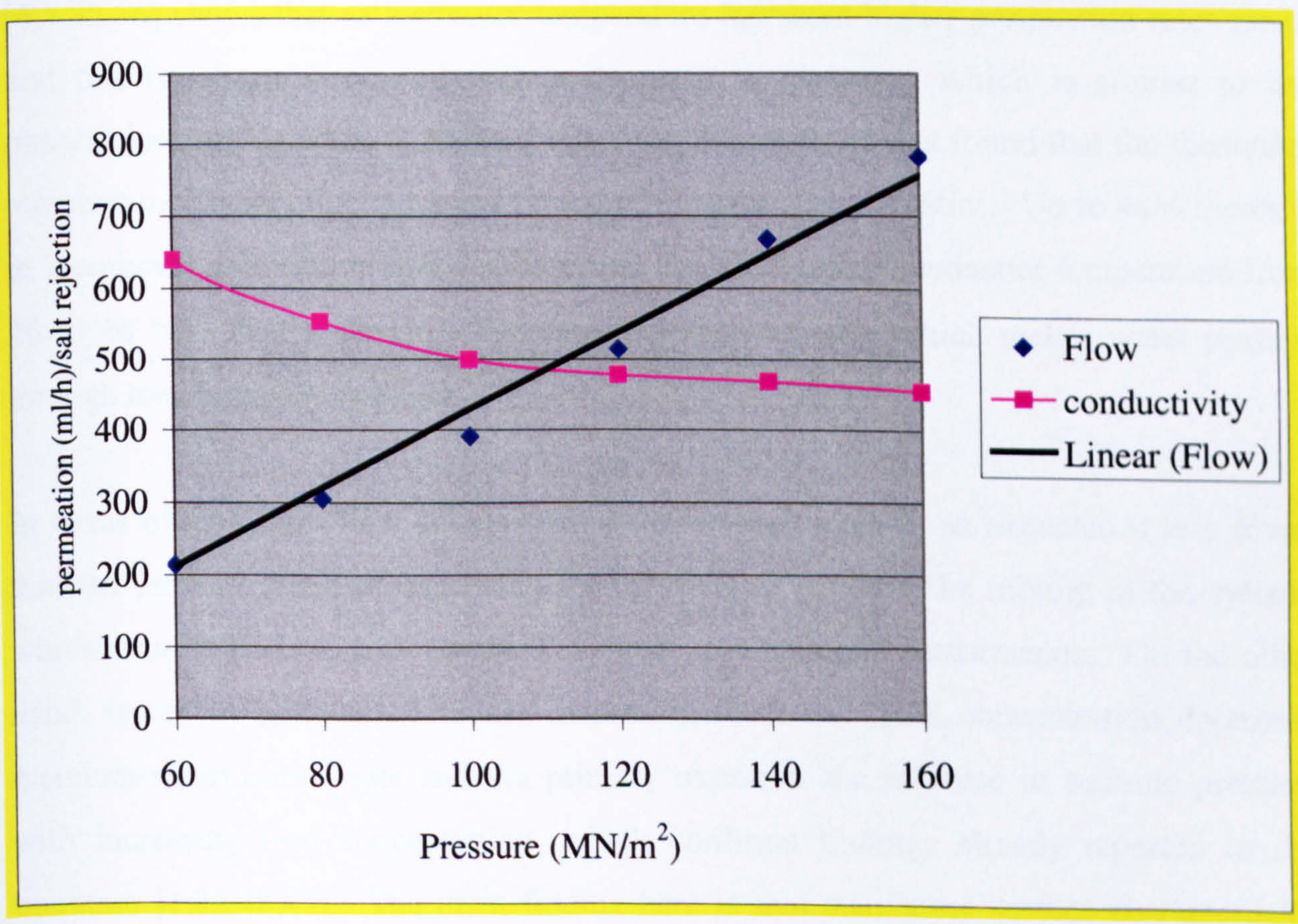

Figure 9.2. Relationship between feedwater pressure, permeation rate and salt rejection for Osmonics SG

From Figure 9.2 which was developed in this study, it can be seen that permeate conductivity does not drop linearly with pressure. Increasing feedwater pressure from 40 to 160 MN/m^2 has increased permeation rate by 5.5 times. If salt passage is constant (as reported by Amjad [4]) and only water passage is increasing then it is expected to dilute permeate by 5.5 times. Permeate conductivity at 40 MN/m^2 is 818 µS/cm and diluting that by 5.5 times gives permeate of 148 µS/cm, however, permeate conductivity was found to be 455 µS/cm. Unfortunately, Amjad has not supported his conclusion based on experimental data to enable proper comparisons with this work.

Therefore, it can be concluded that salt rejection of RO membranes is not directly proportional to feedwater pressure. Increasing feedwater pressure will reduce permeate conductivity but eventually it will stay constant and reaches a plateau.

The influence of temperature varies for different RO membranes. The literature [6,7,32,36] shows that as feedwater temperature increases higher permeation rates result and this has been associated with a decrease in viscosity, which is similar to the observations in this work. Additionally from this work, it was found that the feedwater temperature has an effect on membrane performance characteristics. Up to 40% increase in membrane permeation rate was observed upon increasing feedwater temperature from 26 to 46 °C. That is due to a decrease in water viscosity which makes water passage through membrane pores easier.

In terms of feedwater flow effects on membrane performance, as expected it was found that the primary effect of increasing feed flow is to increase the mixing in the system, which usually leads to a minor improvement in membrane performance. On the other hand, it can be generalized to say increasing feedwater TDS concentration decreases membrane permeation rate and the primary reason is the increase in osmotic pressure with increasing feed concentration, which confirms findings already reported in the literature [1,32,48,49]. The main finding here is that membrane surface characteristics (surface roughness) influence the sensitivity of the membrane to feedwater flow and TDS concentration. Smooth membrane surfaces were found to be more sensitive to feedwater flow and conductivity much more than rough membrane surface. From this work, Osmonics SG (smooth membrane) salt rejection percent decreased from 94 to 80% upon increasing feedwater conductivity from 80 to 25,000 μS/cm whereas for the same feedwater conductivity change, TriSep X20 (rough surface) salt rejection percent has not changed (remained at 94%).

9.4 RO membrane performance in oily water

RO technology is a potential method for wastewater treatment. Current research has shown potential at low oil concentration but there is scope for using this technology in a much more extensive way. This is the first study to consider high levels (up to 50%) of

oil contamination and, as such, expands the current understanding of the applicability and limitations of RO membrane in this field.

It is found that RO membrane technology performance in purifying wastewater is not a simple issue and many interdependent parameters are involved. The experiments showed that Osmonics SG membrane tolerates not only high oil contaminations but also drinking water specification (5 ppm) for TOC level can be achieved by optimizing operating parameters. An increase in permeation rate by up to 20% in some circumstances was observed also possibly due to salt dilution effects with oil in the membrane boundary layer, which results in lower osmotic pressure. The sewer water specification (50 ppm) was met in all experiments. Although the experiments were conducted for water contaminated by oil (refer to chapter 5 for more detail on oil specification) only and other contaminants, which usually exist in sewer water, were not included this finding opens the door for more research in this area. Until today RO membrane processes have never been used in the treatment of up to 30% oil contamination. That is possibly because its application in oily water treatment is not wide and relatively new and the fast developments in membrane materials, which makes RO membranes more tolerance to various contaminants, have not yet been tested in such environment.

While this research is far from complete and field tests would be required to consider all other parameters such as wastewater properties but these initial findings are of great importance in demonstrating a potential use for the applicability of RO membrane technology in wastewater treatment to be widen. This could lead to simpler wastewater treatment plants by bypassing processes needed currently to remove part of the oil prior to RO membranes.

The fouling tendency test for Osmonics SG and TriSep X20 in oil-contaminated water showed that both membranes are not fouled. Based on the literature, membrane fouling tendency by oil is generally correlated with membrane pore size [83,90,140]. Significant fouling and flux decline were reported in purifying oily water by microfiltration processes [88,90,91]. Ultrafiltration membranes in the treatment of oil-in-water emulsions experiences irreversible fouling due to internal pore plugging [100]. High flux declines upon testing nanofiltration membranes in the treatment of wastewater are reported too [119,121]. On the other hand in many papers [35,108,128,129,143-145] RO membranes

are found to be very suitable for treating oily effluents but these papers reports RO performance in low oil contaminations whereas in this work the membrane tested to high oil contamination.

From the above review it appears that membrane pore size has a great influence on the membrane fouling mechanism by oil in oil-contaminated water (refer to Figure 9.3). Microfiltration has the largest pore size among membrane filtration processes and it undergoes severe fouling.

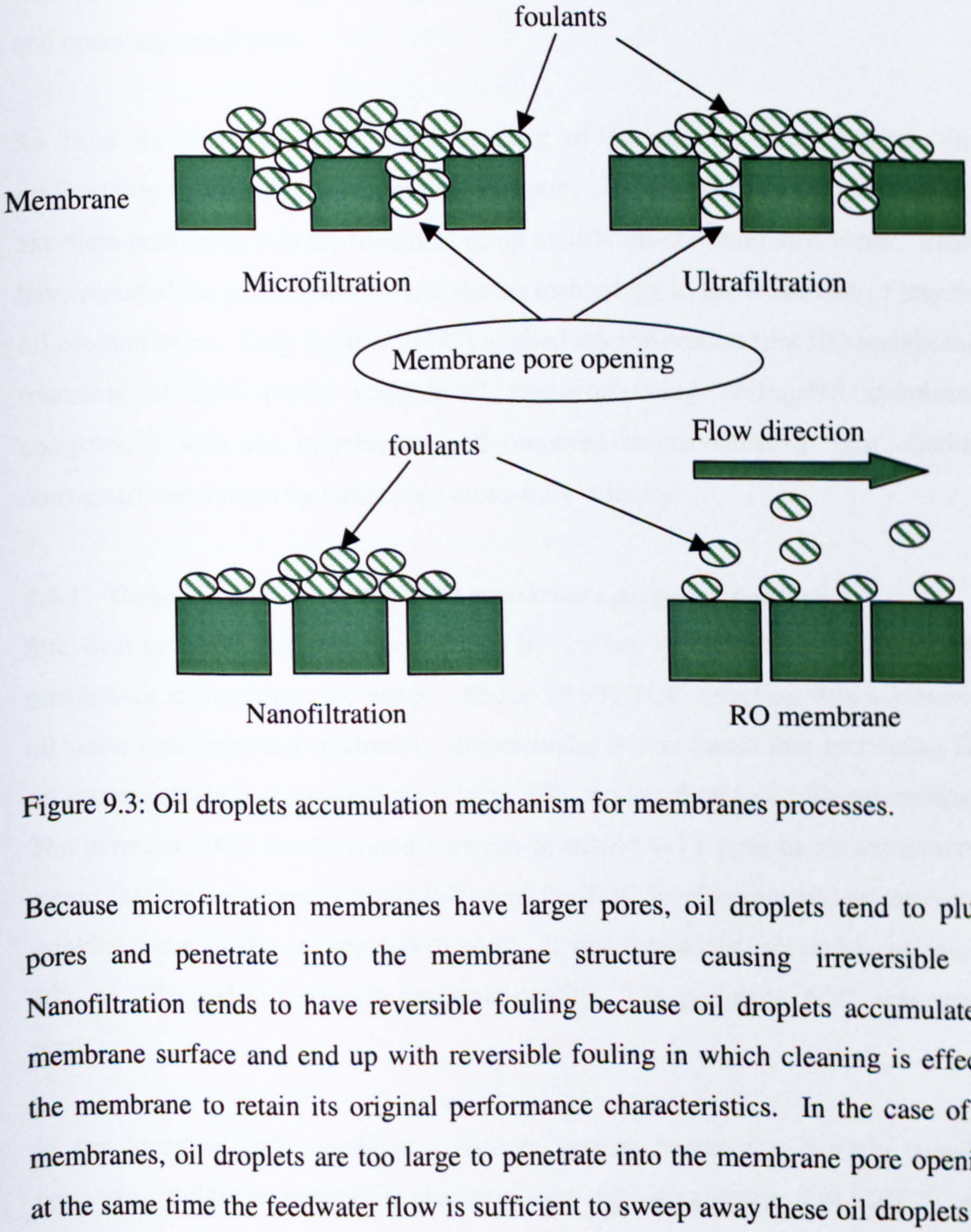

Figure 9.3: Oil droplets accumulation mechanism for membranes processes.

Because microfiltration membranes have larger pores, oil droplets tend to plug these pores and penetrate into the membrane structure causing irreversible fouling. Nanofiltration tends to have reversible fouling because oil droplets accumulate on the membrane surface and end up with reversible fouling in which cleaning is effective for the membrane to retain its original performance characteristics. In the case of the RO membranes, oil droplets are too large to penetrate into the membrane pore openings and at the same time the feedwater flow is sufficient to sweep away these oil droplets because the rate of oil droplets accumulation on the membrane surface is much lower than other

membranes process. The water permeation rate of microfiltration, ultrafiltration and nanofiltration is much higher than RO membrane processes, which make the rate of rejected oil accumulation much faster for these processes than RO membrane processes.

Previous discussion shows that RO membrane pores are too small to be plugged by oily foulant. However, some papers have reported that RO membranes are fouled by organics as a result of absorption of organics present in municipal effluent [128]. This suggests that there are many interdependent parameters that govern membrane performance in oily water treatment such as type of organics, membrane characteristics, feedwater properties and operating conditions.

So from the literature, there are a number of parameters that influence membrane performance in treating oil-contaminated water. In this work, RO membranes showed excellent performance in the treatment of up to 30% oil-contaminated water. Most papers have reported the performance of membrane technology in the treatment of less than 10% oil contamination. Only Scott *et al* [83] applied microfiltration (not RO membrane) in the treatment of 30% (w/w) water-in-oil emulsion using corrugated membranes and compared it with flat membranes and observed enhancement in flux obtained with corrugated membranes by optimizing cross-flow velocity.

9.4.1 Osmonics SG and TriSep X20 membranes permeate quality

Excellent permeate quality was achieved by the use of Osmonics SG and TriSep X20 membranes in purifying oily water. Above 99.9% TOC rejection was achieved in 30% oil water contamination treatment. Interestingly, it was found that increasing feedwater oil contamination percentage from 0.15 to 30% has resulted in a better permeate quality. The permeate TOC levels varied between primarily 4-15 ppm in all experiments. This means that the sewer water limits (50 ppm) for TOC level is met and in some conditions drinking water limits was met too (5 ppm). It was found that increasing oil content from 30% to 50% lead to a drop in permeate quality. The permeate TOC value reached 80 ppm.

In the literature RO membrane permeate quality varies significantly based on the operating conditions, membrane characteristics and oil properties [39,139]. It appears in spite of the extensive experimental work reported, the key factor(s) that directly affect the

rejection of organics are not yet clear. In the following section the effect of operating parameters determined from this work on permeate quality will be presented.

9.4.2 Osmonics SG and TriSep X20 permeate quality at various operating conditions

Optimizing operating parameters significantly improves membrane permeate quality. Increasing feedwater pressure could improve permeate quality by up to 30%. That is possibly due to dilution effects with higher water permeation rate. In the literature some papers have reported similar findings that increasing pressure improves permeate quality whilst others have shown that pressure has no effect [130,134,142]. Different RO membrane processes perform differently with pressure change and that is based on the membrane properties and solute characteristics.

It is found that increasing feedwater temperature increases TOC passage, however the effect is minor and depends on the type of membranes, which is similarly reported in the literature [111].

It was confirmed that at low pH, highest permeate quality is achieved and pH is the most influential parameters on membrane permeate quality possibly as a result of an increase in membrane hydrophilicity at low pH. Ozaki *et al* [129] reported the same finding. But that cannot be generalized because some organics separation is not a function of pH value. Ultra-low pressure RO membrane aromatic polyamide rejection for urea, glucose, benzyl alcohol, and ethylene glycol at pH of 3 and 9 is similar [129].

The feedwater conductivity has no effect on TOC rejection. Sridhar *et al* [134] reported that increasing feedwater-dissolved solids decreases organics rejection. Whereas in this research it was found that dissolved solids has no effect on oil separation. This is most probably because Sridhar tested his membrane in up 50,000 ppm whereas in this research it was limited to 16,000 ppm. More research is needed in the effect of feedwater TDS concentrations on TOC rejection by widening the TDS concentration test range.

9.4.3 Permeate quality of Osmonics SG at 30% oil contamination

The previous discussion is based on RO membranes performance in low oil contamination levels (0.15, 0.25, and 0.6%). In this section the permeate quality at 30%

oil contamination will be presented for Osmonics SG in which interesting findings were observed. At lower oil contaminations it was found that *increasing feedwater pressure leads to lower TOC in permeate.* However, in 30% oil contamination it was found that *higher pressure leads to higher TOC in the permeate.* The most probable cause is that in high oil contamination, the presence of oil in the boundary layer is much significantly higher (about 50 times) than that at low oil contamination. Increasing pressure tends to push oil through membrane pores since water presence is not as much as in low oil contamination.

In high oil contamination feed temperature has no effect on TOC rejection. In low oil contamination, the temperature has an effect; temperature increase leads to lower TOC rejection but that effect is not much and can be ignored. In terms of pH effect, it was found that in low and high oil contamination the pH value has similar effect.

In summary, the effect of operating parameters on membrane TOC rejection properties is a function of oil contamination level. To have a better understanding for the effect of operating parameters and its limitations an extensive research is required to test the membrane in higher than 50% oil contaminations with wider operating range. Also membranes with different chemical and physical properties should be considered in such research to enable recommending the best membranes properties.

9.4.4 Osmonics SG and TriSep X20 permeation in oily water

RO membrane permeation rate is found to be sensitive to oil contamination. At low oil contamination up to 20% increase in permeation rate has been reported in this research in some operating condition and up to 75% was reported at 50% oil contamination.

In oil contamination it was found that RO membranes permeation rate is improved in most circumstances. Most research in oily water treatment with membrane technology is focused on membrane fouling tendency or permeates quality. But RO membrane permeation rate and salt rejection characteristics in oily water treatment were not found in the literature.

It was observed that the effect of oil is more pronounced on Osmonics SG permeation rate than TriSep X20 especially at higher operating pressure due to surface roughness

(TriSep X20 surface roughness value is about 4 times higher than Osmonics SG). A better mixing at the surface of Osmonics SG between oil molecules and water is achieved, which lowers concentration polarization much more effectively than in TriSep X20. From this research, it was found that Osmonics SG permeation rate improves in some circumstances and salt rejection is not affected by oil contamination in up to 30% oil contamination.

At the start of this study it was thought that as oil contamination percent increased the membrane performance in terms of salt rejection and permeation rate would decrease. Also the TOC in the permeate would increase. However, it appears that RO membranes behaviour in oil contamination environment is not as simple as expected. Gradual increase in oil contamination does not imply gradual drop in membrane performance or visa versa. Extensive research is required in this area to come up with a correlation (if exist) between oil contamination percent and RO membranes permeation rate and salt rejection. However, this project has demonstrated that there is RO membrane technology for treating oily waters without associated decrease in performance or increase in permeate TOC.

In short, RO membranes performance in oil water treatment is governed by many parameters although the effect of some parameters where determined in this work it was found that these effects changes with membranes and with operating conditions.

CHAPTER 10 – CONCLUSIONS

This chapter will summarize the main conclusions from this research. It will be divided into three sections: 1) RO membrane structure characterization, 2) RO membranes performance in pure water and 3) RO membranes performance in oily water treatment. Additionally, recommended future research will be addressed.

10.1 RO membrane structure characterization

AFM images analysis of RO membranes have confirmed that RO membranes surface characteristics are not uniform and can vary significantly from one section to another. It was found that RO membrane surface characterization must be handled with caution. Some important findings are summarized in the following points.

- Single AFM images are not sufficient to characterize RO membrane because RO membranes surface morphology vary significantly from one location to another.
- A methodology for AFM imaging has been assessed to properly characterize RO membranes surfaces and that is by collecting at least three images from different locations and from different membrane samples.
- Membrane surface morphology changes upon exposing the membrane to different environments. It was noticed that upon soaking the membrane in water it absorbs water leading in some circumstances to an increase in surface roughness and membrane thickness.
- It was impossible to establish a universal relationship between membrane surface roughness and flux. It was found that Osmonics AG and Osmonics AG have approximately similar surface roughness however, Osmonics AG flux is higher than Osmonics AD by about 10 times.
- A linear relationship between membrane thickness and flux was established. It was observed that the thicker the membrane the lower the permeation rate due to higher pressure drop across the membrane. .

- RO membranes with smooth surfaces are more sensitive to feedwater flow than RO membranes with rough surfaces. But the effect is not significant and can be ignored.
- AFM images of RO membranes surfaces confirmed that generally RO membranes have hills and valley but in some sections the surface is flat.
- For membranes imaged in water by AFM, it was confirmed that contact mode operation can damage some RO membrane surfaces. That is possible due to membrane water absorption, which leads to softer membrane.
- For membranes imaged in air with contact mode, no damage was observed on any of the imaged membranes.
- Varying AFM tip constant force (in the range of 0-60 nA) has a negligible effect on the degree of the membrane surface damage.

10.2. RO membranes performance in pure water

It was found that the operating parameters have a significant effect on RO membranes permeation rate and salt rejection. Some important findings are summarized in the following bullets.

- Feedwater pressure has a great influence on RO membrane performance but the influence of pressure on different RO membranes is different.
- RO membrane salt rejection increases with increasing pressure but eventually it stays constant and reaches plateau.
- As temperature increases RO membranes permeation rate increases and salt rejection decreases. Some RO membranes salt rejection is not effected by temperature.
- At extremely low or high pH value RO membranes salt rejection dropped significantly.
- The pH has minor influence on RO membranes permeation rate.
- Feedwater flow has a minor effect on RO membrane permeation rate and salt rejection.
- As feedwater TDS concentration increases membrane flux deceases significantly.

- The effect of feedwater TDS on RO membranes salt rejection percent varies from one membrane to another.

10.3. RO membranes performance in oily water

It was confirmed that Osmonics SG and TriSep X20 membranes have excellent performance characteristics in the treatment of oil-contaminated water. Operating parameters have a great influence on the membrane performance in oily water treatment in terms of organic rejection and permeation rate. Some important findings are summarized in the following points.

- Osmonics SG performance was not affected in up to 30% oil contamination.
- Osmonics SG and TriSep X20 membranes TOC rejection were above 99% in all tested oil contamination levels.
- It was found that increasing feedwater oil contamination percentage from 0.15 to 30% has reduced TOC level in permeate.
- In some circumstances drinking water specification for TOC level (below 5 ppm) was achieved.
- Increasing oil content in feedwater from 30% to 50% lead to a drop in permeate quality and floating oil is evident in the permeate.
- It was noticed that the best TOC rejection is attained at low pH value.
- It is found that feedwater temperature has minor effect on membrane TOC rejection properties.
- Feedwater conductivity has no effected on RO membrane TOC rejection.
- At low oil contaminations, increasing feedwater pressure leads to lower TOC level in permeate and at high oil contamination, higher pressure leads to higher TOC level in permeate.
- It was observed that the effect of oil concentration on RO membranes permeation varies for different RO membranes.
- Osmonics SG permeation rate in pure water and in high oil contamination is almost similar and in some circumstances better flux is attained in oil contamination.

- Osmonics SG salt rejection doesn't change with changing oil contamination percentage except at high oil contamination (50%).

10.4. Future work

- Evaluate Osmonics SG and TriSep X20 membranes fouling mechanism in the treatment of high oil contaminated wastewater with the presence of various wastewater contaminants for 6 months period in the field to verify the effectiveness of both membranes with their limitations.
- Evaluate the role of RO membranes active layer, micro-porous support layer and polysulfone support layer in membrane permeation rate.
- Investigate the effect of wider ranges of feedwater pressure, temperature, pH, flow, and conductivity on RO membranes TOC rejection properties for wide range of oil contamination levels. Use the results to develop equations that allow calculating membrane performances in various operating conditions. Incorporate these equations with the developed empirical expression in this work.

CHAPTER 11 - APPENDIX

11.1 APPENDIX A

The experimental test rig components details are given below.

PUMP: the pump was purchased from PUMPMASTERS LTD, Edinburgh, Scotland, EH16 4BB (Tel. 0131 661 3982, Fax: 0131 652 0115) at £823.00 and below is its details:

***Pump Details*:**

Pump type: Vertical Multistage Centrifugal

Pump Speed: 2900 RPM

Discharge Branch: 3/8" BSPF

Suction Branch: ¾" BSPF

Casing Material: Stainless Steel

Impeller Material: Stainless Steel

Shaft Material: Stainless Steel

Seal Type: Single mechanical

***Drive Details*:**

Type: TEFV Electric Motor

Power: 3.0 KW

Speed: 2900 RPM

Supply: 240V/1HP/50HZ

Drive arrangement: close coupled

FLOW METER: It was purchased from Cole-Parmer, London, W7 2QA, UK at £86.00. It is spring-loaded flow meter. Its details are below:

Tube material: PVC

Fitting material: brass

Spring and shaft: 316 Stainless steel

Accuracy: $\pm$ 5%

Maximum operating temperature: 65 °C

Maximum operating pressure: 136 MN/m^2

Maximum flow rate: 1.89×10^{-4} m^3/s

Fitting NPT (F): ½"

PIPINGS AND VALVES: Piping and valves were purchased from South Scotland Valve & Fitting Company, Tel. 01294 213341, Fax. 01294-213484, www.swagelok.com. The piping is 316 stainless steel tubing (about 6 meters were used) and the valves were 316 stainless steel. Drain valve was 2" PVC valve.

TANK: It is a common plastic tank.

MIXER: The mixer is a variable speed mixer with a blade width of 3 cm.

SEPA Cell: It is 316 L SS cell (model 1149417) purchased from Osmonics Inc. France. 230 Rue Robert Schuman, ZA des Uselies, 77350 LE MEE SUR SEINE (Tel. ++ 33-1-64-10-20-00), www.osmonics.com

11.2 APPENDIX -B

SEPA CF preparation

The system consists of stainless steel cell body, aluminum cell holder, piston pressure gauge, concentrate flow valve assembly, feed spacer, and 3/8" diameter feed and concentrate tubing. The installation procedure is as follows:

1) Screw the piston-clamping pressure gauge into the 1/4 threaded hole on the top of the aluminum cell holder as shown in Figure 1.

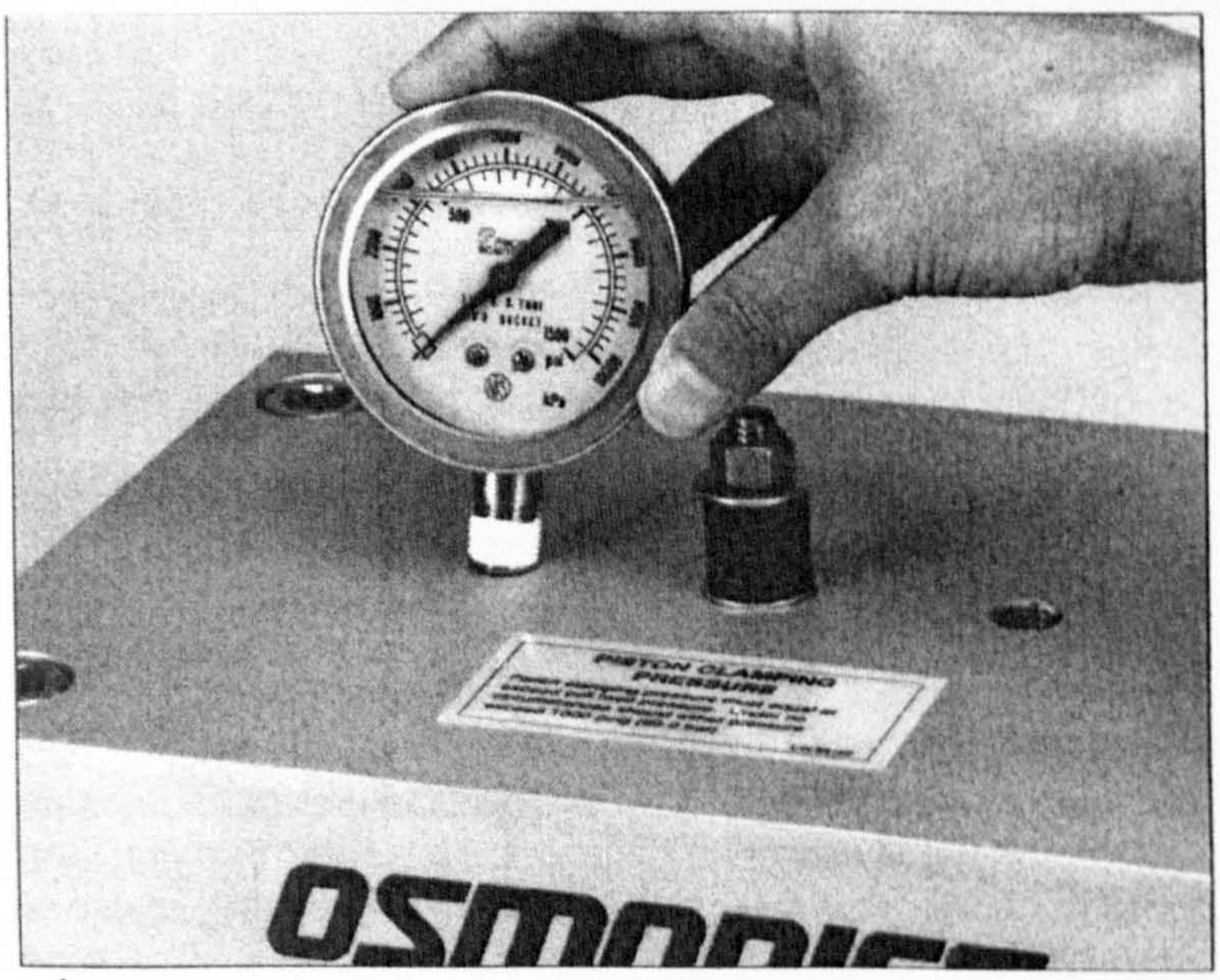

Figure 1. Piston clamping pressure gauge

2) Tighten the gauge with a wrench as shown in Figure 2.

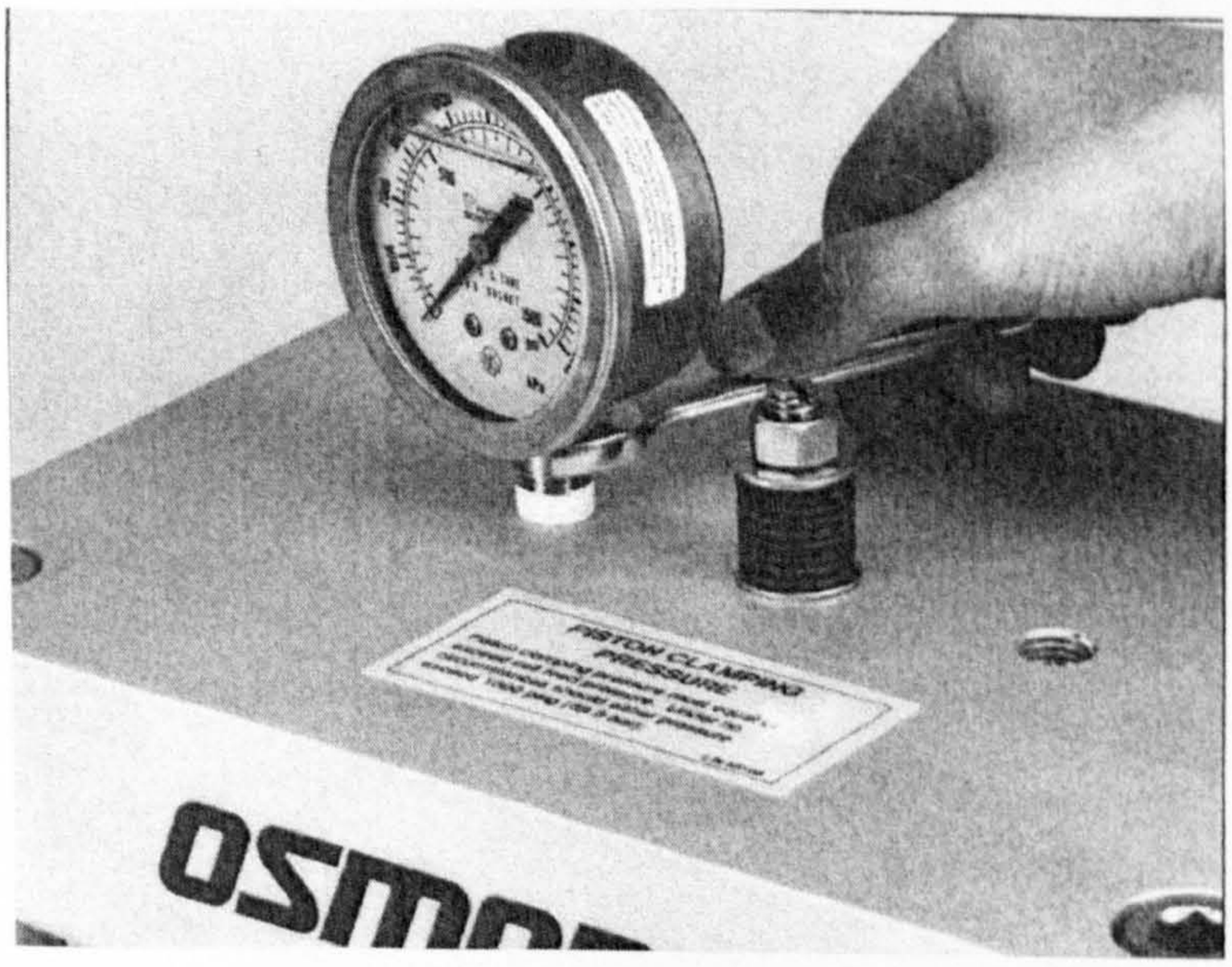

Figure 2. Pressure gauge tightening

3) Install the concentrate flow control valve. Screw the concentrate valve assembly into the open port as shown in Figure 3.

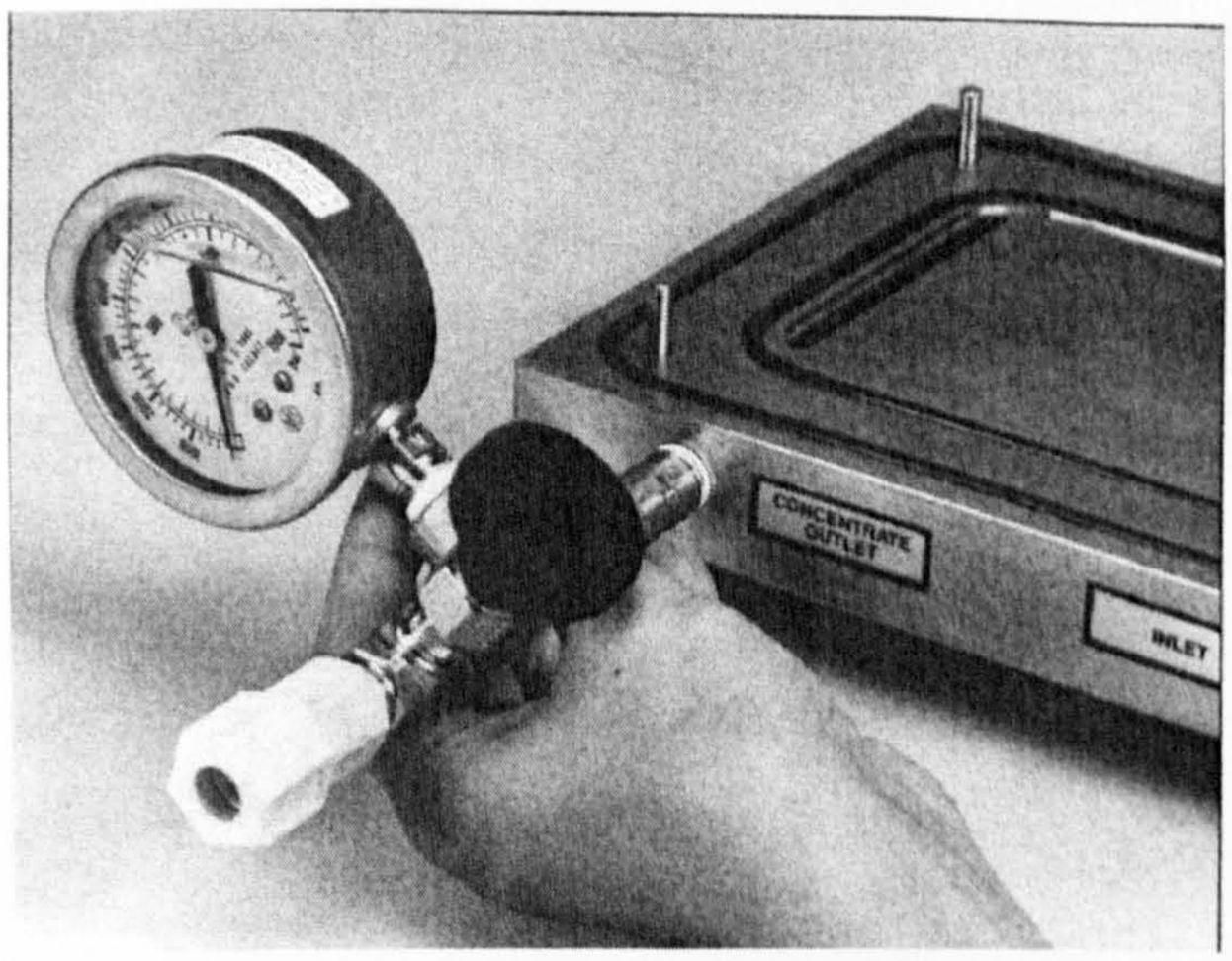

Figure 3. Concentrate flow control valve installation

4) Install the feed spacer. Make sure that the o-rings in the cell body bottom fit properly in the grooves. They should lie flat within the groove as shown in Figure 4.

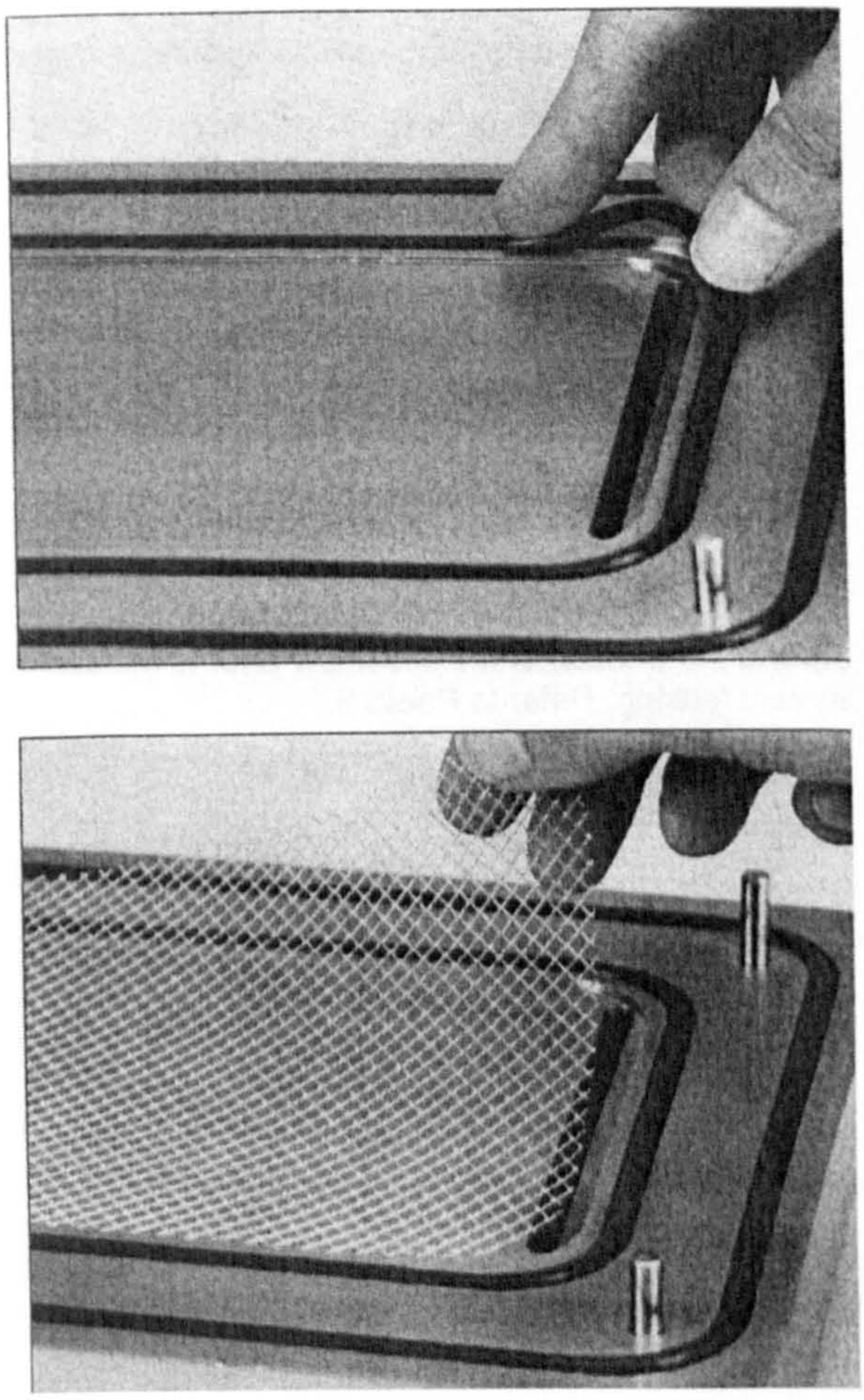

Figure 4. Spacer fitting method

5) Place a piece of pre-cut membrane over the feed spacer using the four alignment pins to hold it in position as shown in figure 5.

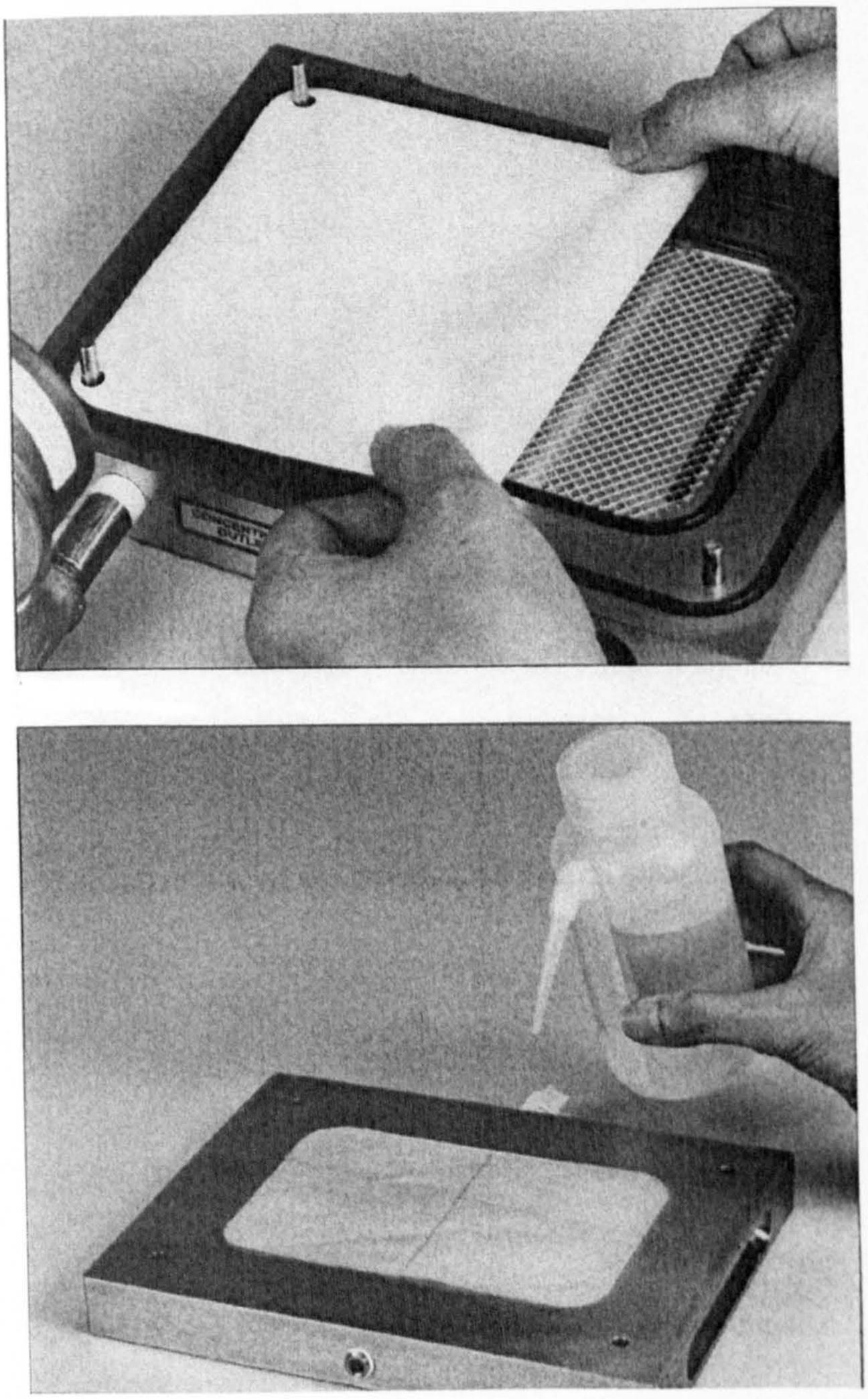

Figure 5. Installation of the membrane sheet

The membrane sheet has a shiny (active side) and dull substrate side. The membrane should be installed with shiny side down toward the feed spacer. After that the permeate carrier holder is installed. Wet the permeate carrier with water as shown in Figure 5.

6) Install the holder as shown in Figure 6.

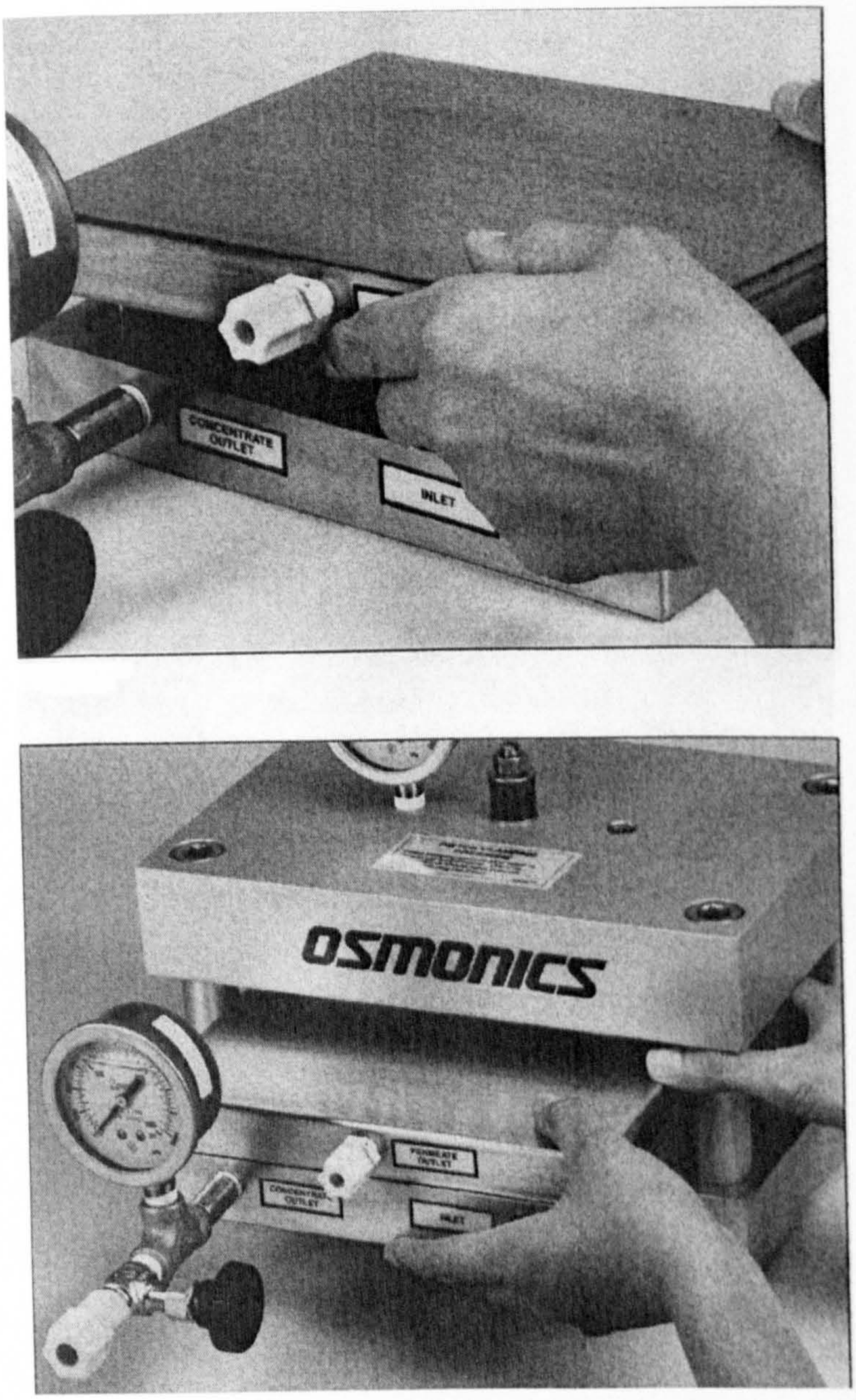

Figure 6. Permeate carrier holder installation

7) Insert the assembled cell body holder into cell holder as shown in Figure 7.

Figure 7. Assembled cell body into cell holder

REFERENCES

1. B. S. Parekh, "*Reverse osmosis technology, application for high-purity water production*", 1988, Marcel Dekker, Inc.
2. R.D. Noble and S.A. Stern, "*Membrane separations technology, Principles and applications*", Elsevier, 1995.
3. W.S. Winston Ho and Kamalesh K. Sirkar, "*Membrane Handbook*", 1992.
4. K. S. Spiegler, *"Principles of water desalination"*, 2nd edition, Academic P. pp. 141.
5. K.S. Spiegler and A.D.K. Laird, "*Principles of desalination*", 2nd Edition, Part B, 1980.
6. A. Porteous, *Desalination Technology, Developments and Practice*, 1983.
7. Z. Amjad "*Reverse osmosis, Membrane technology, water chemistry, and industrial applications*" Chapman & Hall, 1993, New York
8. M. Gama Khedr "*Development of reverse osmosis desalination membrancs composition and configuration: future prospects*" Desalination 153 (2002) 295-304.
9. T. Matsuura "*Progress in membrane science and technology for seawater desalination — a review*" Desalination, Volume 134, Issues 1-3, 20 April 2001, Pages 47-54
10. B. Nicolaisen "*Developments in membrane technology for water treatment*" Desalination, Volume 153, Issues 1-3, 10 February 2003, Pages 355-360
11. S. N. Gaeta, E. Petrocchi, E. Negri and E. Drioli "*Chlorine resistance of polypiperazineamide membranes and modules*" Desalination, Volume 83, Issues 1-3, September 1991, Page 383
12. R. Singh "*Characteristics of a chlorine-resistant reverse osmosis membrane*" Desalination, Volume 95, Issue 1, March 1994, Pages 27-37
13. A. E. Allegrezza, Jr. , B. S. Parekh, P. L. Parise, E. J. Swiniarski and J. L. White "*Chlorine resistant polysulfone reverse osmosis modules*" Desalination, Volume 64, 1987, Pages 285-304
14. M.J. H. Snow, Dirk de Winter, Robert Buckingham, Jeff Campbell and J. Wagner "*New techniques for extreme conditions: high temperature reverse osmosis and nanofiltration*" Desalination, Volume 105, Issues 1-2, June 1996, Pages 57-61
15. H. C. Chu, J. S. Campbell and W. G. Light "*High-temperature reverse osmosis membrane element*" Desalination, Volume 70, Issues 1-3, November 1988, Pages 65-76

16. T. V. Knyazkova and A. A. Kavitskaya "*Improved performance of reverse osmosis with dynamic layers onto membranes in separation of concentrated salt solutions*" Desalination, Volume 131, Issues 1-3, 20 December 2000, Pages 129-136

17. S. Konagaya " *New chlorine-resistant polyamide reverse osmosis membrane with hollow fiber configuration*" J Appl Polym Sci 79 (3): 517-527, Jan 18, 2000.

18. M. Jenkins, "*Operational experience with a new fouling resistant reverse osmosis membrane*" Desalination 119 (1998), pp 243-250.

19. M. Mietton-Peuchot, V. Milisic and P. Noilet "*Grape must concentration by using reverse osmosis. Comparison with chaptalization*" Desalination, Volume 148, Issues 1-3, 10 September 2002, Pages 125-129

20. V. Freger, J. Gilron and S. Belfer "*TFC polyamide membranes modified by grafting of hydrophilic polymers: an FT-IR/AFM/TEM study*" Journal of Membrane Science, Volume 209, Issue 1, 1 November 2002, Pages 283-292

21. V. Alvarez, S. Alvarez, F. A. Riera and R. Alvarez "*Permeate flux prediction in apple juice concentration by reverse osmosis*" Journal of Membrane Science, Volume 127, Issue 1, 30 April 1997, Pages 25-34

22. S. Q. Zhang, A. E. Fouda, T. Matsuura and Kam Chan "*Some experimental results and design calculations for reverse osmosis concentration of green tea juice*" Desalination, Volume 80, Issues 2-3, May 1991, Pages 211-234

23. Permasep Permeators, water treatment by reverse osmosis brochure.

24. Internet: http://www.karcher-vps.com/ProductGroups/WaterPurification/aReverseOsmosis/ReveOsm_main.html

25. http://www.watermakers.com/how.htm.

26. S. Sourirajan "*Reverse osmosis and synthetic membranes, Theroy-Technology-Engineering*" Ottawa, Canda, K1A 0R6, 1977.

27. C. R. Dias, M. J. Rosa and M. N. de Pinho "*Structure of water in asymmetric cellulose ester membranes — and ATR-FTIR study*" Journal of Membrane Science, Volume 138, Issue 2, 21 January 1998, Pages 259-267

28. J. Scott, "*Desalination of seawater by reverse osmosis*", 1981 by Noyes

29. A. Bergen "*Flux enhancement in reverse osmosis using centrifugal membrane separation*" J of Mem Sci, 176 (2): 257-266 AUG 20 2000.

30. C. Visvanathan, N. Boonthanon, A. Sathasivan and V. Jegatheesan "*Pretreatment of seawater for biodegradable organic content removal using membrane bioreactor*" Desalination, Volume 153, Issues 1-3, 10 February 2003, Pages 133-140

31. M. Safar, M. Jafar, M. Abdel-Jawad and S. Bou-Hamad "*Standardization of RO membrane performance*" Desalination, Volume 118, Issues 1-3, 20 September 1998, Pages 13-21

32. M. F. A. Goosen, S. S. Sablani, S. S. Al-Maskari, R. H. Al-Belushi and M. Wilf "*Effect of feed temperature on permeate flux and mass transfer coefficient in spiral-wound reverse osmosis systems*" Desalination 144 (2002) 367-372.

33. S. S. Sablani "*Influence of spacer thickness on permeate flux in spiral-wound seawater reverse osmosis systems*" Desalination 146 (2002) 225-230.

34. M. Abou Rayan and I. Khaled "*Seawater desalination by reverse osmosis (case study)*" Desalination 153 (2003) 245-251.

35. K. Karakulski, M. Gryta and A. Morawski "*Membrane processes used for potable water quality improvement*" Desalination, Volume 145, Issues 1-3, 10 September 2002, Pages 315-319.

36. T. Mohammadi, M. K. Moghadam, S.S. Madaeni "*Hydrodynamic factors affecting flux and fouling during reverse osmosis of seawater*" Desalination 151 (2002) 239-245.

37. Z. Ujang and G. K. Anderson "*Performance of low pressure reverse osmosis membrane (LPROM) for separating mono- and divalent ions*" Water Science and Technology, Volume 38, Issues 4-5, 1998, Pages 521-528.

38. N. M. Al-Bastaki and A. Abbas "*Improving the permeate flux by unsteady operation of a RO desalination unit*" Desalination, Volume 123, Issues 2-3, 10 October 1999, Pages 173-176.

39. H. Ozaki, K. Sharma and W. Saktaywin "*Performance of an ultra-low-pressure reverse osmosis membrane (ULPROM) for separating heavy metal: effects of interference parameters*" Desalination 144 (2002) 287-294.

40. M. R. Pastor, A. F. Ruiz, M. F. Chillón and D. P. Rico "*Influence of pH in the elimination of boron by means of reverse osmosis*" Desalination 140 (2001) 145-152.

41. H. Kurama, J. Poetzschke and R. Haseneder "*The application of membrane filtration for the removal of ammonium ions from potable water*" Water Research, Volume 36, Issue 11, June 2002, Pages 2905-2909.

42. R. Y. Ning "*Arsenic removal by reverse osmosis*" Desalination, Volume 143, Issue 3, 10 June 2002, Pages 237-241

43. T. Koo, Y. J. Lee and R. Sheikholeslami "*Silica fouling and cleaning of reverse osmosis membranes*" Desalination, Volume 139, Issues 1-3, 20 September 2001, Pages 43-56.

44. R. Sheikholeslami and S. Tan "*Effects of water quality on silica fouling of desalination plants*" Desalination, Volume 126, Issues 1-3, 1 November 1999, Pages 267-280.

45. S. D. N. Freeman and R. J. Majerle "*Silica fouling revisited*" Desalination, Volume 103, Issues 1-2, November 1995, Pages 113-115.

46. D. Prats, M. F. Chillon-Arias and M. Rodriguez-Pastor "*Analysis of the influence of pH and pressure on the elimination of boron in reverse osmosis*" Desalination, Volume 128, Issue 3, 10 May 2000, Pages 269-273.

47. R. Sheikholeslami, I. S. Al-Mutaz, S. Tan and S. D. Tan "*Some aspects of silica polymerization and fouling and its pretreatment by sodium aluminate, lime and soda ash*" Desalination, Volume 150, Issue 1, 10 October 2002, Pages 85-92.

48. A. G. Gotor, S. Bachir and C. Argudo "*Analysis and behaviour of chloride solutions in flat reverse osmosis membranes*" Desalination, Volume 119, Issues 1-3, 20 September 1998, Pages 225-227.

49. A. G. Gotor, S. Bachir and C. Argudo "*Analysis and behaviour of chloride solutions in flat reverse osmosis membranes*" Desalination, Volume 119, Issues 1-3, 20 September 1998, Pages 225-227.

50. A. G. Gotor, S. Bachir and C. Argudo "*Analysis and behavior of chloride solutions in flat reverse osmosis membranes*" Desalination, Volume 119, Issues 1-3, 20 September 1998, Pages 225-227.

51. V. Geraldes, V. Semião and M. Norberta de Pinho "*Flow management in nanofiltration spiral wound modules with ladder-type spacers*" Journal of Membrane Science, Volume 203, Issues 1-2, 30 June 2002, Pages 87-102.

52. L. Song "*Performance limitation of the full-scale reverse osmosis process*" Journal of Membrane Science 5530 (2002) 1-6.

53. M. Wilf " *Design consequences of recent improvements in membrane performance*" Desalination 113 (1997) 157-163.

54. M. Hirose, H. Ito and Y. Kamiyama "*Effect of skin layer surface structures on the flux behavior of RO membranes*" Journal of Membrane Science, Volume 121, Issue 2, 11 December 1996, Pages 209-215

55. S. Kwak and D. W. Ihm "*Use of atomic force microscopy and solid-state NMR spectroscopy to characterize structure-property-performance correlation in high-flux reverse osmosis (RO) membranes*" Journal of Membrane Science, Volume 158, Issues 1-2, 1 June 1999, Pages 143-153.

56. N. A. Ochoa, P. Prádanos, L. Palacio, C. Pagliero, J. Marchese and A. Hernández "*Pore size distributions based on AFM imaging and retention of multidisperse polymer solutes: Characterisation of polyethersulfone UF membranes with dopes containing different PVP*" Journal of Membrane Science, Volume 187, Issues 1-2, 15 June 2001, Pages 227-237.

57. J. Y. Kim, H. K. Lee and S. C. Kim "*Surface structure and phase separation mechanism of polysulfone membranes by atomic force microscopy*" Journal of Membrane Science, Volume 163, Issue 2, 1 November 1999, Pages 159-166.

58. D. F. Stamatialis, C. R. Dias and M. N. de Pinho "*Atomic force microscopy of dense and asymmetric cellulose-based membranes*" Journal of Membrane Science, Volume 160, Issue 2, 22 July 1999, Pages 235-242.

59. S.S. Madaeni, " *The effect of surface characteristics on RO membrane performance*" Desalination 139 (2001) 371.

60. J. H. Kim, E. J. Moon and C. K. Kim "*Composite membranes prepared from poly(m-animostyrene-co-vinyl alcohol) copolymers for the reverse osmosis process*" Journal of Membrane Science, In Press, Corrected Proof, Available online 22 March 2003

61. X. Gu, D. Raghavan, T. Nguyen, M. R. VanLandingham and D. Yebassa "*Characterization of polyester degradation using tapping mode atomic force microscopy: exposure to alkaline solution at room temperature*" Polymer Degradation and Stability, Volume 74, Issue 1, 2001, Pages 139-149

62. W. Richard Bowen and T. A. Doneva "*Atomic Force Microscopy Studies of Membranes: Effect of Surface Roughness on Double-Layer Interactions and Particle Adhesion*" Journal of Colloid and Interface Science, Volume 229, Issue 2, 15 September 2000, Pages 544-549

63. M. Elimelech, X. Zhu, A. E. Childress and S. Hong, "*Role of membrane surface morphology in colloidal fouling of cellulose acetate and composite aromatic polyamide reverse osmosis membranes*" Journal of Membrane Science, Volume 127, Issue 1, 30 April 1997, Pages 101-109

64. T. Matsuura, "*Progress in membrane science and technology for seawater desalination- a review*", Desalination 134 (2001) pp 47-54.

65. M. Luo and Z. Wang "*Complex fouling and cleaning-in-place of a reverse osmosis desalination system*" Desalination, Volume 141, Issue 1, 1 December 2001, Pages 15-22

66. M. Gamal Khedr "*Development of reverse osmosis desalination membranes composition and configuration: Future prospects*" Desalination, Volume 153, Issues 1-3, 10 February 2003, Pages 295-304

67. B. J. Trushinski, J. M. Dickson, T. Smyth, R. F. Childs and B. E. McCarry "*Polysulfonamide thin-film composite reverse osmosis membranes*" Journal of Membrane Science, Volume 143, Issues 1-2, 27 May 1998, Pages 181-188

68. B. J. Trushinski, J. M. Dickson, T. Smyth, R. F. Childs and B. E. McCarry "*Polysulfonamide thin-film composite reverse osmosis membranes*" Journal of Membrane Science, Volume 143, Issues 1-2, 27 May 1998, Pages 181-188

69. B. J. Trushinski, J. M. Dickson, T. Smyth, R. F. Childs and B. E. McCarry "*Polysulfonamide thin-film composite reverse osmosis membranes*" Journal of Membrane Science, Volume 143, Issues 1-2, 27 May 1998, Pages 181-188

70. R. I. Urama and B. J. Mariñas "*Mechanistic interpretation of solute permeation through a fully aromatic polyamide reverse osmosis membrane*" Journal of Membrane Science, Volume 123, Issue 2, 22 January 1997, Pages 267-280

71. H. Kim and S. Soo Kim "*Fabrication of reverse osmosis membrane via low temperature plasma polymerisation*" Journal of Membrane Science, Volume 190, Issue 1, 31 August 2001, Pages 21-33

72. S. Kwak, C. Kim, and J. Kim, "*Effects of Bisphenol monomer structure on the surface morphology and RO performance of thin-film composite membranes composed of polyphenyl esters*"J Pol Sci. 24 (1996), pp 2201-2208.

73. N. A. Ochoa, P. Prádanos, L. Palacio, C. Pagliero, J. Marchese and A. Hernández "*Pore size distributions based on AFM imaging and retention of multidisperse polymer solutes: Characterisation of polyethersulfone UF membranes with dopes containing different PVP*" Journal of Membrane Science, Volume 187, Issues 1-2, 15 June 2001, Pages 227-237

74. V. Freger, J. Gilron and S. Belfer "*TFC polyamide membranes modified by grafting of hydrophilic polymers: an FT-IR/AFM/TEM study*" Journal of Membrane Science, Volume 209, Issue 1, 1 November 2002, Pages 283-292

75. J. Y. Kim, H. K. Lee and S. C. Kim "*Surface structure and phase separation mechanism of polysulfone membranes by atomic force microscopy*" Journal of Membrane Science, Volume 163, Issue 2, 1 November 1999, Pages 159-166

76. S. Kwak, M. Yeom, J. Roh, D. Y. Kim and J. Kim "*Correlations of chemical structure, atomic force microscopy (AFM) morphology, and reverse osmosis (RO) characteristics in aromatic polyester high-flux RO membranes*" Journal of Membrane Science, Volume 132, Issue 2, 3 September 1997, Pages 183-191

77. W. R. Bowen, N. Hilal, R. W. Lovitt and P. M. Williams, "*Visualization of an ultrafiltration membrane by non-contact atomic force microscopy at single pore resolution*" Journal of Membrane Science, Volume 110, Issue 2, 21 February 1996, Pages 229-232.

78. S. Kwak, C. K. Kim, and J. Kim "*Effect of bisphoenol monomer structure on surface morphology and reverse osmosis (RO performance of thin-film-composite membranes composed of polyphenyl ester*" J of polm Sci, vol 34, 2201-2208 (1996)

79. E. M. Vrijenhoek, S. Hong and M. Elimelech "*Influence of membrane surface properties on initial rate of colloidal fouling of reverse osmosis and nanofiltration membranes*" Journal of Membrane Science, Volume 188, Issue 1, 30 June 2001, Pages 115-128.

80. M. Hirose, H. Ito and Y. Kamiyama "*Effect of skin layer surface structures on the flux behaviour of RO membranes*" Journal of Membrane Science, Volume 121, Issue 2, 11 December 1996, Pages 209-215.

81. M. Elimelech, X. Zhu, A. E. Childress and S. Hong "*Role of membrane surface morphology in colloidal fouling of cellulose acetate and composite aromatic polyamide reverse osmosis membranes*" Journal of Membrane Science, Volume 127, Issue 1, 30 April 1997, Pages 101-109

82. E. Ferjani, R. H. Lajimi, A. Deratani and M. S. Roudesli "*Bulk and surface modification of cellulose diacetate based RO/NF membranes by polymethylhydrosiloxane preparation and characterization*, Desalination, Volume 146, Issues 1-3, 10 September 2002, Pages 325-330

83. K. Scott, R. J. Jachuck and D. Hall "*Crossflow microfiltration of water-in-oil emulsions using corrugated membranes*" Separation and Purification Technology 22-23 (2001) 431-441.

84. M. Hlavacek "*Break-up of oil-in-water emulsions induced by permeation through a microfiltration membrane*" J of Mem. Sci. 102 (1995) 1-7.

85. I. W. Cumming, R. G. Holdich and I. D. Smith "*The rejection of oil by microfiltration of a stabilised kerosene/water emulsion*" V 169, (2000) Pages 147-155.

86. I. Koyuncu and M. Yazgan "*Application of nanofiltration and reverse osmosis membranes to the salty and polluted surface water*" J Env Sci Health, A36(7), 1321-1333 (2001).

87. W. C. Lai and K. J. Smith "*Heavy oil microfiltration using ceramic monolith membranes*" Fuel 80 (2001) Pages 1121-1130.

88. J. Zhong, X. Sun and C. Wang "*Treatment of oily wastewater produced from refinery processes using flocculation and ceramic membrane filtration*" Separation and Purification Technology 00 (2003) 1-6.

89. S. H. Lee, K. Chung, M. Shin, J. Dong, H. Lee and K. H. Auh "*Preparation of ceramic membrane and application to the crossflow microfiltration of soluble waste oil*" Materials Letters 52 (2002) 266-271.

90. A. B. Kotuniewicz' R. W. Field, "*Process factors during removal of oil-in-water emulsions with cross-flow microfiltration*" Vol. 105, (1996), 79-89.

91. J. Mueller, C. Yanwei and R. H. Davis "*Crossflow microfiltration of oily water*" Vol. 129, (1997) 221-235.

92. H. Ohya, J. J. Kim, A. Chinen, M. Aihara, S. I. Semenova, Y. Negishi, O. Mori and M. Yasuda "*Effects of pore size on separation mechanisms of microfiltration of oily water, using porous glass tubular membrane*" Vol 145, (1998) Pages 1-14.

93. P. Srijaroonrat, E. Julien and Y. Aurelle "*Unstable secondary oil/water emulsion treatment using ultrafiltration: fouling control by backflushing*" J of Mem Sci 159 (1999) 11-20.

94. R. M. Dick "*Ultrafiltration for oily wastewater treatment*" Lubrication Engineering, Vol 38, 4, (1981), pp 219-222.

95. X. Hu, E. Bekassy-Molnar and G. Vatai "*Study of ultrafiltration behaviour of emulsified metalworking fluids*" Desalination 149 (2002) 191-197.

96. S. H. Lin and W. J. Lan "*Treatment of waste oil/water emulsion by ultrafiltration and ion exchange*" Water research, Vol 32, 9, (1998) Pages 2680-2688.

97. A. Duong "*An experimental study of heavy oil ultrafiltration using ceramic membranes*" Fuel, V 76, 9, pp 821-828, (1997).

98. L. E. Fratila-Apachitei, M. D. Kennedy, J. D. Linton, I. Blume and J. C. Schippers "*Influence of membrane morphology on the flux decline during dead-end ultrafiltration of refinery and petrochemical waste water*" J of Mem Sci 182 (2001) 151-159.

99. C. C. Teodosiu, M. D. Kennedy, H. A. V. Straten and J. C. Schippers "*Evaluation of secondary refinery effluent treatment using ultrafiltration membranes*" Water research 133 (1999), Pages 2172-2180.

100. B. Tansel, J. Regula and R. Shalewitz "*Treatment of fuel oil and crude oil contaminated waters by ultrafiltration membranes*" Desalination 102 (1995) 301-311.

101. B. Tansel, J. Regula and R. Shalewitz "*Evaluation of ultrafiltration process perforamance for treatment of petroleum contaminated waters*" Water, Air and Soil Pollution 126, 291-305 (2001).

102. S. Elmaleh and N. Ghaffor "*Cross-flow ultrafiltration of hydrocarbon and biological solid mixed suspensions*" J of Mem Sci 118 (1996) 111-120.

103. S. Elmaleh and N. Ghaffor "*Cross-flow ultrafiltration of hydrocarbon and biological solid mixed suspensions*" Journal of Membrane Science, Volume 118, Issue 1, 4 September 1996, Pages 111-120.

104. K. Karakulski, A. Kozłowski and A. W. Morawski "*Purification of oily wastewater by ultrafiltration*" Separations Technology, Volume 5, Issue 4, November 1995, Pages 197-205.

105. P. Lipp, C. H. Lee, A. G. Fane and C. J. D. Fell "*A fundamental study of the ultrafiltration of oil-water emulsions*" J of Mem Sci 36, 1988, pp 161-177.

106. W. Jian, "*Removal of oil pollutants in seawater as pretreatment of reverse osmosis desalination process*" Water Research 33 (8): 1857-1863 (1999)

107. X. Hu, " *The study of oil/water separation in emulsion by ultrafiltration membranes*" CHEMISCHE TECHNIK, 50 (3): 119-123 MAY-JUN 1998.

108. A. S. Jönsson, J. Lindau, R. Wimmerstedt, J. Brinck and B. Jönsson "*Influence of the concentration of a low-molecular organic solute on the flux reduction of a polyethersulphone ultrafiltration membrane*" J of Mem Sci 135 (1997) 117-128.

109. R. S. Faibish and Y. Cohen "*Fouling-resistant ceramic-supported polymer membranes for ultrafiltration of oil-in-water microemulsions*" J of Mem Sci 185 (2001) 129-143.

110. N. Laitinen, A. Luonsi, E. Levänen and M. Nyström "*Effect of backflushing conditions on ultrafiltration of board industry wastewaters with ceramic membranes*" Separation and Purification Technology 25 (2001) 323-331.

111. T. V. R. Alicieo, E. S. Mendes, N. C. Pereira and O. C. Motta Lima "*Membrane ultrafiltration of crude soybean oil*" Desalination 148 (2002) 90-102.

112. R. S. Faibish and Y. Cohen "*Fouling and rejection behavior of ceramic and polymer-modified ceramic membranes for ultrafiltration of oil-in-water emulsions and microemulsions*" Colloids and Surfaces 191 (2001) 27-40.

113. Z. Xu, T. Chung, K. Loh and B. C. Lim "*Polymeric asymmetric membranes made from polyetherimide/polybenzimidazole/poly(ethylene glycol) (PEI/PBI/PEG) for oil–surfactant–water separation*" Journal of Membrane Science, Volume 158, Issues 1-2, 1 June 1999, Pages 41-53.

114. Internet http://www.mos.org/sln/sem/tour20.html.

115. Internet, Brian Rudie, Hydrophilicity and hydrophobicity, www.osmonics.com/products/Page772htm.

116. Y. Kiso, Y. Nishimura, T. Kitao and K. Nishimura "*Rejection properties of non-phenylic pesticides with nanofiltration membranes*" J of Mem Sci 171 (2000) 229-237.

117. B. V. der Bruggen, L. Braeken and C. Vandecasteele "*Evaluation of parameters describing flux decline in nanofiltration of aqueous solutions containing organic compounds*" Desalination 147 (2002) 281-288.

118. M. Ernst, A. Sachse, C. E. W. Steinberg, and M. Jekel "*Characterization of the DOC in nanofiltration permeates of a tertiary effluent*" Water Research Vol 34, 11, pp 2879-2886 (2000).

119. J. Meier, T. Melin and L. H. Eilers "*Nanofiltration and adsorption on powdered adsorbent as process combination for the treatment of severely contaminated waste water*" Desalination 146 (2002) 361-366.

120. B. V. der Bruggen, L. Braeken and C. Vandecasteele "*Flux decline in nanofiltration due to adsorption of organic compounds*" Separation and Purification Technology Vol 29, 1 (2002), Pages 23-31.

121. M. D. Afonso and R. Bórquez "*Nanofiltration of wastewaters from the fish meal industry*" Desalination 151 (2002) 131-138.

122. C. Jarusutthirak, G. Amy and J. Croué "*Fouling characteristics of wastewater effluent organic matter (EfOM) isolates on NF and UF membranes*" Desalination 145 (2002) 247-255.

123. B. V. der Bruggen, J. Geens and C. Vandecasteele "*Fluxes and rejections for nanofiltration with solvent stable polymeric membranes in water, ethanol and n-hexane*" Chemical Engineering Science 57 (2002) 2511-2518.

124. L. S. White "*Transport properties of a polyimide solvent resistant nanofiltration membrane*" Journal of Membrane Science, Volume 205, Issues 1-2, 1 August 2002, Pages 191-202

125. E. Hindin, P. J. Bennett and S. S. Narayanan "*Organic compounds removed by reverse osmosis*" Water and Sewage Works, December 1969, pp 266-270.

126. V. H. Edward and P. F. Schubert "*Removal of 2,4-D and other persistent organic molecules from water supplies by reverse osmosis*" Water Technology/Quality, AWWA, October 1974, pp 610-616.

127. T. Matsuura and S. Sourirajan "*Physicochemical criteria for reverse osmosis separation of monohydric and polyhydric alcohols in aqueous solution using porous cellulose acetate membranes*" J of App Pol Sci, Vol 17, pp 1043-1071 (1973).

128. R. Gerard, H. Hachisuka, M. Hirose "*New membrane developments expanding the horizon for the application of reverse osmosis technology*" Desalination 119 (1998) 47-55.

129. H. Ozaki and H. Li, "*Rejection of organic compounds by ultra-low pressure reverse osmosis membrane*" Water Research, Volume 36, Issue 1, January 2002, Pages 123-130.

130. H. Odegaard and S. Koottantep "*Removal of humic substances from natural waters by reverse osmosis*" Water Re. Vol 16, pp 613-620 (1982).

131. R. Molinari, P. Argurio and L. Romeo "*Studies on interactions between membranes (RO and NF) and pollutants (SiO_2, NO_3^-, Mn^{++} and humic acid) in water*" Desalination, Volume 138, Issues 1-3, 20 September 2001, Pages 271-281

132. P. A. Maurice, M. J. Pullin, Stephen E. Cabaniss, Qunhui Zhou, Ksenija Namjesnik-Dejanovic and George R. Aiken "*A comparison of surface water natural organic matter in raw filtered water samples, XAD, and reverse osmosis isolates*" Water Research, Volume 36, Issue 9, May 2002, Pages 2357-2371

133. S. S. Deshmukh and A. E. Childress "*Zeta potential of commercial RO membranes: influence of source water type and chemistry*" Desalination, Volume 140, Issue 1, 20 October 2001, Pages 87-95.

134. S. Sridhar, A. Kale and A. A. Khan "*Reverse osmosis of edible vegetable oil industry effluent*" J of Membrane Sci. 205 (2002) 83-90.

135. S. Sridhar, A. Kale and A. A. Khan "*Reverse osmosis of edible vegetable oil industry effluent*" J of Membrane Sci. 205 (2002) 83-90.

136. G. H. Koops, S. Yamada and S. -I. Nakao, "*Separation of linear hydrocarbons and carboxylic acids from ethanol and hexane solutions by reverse osmosis*" Vol. 189, (2001) 241-254.

137. Y. Kiso, T. Kitao, K. Jinno and M. Miyagi "*The effects of molecular width on permeation of organic solute through cellulose acetate reverse osmosis membranes*" Journal of Membrane Science, Volume 74, Issues 1-2, 28 October 1992, Pages 95-103

138. J. Huang, Q. Guo, H. Ohya and J. Fang "*The characteristics of crosslinked PAA composite membrane for separation of aqueous organic solutions by reverse osmosis*" J of Membrane Sci. vol 144, (1998) pp 1-11.

139. L. Katelan-Kunst, K. Kouti, V. Danani and B. Kunst "*FT30 membranes of characterized porosities in the reverse osmosis organics removal from aqueous solutions*" Water Resch, Vol 31, no 11, pp 2878-2884, 1997.

140. K. Kosutic and B. Kunst "*Removal of organics from aqueous solutions by commercial RO and NF membranes of characterized porosities*" Desalination 142, (2002) 47-56.

141. K. Kosutic, L. Kastelan-Kunst, and B. Kunst "*Porosity of some commercial reverse osmosis and nanofiltration polyamide thin film composite membrane*" J of membrane Sci 168 (2000) 101-108.

142. S. H. Lin and W. J. Lan "*Waste oil/water emulsion treatment by membrane processes*" J of Hazrd Mtrl 59 (1998) 189-199.

143. G. H. Koops, S. Yamada and S. I. Nakao "*Separation of linear hydrocarbons and carboxylic acids from ethanol and hexane solutions by reverse osmosis*" Journal of Membrane Science, Volume 189, Issue 2, 15 August 2001, Pages 241-254.

144. S. Sridhar, A. Kale and A. A. Khan "*Reverse osmosis of edible vegetable oil industry effluent*" Journal of Membrane Science, Volume 205, Issues 1-2, 1 August 2002, Pages 83-90.

145. H. Ma, H. E. Allen and Y. Yin "*Characterization of isolated fractions of dissolved organic matter from natural waters and a wastewater effluent*" Water Research, Volume 35, Issue 4, March 2001, Pages 985-996.

146. V. V. Goncharuk, D. D. Kucheruk, V. M. Kochkodan and V. P. Badekha "*Removal of organic substances from aqueous solutions by reagent enhanced reverse osmosis*" Desalination, Volume 143, Issue 1, 10 May 2002, Pages 45-51.

147. T. Hodgkiess, W. T. Hanbury, G. B. Law and T. Y. Al-Ghasham, "*Effect of hydrocarbon contaminants on the performance of RO membranes*" Desalination, Volume 138, Issues 1-3, 20 September 2001, Pages 283-289.

148. FILMTEC membranes products information, page 75 http://www.membraneonline .com/Companies/Listings/Filmtec.htm

149. M. Teng, K. Lee, D. Liaw, Y. Lin and J. Lai "*Plasma deposition of acrylamide onto novel aromatic polyamide membrane for pervaporation*, European Polymer Journal, Volume 36, Issue 4, 1 April 2000, Pages 663-672

150. R. Rautenbach, T. Linn " *High-pressure reverse osmosis and nanofiltration, a "zero discharge" process combination for the treatment of waste water with severe fouling/scaling potential*" Desalination 105 (1996) 63-70.

151. A. M. Alsari, K. C. Khulbe and T. Matsuura "*The effect of sodium dodecyl sulfate solutions as gelation media on the formation of PES membranes*" Journal of Membrane Science, Volume 188, Issue 2, 15 July 2001, Pages 279-293

152. M. Pontié, P. Cowache, L. H. Klein, V. Maurice and F. Bedioui "*Preparation and characterization of an electronically conductive and chemically modified ultrafiltration type membrane"* Journal of Membrane Science, Volume 184, Issue 2, 30 March 2001, Pages 165-173

153. J. B. Evett, C. Liu "Fluid Mechanics and hydraulics" McGraw Hill, 1988

154. http://stm2.nrl.navy.mil/how-afm-afm/how-afm.html

155. www.chembio.uoguelph.ca/educmat/chm729/afm/details.htm

156. G. Wen, X. Li, Y. Liao and L. An "*Surface phase separations of PMMA/SAN blends investigated by atomic force microscopy*" Polymer, Volume 44, Issue 14, June 2003, Pages 4035-4045.

157. F. Dinelli, H. E. Assender, K. Kirov and O. V. Kolosov "*Surface morphology and crystallinity of biaxially stretched PET films on the nanoscale*" Polymer, Volume 41, Issue 11, May 2000, Pages 4285-4289